ERICSSON technics

Ericsson LM

NUMBER 1 / 1960 - 62

Ericsson Technics

ADVISORY BOARD

H THORELLI, Senior Vice President (ret.)

E A ERICSSON, Vice President

H BLOMBERG, President, Svenska Radio AB, Stockholm

EDITORIAL COMMITTEE

C JACOBÆUS, Dr Techn, Vice President, Chairman

S EKLUND, D.H.S., Editor

O BAGER, M.Sc. (El. Eng.)

Ericsson Technics is published by
Telefonaktiebolaget L M Ericsson
Stockholm 32, Sweden

Ericsson Technics

VOLUME 16 (1960) · No. 1

CONTENTS

TELEFONAKTIEBOLAGET L M ERICSSON
STOCKHOLM 32

Some Problems Concerning Noise in Wide-Band Carrier Systems

BY

STIG JANSON* & VIKING STENDING*

UDC 621.395.82
621.395.44

This article is primarily intended to give information on the various types of noise which arise in modern wide-band systems for telephony. General formulæ for second and third order intermodulation noise and certain optimum conditions for noise are derived. Finally, a practical example is worked out.

This article corresponds to »Några problem behandlande störningar i bredbandssystem» by S Janson & V Stending, printed in Tele No. 3/1959.

* The Swedish Board of Telecommunications, Stockholm

Contents

Introduction

The types of transmission systems which today are available for long distance transmission of large numbers of telephone circuits are those for coaxial cables and radio links. They have many factors in common, viz. the terminal equipment is the same, and the number of circuits per system is of the same order of magnitude. The number of circuits is increased in both cases in step with development in technique. Radio links have for several years been able to transmit 600 telephone circuits per system, and are now being designed for 960 circuits. The capacity of the coaxial cable systems is now being increased from 960 to 2,700 circuits per system. In both types of system, the problem of crosstalk *between* different systems on the same route can be overcome nowadays using relatively simple means. The main problem in both cases is the interference which arises within systems at the many points of amplification. Interference occurs there just as inevitably as friction in a machine and it is a difficult technical problem to design equipment in such a way that high transmission quality is obtained. The types of interference which occur most often are "babble" and noise—thermal noise and intermodulation noise.

In the following article, emphasis has been placed on the coaxial systems, as the authors are most acquainted with these.

CHAPTER 1

CCITT Recommendations

The original recommendations on noise are very old and go back to the open-wire line era where interference due to power lines etc. was the dominating factor. The peculiarity is that practically the same recommendations are still in use today and the requirements have not been increased but reduced instead. Thus for open-wire lines the earlier recommendation for the psophometric e.m.f. was that this should not exceed 5 mV. For cable routes this maximum value was recalculated to be 2 mV in a point of relative level —0.8 N (—7 db). This value, however, is not, as was the case previously, the maximum value but the mean value in the busy hour. This shall be maintained for each international circuit.

CCITT have proposed some hypothetical reference circuits to act as guides for designers. Hypothetical reference circuits for 2.6 and 4 Mc/s and also for the 12 Mc/s coaxial systems are shown in *fig. 1*. These reference circuits are 2,500 km (1,550 miles) long and are divided into three uniform sections connected together at voice frequency. Each of these sections is again divided up into 3 equally long homogeneous sections (each section is thus $\frac{2{,}500}{9} \approx 280$ km (or 170 miles). The connexion of these sections together is on basic supergroup and basic group basis for 2.6 Mc/s and 4 Mc/s coaxial systems and on a basic mastergroup and basic supergroup basis for the 12 Mc/s coaxial system.

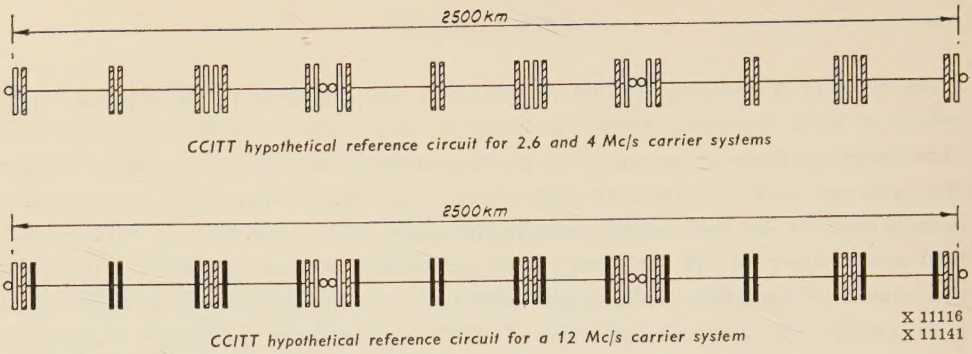

Fig. 1. CCITT hypothetical reference circuits for coaxial systems.

o Channel translating equipment

▯ Group translating equipment

▨ Supergroup translating equipment

▌ Mastergroup translating equipment

It has also been stated that of the 10,000 pW[1] total noise permitted for a hypothetical reference circuit (at a zero relative level point), the noise contributions from all the terminal equipment should not exceed 2,500 pW and those from the h.f. line should not exceed 7,500 pW (corresponding to 3 pW/km).

The following recommendations have been made for summation of the noise contributions due to the different parts:

1. At the end of each homogeneous section, the channels, groups and supergroups will be connected through at random.
2. Within each homogeneous section, the telephone channels will occupy the same position in relation to each other. If, within these sections, certain intermodulation products (those of odd order) tend to add according to a law of linear addition of voltages, it may be considered that a power addition law only applies between the sections in respect of noise.

These values, however, can give relatively poor quality. In Sweden alone it is possible to have very long circuits, and with international calls between, for example, Kiruna and Southern Europe, lines of 5,000 km length can occur. Better values than the above mentioned 3 pW/km are therefore being aimed at by several administrations. In addition, it should also be remembered that if new plant can only just maintain the requirement of 3 pW/km, there is a very great risk that this value is later exceeded due to ageing of tubes and other components, etc.

[1] Corresponds to 2.2 mV psophometric e.m.f. at a point of relative level —0.8 N (—7 db). The permitted value of 2 mV corresponds to approx. 8,000 pW or a noise level equal to — 5.9 N (— 53 db).

CHAPTER 2

Thermal Noise

Thermal noise occurs mainly only on the input side of amplifiers where the level is lowest. This is caused by resistance noise and tube noise. Resistance noise is caused by the internal energy of the free electrons. It is evenly distributed over the frequency band (white noise) and the corresponding mean value of voltage across a terminated four-terminal network of real image impedance R is

$$E = \sqrt{2kTR\Delta f}$$

where k is BOLTZMANN's constant 1.38×10^{-23} Ws/degree KELVIN, T is the absolute temperature, which is about 300° KELVIN and Δf is the bandwidth in c/s.

The corresponding mean power is

$$\frac{E^2}{R} = 2kT\Delta f$$

The disturbance value of noise in a telephone channel is less than this power due to the noise at low and high frequencies not being so disturbing as at frequencies in the middle of the speech band. With a frequency band of 300—3,400 c/s the power given by the above formula is thus reduced to a half by the psophometric weighting. For a telephone channel with 4 kc/s bandwidth, the resistance noise level may be calculated using the above to be —15.9 nepers below zero level. According to the previous chapter the total permissible interference level in a channel is 2 mV or — 5.9 N. From the above it is seen that the resistance noise alone gives maximum permissible noise if the level at one point only is allowed to go to the value — 10.0 N. As the noise from different sources of interference add, the input level of the amplifiers in a long transmission line must clearly have a safe margin from this value.

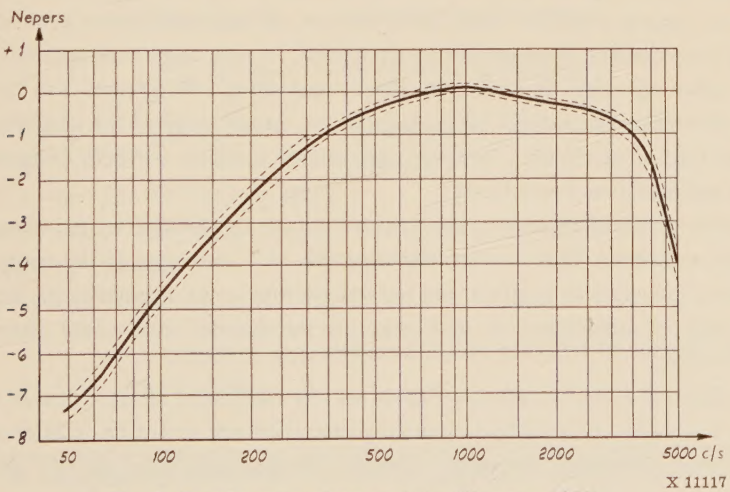

Fig. 2. Psophometer characteristic (Florence 1951).

Tube noise is of about the same magnitude as the resistance noise alone. The easiest method of calculating tube noise is to use the value normally given for the equivalent noise resistor for the input tube.

When coupled immediately before the input this fictitious resistor shall give the same thermal noise according to the formula given above as that given by the tube. The tubes used in the coaxial system amplifiers normally have a noise resistance of several hundred ohms. The input impedance of a coaxial system amplifier is 75 ohms. This value, however, is transformed by the input transformer up to a value of 700 to 800 ohms which gives a noise resistance of 350 to 400 ohms. The tube noise, therefore, gives a not unappreciable contribution to the total thermal noise.

CHAPTER 3

Intermodulation Noise

General

Intermodulation noise varies appreciably with loading, as will be shown later. It is therefore greatest in the busy hour. The main cause of this type of interference is that the characteristics of the amplifier tubes are not absolutely linear. Within the working region i.e. for small amplitudes, an appreciable improvement in the linearity of an amplifier can be obtained by using feedback, but to have so much feedback on the amplifiers that almost ideal conditions in this respect are obtained—even if it were technically possible—would be too expensive.

Consider the case when the amplifiers are overloaded. As long as an amplifier works within its linear range, it is mainly the second and third order intermodulation products which determine the level of the intermodulation noise. Their power increases within this range by the square and the cube of the fundamental power. If, however, the power of the fundamental exceeds a certain value, the power of the intermodulation products increases very much more quickly; the amplifier is overloaded. In such cases intermodulation products of higher order will also be important when considering interference. The limit of overloading is determined in general by the tube in the output stage of the amplifier.

The latter type of interference, however, very seldom occurs in correctly designed amplifiers if the tube maintenance is satisfactory.

Both types of the interference above can of course be reduced by lowering the output level of the amplifiers. This is relatively expensive as a reduction in the output level must either mean a reduction in length of the repeater section or an increase in the dimensions of the cable (reduced attenuation per unit length) as the thermal noise would otherwise exceed acceptable values.

Besides electron tubes, transformers must also be mentioned as components which cause distortion. It has also occurred that capacitors have given rise to distortion of such magnitude that it has been disturbing. Normally, however, the distortion from the two last-mentioned components is negligible.

Distortion and Intermodulation

When an amplifier, even if it has negative feedback, does not have completely linear characteristics, the output voltage is not a linear function of the input voltage. With a pure sinusoidal voltage at the input, harmonics of this are also obtained at the output. If there are voltages of different frequencies at the input, combinations of the various frequencies, intermodulation products[1] as well as the fundamentals and harmonics are obtained at the output.

The relation between the input and output voltages (*fig. 3*) can be most suitably expressed as a power series

$$u_2 = a_1 u_1 + a_2 u_1^2 + a_3 u_1^3 + \ldots$$

where u_2 refers to the output voltage at the final tube. It is assumed that the input voltage u_1 consists of a number of sinusoidal voltages of various frequencies f_A, f_B, f_C etc. and having amplitudes of U_A, U_B, U_C etc.

If this is substituted in the power series, the following is obtained:

$$\begin{aligned} u_2 = {} & a_1 [U_A \cos 2\pi f_A t + U_B \cos 2\pi f_B t + U_C \cos 2\pi f_C t + \ldots] + \\ & + a_2 [U_A \cos 2\pi f_A t + U_B \cos 2\pi f_B t + U_C \cos 2\pi f_C t + \ldots]^2 + \\ & + a_3 [U_A \cos 2\pi f_A t + U_B \cos 2\pi f_B t + U_C \cos 2\pi f_C t + \ldots]^3 + \\ & + \ldots\ldots \end{aligned}$$

If the above expression is developed it is found that the output voltage contains the frequencies

1)		f_A, f_B etc.	= fundamentals
2)		$2f_A$, $2f_B$ etc.	= second order harmonics
3)		$3f_A$, $3f_B$ etc.	= third order harmonics
4)		$f_A \pm f_B$ etc.	= second order intermodulation products
5)	I a)	$f_A + f_B + f_C$, $f_A - f_B - f_C$ etc.	third order intermodulation products
	I b)	$2f_A + f_B$ $f_B - 2f_A$	
	II a)	$f_A + f_B - f_C$ etc.	
	II b)	$2f_A - f_B$,,	
6)		harmonics and intermodulation products of higher order and also d.c. terms.	

[1] It sometimes occurs that correction networks of various types are placed at the output of the amplifier. All reasoning from this point considers the conditions immediately after the final tube, that is before any correction network.

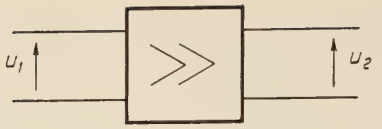

X 11118

Fig. 3. Amplifier.

The amplitudes are for

1) $a_1 U_A$, $a_1 U_B$

2) $\frac{a_2}{2} U_A^2$, $\frac{a_2}{2} U_B^2$

3) $\frac{a_3}{4} U_A^3$, $\frac{a_3}{4} U_B^3$

4) $a_2 U_A U_B$

5) Ia) $\frac{6a_3}{4} U_A U_B U_C$

5) Ib) $\frac{3a_3}{4} U_A^2 U_B$

5) IIa) $\frac{6a_3}{4} U_A U_B U_C$

5) IIb) $\frac{3a_3}{4} U_A^2 U_B$

The total harmonic ratio for second and third order harmonics is

$$a_{k_2} = \ln \frac{2a_1 U}{a_2 U^2}$$

$$a_{k_3} = \ln \frac{4a_1 U}{a_3 U^3}$$

If $U = ke^N$, the expressions become

$$a_{k_2} = \ln \frac{2a_1}{k a_2} - N$$

$$a_{k_3} = \ln \frac{4a_1}{k^2 a_3} - 2N$$

It will be seen that the total harmonic ratio is dependent on the output voltage. An increase in the level of the fundamental by S nepers results in a_{k2} and a_{k3} decreasing by S and $2S$ nepers respectively, or in other words the second and third order distortion voltages increase by the square and cube of the amplitude of the associated fundamental.

If $U_A = U_B = U_C$, it is found in addition that the level of the intermodulation products is greater than the level of the harmonic products of the same order. (See *table 1.*)

Table 1.

Type of intermodulation product	Level difference	Order of harmonic
$A \pm B$	0.7 neper higher than	$2A$
$A \pm B \pm C$	1.8 „ „ „	$3A$
$2A \pm B$	1.1 „ „ „	$3A$

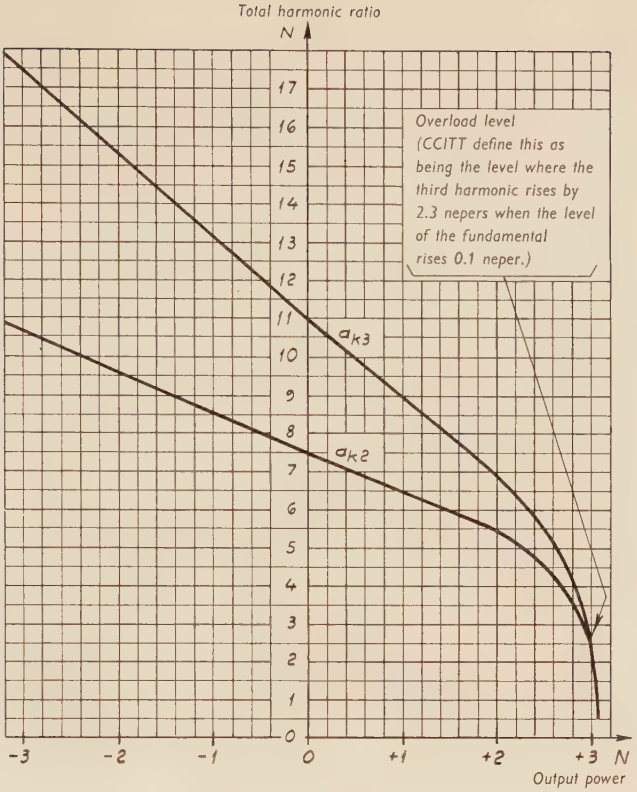

Fig. 4. Total harmonic ratio as function of the output power for a coaxial amplifier for 960 channels.

Table 2.

Order	Type	Number	
2nd	$2A$	n	60
	$A \pm B$	$n\,(n-1)$	3540
3rd	$3A$	n	60
	$2A \pm B$	$2n\,(n-1)$	7080
	$A \pm B \pm C$	$\frac{2}{3}\,n\,(n-1)\,(n-2)$	136880

The number of intermodulation products is easily seen to be appreciably greater than the number of harmonic products and thus no account of the latter need be taken in the calculation of intermodulation noise. The number of products which can be formed from the various types is seen in *table 2*. The number which can be formed from a supergroup has been given in column 3 (a large number of these, however, fall outside the transmitted

frequency band). As will be seen, the number of harmonic products is negligible in relation to the intermodulation products, even with this low number of channels.

It is easily seen that the width of the transmitted frequency band must be at least one octave before second order harmonics and intermodulation products give rise to interference within the band. On the other hand, third order products of the type $A + B - C$ and $2A - B$ give rise to interference even in small bands.

Reduction of Distortion and Intermodulation by means of Negative Feedback

If negative feedback is introduced in an amplifier, all types of interference voltages present in the μ path of the amplifier are reduced. As is known, the principle of negative feedback consists of feeding back a part of the output voltage to the input of the amplifier in such a phase that the amplifier cannot oscillate (*fig. 5*). Interference voltages (noise, hum, distortion, intermodulation etc.) which are present in the μ path of the amplifier are thus fed back to its input out of phase, whereby a reduction of the interference is obtained.

In this connexion, the part of greatest interest is the reduction of harmonic and intermodulation products which are present as a result of the distortion in the tubes used in the amplifier.

The characteristic of the μ path of the amplifier is written as previously as a power series.

$$u_2 = a_1 u_g + a_2 u_g^2 + a_3 u_g^3 + \ldots\ldots$$

As $u_g = u_1 - b u_2$, the following is obtained for the amplifier with negative feedback

$$u_2 = a_1 (u_1 - b u_2) + a_2 (u_1 - b u_2)^2 + a_3 (u_1 - b u_2)^3 + \ldots\ldots$$

If this equation is solved for u_2, then

$$u_2 = u_1 \frac{a_1}{1 + a_1 b} + u_1^2 \frac{a^2}{(1 + a_1 b)^3} + u_1^3 \left[\frac{a_3}{(1 + a_1 b)^4} - \frac{2 a_2^2 b}{(1 + a_1 b)^5} \right] + \ldots\ldots$$

If in this equation the amplified fundamental is put equal to u_2', then

$$u_2 = u_2' + \left(\frac{u_2'}{a_1} \right)^2 \frac{a_2}{1 + a_1 b} + \left(\frac{u_2'}{a_1} \right)^3 \left[\frac{a_3}{1 + a_1 b} - \frac{2 a_2^2 b}{(1 + a_1 b)^2} \right] + \ldots$$

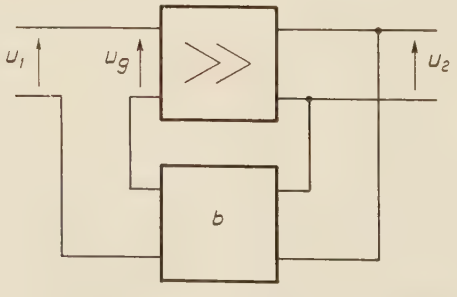

X 11120

Fig. 5. Negative feedback amplifier.

or, as $a_1 b \gg 1$

$$u_2 = u_2' + \left(\frac{u_2'}{a_1}\right)^2 \frac{a_2}{a_1 b} + \left(\frac{u_2'}{a_1}\right)^3 \frac{a_3 - \dfrac{2a_2^2}{a_1}}{a_1 b} + \ldots$$

The third coefficient has received the additional term $\dfrac{-2a_2^2}{a_1}$. As a_3 in general is negative, this term means a contribution. In many cases it is, however, negligible. It can be explained as follows. A second harmonic of frequency $2f_A$ is first formed from the fundamental f_A. As a result of negative feedback this is returned to the input and passes through this amplifier again. Thus the frequency $2f_A$ together with the fundamental forms an intermodulation product of type $A + B$ $(f_A + 2f_A = 3f_A)$.

For the same output voltage but without negative feedback the expression for u_2 is

$$u_2 = u_2' + \left(\frac{u_2'}{a_1}\right)^2 a_2 + \left(\frac{u_2'}{a_1}\right)^3 a_3 + \ldots$$

As will be seen, the second and third order harmonic and intermodulation products have been reduced by a factor $\dfrac{1}{a_1 b}$ due to negative feedback.

It is immediately seen that the total harmonic ratio is determined by $a_1 b$ at the distortion frequency or, in other words, if the total harmonic ratio for a given frequency $2f$ (fundamental frequency f) is a_{k2} neper, the attenuation a_{k2} of the intermodulation products (for example $f_A + f_B$) is a_{k_2}— 0.7 neper for all combinations giving $f_B + f_A = 2f$.

For the sake of completeness, it will also be shown how incoming interference (noise, hum) is reduced by negative feedback in the amplifier part.

From *fig. 6* is obtained

$$[(U_1 - bU_2)a' + U_S]\, a'' = U_2$$

From this is obtained

$$U_2 \approx \frac{U_1}{b} + \frac{U_s}{ba'}$$

Clearly, the earlier the interference enters the amplifier, the less it is reduced by negative feedback.

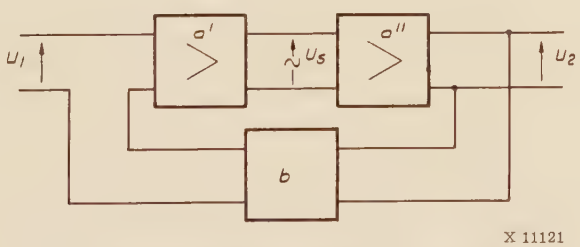

X 11121

Fig. 6. Negative feedback amplifier (μ-part divided).

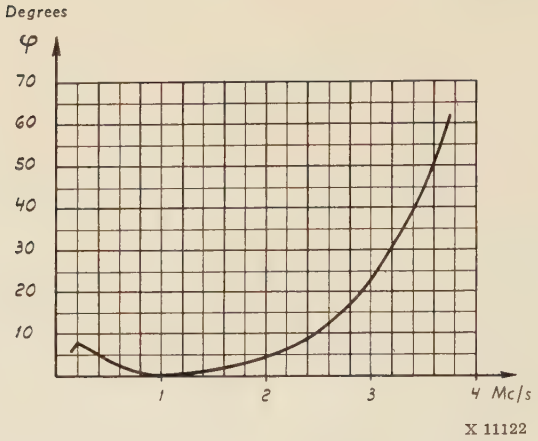

Fig. 7. Deviation in phase shift from the tangent at 1 Mc/s for a 4 Mc/s h.f. line repeater section.

Addition of Intermodulation Products

Fig. 7 shows the deviation of the phase shift from the tangent at 1 Mc/s for a repeater section of a 4 Mc/s h.f. line. If the tangent at an arbitrary point is written as $b_0 + kf$, the phase shift may be written as

$$b = b_0 + kf + \varphi(f)$$

where $\varphi(f)$ corresponds to terms of second and higher orders.

It is shown below how intermodulation products from successive repeaters add together.

$$\left.\begin{aligned} &2\pi f_A t \\ &2\pi f_B t \\ &2\pi f_C t \end{aligned}\right\} \xrightarrow{T_2} \left\{\begin{aligned} &2\pi f_A t + b_0 + kf_A + \varphi(f_A) \\ &2\pi f_B t + b_0 + kf_B + \varphi(f_B) \\ &2\pi f_C t + b_0 + kf_C + \varphi(f_C) \end{aligned}\right\} \xrightarrow{T_4}$$

$$\left\{\begin{aligned} &2\pi(n_A f_A + n_B f_B + n_C f_C)\,t + \\ &+ n_A[b_0 + kf_A + \varphi(f_A)] + \\ &+ n_B[b_0 + kf_B + \varphi(f_B)] + \\ &+ n_C[b_0 + kf_C + \varphi(f_C)] \end{aligned}\right\} = \phi_1$$

$$2\pi(n_A f_A + n_B f_B + n_C f_C)\,t \xrightarrow{T_3} \left\{\begin{aligned} &2\pi(n_A f_A + n_B f_B + n_C f_C)\,t + \\ &+ b_0 + k(n_A f_A + n_B f_B + n_C f_C) + \\ &+ \varphi(n_A f_A + n_B f_B + n_C f_C) \end{aligned}\right\} = \phi_2$$

At the output of repeater I there are fundamentals and intermodulation products (arrow T_1) having frequencies $n_A f_A + n_B f_B + n_C f_C$ (n_A, n_B and n_C are order numbers) formed in the repeater. Both fundamentals and intermodulation products are transmitted and appear at the output of repeater II (arrows T_2 and T_3). Intermodulation products (arrow T_4) are again formed from fundamentals in this repeater.

The phase angles of the intermodulation products (arrows T_4 and T_3 respectively) are

$$\phi_1 = n_A[b_0 + kf_A + \varphi(f_A)] + n_B[b_0 + kf_B + \varphi(f_B)] + n_C[b_0 + kf_C + \varphi(f_C)]$$

$$\phi_2 = b_0 + k(n_A f_A + n_B f_B + n_C f_C) + \varphi(n_A f_A + n_B f_B + n_C f_C)$$

The phase differences ($\phi_1 - \phi_2$) are thus obtained for second and third order harmonic and intermodulation products.

n_A	n_B	n_C	Type	$\phi_1 - \phi_2$
2	0	0	$2A$	$b_0 + 2\varphi(f_A) - \varphi(2f_A)$
1	1	0	$A + B$	$b_0 + \varphi(f_A) + \varphi(f_B) - \varphi(f_A + f_B)$
1	—1	0	$A - B$	$-b_0 + \varphi(f_A) - \varphi(f_B) - \varphi(f_A - f_B)$
3	0	0	$3A$	$2b_0 + 3\varphi(f_A) - \varphi(3f_A)$
1	1	1	$A + B + C$	$2b_0 + \varphi(f_A) + \varphi(f_B) + \varphi(f_C) - \varphi(f_A + f_B + f_C)$
1	—1	—1	$A - B - C$	$-2b_0 + \varphi(f_A) - \varphi(f_B) - \varphi(f_C) - \varphi(f_A - f_B - f_C)$
2	1	0	$2A + B$	$2b_0 + 2\varphi(f_A) + \varphi(f_B) - \varphi(2f_A + f_B)$
1	—2	0	$A - 2B$	$-2b_0 + \varphi(f_A) - 2\varphi(f_B) - \varphi(f_A - 2f_B)$
1	1	—1	$A + B - C$	$\varphi(f_A) + \varphi(f_B) - \varphi(f_C) - \varphi(f_A + f_B - f_C)$
2	—1	0	$2A - B$	$2\varphi(f_A) - \varphi(f_B) - \varphi(2f_A - f_B)$

It will be seen that the phase difference φ for certain third order intermodulation products $A + B - C$ and $2A - B$ does not contain b_0. The phase difference for these products therefore becomes practically zero if the phase curve within a certain range approximates to a straight line and if f_A, f_B, f_C and $f_A + f_B - f_C$ respectively f_A, f_B and $2f_A - f_B$ lie within this region. In other words they add on a voltage basis.

In general for $A + B - C$, voltage addition is obtained if

$$\varphi(f_A) + \varphi(f_B) \approx \varphi(f_C) + \varphi(f_A + f_B - f_C)$$

Addition on a voltage basis is thus obtained if the four frequencies lie within a small frequency band, but this is not a necessary condition. If, for example, f_A is nearly equal to f_C, voltage addition is also obtained for arbitrary values of f_B because $f_A + f_B - f_C$ becomes approximately equal to f_B, whereby the above requirement is fulfilled. The first case where the four frequencies lie within a relatively small frequency band is, however, the most important.

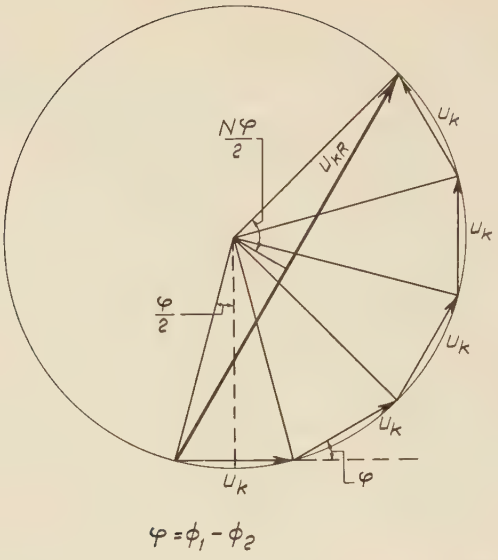

X 11123

Fig. 8. Addition of harmonic and intermodulation products.

It should be observed that even if the repeater sections have different lengths i.e. b_0 and k differ from one repeater section to the next, voltage addition is obtained despite this, thus the most unfavourable.

A voltage polygon (*fig. 8*) can be used with advantage for calculation of the resulting harmonic or intermodulation voltage along a number (N) of repeaters. The harmonic or intermodulation product generated in each repeater is denoted by U_k and that resulting after N repeaters by U_{kR}. From the figure the resulting voltage U_{kR} is

$$U_{kR} = U_k \frac{\sin \frac{N\varphi}{2}}{\sin \frac{\varphi}{2}}$$

For $\varphi \neq 0$, U_{kR} will steadily increase to a maximum and then decrease.

The results of measurements carried out on the addition of intermodulation products of type $A + B - C$ are given in *fig. 9*. The measurements have been made using pure tones, distributed as given in the figure. The wider the frequency band chosen, the more rapidly does the addition depart from voltage addition, which is to be expected in this case as the deviation of the phase curve from the straight line increases with increase in the width of the frequency band.

More favourable conditions of addition for intermodulation products of second order are obtained if $\frac{\pi}{2} < \varphi < \frac{3\pi}{2}$ (the conditions of addition for the third order are unfortunately

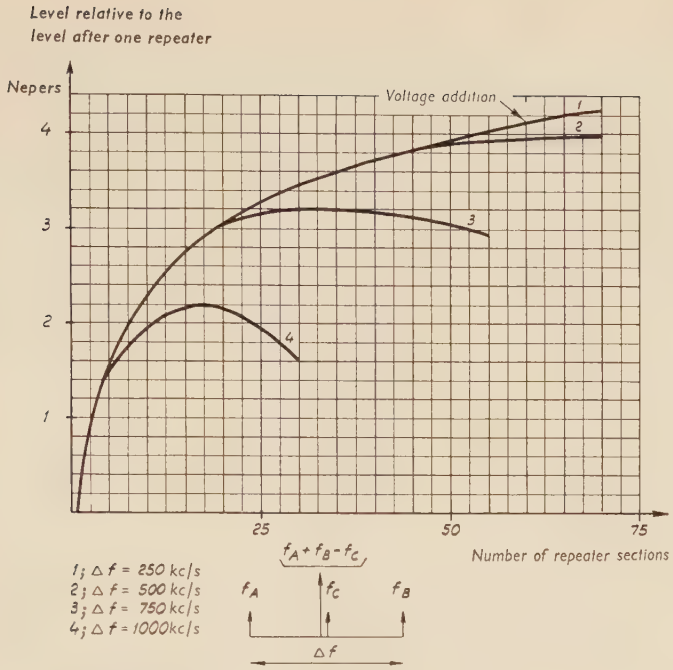

Fig. 9. Addition of $A+B-C$-products along a 4 Mc/s h.f. line.

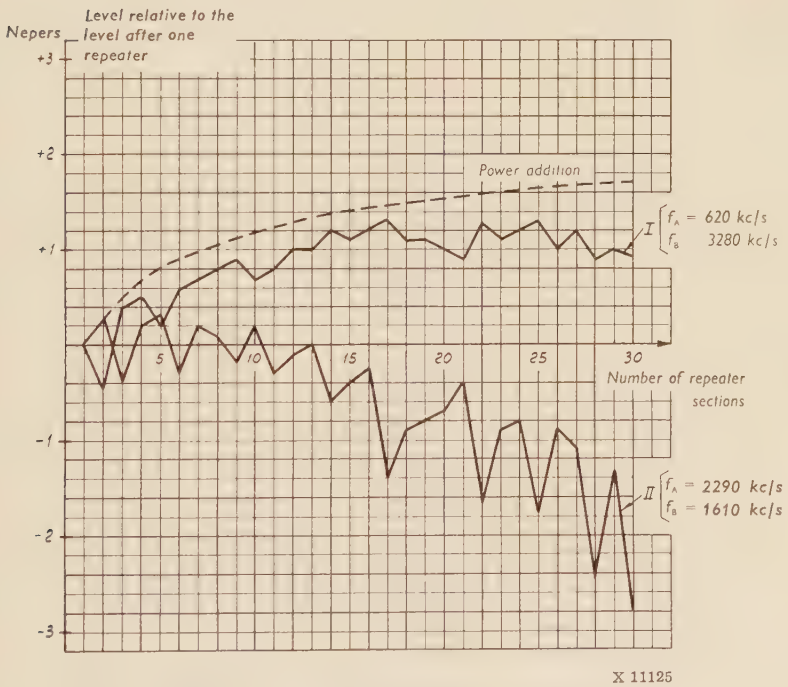

Fig. 10. Addition of $A+B$-products along a 4 Mc/s h.f. line.

not affected by this). U_{kR} is then always $\leqq U_k\sqrt{2}$. The repeaters are generally designed so that this applies to most intermodulation products of second order. Due to variations in the lengths of repeater sections and differences in the contributions from the various repeaters etc., the addition conditions are, however, in practice not quite so favourable.

Fig. 10 shows how the levels of two different $A + B$ products vary along a 4 Mc/s coaxial h.f. line. The difference in the characteristics is a result of the difference in φ.

If the measurements which are the basis of graph II were made on a longer h.f. line they would have given a curve which had a minimum at approx. 35 repeater sections and which then increased. The A — B products and the third order type I products will add on a similar basis to that described above for $A + B$ products.

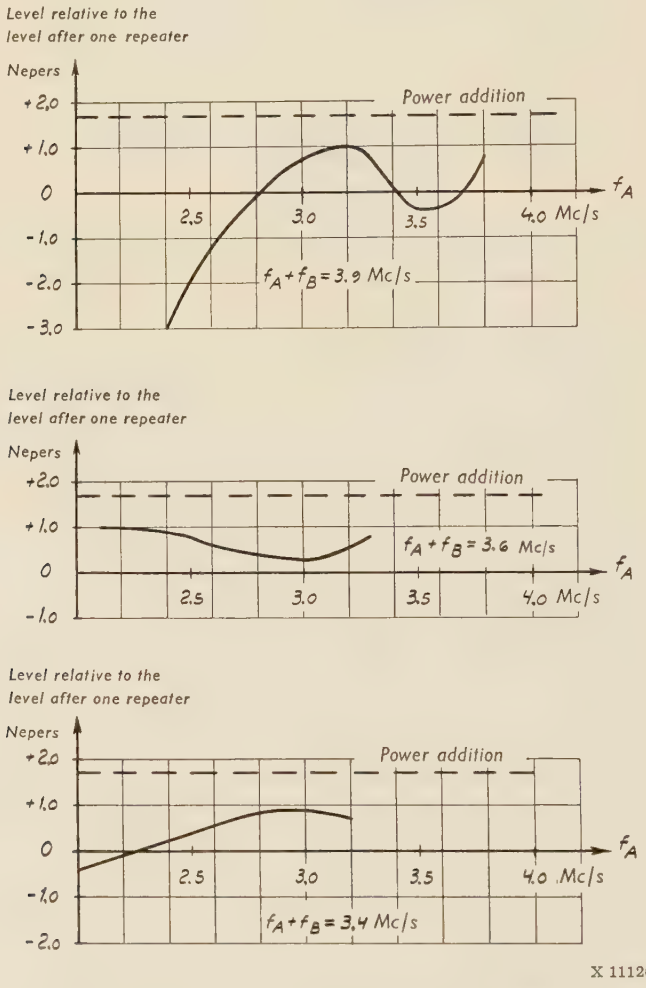

Fig. 11. Relative level for $A + B$-products after 30 repeater sections.

The results of intermodulation measurements on a coaxial h.f. line with 30 repeater sections are given in fig. *11*. It will be seen that the power of the intermodulation products varies appreciably, and with certain intermodulation combinations it is even lower than after one repeater. It is doubtful whether it is possible to produce an "exact" method for calculation of noise due to second order intermodulation.

For rough calculations a power addition minus 0.4 to 0.7 neper depending on length of the system can be used (see *fig. 10* graph I), it being assumed that the repeater phase shift has been chosen as mentioned previously.

Distribution of Intermodulation Products over the Band

The most dangerous intermodulation products from the point of view of disturbance are those of second order $A + B$ and $A - B$ and third order $A + B - C$. Other products of third order, and products of higher order are in general of little practical interest as long as the repeater is not overloaded. In the following calculations it is assumed that the repeaters work in their "linear" region. It will first be shown how the above intermodulation products are distributed over the band and then the intermodulation interference in the channels most likely to be affected, will be calculated. The following symbols are used:

F – "frequency" for one channel (frequency unit = 4 kc/s) or the order number for the channel reckoned from zero frequency.
F_1 and F_2 = lowest and highest channel transmitted.

The number of intermodulation products of type $A + B$ in channel xF_2 will first be calculated (see *fig. 12*). The number of intermodulation products of this type in channel xF_2 are clearly

$$y = \frac{xF_2}{2} - F_1 = \frac{xF_2}{2}\left[1 - \frac{2F_1}{xF_2}\right]$$

The number of type $A - B$ in channel XF_1 is calculated in a similar manner (see *fig. 13*).

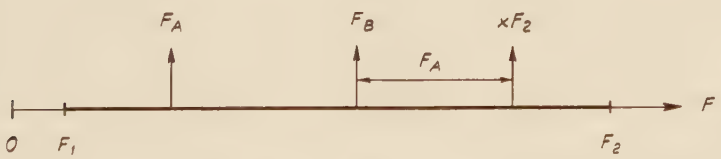

Fig. 12. $F_A + F_B = XF_2$.

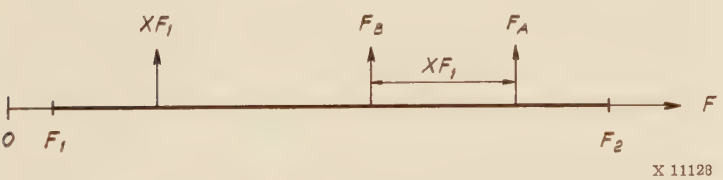

Fig. 13. $F_A - F_B = XF_1$.

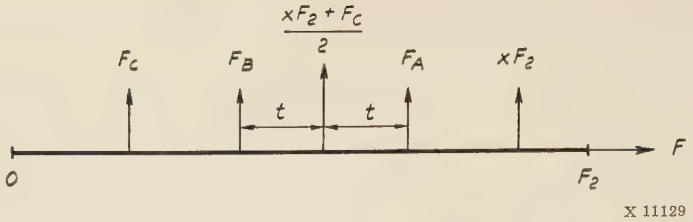

X 11129

Fig. 14. Positions of F_A, F_B and F_C relative to the disturbed channel (xF_2).

The number of products of this type in channel XF_1 is

$$y = F_2 - XF_1 - F_1 = F_2\left[1 - \frac{F_1}{F_2}(1 + X)\right]$$

As will be seen from the above, the number of $A-B$ products in the lowest channel is always double the number of $A+B$ products in the highest channel and this is independent of the ratio $\frac{F_2}{F_1}$.

In calculating the number of products of type $A+B-C$, a certain simplification is obtained if F_1 is assumed to be zero and F then calculated from there. It is easily seen that this is permissible as the number of products of this type is only dependent on the absolute and not the relative bandwidth (see *fig. 14*). The following applies for these intermodulation products

$$F_A + F_B = xF_2 + F_C$$

or in other words, F_A and F_B lie symmetrically in relation to $\frac{xF_2 + F_C}{2}$.

For each value of F_C which is $\leqq F_2(1-x)$, $\frac{xF_2 + F_C}{2}$ intermodulation products are obtained.

If $F_c \geqq F_2(1 - x)$, the number of products is equal to $F_2 - \frac{xF_2 + F_C}{2}$.

The total number in the channel xF_2 is clearly

$$y = \int_0^{F_2(1-x)} \frac{xF_2 + F}{2}\, dF + \int_{F_2(1-x)}^{F_2} \left(F_2 - \frac{xF_2 + F}{2}\right) dF = \frac{F_2^2}{4}\left[1 + 2x(1-x)\right] = \frac{F_2^2}{4} \cdot Z$$

This function has its maximum when $x = 0.5$. Z is then $\frac{3}{2}$.

When $x = 0$ or 1, Z is equal to 1.

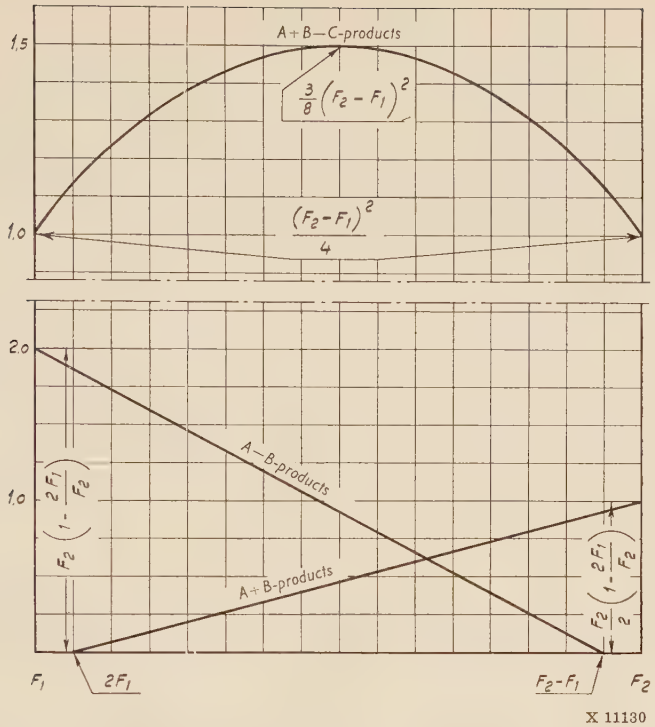

Fig. 15. Distribution of the relative number of intermodulation products.

The distribution of the intermodulation products is shown in *fig. 15*. The $A+B$ and $A-B$ products reach their maxima in the highest and lowest channels respectively, whereas the $A + B - C$ products reach their maximum in the middle channel. It will be seen from the expressions that the number of combinations of type $A + B - C$ which give rise to interference within the band is very large. Thus, for a 12 Mc/s coaxial system the number of combinations which interfere with the highest and middle channels is $\frac{2700^2}{4}$ and $\frac{3}{8} \cdot 2700^2$ respectively ($\approx 1.8 \times 10^6$ and 2.7×10^6 respectively).

CHAPTER 4

Calculation of Intermodulation Noise

The frequency dependence of the cable attenuation is generally compensated completely or partly in the amplifier feedback circuit. The degree of negative feedback falls off as the frequency increases, which means among other things that even the total harmonic ratio decreases with increase in frequency.

With a constant output level the channels in the upper part of the band would consequently be appreciably worse than the channels in the lower part. In order to even out the quality it is therefore usual to allow the output level to increase with frequency, a measure which is termed pre-emphasis. The uppermost channels are thus sent at a higher level and are therefore less exposed to thermal noise and intermodulation noise of type $A + B$. The lower channels, on the other hand, due to this measure are more exposed to noise, and the problem arises of obtaining the optimum pre-emphasis. This problem will be treated in a subsequent section.

The intermodulation noise will now be calculated. The contribution from one amplifier is calculated and approximate methods for the calculation of the noise on an h.f. line section are given. It is assumed that the graph of the output level (pre-emphasis) is known. The following symbols are used:

a_{k_2} and a_{k3} = total harmonic ratio in nepers for the second and third harmonics respectively with a fundamental output power of 1 mW (0 neper).

n_{mk} = average power in nepers per telephone channel at a relative level of 0 neper $= -1.73$ nepers (see next section).

F = "frequency" of a channel (frequency unit = 4 kc/s) or the order number reckoned from zero frequency.

F_1 and F_2 = lowest and highest transmitted channels.

N = number of repeater sections.

Loading Conditions

The load or useful power in an amplifier carrying many channels consists of a frequency mixture having many components U_A, U_B, U_C ..... U_n. It has been shown previously that the harmonic and intermodulation products which are present have practically the whole power concentrated in terms of the type $2U_A\,U_B$, $2U_A\,U_C$ ..... $2U_A\,U_n$, $2U_B\,U_C$ etc. and $6U_A\,U_B\,U_C$, $6U_A\,U_B\,U_D$ ..... $6U_A\,U_B\,U_n$, $6U_B\,U_C\,U_D$ etc. for the second and third order intermodulation respectively. It can also be shown that the power in the intermodulation products is solely dependent on the total amount of the useful power but independent of the number of components, assuming that the number is large and that

they are fairly evenly distributed over the band. In the design of multi-channel systems therefore, it can be assumed that the average loading consists of white noise evenly distributed over the frequency band.

According to investigations carried out, the speech volume has approximately statistically normal distribution with a deviation σ of 4 to 6 db[1] and an average value of about — 15 dbm0. The results of some investigations carried out in America, England and France which have been submitted to CCITT are given in *table 3*.

Table 3.

	Col. 1	Col. 2	Col. 3	Col. 4	
	dbm0	dbm0	dbm0	dbm0	μW
America 1953	—14.4	5.6	—10.8	—16.8	20.8
England 1955					
London—Birmingham	—15.5	4.4	—13.3	—19.3	11.8
London—New York	—13.2	4.6	—10.8	—16.8	20.8
France 1955	—12.0	4.0	—10.0	—16.0	25.0

Col. 1 Average volume
Col. 2 Deviation
Col. 3 Average power with continuous speech
Col. 4 Average power per channel during the busy hour

The volume variation is due to several causes e.g. the loss in the subscriber's line, the subscriber's habits, telephone equipment etc.

According to investigations carried out by SUBRIZI at Bell Telephone Laboratories, the crow flight distances between subscribers also have their effect. Thus the volume increases by about 1 db for every 1,000 km increase in distance. When men speak in the telephone, the volume in general is 1 to 2 db higher than when women talk. Lines with high levels of noise also contribute to increase the volume.

If the results of volume investigations carried out previously are studied, it is found that the average volume has decreased appreciably (in America from — 8 dbm0 in 1939 to — 10 dbm0 in 1949 and to — 14.4 dbm0 in 1953). The reason for this is to be found, among other things, in that better telephone sets are used and also that the transmission properties of the lines have been improved.

Column 3 of *table 3* gives the average power per active channel with continuous speech, calculated from the average volume and deviation (columns 1 and 2 respectively). Even if

[1] In this section the unit db is used instead of neper as the unit db is used in the corresponding CCITT document.

conversations were on all circuits, a maximum of only half the channels would be active, as it must be assumed that the two subscribers participating in a telephone conversation each speak half of the time. Further time is lost in pauses in conversation, preparations, connecting up, signalling etc. According to investigations made by HOLBROOK and DIXON among others, a channel is not active for more than 25 % of the time, which value is used by CCITT in the calculation of the average channel power during the busy hour. This average power has been given in column 4 of *table 3*. It is seen that this varies appreciably for various countries. CCITT recommend that when designing a carrier system having a number of channels not less than 240, an average power of 32 μW per channel (corresponding to − 15 dbm0) of which 22 μW for speech and carrier leaks and 10 μW for signalling and buzzer tones should be assumed.

In the determination of the performance of a wideband amplifier it is also necessary to know the instantaneous peak voltage. According to HOLBROOK and DIXON the 1 % value is approximately 12 db above the value of average power if the number of channels is above 500. With tube ageing, level variations, test tones etc., this value should be raised appreciably, however, in the determination of the overload point.

Intermodulation Noise of Types $A + B$ and $A - B$

If a test tone having a relative level of 0 neper is sent in each of the channels, F_A and F_B (see *fig. 16*), a disturbance having a relative channel level of

$$-\left[a_{k_2} - 0.7 + (n_1 + Y_{xF_2}) - (n_1 + Y_{F_A}) - (n_1 + Y_{F_B})\right]$$

is obtained in the channel xF_2 for the $A + B$ product.

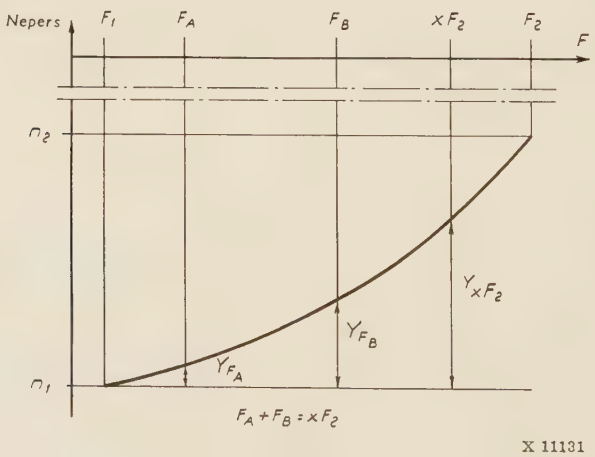

Fig. 16.

The loading is instead made with "white" noise having a relative average power of n_{mk} per channel. A narrow band ΔF_A gives with channel F_B a disturbance in xF_2 having a relative level of

$$-\left[a_{k_2} - 0.7 + Y_{xF_2} - n_1 - 2n_{mk} - Y_{F_A} - Y_{F_B} - \frac{1}{2} \ln \Delta F_A\right]$$

When expressed in pW in a zero level point this becomes

$$p = 10^9 \cdot e^{-2(a_{k_2} - 0.7 + Y_{xF_2} - n_1 - 2n_{mk})} e^{2(Y_{F_1} + Y_{F_B})} \Delta F_A = K_{xF_2}^{A+B} \cdot \psi(F_A) \cdot \psi(F_B) \Delta F_A$$

The total noise in channel xF_2 is

$$p = K_{xF_2}^{A+B} \int_{F_1}^{\frac{xF_2}{2}} \psi(F) \cdot \psi(xF_2 - F)\, dF \qquad \text{pW}$$

In many practical cases $\psi(F)$, with a good approximation, can be written as $1 + k_1 e^{k_2 F}$. The expression for the noise is then

$$p = K_{xF_2}^{A+B} \int_{F_1}^{\frac{xF_2}{2}} \left(1 + k_1 e^{k_2 F}\right)\left(1 + k_1 e^{k_2 (xF_2 - F)}\right) dF =$$

$$= K_{xF_2}^{A+B} \left[\frac{xF_2}{2}\left(1 - \frac{2F_1}{xF_2}\right)\left(1 + k_1^2 e^{k_2 xF_2}\right) + \frac{k_1}{k_2} e^{k_2 F_1} \cdot \left(e^{k_2 xF_2\left(1 - \frac{2F_1}{xF_2}\right)} - 1\right)\right]$$

In general $\frac{F_1}{2F_2} \ll 1$. With this assumption the noise in the highest channel F_2 is

$$p = K_{F_2}^{A+B}\left[\frac{F_2}{2}\left(1 + k_1^2 e^{k_2 F_2}\right) + \frac{k_1}{k_2}\left(e^{k_2 F_2} - 1\right)\right] \approx K_{F_2}^{A+B}\left[\frac{F_2}{2} + \frac{e^{2(n_2 - n_1)} - 1}{k_2}\right] \qquad \text{pW}$$

If the pre-emphasis is a linear function of frequency, the noise in channel xF_2 is

$$p = y \cdot 10^9 e^{-2(a_{k_2} - 0.7 - n_1 - 2n_{mk})}$$

where $y = \frac{xF_2}{2}\left(1 - \frac{2F_1}{xF_2}\right)$ = number of intermodulation products of this type which lie in the channel in question. With this type of pre-emphasis, the noise is clearly completely independent of the slope $\frac{n_2 - n_1}{F_2 - F_1}$ and is only determined by the level n_1, to a certain extent a curious result.

In a similar manner, the intermodulation noise in channel XF_1 of type $A - B$ is

$$p = 10^9 e^{-2(a_{k_2} - 0.7 + Y_{XF_1} - n_1 - 2n_{mk})} \int_{F_1}^{F_2 - XF_1} \psi(F)\,\psi(XF_1 + F)\,dF = K_{XF_1}^{A-B} \int_{F_1}^{F_2 - XF_1} \psi(F)\,\psi(XF_1 + F)\,dF =$$

$$= K_{XF_1}^{A-B} \left\{ F_2 - F_1(1 + X) + \frac{k_1}{k_2} \left[e^{k_2 F_2} + e^{k_2 (F_2 - XF_1)} - e^{k_2 F_1 (1+X)} - e^{k_2 F_2} \right] + \right.$$

$$\left. + \frac{k_1^2}{2k_2} \left[e^{k_2 (2F_2 - XF_1)} - e^{k_2 F_1 (X+2)} \right] \right\}$$

With the same assumptions as were made for the $A + B$ products, the noise in the lowest channel F_1 is

$$p = K_{F_1}^{A-B} \left[F_2 + \frac{2k_1}{k_2} e^{k_2 F_2} \left(1 + \frac{k_1}{4} e^{k_2 F_2} \right) \right] \approx K_{F_1}^{A-B} \left[F_2 + \frac{2e^{2(n_2 - n_1)} - 2}{k_2} \right] \quad \text{pW}$$

The distribution of intermodulation noise of types $A+B$ and $A-B$ is shown in *figs. 17* and *18* respectively. The calculations have been carried out for the pre-emphasis shown in *fig. 21*. The curves 1 show the noise distribution with constant a_{k_2} while curves 2 and 3 show the same when a_{k_2} decreases linearly by 1 and 2 nepers respectively from the lowest to the highest channel. As shown previously, when the degree of negative feedback in general decreases with increase in frequency and thereby also the total harmonic ratio, the noise of type $A+B$ and $A-B$ will in general reach a maximum in the upper and lower parts respectively of the band.

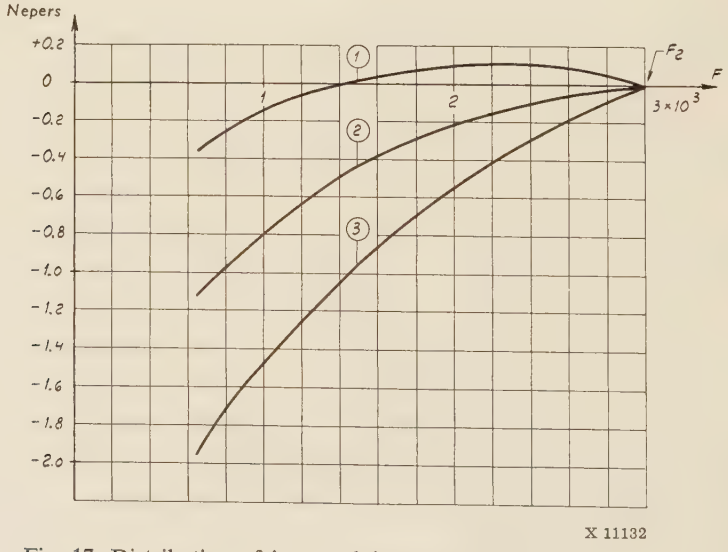

Fig. 17. Distribution of intermodulation noise of type $A+B$.

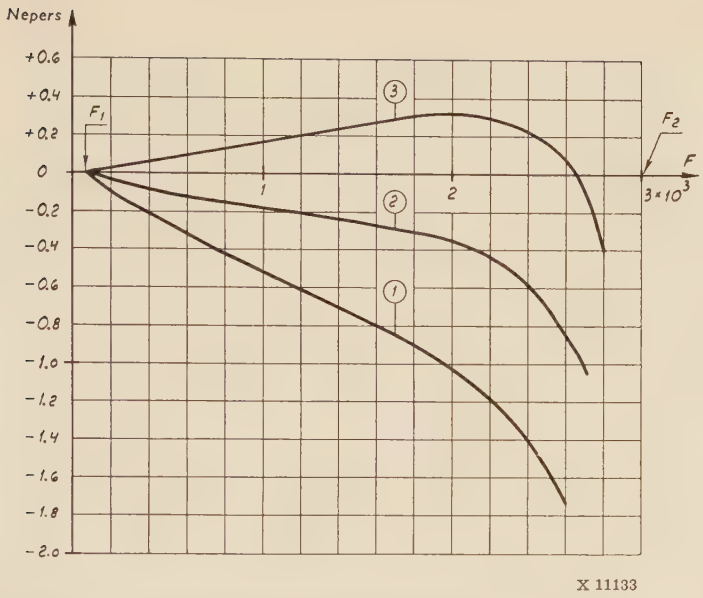

Fig. 18. Distribution of intermodulation noise of type $A - B$.

The noise calculations carried out above have only given the contribution from a single amplifier. In the determination of the noise for an h.f. line link of 200 to 300 km length, power addition minus 0.7 neper can be assumed in accordance with the above, giving satisfactory accuracy for practical purposes.

Intermodulation Noise of Type $A + B - C$

The treatment of intermodulation noise of type $A + B - C$ will now be dealt with. As the expressions for this are particularly complicated and not easily surveyed, only the general expression for their calculation after a single repeater is given and the distribution in the transmission band is shown in the diagram. It is then shown how rough calculations of the noise for an h.f. line link may be carried out in a simple manner. It seems not possible to calculate "exactly" the noise for an h.f. line link with pre-emphasis and non-linear phase shift. Solutions have been published for certain special cases and without pre-emphasis (output level independent of frequency).

With reasoning similar to that made previously and with the help of *fig. 19*, the following expression for intermodulation noise of type $A + B - C$ after a single repeater in an arbitrary channel xF_2 is obtained.

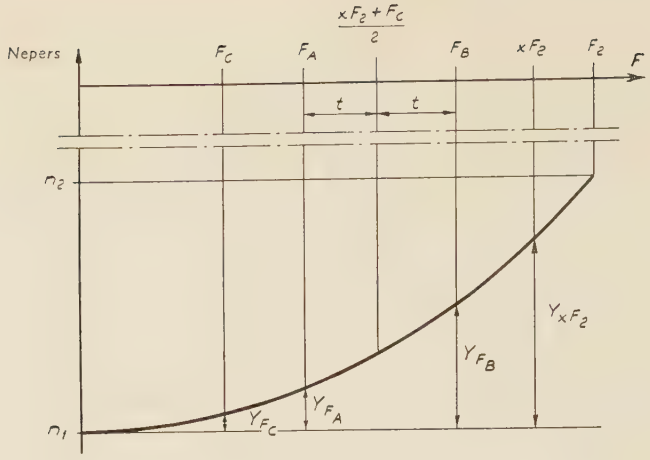

Fig. 19.

$$p = K_{xF_2}^{A+B-C}\left[\int_0^{F_2(1-x)}\int_0^{\frac{F_c+F_2}{2}}\psi(F_c)\,\psi\left(\frac{F_c+xF_2}{2}+t\right)\psi\left(\frac{F_c+xF_2}{2}-t\right)dF_c\,dt+\right.$$

$$\left.+\int_{F_2(1-x)}^{F_2}\int_0^{\frac{F_2(2-x)-F_c}{2}}\psi(F_c)\,\psi\left(\frac{F_c+xF_2}{2}+t\right)\psi\left(\frac{F_c+xF_2}{2}-t\right)dF_c\,dt\right]$$

In this case

$$K_{xF_2}^{A+B-C} = 10^9 \cdot e^{-2(a_{k_3}-1{\cdot}8+Y_{xF_2}-2n_1-3n_{mk})}$$

The distribution of the intermodulation noise (type $A+B-C$) has been drawn in *fig. 20* for two different variations of a_{k3}. The calculations have been made for the pre-emphasis shown in *fig. 21*. In both cases it has been assumed that a_{k3} is a linear function of frequency. If the total harmonic ratio is independent of frequency within the transmission band (curve 1), the channels in the lower part of the band are most exposed to this type of interference. As the frequency dependence of the cable loss is wholly or partly compensated in the feedback path of the amplifier, the degree of negative feedback and thereby the total harmonic ratio falls with increase in frequency and consequently the noise maximum is shifted to higher frequencies. Curve 2 in *fig. 20* shows the distribution of noise when a_{k3} is reduced by 2 nepers from the lowest to the highest frequency. For most practical cases therefore, the relative noise maximum should lie in the upper part of the band. It will easily be seen that the major part of this noise comes from channels in the upper part of the band. These give the strongest intermodulation products as they have high output level from the repeaters due to pre-emphasis.

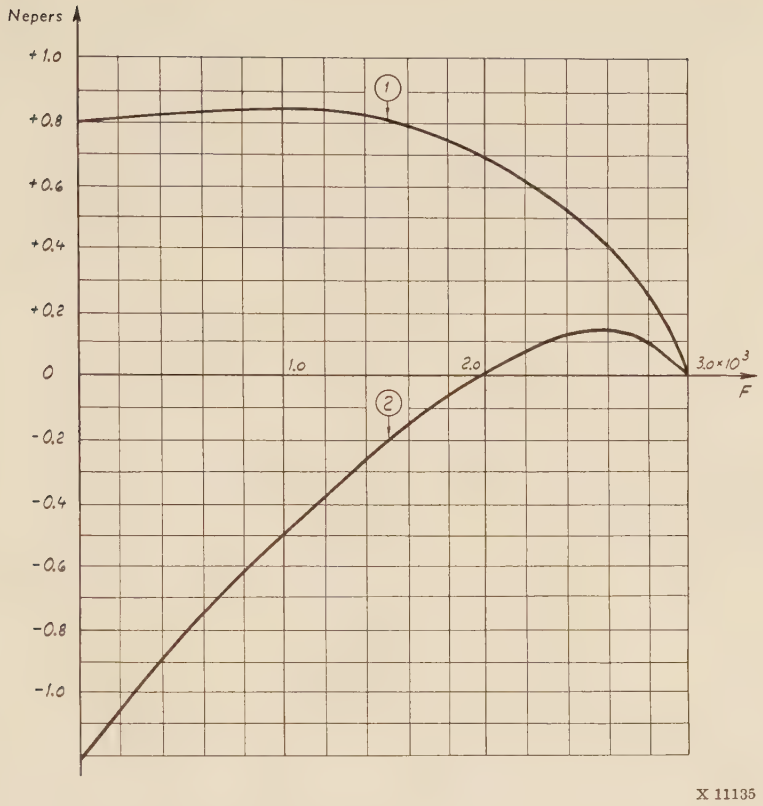

Fig. 20. Distribution of intermodulation noise of type $A+B-C$.

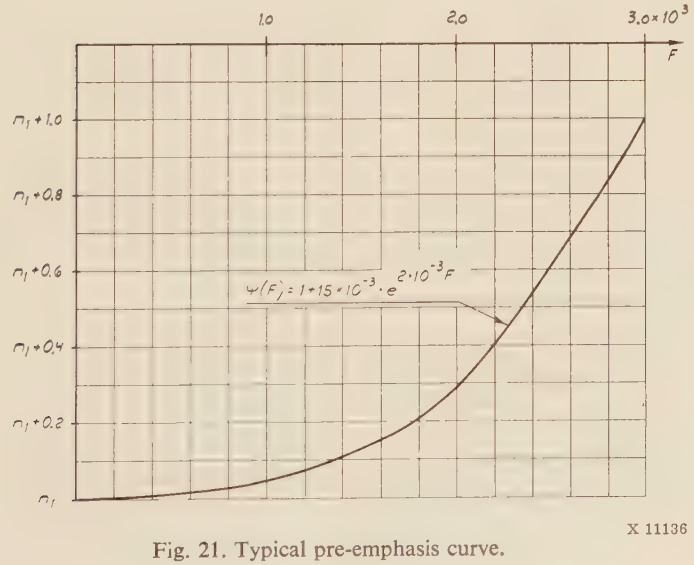

Fig. 21. Typical pre-emphasis curve.

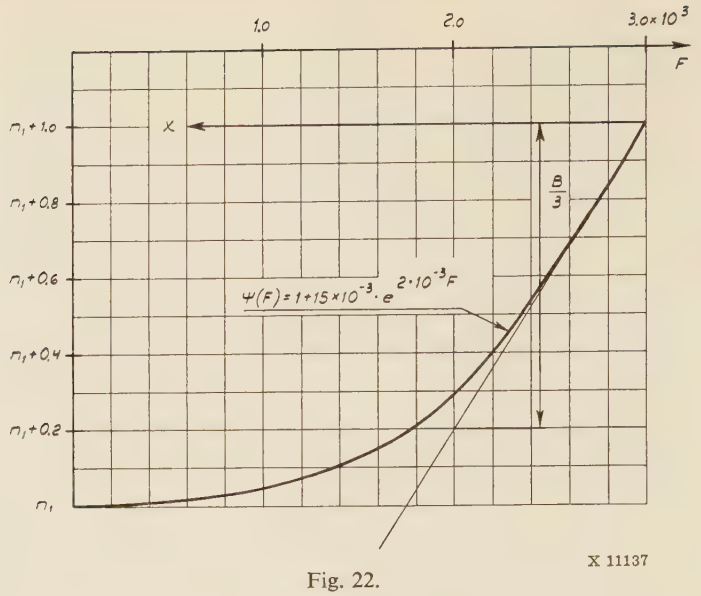

Fig. 22.

If for a single amplifier the major part of the intermodulation noise in the upper part of the band originates from the highest channels, it is quite safe to presume for an h.f. line link that practically all noise in the upper channels originates from channels in this part of the band, due to the $A+B-C$ products adding on a voltage basis within narrow bands (cf. page 17).

With wider bands the addition deviates to a certain extent from that on a voltage basis and within very wide bands the deviation is appreciable. Consequently the channels in the lowest and centre parts of the band give practically no contribution to the intermodulation noise in the upper part.

The calculation of the noise in the upper part of the band can clearly be appreciably simplified when — as will be seen from the above — it is only necessary to consider this part of the band. Here the pre-emphasis can be replaced with relatively good accuracy by a straight line (see *fig. 22*). For an h.f. line link having N repeater sections the following value of the noise in the top channel is obtained:

$$P_{F_2} = N^2 \cdot 10^9 \cdot \underbrace{e^{-2(a_{k_3} - 1.8 - 2n_2 - 3n_{mk})}}_{2K} \int_0^{\Delta F_2} \frac{x}{2} \cdot e^{-4\frac{B}{F_2}x} dx$$

$$P_{F_2} = N^2 \cdot K \left[\left(\frac{F_2}{4B} \right)^2 \left(1 - e^{-\frac{4B}{F_2}\Delta F_2} \right) - \frac{F_2}{4B} \Delta F_2 \cdot e^{-\frac{4B}{F_2}\Delta F_2} \right]$$

In this case ΔF_2 is the effective bandwidth, about 10 to 20 % of the whole band, within which voltage addition can be assumed. $\frac{B}{F_2}$ is the pre-emphasis slope in the upper part of the band.

As is seen in *fig. 20*, the noise does not reach its maximum value in the highest channel but somewhat below this. A sufficiently accurate value of the maximum noise with normal pre-emphasis is therefore obtained if in the above expression the integration is carried out over the whole band. Thus

$$P_{max} \approx N^2 K \left[\left(\frac{F_2}{4B} \right)^2 (1 - e^{-4B}) - \left(\frac{F_2}{4B} \right)^2 \cdot e^{-4B} \right] \approx K \left(\frac{NF_2}{4B} \right)^2$$

It has been assumed in the calculations carried out so far that the loading consists of white noise and the noise values calculated also concern white noise in the disturbed channel. Having regard to the distribution of speech power in the telephone channels among other things, the shape of the psophometer curve etc. these values must be corrected by a certain factor α. The most suitable values are

$\alpha = 0.25$ for $A - B$ products
$\alpha = 0.5$ for $A + B$ products and thermal noise
$\alpha = 0.5$ to 1.0 for $A + B - C$ products.

CCITT here recommend $\alpha = 0.5$ with white noise loading.

CHAPTER 5

Method for Measurement of Noise

Special measuring equipment for measurement of noise (thermal noise and intermodulation noise) in certain pre-determined parts of the band are now manufactured by several instrument firms. The method of measurement is seen in *fig. 23* and from the following details. The object under test, for example an h.f. line, is loaded with white incorrelated noise within the whole of its transmission band. A small band within which the noise is to be measured is, however, kept "pure". The method of test seems to be satisfactory. However for practical reasons it is almost impossible to make the band-stop filters (a) sufficiently narrow which can mean that altogether too good test results are obtained. It will be seen from the above that practically all intermodulation noise of type $A + B - C$ in a certain channel originates in general from channels in the same part of the band, owing to this type of intermodulation product adding on a voltage basis within narrow bands. If the filter is wide there is a risk that the channels which should give the most interference are not loaded and consequently not unappreciable measuring errors can arise.

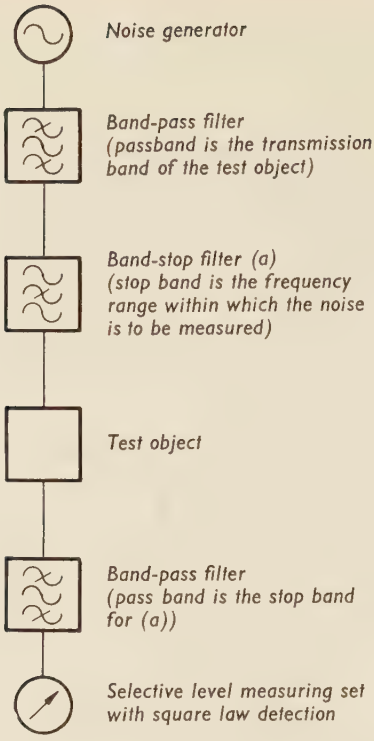

Fig. 23.

A method of measurement will be given below which has been used with success by the Board of Telecommunications in noise measurements on 4 Mc/s h.f. lines. The method utilizes the terminal equipment associated with the h.f. line. Similar measuring techniques may be used for noise investigations on, for example, a 12 Mc/s system.

The only extra equipment which is required is a noise generator and a psophometer. The method assumes, however, that the noise contributions from the various parts of the terminal equipment are known. The test arrangements are as shown in *fig. 24*.

White uncorrelated noise is injected into the supergroup translating equipment (receiving side). All supergroups except one are through connected on a supergroup basis to supergroup translating equipment (sending side). Four basic groups are through connected on a group basis in this supergroup. Eleven channels are through connected in the fifth basic group. The noise measurement is carried out on the channel which is not through connected. It will be seen that this method gives possibilities of measurement of noise anywhere in the band where required. All channels are correctly loaded and reliable measurement results will be obtained.

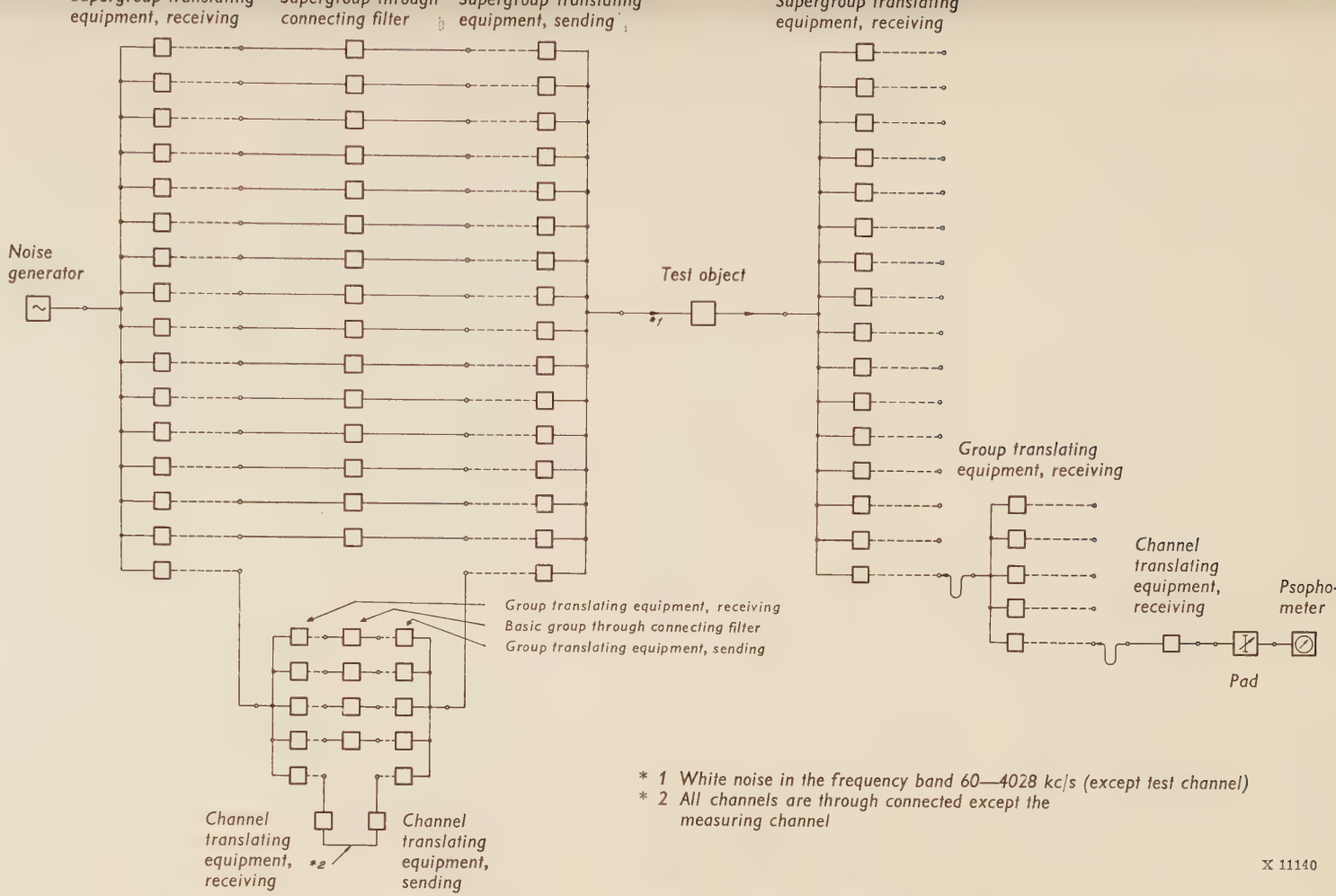

Fig. 24. Circuit for measurement of noise (thermal and intermodulation noise) due to 4 Mc/s h.f. line equipment.

CHAPTER 6

Design with Regard to Noise

It will be seen from the above that the noise contributions from various repeaters in a long h.f. line add in different ways. The thermal noise (resistance and tube noise) thus add on a power basis and the same applies to the intermodulation products of the second order, where, however, in favourable cases a certain reduction factor—about 0.7 neper—may be introduced. The most dangerous intermodulation products of the third order, however, add on a voltage basis.

Relationship between Bandwidth, Section Loss and Number of Repeaters

The way in which a change in the number of repeaters in an h.f. line affects the total noise will now be studied. It is assumed here that the repeater characteristics as regards thermal noise and distortion are identical at the same levels, although their gain is altered.

To obtain a clear picture of the conditions, it is assumed at the start that the number of repeaters in an h.f. line is doubled, the frequency band is increased and that in so doing the total noise power is required to be unchanged. The number of noise contributions of different types is thus also doubled, and the power contribution from each repeater must then be reduced to a half i.e. by 0.35 neper ($-\ln\sqrt{2}$). The input level must therefore be raised by 0.35 neper so as to reduce the thermal noise by a similar value. It is also required that the output level is reduced by 0.35 nepers to reduce the intermodulation products of the second order. The absolute power of the intermodulation power is then reduced by double this value or 0.7 neper, but as the noise in the disturbed channel has also been decreased by 0.35 neper the relative power contribution is reduced by the difference i.e. by a half. In addition, the reduction of the output level by 0.35 neper means that the intermodulation products of the third order are reduced by 3 times this value or by 1.05 nepers as far as the absolute values are concerned. In the same way as previously, the level in "disturbed channel" is reduced by 0.35 neper and thus the relative noise level has been reduced by 0.7 neper i.e. their voltage from each repeater has been reduced to a half and the power to a quarter.

As mentioned above, the dangerous products of this type add on a voltage basis. As there are twice as many repeaters in the line link the total voltage is unchanged and thus too the total power contribution of this type. Thus with a doubling of the number of repeaters in an h.f. line, the input level must be raised by 0.35 neper and the output level reduced by an equal amount in order that the total noise from the three most important sources of interference shall remain unchanged. In total, therefore, the gain per repeater is reduced by 0.7 neper i.e. the loss of each line section is reduced by 0.7 neper = ln 2.

It can easily be shown that in general with a change of the number of wide-band amplifiers in a section e.g. due to changed conductor dimensions or frequency band, the loss of the line sections should be changed by the natural logarithm of the ratio of the number of amplifiers.

Expressed in another way, for unchanged noise quality it is required that the maximum attenuation, a neper of the repeater sections shall be

$$a = \text{constant} + \ln L$$

where L is their length in suitable units. As Americans and Englishmen have been pioneers in coaxial technique, the lengths of repeater sections were standardized at an early stage in English miles e.g. 8 miles for the American L-1 system and 6 miles (9.6 km) for the European 4 Mc/s system. Later on these section lengths have been halved to 4 and 3 miles respectively. If the unit of length in English miles is used in the attenuation formula above, the constant is approximately equal to 3.7. *Table 4* gives the maximum attenuation for the various systems calculated in this way and the true attenuation of the system in the normal coaxial cable.

The last column is given as a curiosity and shows what the result might be with a possible future division of our coaxial cable repeater sections into two parts.

It will be seen that the values of the table agree fairly well. It must not be concluded, from what is said above, that it would be as easy to realize various coaxial systems, but only that they can be made fairly well equivalent from the noise point of view. The difficulties in designing good amplifiers increase very much instead with increasing frequency and bandwidth. Among other things, better tubes are required and a factor in this connexion which has not been mentioned previously is that the distortion requirements with the output level of the repeaters at a constant value must be increased due to the wider bandwidth and the resulting larger number of intermodulation products which arise due to combinations of different channels.

Optimum Section Attenuation

The associated problem of how the number of repeaters in an h.f. line shall be chosen so as to obtain minimum interference noise for unchanged conductor dimensions and constant frequency band will now be investigated. H. F. MAYER has shown in a simple manner that if account is only taken of the thermal noise, the number of repeaters shall be chosen so that the line attenuation is only 0.5 neper.

If account is also taken of the intermodulation products of second and third order, the conditions are somewhat more complicated. The following symbols are used:

Output level of the repeaters	n_u neper
Input level of the repeaters	n_i neper
Total attenuation of the h.f. line	A neper
Number of repeaters	N
Total noise power	P pW
Noise power per repeater:	
thermal noise at $n_i = 0$	p_t pW
second order intermodulation at $n_u = 0$	p_2 pW
third order intermodulation at $n_u = 0$	p_3 pW

A possible reduction factor is included in p_2 for more favourable addition than on a power basis. Only the most dangerous intermodulation products which are added on a voltage basis are included in p_3. It is easily seen that the total thermal noise will be equal to $N \cdot p_t \cdot e^{-2n_i}$. In a similar manner the total second order intermodulation products are equal to $N \cdot p_2 \cdot e^{2n_u}$. The corresponding third order products added on a voltage basis are equal to $p_3 [N \cdot e^{2n_u}]^2$.

The total noise power is then

$$P = Np_t e^{-2n_i} + Np_2 e^{2n_u} + N^2 p_3 e^{4n_u}$$

The attenuation of the repeater sections is equal to $n_u - n_i = \frac{A}{N}$. Replace n_i by the term $n_u - \frac{A}{N}$ in the expression for P and at the same time put $e^{2n_u} = X$. The following is then obtained

$$P = \frac{N}{X} p_t e^{2\frac{A}{N}} + Np_2 X + N^2 p_3 X^2$$

In this expression, N and X are independent variables and a minimum in P is obtained by putting

$$\frac{\partial P}{\partial X} = \frac{\partial P}{\partial N} = 0$$

The following are obtained

$$-\frac{N}{X^2} \cdot p_t \cdot e^{2\frac{A}{N}} + Np_2 + 2N^2 p_3 X = 0$$

$$\frac{1}{X} p_t \cdot e^{2\frac{A}{N}} \left(1 - \frac{2A}{N}\right) + p_2 X + 2Np_3 X^2 = 0$$

The first of these gives

$$p_2 X + 2Np_3 X^2 = \frac{1}{X} p_t e^{2\frac{A}{N}}$$

which is put in the other expression, thus giving

$$\frac{1}{X} p_t \cdot e^{2\frac{A}{N}} \left(2 - 2\frac{A}{N}\right) = 0$$

of which $\frac{A}{N} = 1$

The repeater section attenuation shall thus be 1 neper for a minimum of noise. This value is very low in relation to the normally used values of attenuation in accordance with *table 4*. Economic considerations have naturally affected this. The average attenuation

for the whole frequency band is, however, lower than that given in the table which applies to the attenuation at the highest frequency. In addition, it is clear that the new coaxial systems tend to lower values of attenuation and it is not precluded that in the future, transistorized repeaters may be introduced in the coaxial cables on relatively short distances if sufficiently good transistors are developed.

Table 4.

System type	*L*—1	4 Mc/s	*L*—3	12 Mc/s	?
Section length (*L*) miles	8	6	4	3	1.5
ln *L*	2.1	1.8	1.4	1.1	0.4
$a = 3.7 + \ln L$ nepers	5.8	5.5	5.1	4.8	4.1
Actual loss nepers	5.9	5.5	5.2	4.8	?
Max. frequency Mc/s	2.6	4.1	8.3	12.4	approx. 35
No. of telephone circuits	600	960	1800	2700	approx. 8000

Division of Thermal Noise and Intermodulation Noise

One of the minimum requirements given above was

$$\frac{1}{X} p_t \cdot e^{2\frac{A}{N}} = p_2 X + 2Np_3 X^2$$

If this expression is multiplied by N it becomes

$$\frac{N}{X} p_t \cdot e^{2\frac{A}{N}} = Np_2 X + 2N^2 p_3 X^2$$

When expressed in words this means that the levels shall be so chosen for minimum total noise that the thermal noise is equal to the sum of the second order and twice the third order intermodulation noise. As the minimum is very flat, it is usual in practice to select the level so that the thermal noise is equal to twice the intermodulation noise (sum of the second and third order) so as to obtain the same worsening of quality with level deviations in both directions.

The total noise shall thus be about 0.2 neper $\left(= \frac{1}{2} \ln \frac{3}{2} \right)$ stronger than the thermal noise alone.

Optimum Pre-Emphasis

It has been assumed previously that optimum pre-emphasis has been chosen. Frogging is used in a widely dispersed coaxial network. This means that for long connexions, blocks of circuits (supergroups, mastergroups etc.) systematically change places in the frequency band at the through routing stations. An equalization of the quality is thereby obtained. The

requirement for optimum pre-emphasis means then that pre-emphasis shall be chosen so that the sum of the noise power in the various channels is a minimum.

The choice of pre-emphasis is a complicated problem, where account must be taken of the frequency dependence of the line attenuation, noise factor and total harmonic ratios etc. It is now shown, using very simplified assumptions, that the optimum frequency dependence of pre-emphasis should correspond to about $^2/_3$ of the gain of the negative feedback amplifiers used. It is hereby assumed that the frequency dependence of the gain is solely dependent on the feedback i.e. the possible correction networks are not included in the amplifiers and that the gain of the μ path is constant. The thermal noise per channel without pre-emphasis varies with frequency and in general rises with this. With a constant amplifier noise factor the noise is proportional to e^{2F} where F is the gain at the respective frequency. In addition, it is proportional to e^{-2n} where n is the level of the respective channel after the amplifier.

In addition, it is assumed, that the power of the intermodulation products is only dependent on the power of the disturbing channels and the degree of feedback at the frequency of the disturbed channel.

As the gain varies inversely with the degree of feedback, the power of the intermodulation products in a certain channel is proportional to e^{2F}. With a complete derivation of the optimum pre-emphasis, account must be taken of the fact that all the channels can give intermodulation noise in a certain channel and that this in its turn disturbs all the others. With the simplified derivation, only the conditions in two arbitrary channels denoted by 1 and 2, will be investigated. For the most important intermodulation products $A + B$ and $A - B$ of the second order and $A + B - C$ of the third order, a certain reversibility prevails in that two arbitrary channels interfere with each other by intermediation of the same channels in both cases. If, for example, consideration is made of the third order disturbance $A + B - C = D$ where A, B, C and D are designations of the respective channel frequencies, it can be said that channel A interferes with D by intermediation of channels B and C. In this way channel D can also interfere with A due to exactly the same channel intermediation as $A = D + C - B$. The same applies for second order intermodulation. As the most suitable level n_1 and n_2 in channels 1 and 2 are to be investigated, the levels of the remaining channels are not varied. The interference from channel 1 to channel 2 and vice versa is then regulated by one and the same factor k_{12} which is dependent on the type of interference and the levels of the intermediary channels. In accordance with the above, the intermodulation interference from channel 1 to channel 2 can therefore be put equal to $k_{12} \cdot e^{2F_2} \cdot e^{2n_1 - 2n_2}$. The interference from channel 2 to channel 1 is then equal to $k_{12} \cdot e^{2F_1} \cdot e^{2n_2 - 2n_1}$. These intermodulation interferences are only a small fraction of the total intermodulation noise in the respective channels. However, as all channels affect each other in the same way, these expressions can represent the total intermodulation noise in the two channels.

The corresponding thermal noise in the two channels is $p_t e^{2F_1 - 2n_1}$ and $p_t e^{2F_2 - 2n_2}$ respectively, where p_t is a constant. The total noise contribution in both channels is therefore

$$P = p_t \cdot \left(e^{2(F_1 - n_1)} + e^{2(F_2 - n_2)}\right) + k_{12}\left(e^{2(F_2 + n_1 - n_2)} + e^{2(F_1 + n_2 - n_1)}\right)$$

The first term in this expression corresponds to the thermal noise and the second term corresponds to the intermodulation noise. The factor $e^{-(n_1 + n_2)}$ is taken out of the first term and written as

$$p_t \cdot e^{-(n_1 + n_2)} \cdot \left(e^{2F_1 - (n_1 - n_2)} + e^{2F_2 + (n_1 - n_2)}\right)$$

In this expression, the pre-emphasis, $n_1 - n_2$ will be varied so as to obtain minimum for P. The average level $\frac{n_1 + n_2}{2}$ is assumed, in accordance with previous derivations, to be chosen so that the thermal noise is twice as large as the intermodulation noise. If $n_1 - n_2$ is put equal to X the following is obtained

$$p_t \cdot e^{-(n_1 + n_2)} \cdot \left(e^{2F_1 - X} + e^{2F_2 + X}\right) = 2k_{12} \cdot \left(e^{2(F_2 + X)} + e^{2(F_1 - X)}\right)$$

Now $\frac{dP}{dX}$ is put equal to 0 and so

$$p_t \cdot e^{-(n_1 + n_2)}\left(-e^{2F_1 - X} + e^{2F_2 + X}\right) + k_{12}\left(2e^{2(F_1 + X)} - 2e^{2(F_1 - X)}\right) = 0$$

By combination of these two expressions, the following are obtained successively:

$$\frac{e^{2F_1 - X} + e^{2F_2 + X}}{e^{2F_1 - X} - e^{2F_2 + X}} = \frac{e^{2(F_2 + X)} + e^{2(F_1 - X)}}{e^{2(F_2 + X)} - e^{2(F_1 - X)}}$$

$$\frac{e^{2F_1 - X}}{e^{2F_2 + X}} = \frac{e^{2(F_2 + X)}}{e^{2(F_1 - X)}}$$

$$e^{4F_1 - 3X} = e^{4F_2 + 3X}$$

$$4F_1 - 3X = 4F_2 + 3X$$

$$6X = 4(F_1 - F_2)$$

Thus at the minimum

$$X = n_1 - n_2 = \frac{2}{3}(F_1 - F_2)$$

As this must apply for two arbitrary channels, it can be said in general that

$$n = \frac{2}{3}F + k$$

where k is a constant which is to be chosen so that at the minimum the thermal noise in all channels together shall be twice as large as the total intermodulation noise.

It should again be pointed out that a rough estimate of the frequency dependence of the pre-emphasis has been derived. A more accurate theoretical derivation, however, is very difficult. Possibilities exist of trying out practically the optimum pre-emphasis with different conditions. A suitable method of procedure appears to be the following.

In a regulated section of normal length (e.g. 280 km, in accordance with CCITT) the noise is measured in a suitable number of channels spread out over the whole frequency band. Variable correction networks are connected at the beginning and end of the line e.g. cosine equalizers, which simultaneously can be regulated in opposite directions so that they cancel each other's influence on the attenuation in the transmitted frequency band. The total noise in the test channels is measured and the correction networks regulated to give a total noise minimum. At the minimum the correction network at the sending end clearly corresponds to optimum pre-emphasis.

Necessary Harmonic Ratio

An attempt will now be made to calculate the needed harmonic ratio at the highest frequency, for a 12 Mc/s coaxial amplifier, using the expressions derived in the previous section for the intermodulation noise. The length of the coaxial line link is assumed to be the same as that of the CCITT reference line i.e. $\frac{2{,}500}{9} \approx 280$ km. The cable attenuation at 12 Mc/s between two repeater stations is assumed to be 4.5 nepers* which in the case of the Swedish coaxial cable corresponds to a length of about 4.6 km. The coaxial line link therefore contains about 60 repeater sections.

The average value of the noise in a coaxial line link must not, according to CCITT, in any hour exceed $\frac{7{,}500}{9} \approx 830$ pW, or in other words may in the worst case be equal to this value. About half this value or 400 pW will be reckoned with here and it is assumed that $^2/_3$ of this is thermal noise, $^1/_6$ is intermodulation noise of second order and $^1/_6$ is intermodulation noise of third order.

For the tube types in question here, the value of equivalent noise resistance is about 150 ohms. The input transformer can hardly be designed to have a greater impedance ratio than 1/10 or 75/750 for this frequency range. Tube noise clearly gives a not unappreciable contribution to the total thermal noise. If the attenuation in the input transformer is 0.05 neper (a reasonable value) the absolute level of the thermal noise (psophometrically weighted, bandwidth = 3 kc/s) at the repeater input must clearly be reckoned as being not less than

$$-16.0 + \ln \frac{375 + 150}{375} + 0.05 = -15.6 \text{ nepers}$$

* At the first discussions of the CCIF concerning the structure of this system, it was assumed that the 12 Mc/s system repeater sections would be obtained dividing those of the 4 Mc/s into two parts. A recommendation for the attenuation of the repeater sections in a 12 Mc/s system is not available, however.

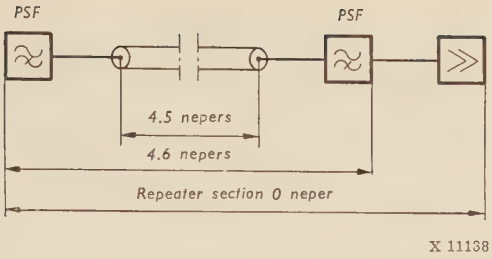

Fig. 25. Repeater section.

The lowest output level from the repeater at 12 Mc/s is then (see *fig. 25*):

$$n_u = -15.6 + \frac{1}{2}\ln\frac{10^9}{\frac{400\cdot 2}{3}} + \frac{1}{2}\ln 60 + 4.6 = -1.4 \text{ nepers}$$

Now that the output level from the repeater is known, expressions for the second and third order intermodulation noise a_{k2} and a_{k3} may be calculated with the help of the previous section, assuming that the pre-emphasis is known. The pre-emphasis given in *fig. 21* is assumed to apply here. This gives for the top channel

$$\frac{400}{6} = 10^9 \cdot e^{-2(a_{k_2} - 0.7 + 1.0 + 2.4 + 3.5)}\left[\frac{2{,}700}{2} + \frac{e^2 - 1}{2\cdot 10^{-3}}\right]\frac{60}{4}\cdot\frac{1}{2}$$

from which $a_{k2} = 7.5$ nepers

$$\frac{400}{6} = 10^9 \cdot \frac{e^{-2(a_{k_3} - 1.8 + 2.8 + 5.2)}}{2}\left[\frac{2{,}700\cdot 60}{4\times 2.4}\right]^2\cdot\frac{1}{2}$$

from which $a_{k3} = 11.2$ nepers.

Bibliography

1 Bennet, W R: *Cross Modulation in Multi-Channel Amplifiers below Overload.* Bell Syst. tech. J *19*(1940): 4, pp. 587—610.

2 Black, B S: *Stabilized Feedback Amplifiers.* Bell Syst. tech. J *13*(1934): 1, pp. 1—18.

3 Brockbank, R A & Wass, C A A: *Non-Linear Distortion in Transmission Systems.* J Instn Elect. Engrs *92*(1945): Part III, pp. 45—56.

4 Holbrook, B D & Dixon, J T: *Load Rating Theory for Multi-Channel Amplifiers.* Bell Syst. tech. J *18*(1939): 4, pp. 624—644.

5 Jacobsen, B B: *The Effect of Non-Linear Distortion in Multi-Channel Amplifiers.* Elect. Commun. *19*(1940/41): 1, pp. 29—54.

6 Martin, G: *Klirrspannungsmessungen an Trägerfrequenzsystemen für symmetrische Kabel.* Nachrichtent. Z *9*(1956): 5, pp. 199—210.

7 Ring, F & Zerbel, W: *Die Reichweite von Trägerfrequenzsystemen.* Fernmeldetechn. Z *3*(1950): 10, pp. 377—384.

8 Ring, F: *Übertragungseigenschaften der V 60-Trägerfrequenzgeräte.* Fernmeldetechn. Z *5*(1952): 3, pp. 101—108 & 179—186.

9 Steinbuch, K & Marko, H: *Ein Beitrag zur Frage des Additionsgesetzes des Klirrgeräusches in Weitverkehrsystemen.* Fernmeldetechn. Z *8*(1955): 2, pp. 71—78.

10 Subrizi, V: *A Speech Volume Survey on Telephone Message Circuits.* Bell Labor. Record *31* (1953): 8, pp. 292—295.

11 Zuhrt, H: *Ein Beitrag zum Additionsgesetz der Klirrspannungen in Weitverkehrsystemen mit Amplitudenmodulation.* Entwicklungsberichte Siemens & Halske *21*(1958): 4, pp. 337—343.

Manuscript received by the editors December 1959.

Oscillations in Long Electron Beams

BY

BERTIL AGDUR*

UDC 537.525.6
538.69
LME 5371,5376,7223

Two types of instabilities in long electron beams, confined by magnetic fields, are investigated. One of them, which is dependent upon the presence of positive ions trapped in the beam, occurs at frequencies near the plasma frequency of the ions and gives rise to a rotational motion of the electron beam. The other, which is dependent upon the presence of slow electrons in the beam, occurs at frequencies close to the gyrofrequency of the electrons.

* Electronics Department of the Royal Institute of Technology and the Research Department of Telefonaktiebolaget L M Ericsson, Stockholm. Now at the Microwave Department of the Royal Institute of Technology.

Introduction

Long electron beams confined by d.c. magnetic fields are used in many microwave tubes and much attention has been paid to the stability properties of such beams. The first part of the investigation reported here concerns the oscillations that can occur when positive ions are trapped in the beam so that the beam is in fact passing through a cloud of positive ions. Such oscillations have been studied earlier by several authors. Of these, C. CUTLER[1] and H. MIHRAM[2] have given the most complete experimental information. The experiments presented here aim at a more detailed insight in some aspects of these oscillations. Even if the investigation is concerned with a type of system used in microwave tubes, we feel that some of the results may also be applicable to more general systems such as, for instance, certain types of gas discharges.

One of the main features of these oscillations is that the beam as a whole performs a rotational motion around the axis of symmetry of the tube. The frequency of rotation corresponds to the plasma frequency of the positive ions if we assume that the ion density is such that the space charge in the electron beam is neutralized. Measurements of the variation in amplitude along the beam—which are difficult to make accurate enough—indicate that the amplitude increases from the gun to the collector end and that there is generally a certain phase difference in the rotation between the gun and the collector end of the tube. When the magnetic field is increased, the amplitude of the beam oscillations first decreases but appears to approach a constant value for strong magnetic fields ($>$ 3,000 gauss). The a.c. current in the axial direction, which is simply the current measured in the collector circuit, is generally less than 1 % of the d.c. current to the collector. An ion current, modulated with a frequency that in most cases is an order of magnitude lower than the frequency mentioned above, reaches the walls of the tube.

Experiments have been made on the effect of the secondary electrons, slow as well as fast, that leave the collector. The measurements show that the amplitude of the oscillations can be decreased by suppressing the secondaries but we have not been able to reduce the amplitude in this way by more than a factor of 5.

The second part of this paper describes phenomena occurring at frequencies around the gyrofrequency of the electrons when the pressure in the tube is high enough ($\approx 10^{-4}$ mm Hg). A signal impressed on the beam is amplified as long as the beam current is below a certain value. When the current is above this value the tube breaks into oscillation. The amplification, at a frequency of 3,000 Mc/s, along a 30 cm long beam can be of the order of 40 db at a beam current of 20 mA and an accelerating voltage of 1,000 volts. These phenomena occur only when the beam region contains a certain number of secondary electrons, created by the primary beam through ionizing collisions with the rest-gas molecules. Measurements show that the density of secondary electrons is higher than the density of the primary beam at a pressure of 10^{-4} mm Hg.

At a pressure of 10^{-4} mm Hg the beam gives rise to enough light to permit visual observation. When the system is working as an amplifier, this light is sharply confined to an area roughly corresponding to the beam area. However, when the system breaks into oscillations, the light comes from a region much greater than the beam region. This seems to indicate that the microwave fields have become strong enough to cause the electrons that have "diffused" out from the beam region, to excite the gas molecules.

CHAPTER 1

Experimental Investigations of the Ion Oscillations

1.1 Description of the Tube and the Measurements

The tube used for the measurements is shown in *fig. 1*. The longitudinal magnetic field extends beyond both the cathode and the collector and can be varied up to 5,000 gauss. Owing to the heat developed, fields above 1,500 gauss can be used only for short periods. The cathode has a diameter of 3 mm and gives a solid cylindrical beam with a beam current up to 50 mA. The diameter of the surrounding metal tube is 5.5 cm and the length of the beam is about 50 cm. Most of the measurements were made with accelerating voltages between 200 and 1,000 volts and at pressures between $5 \cdot 10^{-6}$ and $2 \cdot 10^{-5}$ mm Hg.

Three different types of collectors have been used. The first, C_1, was simply a solid copper rod with a diameter about 10 times the beam diameter. In the second type, C_2, a semicircular nickel plate covered half the end surface of the copper collector. The nickel plate made good

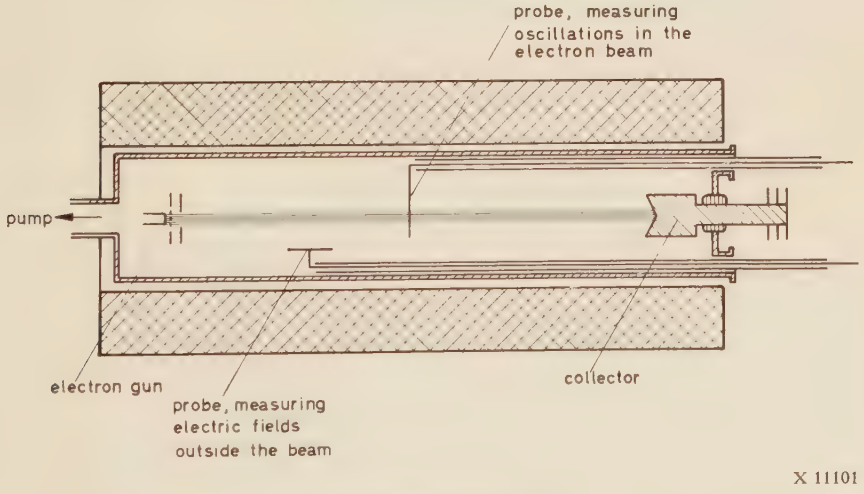

Fig. 1. The experimental tube.

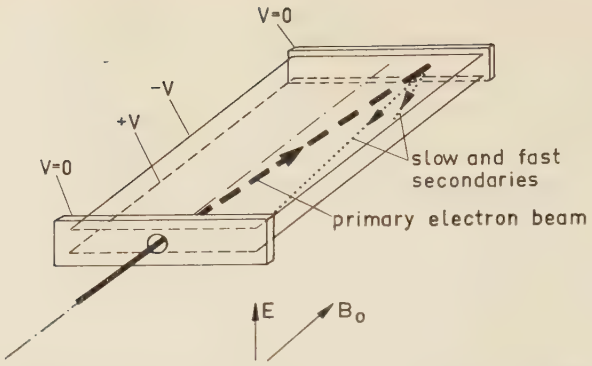

Fig. 2. Collector system using crossed electric and magnetic fields.

electric and mechanic contact with the copper. The beam could be directed so that it hit the copper and nickel surfaces simultaneously. With this collector we could study the influence that inhomogeneities in the secondary emission properties of the collector surface have on the oscillations. The third type of collector, C_3, which makes use of deflection in crossed electric and magnetic fields, is shown in *fig. 2.* The magnetic field is the longitudinal field confining the electron beam. With this arrangement, we can prevent both slow and fast secondaries leaving the collector surface from going back into the beam.

To measure the d.c. and a.c. properties of the beam we used two very thin wire probes. These probes were independent and movable in the axial direction and they could be made to sweep over the cross section of the tube. Measurements of the a.c. fields outside the beam region including their rotation were made by means of electric (capacitive) probes that could be displaced axially and radially. These probes were 3 cm long and 1 cm wide metal plates. *Fig. 3* shows the arrangement of the probes.

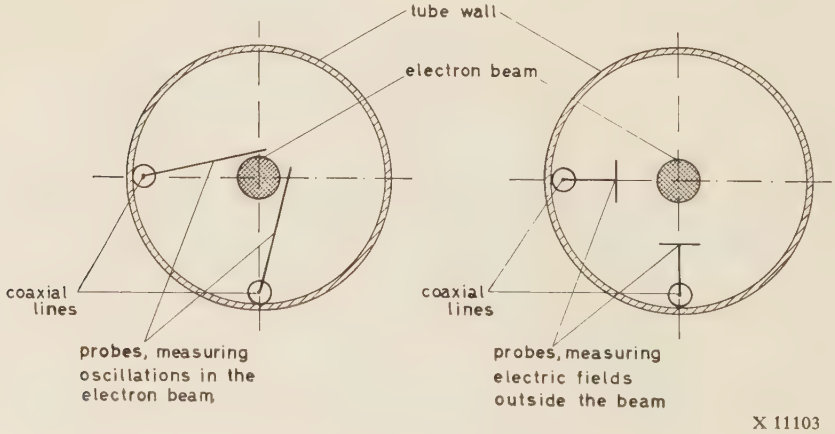

Fig. 3. Probe arrangements.

By using two identical probes that could be moved independently over the cross section of the tube, we could estimate the effect of any one of the probes on the oscillating system. Such measurements show that the disturbances caused by the electric probes are extremely small even when the probes are very close to the beam. The wire probes disturb the system more but the results obtained from such probes should be qualitatively correct.

When the ion current going to the tube wall was measured, a fine-mesh cylindrical net was placed close to the tube wall. This arrangement allows measurement of the energy of the ions and simplifies the measurement of the ion current to the tube wall when the electron beam is pulsed.

1.2 D.C. Fields and Space Charge

The electron beam creates positive ions and electrons by collisions with the gas molecules. The main part of the electrons formed at the collisions have much higher energies than the positive ions and quickly reach the collector. The positive ions have low velocities and are confined radially if there is a net negative charge in the beam. The axial drift of the positive ions is determined mainly by gradients in the axial direction.

When the ion production exceeds the axial losses, the negative charge will tend to become neutralized so that the ions are no longer confined radially (the ions are almost unhindered by magnetic fields less than about 2,000 gauss). If it can be assumed that the secondary electrons leave the system instantaneously and that the axial ion losses are negligible, an upper limit to the concentration of positive ions can be found. As the collector was always kept at -100 volts with respect to the tube wall, it is probable that these assumptions are reasonable (at least for pressures around 10^{-5} mm Hg). The potential difference between the centre of the tube and the wall is then determined by the condition that the potential, created in the centre of the beam by accumulation of positive charge, is large enough to give a radial out-flow of ions equal to their rate of production. The beam radius, inside which the positive ions are formed, is very small compared to the radius of the metal tube and it should be justified to assume that the field at the beam boundary is zero (space-charge limited current). The potential difference between the beam and the tube wall (V) then becomes

$$V \cong 4 \cdot 10^7 \cdot \left(\frac{p \cdot i_c \cdot r_a}{V_{\text{acc}}} \right)^{2/3} \text{ volts}, \tag{1}$$

where p is the pressure in mm Hg, i_c the collector current in amperes, r_a the radius of the metal tube in cm and V_{acc} the accelerating voltages in volts. For the following typical values — $p = 10^{-5}$, $i_c = 2 \cdot 10^{-2}$, $r_a = 3$, $V_{\text{acc}} = 1{,}000$ — we obtain $V \simeq 29$ volts. Under these conditions, the ion current to the tube wall would be 3.1 μA, which is about half of the measured value. More general calculations show that the ion concentration is very nearly the same as the concentration of primary electrons. The potential determined by eq. (1) is, in most of the experiments, greater than the cut-off voltage for the ions in the crossed electric and magnetic fields.

1.3 Some General Remarks on the Oscillations

In the first measurements we pulsed the beam current and observed the fluctuations in the current to a wire probe barely touching the beam. During the first part of the pulse there are no oscillations in the probe current but after a certain time oscillations start. At constant beam current, the time interval, Δt, between the beginning of the pulse and the start of the oscillations is inversely proportional to the gas pressure in the tube. When Δt is studied as a function of the beam current at constant pressure we obtain the result shown in *fig. 4.*

If it were assumed that the oscillations start when the beam is neutralized by positive ions Δt should be independent of the beam current, vary inversely as the gas pressure and have the approximate value 42 μs under the conditions of *fig. 4.* Thus, both the magnitude of Δt and its variation with the beam current show that the start of oscillations is a more complex phenomenon.

The solid line in *fig. 5* shows the observed oscillation frequency versus the square root of the collector current, i_c. The vertical lines represent the spread in the measurements. A magnetic field of 750 gauss was used to ensure that the beam was well confined. The dotted line in *fig. 5* gives the variation of the resonance frequency, $\nu_r = \nu_{\text{plasma}}/\sqrt{2}$. In calculating the plasma frequency we have assumed that the space charge in the beam is completely neutralized and that the ions have an atomic weight of 30. The diameter of the beam, taken as the distance between points where the current density is half its maximum value, was

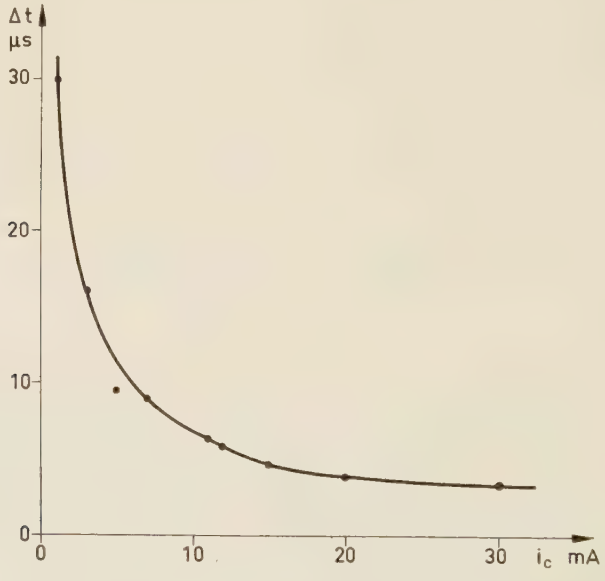

Fig. 4. Time for start of oscillations, Δt, versus collector current, i_c. Pressure 10^{-5} mm Hg, magnetic field 1,000 gauss, accelerating voltage 800 volts.

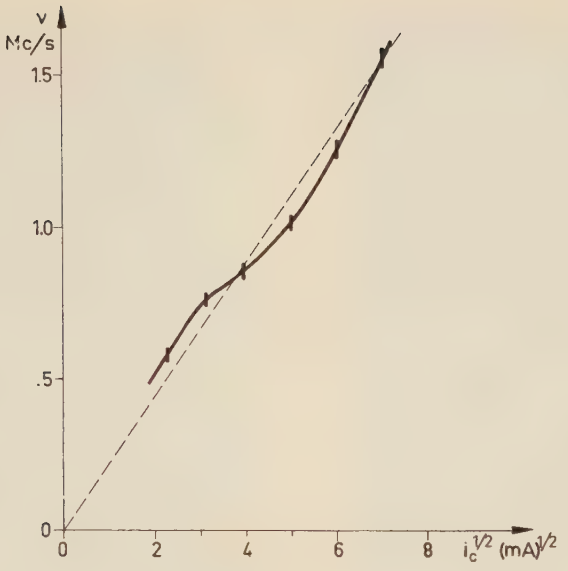

X 11105

Fig. 5. Measured oscillation frequency versus square root of collector current, solid line. The dotted line shows $\nu_r = \nu_{plasma}/\sqrt{2}$.

measured with the arrangement shown in *fig. 6*. The beam diameter was estimated to be 2.7 mm, which also is the value that gives the best fit to the experimental curve.

The pressure dependence of the oscillations is quite complicated in its details. The general nature of the oscillations remains almost unchanged in the pressure range 10^{-6} — $5 \cdot 10^{-5}$ mm Hg. Above $5 \cdot 10^{-5}$ mm Hg, however, the type of oscillations discussed here gradually disappears.

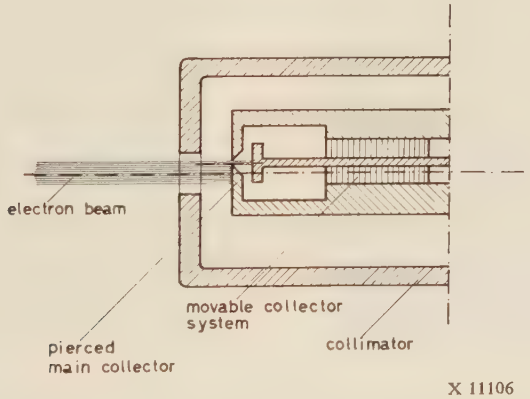

X 11106

Fig. 6. Collector system for measuring the beam diameter. The pierced main collector is movable in radial direction and can also be rotated.

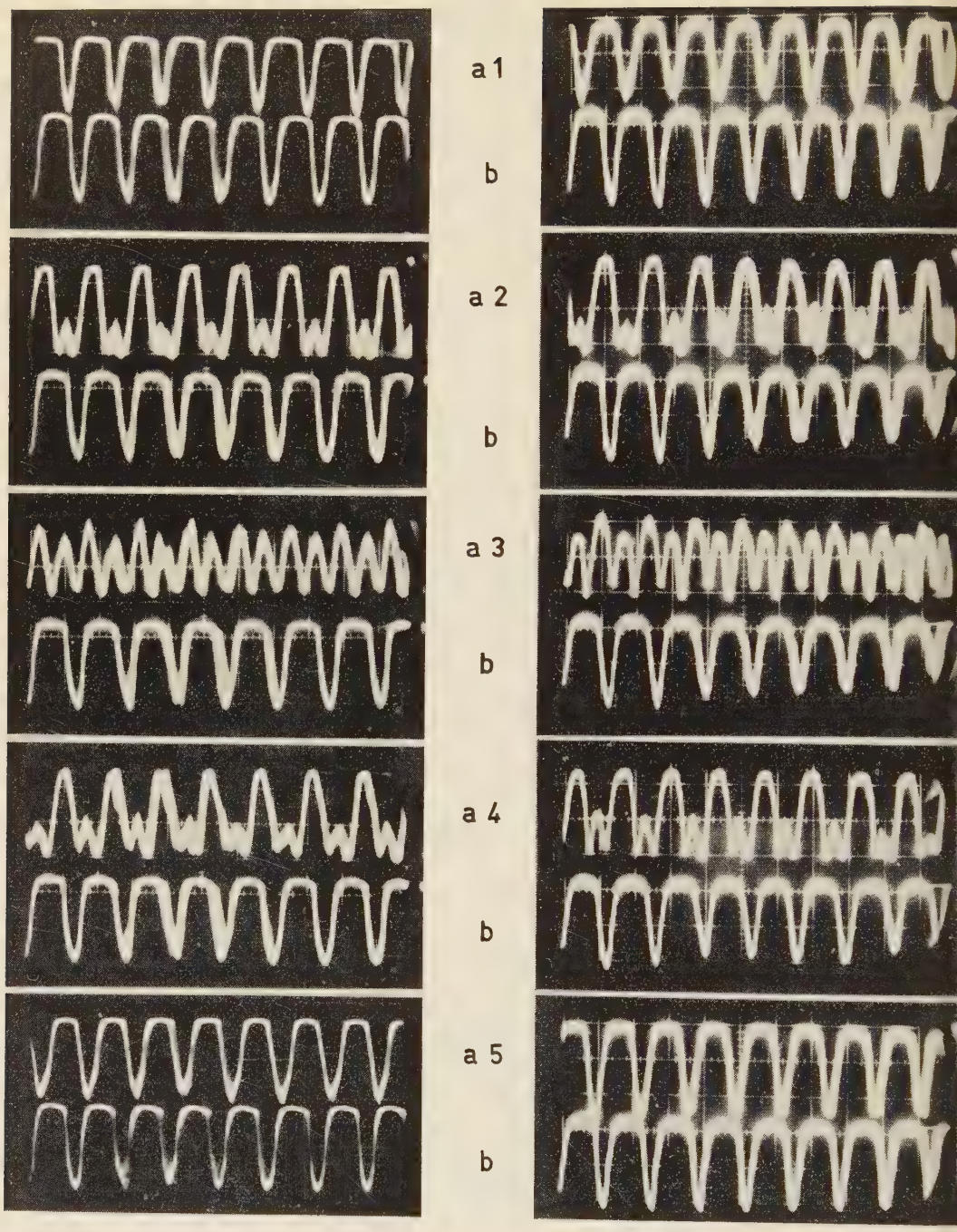

X 11107

Fig. 7. Current to the wire probes versus time. Probe b is fixed and probe a has the different positions indicated in fig. 8. The two series of pictures are taken for different directions of the magnetic field, B_0.

Next, we used the different types of collectors described above to obtain some general information about the main character of the current modulation. In these experiments great precaution was taken to avoid all interception currents. If the current fluctuations are mainly transverse, there should be only a very small a.c. component in the collector current when the all-copper collector, C_1, is used. Owing to the different secondary emission properties of copper and nickel, one would, however, expect much greater fluctuations when the copper-nickel collector, C_2, is used. The observed current fluctuations were at least a hundred times greater for C_2 than for C_1. This and the results from the wire probe measurements prove the oscillations to be essentially transverse, which does not mean that the longitudinal velocity fluctuations are necessarily small. It is obvious that the nature of the collector surface greatly influences the a.c. collector current, which makes it difficult to achieve a good reproducibility with demountable systems.

Measurements with the deflection collector, C_3, (*fig. 2*) show that the oscillations become much "cleaner", when the secondary electrons are retained inside the collector. Capturing the secondaries also decreases the amplitude of the oscillations to about a fifth, but it has not been possible to stop the oscillations completely by these means. The secondaries are apparently not necessary for sustaining the oscillations.

1.4 A Study of the Transverse Beam Oscillations

According to the results presented above, the longitudinal fluctuations are generally very small when interception currents are eliminated and the electrons that are released from the collector through secondary emission are prevented from reaching the beam. In the next stage of the experiment we studied the transverse oscillations by means of the probes under such conditions that this should be valid.

The series of oscillograms in *fig. 7* shows the current to the wire probes versus time. Probe *b* was fixed and probe *a* had the different positions indicated in *fig. 8*. The measurements were made with a beam current of 20 mA, an accelerating voltage of 1,000 volts, a magnetic

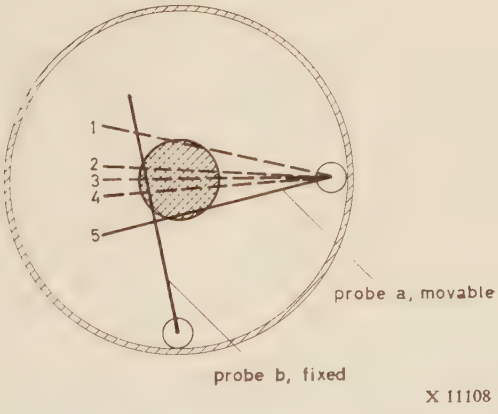

Fig. 8. Probe positions.

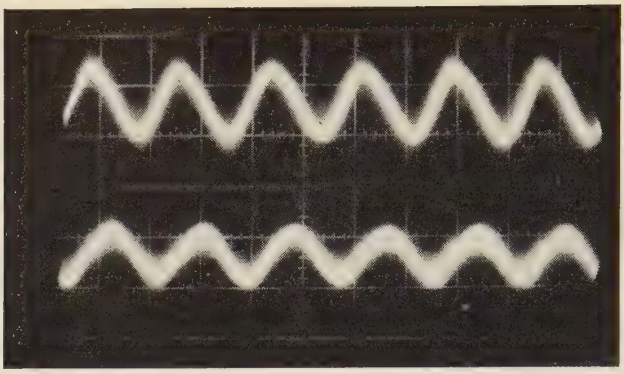

X 11109

Fig. 9. Oscillations measured with two electric probes placed as is shown in fig. 3.

field of 1,000 gauss and at a pressure of 10^{-5} mm Hg. The phase difference between the position of probe *b* and the two positions, 1 and 5, of probe *a* are, roughly, 90° and 270° respectively; i.e. the phases at positions 1 and 5 are opposite (180° difference). This and the fact that the frequency is approximately doubled when the probe passes through the axis of the beam indicates that the beam has a rotational motion. The direction of rotation changes with the direction of the magnetic field and is the same as that of the gyro-rotation of the electrons.

The next picture, *fig. 9*, shows the oscillations measured with two capacitive probes placed as is shown in *fig. 3*. We see that there is a phase difference of about 90° between the two probe curves. It has been clearly demonstrated by means of probes placed between these two that the fields outside the beam also rotate. The relative variation of the field along the axis of the tube, measured with a capacitive probe, is shown in *fig. 10* for two different magnetic

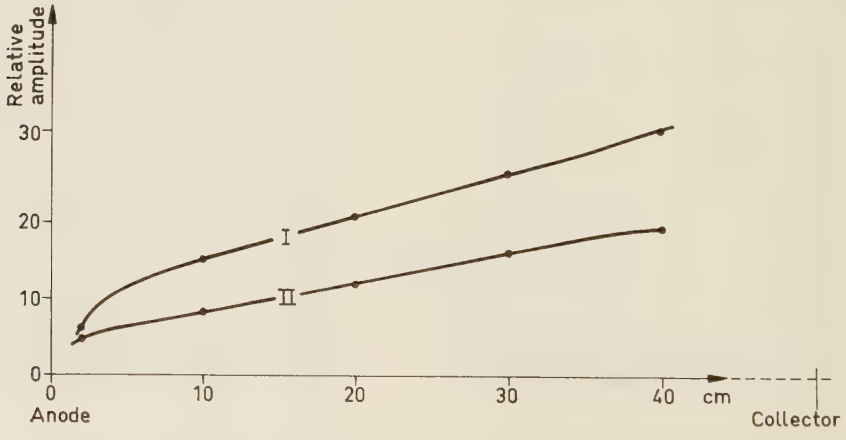

X 11110

Fig. 10. Electric field outside the beam region versus distance from the anode at two different magnetic fields; curve *I* 1,300 gauss, curve *II* 2,500 gauss. Collector current 25 mA, accelerating voltage 900 volts and pressure 10^{-5} mm Hg.

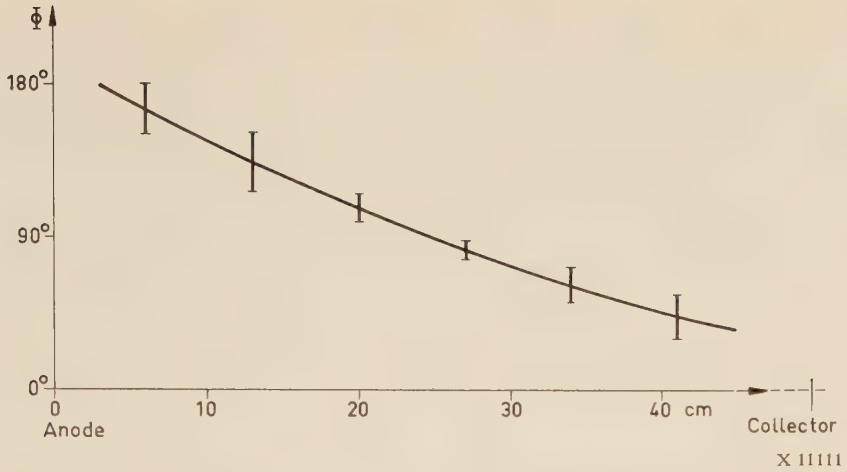

Fig. 11. Phase difference, Φ, between the signals to two electric probes one of which is fixed and the other movable in axial direction. Collector current 20 mA, accelerating voltage 500 volts, magnetic field 800 gauss and pressure $2 \cdot 10^{-5}$ mm Hg.

fields. The probe was placed half-way between the axis of the tube and the metal wall. Measurements show that the form of these curves depends upon the space charge of the beam. If the beam current is halved, the curves are almost flat from the collector to about 5 cm from the anode.

Fig. 11 shows the phase difference between the signals to two electric probes one of which is fixed and the other movable in axial direction. The vertical lines represent the spread in the measurements. The probes are placed as is shown in *fig. 3*; one is half-way between the anode and the collector and the other can be moved from the anode to the collector region. The phase difference depends both on the space charge in the beam and on the accelerating voltage.

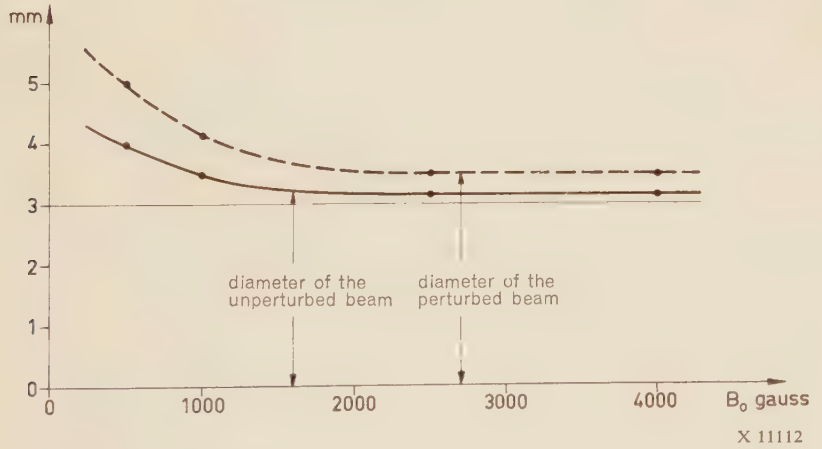

Fig. 12. Beam diameter versus magnetic field. Collector current 25 mA, accelerating voltage 900 volts and pressure 10^{-5} mm Hg.

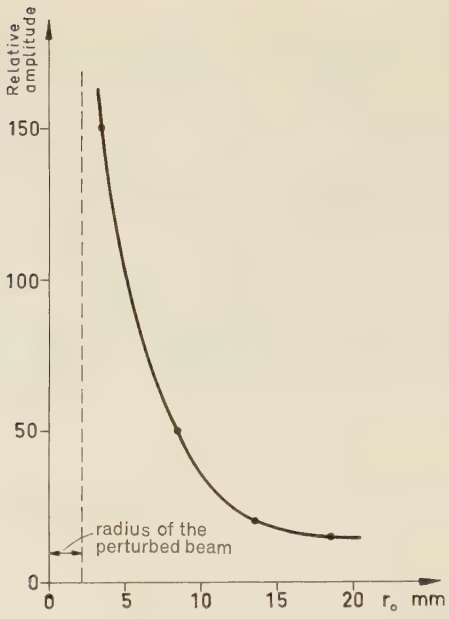

Fig. 13. Electric field outside the beam region versus radius. Collector current 25 mA, accelerating voltage 800 volts, magnetic field 1,000 gauss and pressure $2 \cdot 10^{-5}$ mm Hg. The field decreases with radius roughly as $r^{1.5}$

Fig. 12 shows the beam diameter—measured with the arrangement in *fig. 6*—as a function of the magnetic field. The measurements are made after the oscillations have started. (The beam diameter is here taken as the distance between the points where the current density is 10 % of its maximum value. The perturbation in the diameter is independent of how the diameter is defined.) The accuracy of the measurements is 0.1 mm. We note that the perturbations seem to approach a constant value for strong magnetic fields. The electric field outside the beam has been measured at magnetic fields up to 10,000 gauss. The amplitude and frequency of the field are almost constant for magnetic fields above 3,000 gauss.

The variation of the field outside the beam region with the distance from the axis of the tube is shown in *fig. 13*. The capacitive probe was placed half-way between the anode and the collector; the beam current was 25 mA, the accelerating voltage 800 volts, the magnetic field 1,000 gauss and the pressure $2 \cdot 10^{-5}$ mm Hg.

Attempts to give a theoretical description of the phenomena have not yet been successful and we will only give a few concluding remarks. The measured frequency of oscillation is close to the resonance frequency that theoretically should be expected if the positive ions oscillated in an electric dipole field and the transverse displacements of the electrons were

negligible. With this model—assuming that the dipole rotates—we could qualitatively explain some of the observations. However, the displacement of the electrons due to the transverse drift motion caused by this electric field, will be larger than the displacement of the ions (at least for magnetic fields below 2,000 gauss). Furthermore, the observations that the beam oscillations as well as the electric field outside the beam seem to approach constant values for strong magnetic fields also contradict this simple hypothesis. If the beam perturbations were caused by a drift in the crossed electric (dipole) and magnetic fields, this result would imply, that the dipole field increases with increasing magnetic field, which is not consistent with the measurements.

Phenomena in the gun region may be important for the oscillation mechanism. Measurements of the beam oscillations show that the amplitudes close to the anode and at the collector end are comparable.

CHAPTER 2

Electron Oscillations

Electron oscillations were studied in the same tube as was used for the previously described experiments, *fig. 1.* Two short helices were, however, introduced for modulating and demodulating the beam, *fig. 14.* Magnetic fields of the order of 1,000 gauss were used to ensure that the beam should be well confined. To get a rough estimate of the density of the secondary electrons (created through ionizing collisions in the primary beam), the beam was pulsed and the current going to the collector immediately after the end of the pulse was studied.

An amplification was obtained which varied with a factor of about three in the frequency range studied; the highest amplification obtained was 40 db with a distance between the two helices of 30 cm. The bandwidth, within which a gain was observed, was about 40 Mc/s.

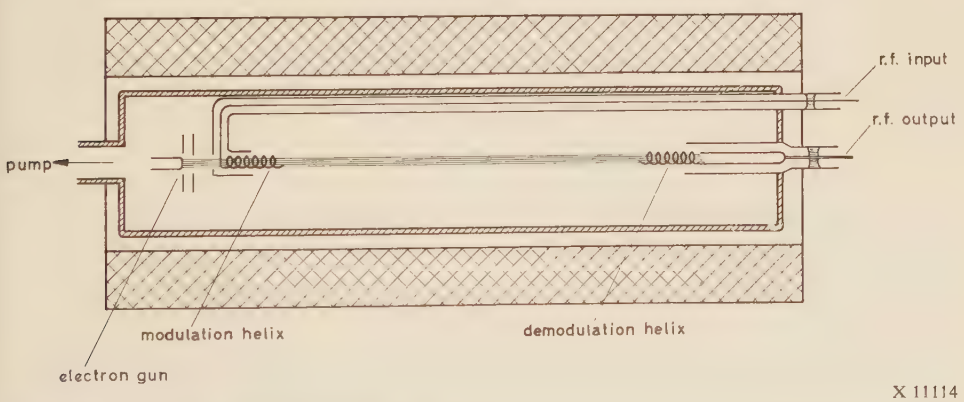

Fig. 14. Experimental tube for studying instabilities connected with the gyromotion of the electrons.

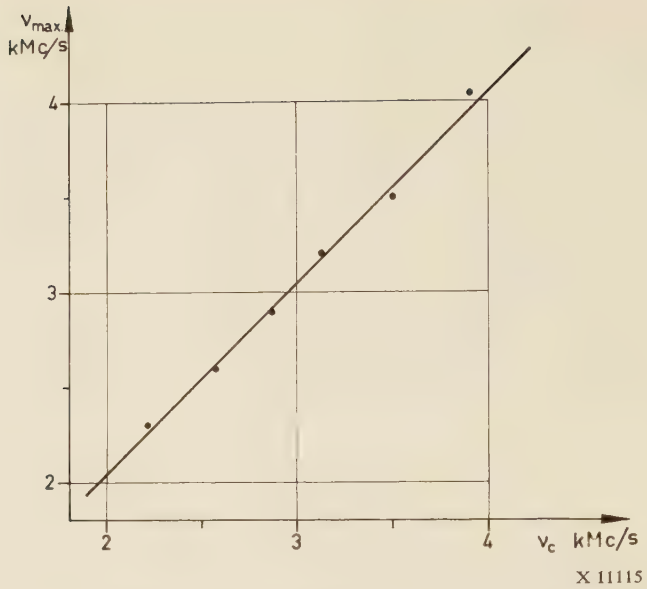

Fig. 15. Signal frequency for maximum amplification versus the gyrofrequency of the electrons.

Fig. 15 shows the signal frequency for maximum amplification versus the gyrofrequency of the electrons. The beam current was 20 mA, the accelerating voltage 800 volts and the pressure 10^{-4} mm Hg. The density of secondary electrons in the beam region was estimated to be three times the density of the electron beam, which means that the "plasma frequency" of the secondary electrons was 500 Mc/s.

This phenomenon may be explained if we assume that the beam interacts with slow waves carried by secondary electrons in the beam region. As long as the velocities of the secondary electrons are much smaller than the velocity of the slow waves, the secondary electrons may, in a first approximation, be taken as being at rest. With this assumption it can be shown that, when $\omega > \omega_e$, slow waves can exist only in the frequency range determined by the relation,

$$\omega_c^2 < \omega^2 < \omega_c^2 + \omega_e^2 \tag{2}$$

where ω_c is the gyrofrequency of the electrons and ω_e the plasma frequency of the slow electrons. This relation shows that—under the experimental conditions, where $\omega_e \ll \omega$ — slow waves exist only when $\omega \simeq \omega_c$.

One possible starting mechanism for the oscillations is the internal feed-back of energy that occurs when, as in the frequency range defined by eq. 2, the phase and group velocities are oppositely directed. In this frequency range the phase velocity changes with the param-

eters of the medium so that a continuous transition from slow to fast waves can be obtained. Thus the energy of the amplified waves may radiate out from the medium if the magnetic field and/or the plasma density varies along the plasma column so that the slow waves are transformed into fast waves.

Acknowledgements

I wish to express my gratitude to Professor HANNES ALFVÉN for his encouragement during the course of this work. I also wish to acknowledge my great indebtedness to Mr. G. BÖLING, who has constructed the tubes and with never failing interest and great personal engagement has made most of the measurements.

This work is part of a series of investigations carried out by a group supported by Telefonaktiebolaget L M Ericsson, the Swedish Technical Research Council and the Research Institute of National Defence.

Bibliography

1. CUTLER, C C: *Spurious Modulation of Electron Beams.* Proc. IRE *44*(1956): 1, pp. 61—64.

2. MIHRAM, T G: *Positive Ion Oscillations in Long Electron Beams.* IRE Trans. Electron Devices *3*(1956): 3, pp. 117—121.

3. AGDUR, B: *Notes on the Propagation of Guided Microwaves through an Electron Gas in the Presence of a Static Magnetic Field.* Proc. Symposium on Electronic Waveguides, pp. 177—197. New York 1958.

Manuscript received by the editors February 1960.

On Microwave Propagation in a Plasma-Filled Coaxial Line

BY

BENGT ENANDER*

UDC 621.372.2.029.6
537.525.1
621.315.212
LME 5375,5376,762

Experiments on microwave propagation in a coaxial line containing a glow discharge in a magnetic field are described. A signal passing through the discharge is attenuated if the signal frequency lies within a certain band, the lower limit of which is the gyromagnetic frequency. The attenuation is caused by absorption of the signal in the discharge. According to a simplified theory, there should be a frequency band with low transmission, similar to the one measured, but the transmission attenuation should be caused by reflections from the discharge and not by absorption.

* Electronics Department of the Royal Institute of Technology and the Research Department of Telefonaktiebolaget L M Ericsson, Stockholm. Now at the Microwave Department of the Royal Institute of Technology.

Introduction

During the last few years many investigations have been made of microwave propagation in plasma-filled wave guides[1, 2]. This paper describes experiments with a coaxial line containing a glow discharge in a magnetic field *(fig. 1)*. A microwave signal passing through the discharge is attenuated if the signal frequency lies within a certain band, extending from the gyro-

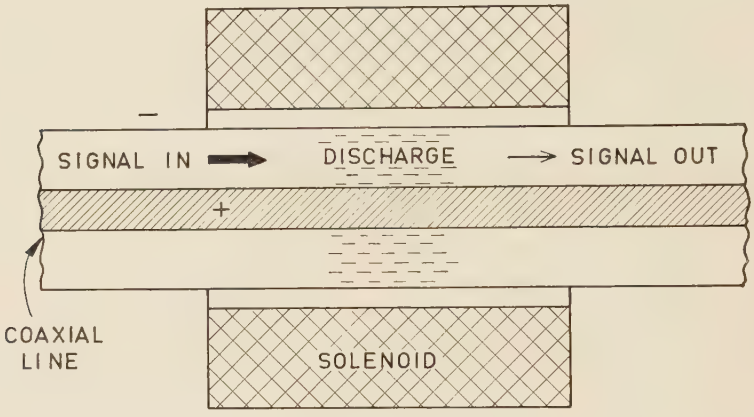

Fig. 1. Principle of the experimental tube.

magnetic frequency up to a frequency that increases with the discharge current. Reflections from the discharge boundaries are found to be very small and the attenuation seems to arise from absorption in the discharge. The attenuation band can easily be made several 1000 Mc/s wide. A device of this kind may be used as a microwave circuit element having a rapidly variable wide-band attenuation.

Apparatus

The tube used in the experiments *(fig. 2)* is essentially a coaxial line filled with argon gas of low pressure. A discharge is initiated by applying a voltage between the outer and inner conductors with the outer one as cathode. Without magnetic field the breakdown voltage is very high at low pressures, i.e. when the mean free path for electrons is comparable to or larger than the distance between the electrodes. In our experiments a longitudinal magnetic

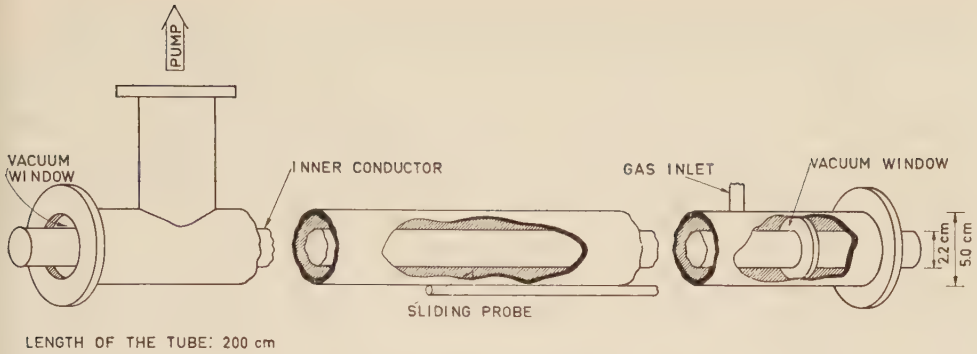

X 11078

Fig. 2. Experimental tube.

field in the central region is produced by a 40 cm long solenoid around the tube. This field lowers the breakdown voltage and the discharge occupies a rather short region inside the solenoid where the magnetic field is almost uniform (PENNING[3]). Yet, the tube must be long to prevent sputtered cathode material from reaching the perspex vacuum windows at the ends. As the tube cannot be baked out, contaminating gases will be released from the electrodes. The effects of these gases are reduced by letting the argon gas flow through the tube from a needle valve at one end to a pump outlet at the other end. The pump is an oil diffusion pump with a liquid-air trap and gives a base vacuum of a few times 10^{-6} mm Hg in the tube. In some experiments the tube has to dissipate a power of several kilowatts, which makes water cooling of the electrodes necessary.

The tube has been designed to have a characteristic impedance of approximately 50 ohms, and tapered transitions are used to connect it to standard coaxial components. Only the TEM mode can propagate in the empty line for frequencies below 2600 Mc/s.

Three different tubes have been used, all having inner electrodes of copper, with dimensions according to *fig. 2*. The first tube (tube I) had a stainless-steel outer electrode; tube II had an

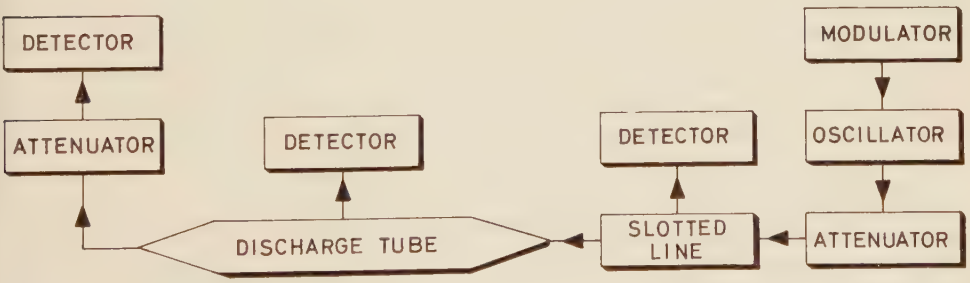

X 11079

Fig. 3. Block diagram of the microwave set-up.

aluminum outer electrode and was provided with a sliding probe to measure the microwave field in the discharge region. The discharges in these two tubes were far from uniform in the axial direction (see *fig. 5* below). To obtain a more uniform discharge tube III was constructed. It has a copper outer electrode and the central portion of the inner electrode consists of 26 copper sleeves, 1.5 cm long, insulated from each other by small gaps. With each sleeve connected to the D.C. supply through a separate resistor, an even current distribution over the 26 sleeves can be produced.

A block diagram of the microwave set-up is shown in *fig. 3*. The signal from a microwave oscillator, modulated by a 1000 c/s square wave, is sent through the tube via a padding attenuator and a slotted line. The signal transmitted through the tube is measured with a detector and the reflected signal is measured by means of the slotted line. Another detector is connected to the sliding probe. The detectors contain 1000 c/s filters that separate the signal from the, usually large, noise of the discharge.

Measurements

Some D.C. characteristics of the discharge are shown in *figs. 4* and *5*. Probe measurements of electron density and temperature have not been attempted. In a discharge of this type a probe would probably perturb the plasma badly.

The microwave measurements are made at so low gas pressures that the electron collision frequency is small compared to the signal frequency. At an argon pressure of 10^{-3} mm Hg the collision frequency for electrons with an energy of a few eV is of the order 10^6 sec^{-1}. The microwave power input is generally so small (<10 mW) that nonlinearities are unimportant. Nonlinear effects become appreciable at a power level of about 1 W, and the attenuation is then no longer independent of the input power.

Microwave transmission characteristics for small discharge currents *(figs. 6, 7, 8, 9)* have been obtained by varying the magnetic field, while keeping the discharge current, the pressure and the signal frequency constant. The attenuation peak observed in these measurements occurs at gyromagnetic resonance, i.e. when the signal frequency, f, is equal to the gyrofrequency of the electrons in the applied magnetic field, B. The resonance condition is

$$f = 2.8 \times 10^{10}\ B \text{ (MKSA units)}$$

At low pressures the attenuation curve exhibits secondary peaks *(fig. 6)*. For signal frequencies above 1000 Mc/s, the attenuation caused by the discharge is very small when the magnetic field is much higher or much lower than the resonance value. An exception is, however, evident from *fig. 9*, which shows that at pressures around 0.1 mm Hg another attenuation band appears at low magnetic fields.

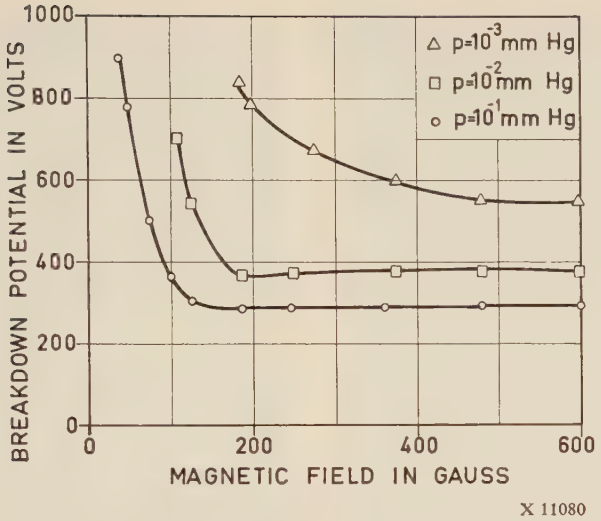

Fig. 4. Breakdown potential for the discharge in argon. (Tube III.)

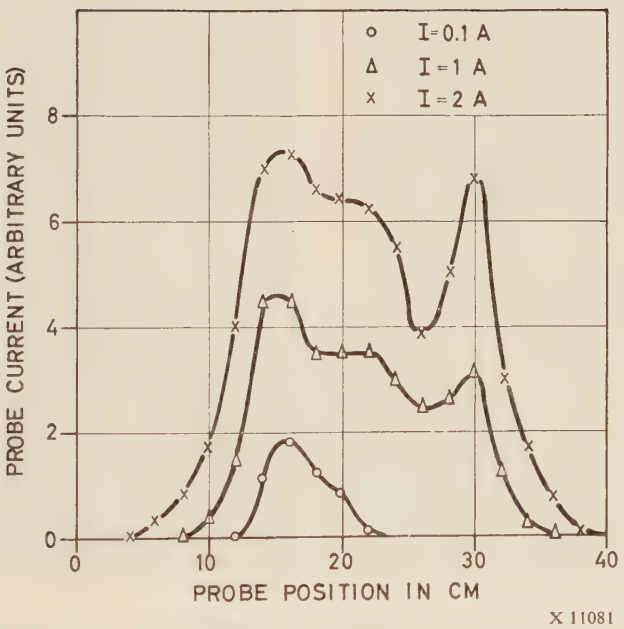

Fig. 5. Current distribution at the cathode for different values of the discharge current (I). The distance is measured from one end of the solenoid. $B = 1000$ gauss; $p = 3 \cdot 10^{-2}$ mm Hg. (Tube II.)

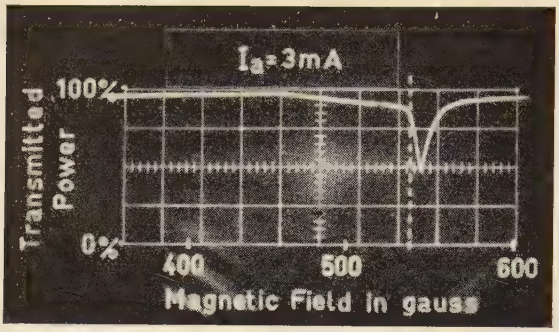

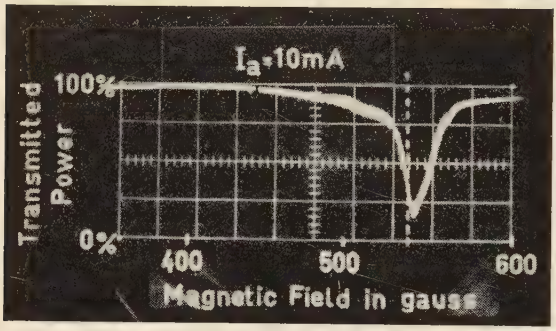

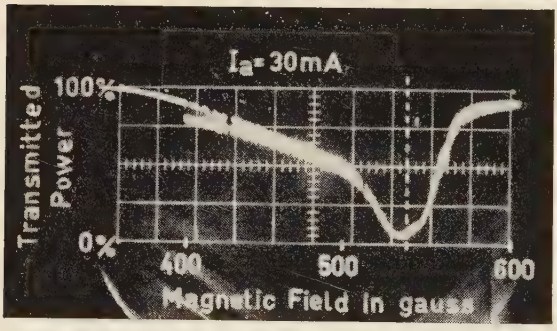

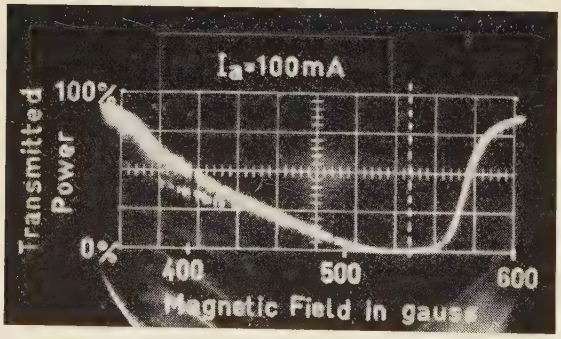

X 11082—X 11085

Fig. 6. Power transmitted through the discharge vs magnetic field for different values of the discharge current (I). $p = 3 \cdot 10^{-3}$ mm Hg; frequency 1500 Mc/s. (Tube III.) Gyromagnetic resonance occurs at the dashed line.

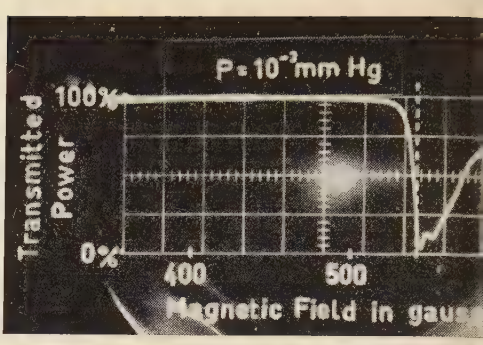

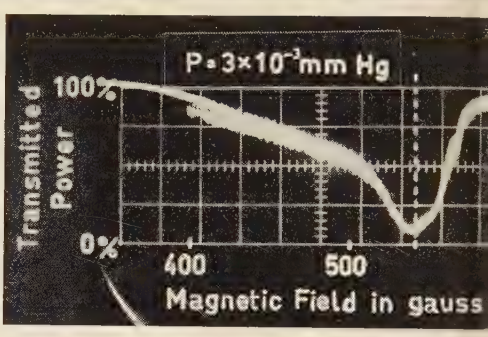

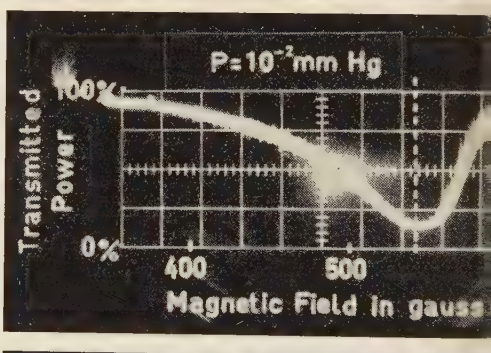

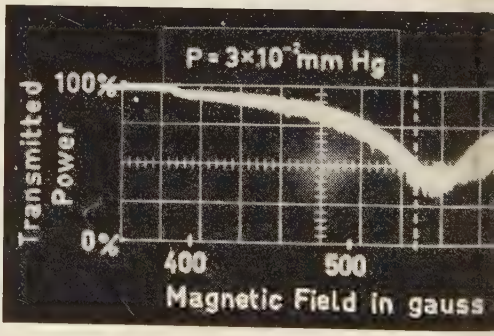

X 11086—

Fig. 7. Power transmitted through the discharge v
netic field. Discharge current 30 mA; frequency 150
(Tube III.) Gyromagnetic resonance occurs at the
line.

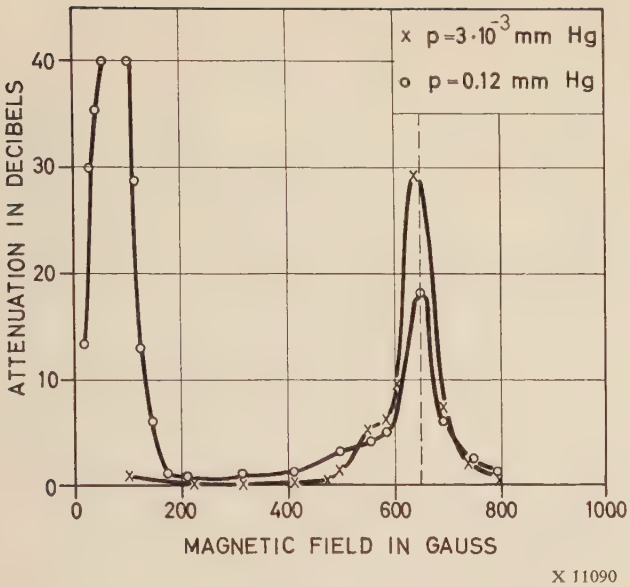

Fig. 8. Attenuation of the transmitted signal. Discharge current 0.1 A; frequency 1800 Mc/s. (Tube I.) Gyromagnetic resonance occurs at the dashed line.

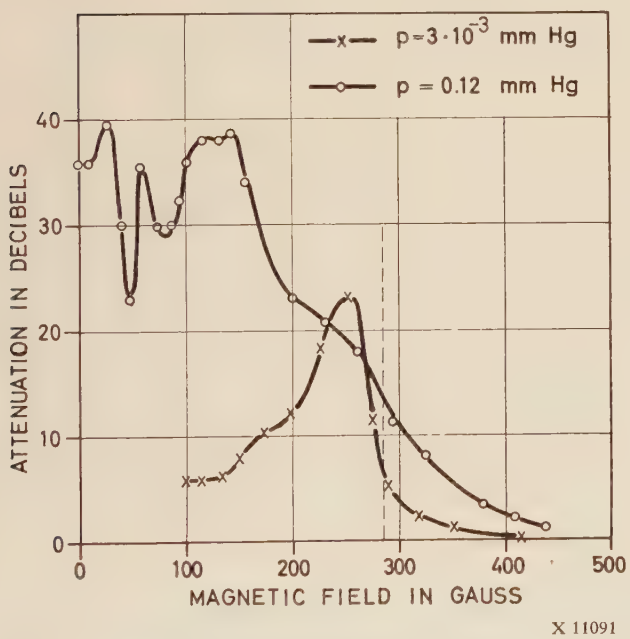

Fig. 9. Attenuation of the transmitted signal. Discharge current 0.1 A; frequency 800 Mc/s. (Tube I.) Gyromagnetic resonance occurs at the dashed line.

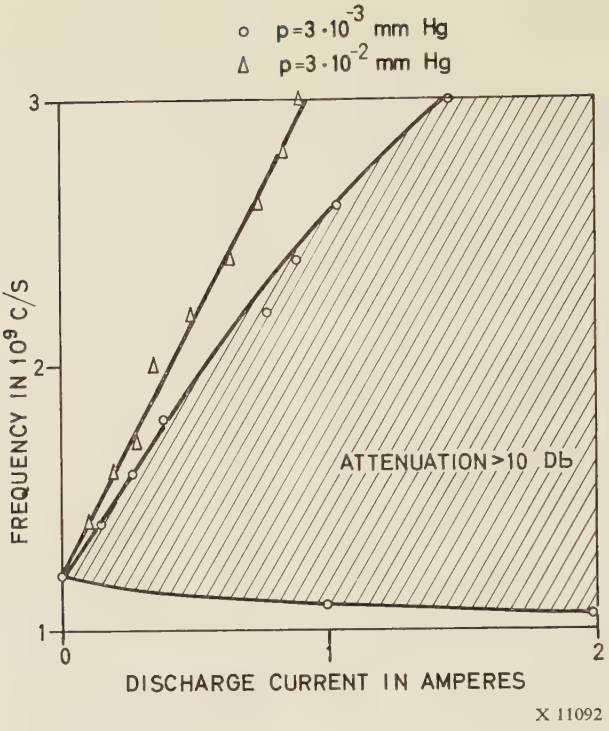

Fig. 10. Attenuation band vs discharge current. $B = 440$ gauss. (Tube II.)

For high discharge currents (> 0.1 A) the peak attenuation in the resonance attenuation band is so large (> 40 db) that—with our apparatus—the output signal could not be separated from the noise. The peak attenuation could thus not be measured. Instead the points on the transmission curve that correspond to 10 db attenuation were determined and taken to define the attenuation band. Data from such measurements are plotted in *figs. 10—14*. *Figs. 10—12* show how the attenuation band varies with the discharge current at constant magnetic field; in *fig. 12* results for other gases than argon have been included. The variation of the attenuation band with the magnetic field and the pressure are shown in *figs. 13* and *14* respectively. For small discharge currents the attenuation is greater than 10 db in a narrow band near the gyromagnetic frequency. As the current is increased the band widens. The upper frequency limit of the band increases rapidly whereas the lower limit decreases only slightly.

Reflections from the discharge were small under all conditions used in the measurements and the reflected power was always found to be less than ten percent of the input power. This indicates that the large attenuation of the microwave signal must be caused by absorption in the discharge.

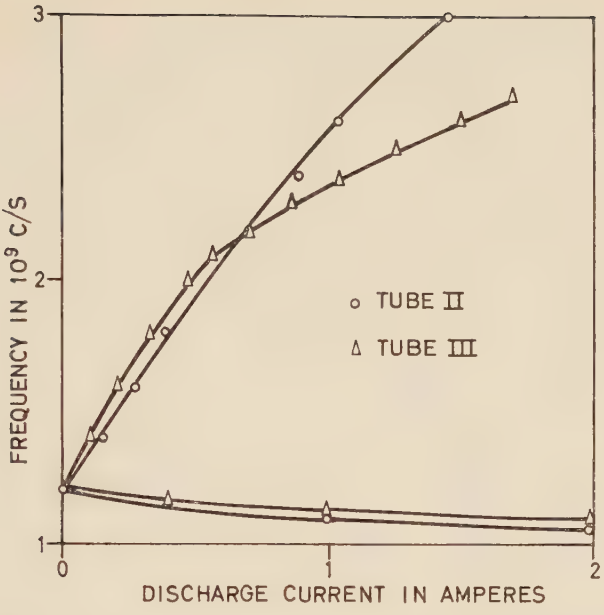

Fig. 11. Attenuation band vs discharge current. $B = 440$ gauss; $p = 3 \cdot 10^{-3}$ mm Hg.

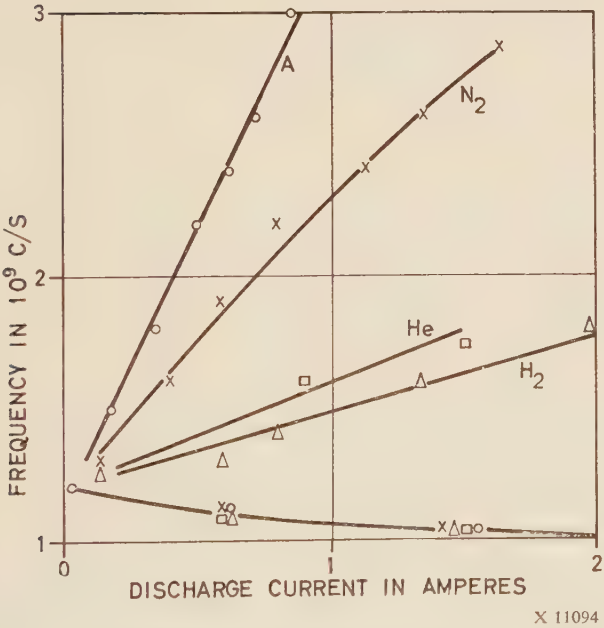

Fig. 12. Attenuation band vs discharge current. $B = 440$ gauss; $p = 3 \cdot 10^{-2}$ mm Hg.

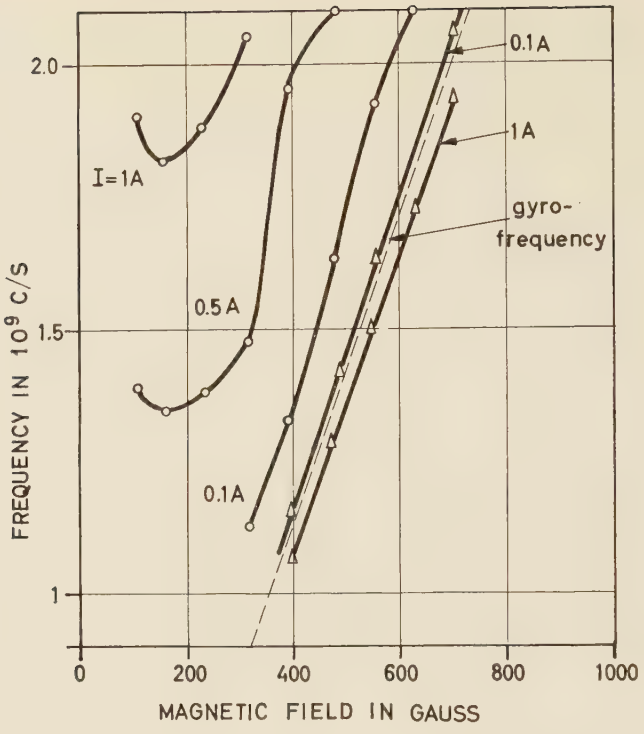

X 11095

Fig. 13. Attenuation band vs magnetic field. $p = 5 \cdot 10^{-3}$ mm Hg. (Tube I.)

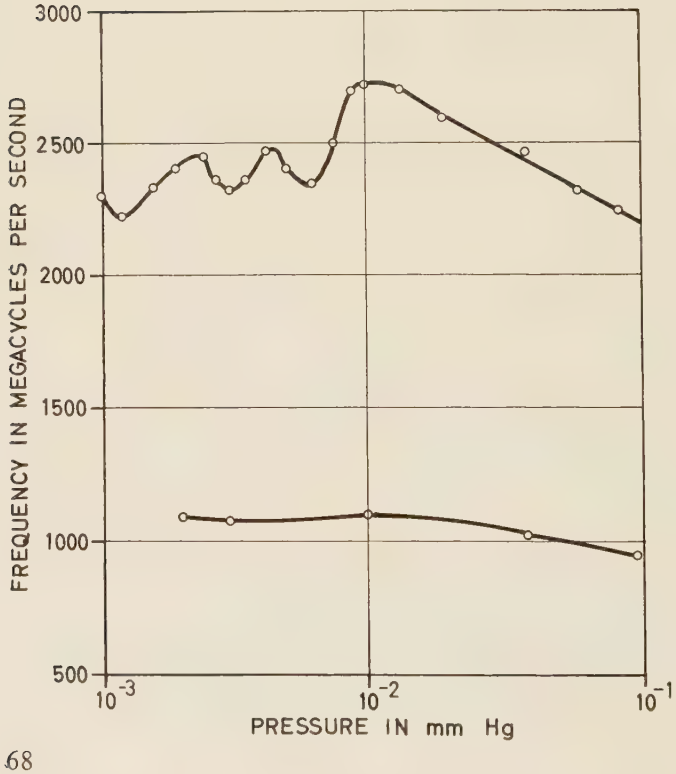

X 11096

Fig. 14. Attenuation band vs pressure. Discharge current 1 A; $B = 440$ gauss. (Tube III.)

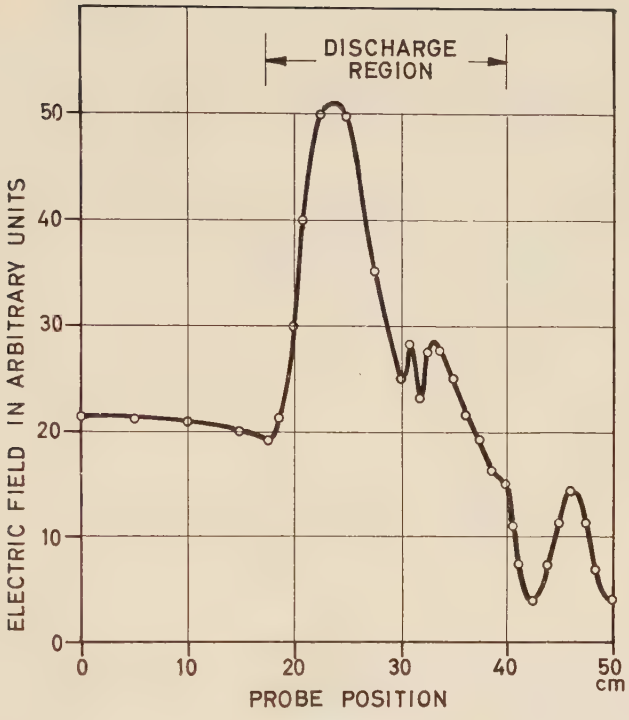

Fig. 15. Radial electric R.F. field. The probe position is measured from the input end towards the output end. Discharge current 330 mA; frequency 2000 Mc/s; $B = 940$ gauss; $p = 10^{-2}$ mm Hg. (Tube II.)

A comparison between data from tube II, with an axially non-uniform discharge, and tube III, with an almost uniform discharge, shows that axial non-uniformities do not have a major influence on the width of the attenuation band *(fig. 11)*. Nor does the band change greatly with the pressure within the pressure range 10^{-3}—10^{-1} mm Hg *(figs. 14* and *10)*.

The wavelength in the plasma was measured by means of the sliding probe and a phase-sensitive detector arrangement. Deviations from the free-space wavelength were found at signal frequencies near the gyromagnetic frequency. The wavelength was shorter than the free-space wavelength at frequencies below the gyromagnetic frequency and longer at frequencies above it. It was also found that the radial electric R.F. field could sometimes be greater in the discharge region than in front of it. The effect was large at frequencies just below the gyrofrequency; in *fig. 15* the maximum field in the discharge is 2.5 times the field outside.

Comparison between Theory and Experiments

In order to see how the experimental results compare with the theory of microwave propagation in plasma-filled waveguides (SUHL and WALKER[4], AGDUR[5]), we will here discuss the propagation in a plane plasma cable *(fig. 16)*. The cable consists of two infinite parallel conducting planes (at $y = \pm\delta$) bounding a homogeneous plasma magnetized in the propagation direction (z-axis). The microwave fields are assumed not to vary along the x-axis. The modes that propagate in this structure will exhibit all the salient features of those modes in the coaxial cable that have no azimuthal variation—provided the distance between the conductors of the coaxial line is small compared to their radii.

AGDUR[6] has arrived at the following characteristic equation for the antisymmetric modes (E_z and B_z antisymmetric with respect to the x—z plane) in the plane plasma cable:

$$\frac{M_1\left(\frac{\varepsilon_2^2}{\varepsilon_1} - \varepsilon_1 + \tau^2 + M_1^2\right)\tan kM_1}{M_2\left(\frac{\varepsilon_2^2}{\varepsilon_1} - \varepsilon_1 + \tau^2 + M_2^2\right)\tan kM_2} = 1 \tag{1}$$

where

$$M_{1,2}^2 = \frac{1}{2}\left\{\left(\varepsilon_1 - \tau^2\right)\left(1 + \frac{\varepsilon_3}{\varepsilon_1}\right) - \frac{\varepsilon_2^2}{\varepsilon_1} \pm \sqrt{\left\{\left(\varepsilon_1 - \tau^2\right)\left(1 - \frac{\varepsilon_3}{\varepsilon_1}\right) - \frac{\varepsilon_2^2}{\varepsilon_1}\right\}^2 + 4\tau^2\varepsilon_3\frac{\varepsilon_2^2}{\varepsilon_1}}\right\}$$

$$\varepsilon_1 = 1 - \frac{\left(\frac{\omega_p}{\omega}\right)^2}{1 - \left(\frac{\omega_c}{\omega}\right)^2}; \quad \varepsilon_2 = \frac{\left(\frac{\omega_p}{\omega}\right)^2\frac{\omega_c}{\omega}}{1 - \left(\frac{\omega_c}{\omega}\right)^2}; \quad \varepsilon_3 = 1 - \left(\frac{\omega_p}{\omega}\right)^2$$

$$\omega_p = \sqrt{\frac{ne^2}{m\varepsilon_0}} \qquad \omega_c = \frac{eB}{m} \qquad \tau = \frac{\beta}{\beta_0} = \frac{c}{v}$$

$$k = \frac{2\pi\delta}{\lambda_0}$$

and

n = electron density
B = static magnetic field
β = propagation constant
β_0 = propagation constant for free space
c = velocity of light
v = phase velocity
λ_0 = free-space wavelength
(MKSA-units are used)

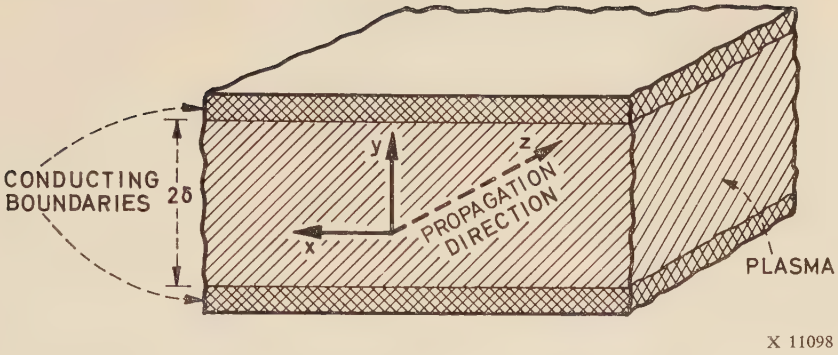

Fig. 16. Plane cable filled with plasma magnetized along propagation direction.

The characteristic equation was obtained by solving Maxwell's equations with appropriate boundary conditions under the assumption that all field components vary as $\exp\{j(\omega t - \beta z)\}$. The plasma was assumed macroscopically neutral and collisions and thermal velocities were neglected.

We will here give solutions of equation (1) for the case when the distance between the planes, 2δ, is small compared to the free-space wavelength. Only the TEM-mode will then propagate in the empty cable. The discussion will mainly be limited to the dominant mode which originates from this mode; following SUHL and WALKER[4] we will call this the TEM-limit mode.

If $k \ll 1$ an approximate solution of (1) is given by

$$\tau^2 \approx \varepsilon_1 + \frac{k^2 \varepsilon_2^2}{3} \tag{2}$$

This solution corresponds to the TEM-limit mode and the approximation is valid except for $\varepsilon_1 \ll 1$. Neglecting the second term on the right we get

$$\tau^2 \approx 1 - \frac{\left(\frac{\omega_p}{\omega}\right)^2}{1 - \left(\frac{\omega_c}{\omega}\right)^2} \tag{2a}$$

which is very similar to the corresponding equation for the extraordinary plane wave in an unbounded plasma magnetized in the propagation direction:

$$\tau^2 = 1 - \frac{\left(\frac{\omega_p}{\omega}\right)^2}{1 - \frac{\omega_c}{\omega}} \tag{3}$$

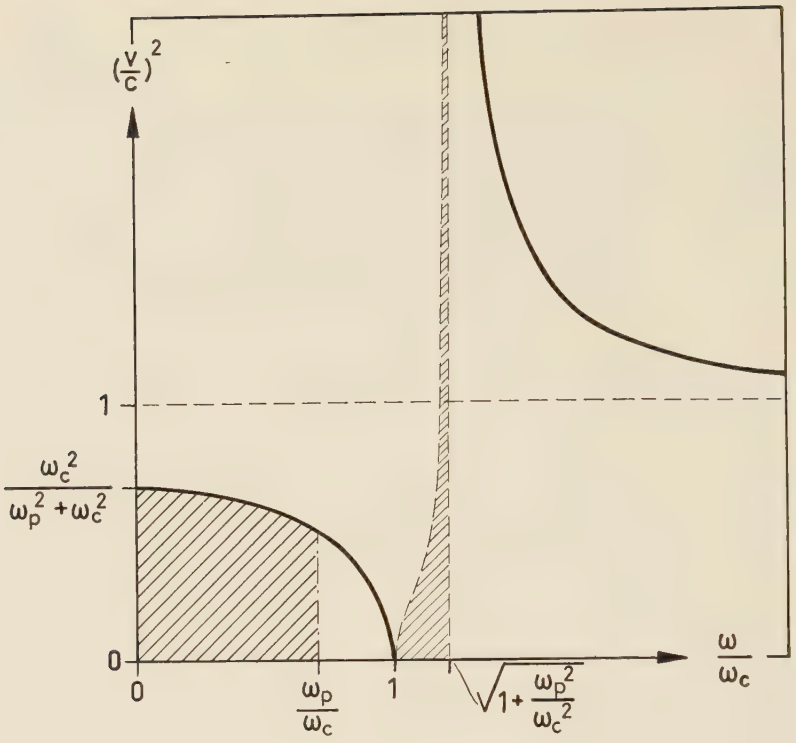

Fig. 17. Phase velocity of the TEM-limit mode. Higher order modes exist in the shaded regions. $\frac{\omega_p}{\omega_c} < 1$.

The solution (2a) is plotted in two $\left(\frac{v}{c}\right)^2$ vs $\frac{\omega}{\omega_c}$ diagrams *(figs. 17* and *18)* which also show the regions in which other (incipient) modes exist. Symmetric modes are obtained from a characteristic equation very similar to eq. (1). All the symmetric modes are incipient and exist in the same regions as the antisymmetric incipient modes. Unlike the TEM mode in the empty waveguide, the TEM-limit mode has field components in the propagation direction. The field for the solution (2a) is

$$E_y = \cos m_1 y - \frac{m_2^3 \sin m_1\delta}{m_1^3 \sin m_2\delta} \cos m_2 y$$

$$E_z = \frac{j\varepsilon_2^2}{\sqrt{\varepsilon_1}\, M_1^3} \left(\sin m_1 y - \frac{\sin m_1\delta}{\sin m_2\delta} \sin m_2 y\right)$$

$$E_x = -\frac{j\varepsilon_2}{M_1^2} \left(\cos m_1 y - \frac{\cos m_1\delta}{\cos m_2\delta} \cos m_2 y\right)$$

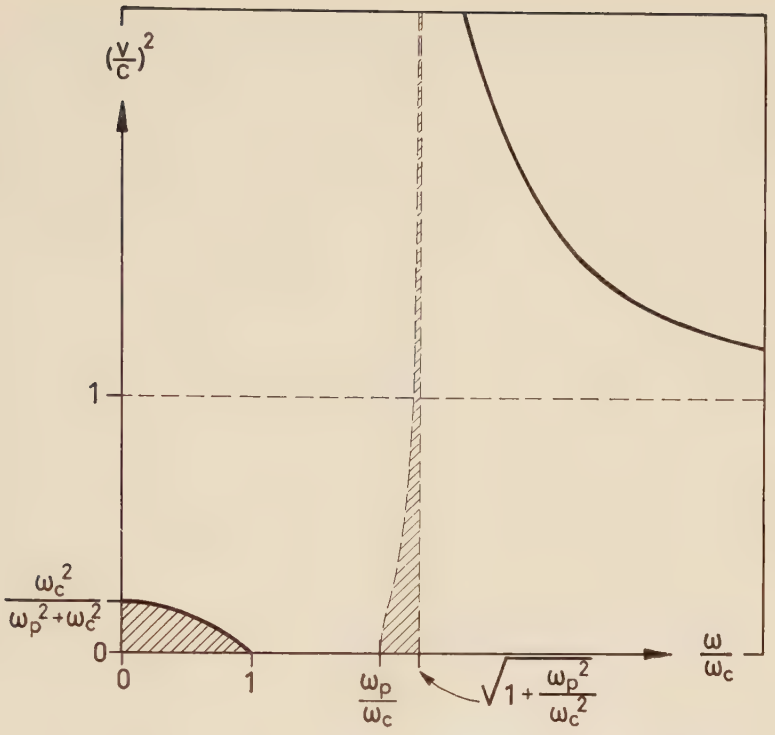

Fig. 18. Phase velocity of the TEM-limit mode. Higher order modes exist in the shaded regions. $\frac{\omega_p}{\omega_c} > 1$.

$$B_y = \frac{\sqrt{\varepsilon_1}}{c} E_x$$

$$B_z = \frac{\varepsilon_2}{c M_1} \left(\sin m_1 y - \frac{m_2^2 \sin m_1 \delta}{m_1^2 \sin m_2 \delta} \sin m_2 y \right)$$

$$B_x = -\frac{\sqrt{\varepsilon_1}}{c} E_y - \frac{j\varepsilon_2}{\sqrt{\varepsilon_1} c} E_x$$

where

$$m_{1,2}^2 = \beta_0^2 M_{1,2}^2$$

The TEM-limit mode propagates in the frequency region below the gyromagnetic frequency with a phase velocity smaller than c and a wavelength smaller than the free-space wavelength *(figs. 17* and *18)*. In the region $\omega_c < \omega < \sqrt{\omega_c^2 + \omega_p^2}$ the TEM-limit mode is "cut-off" and corresponds to an evanescent wave with an amplitude decreasing as $e^{-|\beta| z}$ in the propagation

direction. Higher order modes may, however, propagate at these frequencies. At frequencies above the "cut-off" band the TEM-limit mode is the only propagating mode, and has a phase velocity larger than c.

Let us now consider a coaxial cable—such that the theory for the plane cable is applicable—in which a section is filled with homogeneous plasma. An R.F. signal, propagating in the empty cable towards the plasma boundary, excites mainly the TEM-limit mode in the plasma, if the frequency is outside the "cut-off" band. The reflections from the boundary should be small (except near the "cut-off" limits) and the transmission through the plasma large. For frequencies in the "cut-off" band the signal may propagate in the higher order modes through the plasma. However, the reflections should be large in this case, as the field configurations of these modes are very different from the field configuration of the TEM mode.

The agreement between the experimental results and the idealized theory is only partial. There is, in both, a band with low transmission that extends from the gyrofrequency toward higher frequencies. Also, the measured variation of the wavelength in the plasma with frequency is consistent with the theory. However, there is an important discrepancy: whereas in the theory the low transmission should be caused by reflections, the experiments show that it is caused by absorption.

At present we have no satisfactory explanation of the absorption. If collisions are taken into account in the case of a plane wave, eq. (3) is modified to

$$\tau^2 = 1 - \frac{\left(\frac{\omega_p}{\omega}\right)^2}{1 - \frac{\omega_c}{\omega} - j\frac{\nu}{\omega}} \tag{4}$$

where ν is the collision frequency. When $\frac{\nu}{\omega} \ll 1$ (as in our experiments), the influence of the collisions should according to (4) be large only in a narrow frequency band around the gyrofrequency with a bandwidth $\triangle\omega$, where $\frac{\triangle\omega}{\omega}$ is of the order $\frac{\nu}{\omega}$. For physical reasons this should hold for the TEM-limit mode also. The discussion above (predicting reflections) should therefore still be valid, except in the band $\triangle\omega$.

The plasma in the experiments is not homogeneous, but has large variations in density both in axial and radial direction. The experiments indicate that the axial inhomogeneities are not important for the absorption effects. The radial density variations may, however, be of major importance.

Acknowledgement

The author wishes to express his thanks to Professors Hannes Alfvén and Bertil Agdur for encouragement and stimulating discussions during the course of this work. The technical assistance of Mr Christopher Wilson is gratefully acknowledged. The investigation has been sponsored by Telefonaktiebolaget L M Ericsson.

Bibliography

1. *Proceedings of the Symposium on Electronic Waveguides.* New York 1958. 418 pp.

2. Goldstein, L: *Electrical Discharge in Gases and Modern Electronics.* Advances in Electronics and Electron Physics *7*(1955): pp. 399—503.

3. Penning, F M: *Die Glimmentladung bei niedrigem Druck zwischen Koaxialen Zylindern in einem Axialen Magnetfeld.* Physica *3*(1936): 9, pp. 873—894.

4. Suhl, H & Walker, L R: *Topics in Guided-Wave Propagation through Gyromagnetic Media.* Bell Syst. tech. J *33*(1954): 3, 4, 5, pp. 579—659; 939—986; 1133—1194.

5. Agdur, B: *Notes on the Propagation of Guided Microwaves through an Electron Gas in the Presence of a Static Magnetic Field.* Proc. Symposium on Electronic Waveguides, pp. 177—197. New York 1958.

6. Agdur, B: *On Propagation of Guided Microwaves through an Electron Gas in the Presence of a Static Magnetic Field.* Stockholm 1957. Royal Inst. of Technol., Department of Electronics (Internal Report).

Manuscript received by the editors February 1960.

Aspects on Wide-Band Parametric Travelling-Wave Amplifiers

BY

BENGT T HENOCH*

UDC 621.375.9.029.6

The interaction between signal and idling waves in a filter ladder containing non-linear reactances and exposed to a pump wave is investigated theoretically. The cases of homogeneous lines and circuits with concentrated elements are considered. Satisfaction of certain phase and dispersion conditions leads to wide-band parametric amplification. The properties of such systems are determined. From the theoretical results filter structures applicable to parametric amplification can be derived. Various filter structures of low-pass and band-pass types which are suitable for different frequency ranges are treated.

Finally the influence of losses and generation of noise are determined. Different measures to minimize the noise figure are discussed.

* Research Institute of National Defence, Electronics Department, Stockholm.

Contents

Introduction

Parametric circuits are distinguished by the fact that they contain a non-linear reactance varying with time in synchronism with an applied pump voltage having an angular frequency ω_p. A signal having an angular frequency ω_s is applied to the circuit, and a mixed voltage, i.e. idling voltage with an angular frequency $\omega_i = \omega_p \pm \omega_s$, is generated in the circuit by the non-linear reactance. Parametric circuits may work as frequency converters or amplifiers.

Parametric amplifiers with the frequency relation $\omega_s + \omega_i = \omega_p$ have recently attracted great attention, and they have been treated in several papers. The great advantage of these amplifiers is the fact that they have a low noise figure and that solid state amplification can be carried out. The parametric amplifiers with a simple parametric circuit that have been built have a very small bandwidth, and in order to obtain the large bandwidths desired, it was necessary to apply parametric travelling-wave amplification. Parametric amplification of electromagnetic waves in two homogeneous lines with non-linear coupling has been treated by P. K. Tien and H. Suhl,[1,2] and parametric amplification of space-charge waves in an electron beam has been described by W. H. Louisell and C. F. Quate[3].

The principles of parametric travelling-wave amplification can easily be understood if a filter ladder containing distributed non-linear reactances is considered. A signal and a pump wave are applied to the filter ladder. Small-signal theory is valid, meaning that the signal amplitude is considerably smaller than the pump amplitude, and that the time-varying reactance caused by the pump wave is small. By mixing of signal and pump voltages in the non-linear reactances, harmonics with the frequencies $m\omega_p + n\omega_s$ are formed. As small-signal theory and a certain filter structure are assumed, only the idling frequency $\omega_i = \omega_p - \omega_s$ is considered. Thus from the distributed non-linear reactances, idling wavelets are emitted in both directions. In order to obtain a strong interaction between signal and idling waves these idling wavelets should add in phase in one direction, which requires the satisfaction of certain phase conditions in the filter ladder. This integrated idling wave is in turn mixed with the pump wave, with the result that signal wavelets adding in phase with the incident signal wave are emitted from the distributed non-linear reactances. In these circumstances coupled pairs of signal and idling waves are obtained. Power is transferred from the pump wave to the signal and idling wave, and thus the signal wave is amplified.

There are similarities between parametric travelling-wave amplifiers and travelling-wave amplifiers utilizing the coupling between waves in an electron beam and a slow-wave structure. The mechanisms of amplification are different, but the signal and idling waves are coupled to each other in a way similar to that in which the waves in an electron beam and a slow-wave structure are coupled to each other.

In an ordinary travelling-wave tube the waves in the electron beam and the slow-wave structure have parallel group velocities, and an amplifier with exponential gain and wide bandwidth is obtained. In the same way parallel signal and idling group velocities will give a stable amplifier having exponential gain and wide bandwidth.

In a backward-wave tube the waves in the electron beam and the slow-wave structure have reversed group velocities, and as a result of the feedback caused by the reversed group velocities, a regenerative amplifier having a narrow bandwidth is obtained. In a parametric travelling-wave amplifier, reversed signal and idling group velocities will introduce continuous feedback along the filter ladder, and the amplifier will be regenerative and narrow-banded. The wave pattern of the backward-wave parametric amplifier is similar to the wave pattern of the backward-wave tube. The signal wave amplitude varies according to a cosine curve with maximum amplitude at the signal output. If the coupling between the signal and idling waves is strong enough, the amplifier will burst into oscillation. Like the backward-wave tube the backward-wave parametric amplifier can be used as an oscillator tunable over a wide frequency range.

In the following the treatment will be confined to forward-wave parametric amplifiers giving stable, unidirectional gain and wide bandwidth.

The purpose of this paper is to show the methods of calculation that can be used for calculation of amplification, bandwidth, phase condition and noise figure for a parametric travelling-wave amplifier, as well as to obtain the different types of circuits to be used for parametric travelling-wave amplification. The theoretical treatment in chapter 1 follows principally that of P. K. Tien and H. Suhl,[1,2] but the theory has been expanded to include circuits with concentrated circuit elements. The calculations have been made for the case where the non-linear reactance is a voltage-dependent capacitance inserted at an arbitrary point in the parallel susceptances of a filter ladder.

The calculations show that parametric travelling-wave amplifiers can be classified on theoretical principles into three groups according to the three phase conditions necessary for the amplification, and satisfied by signal, idling and pump waves. The circuits for parametric travelling-wave amplifiers are classified according to the circuit elements that are the fundamental elements of the circuits. The circuits can then be built of LC-circuits, transmission lines or periodic slow-wave structures, as well as according to the number of pass-bands used in the circuits.

When classified according to the fundamental elements these circuits are treated separately in chapters 2, 3 and 4.

In chapter 5 the effect of losses in a parametric travelling-wave amplifier is discussed. The wave propagation is investigated in a lossy circuit. The generation of noise is investigated in chapter 6, and different measures to minimize the noise figure are discussed. Chapter 7 gives a final discussion of the results.

CHAPTER 1

Theoretical Treatment

1.1 Parametric Circuit

In the calculations, a filter ladder with the series reactance jX and the parallel susceptance jB is assumed. A pump wave having an angular frequency ω_p and a signal wave having an angular frequency ω_s are applied to the circuit, and an idling wave of angular frequency ω_i is generated by the non-linear reactances inserted in the filter ladder. For parametric travelling-wave amplification, power is transferred from the pump wave to the signal and idling waves. The frequency condition where $\omega_s + \omega_i = \omega_p$, is always satisfied. In the following, it is assumed that $\omega_s \leqq \omega_i$. This assumption does not restrict the validity of the calculations, but has been made because the amplifier has a lower noise figure when $\omega_s \leqq \omega_i$. The frequencies can simply be reversed.

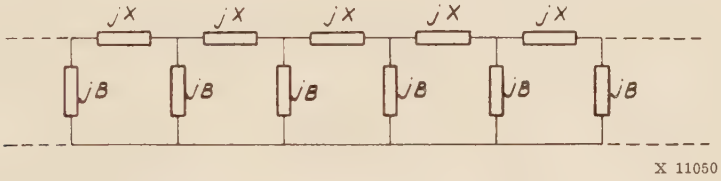

Fig. 1. Equivalent circuit for parametric travelling-wave amplifier.

For the reactances and susceptances of the circuit,

$$\text{at frequency } \omega_s \qquad \begin{cases} X = X_s \\ B = B_s \end{cases} \tag{1}$$

$$\text{at frequency } \omega_i \qquad \begin{cases} X = X_i \\ B = B_i \end{cases} \tag{2}$$

$$\text{at frequency } \omega_p \qquad \begin{cases} X = X_p \\ B = B_p \end{cases} \tag{3}$$

hold true.

φ_s is signal wave phase shift per section
φ_i is idling wave phase shift per section
φ_p is pump wave phase shift per section
$(Z_0)_s$ is the characteristic impedance of the circuit at signal frequency
$(Z_0)_i$ is the characteristic impedance of the circuit at idling frequency
$(Z_0)_p$ is the characteristic impedance of the circuit at pump frequency

Susceptance B contains a capacitance inserted at an arbitrary point —a varicap—having a static d.c. capacitance $C_{dc}(\overline{V})$ and a dynamic a.c. capacitance $C_v(\overline{V})$. The values of the capacitance depend on the applied d.c. voltage $\overline{V}$, and provided the a.c. voltage is small, the following holds

$$C_v(\overline{V}) = C_{dc}(\overline{V}) + \frac{dC_{dc}}{d\overline{V}} \cdot \overline{V} \tag{4}$$

A pump wave giving a voltage V_p across the varicap is applied to the circuit, and the wave propagates according to

$$V_p = \frac{1}{2}(V_p)_0 \left[e^{j(\omega_p t - n \cdot \varphi_p)} + e^{-j(\omega_p t - n \cdot \varphi_p)} \right] \tag{5}$$

where n is the number of filter sections from the filter input. This pump wave now causes the varicap to vary with time according to

$$C = C_v + \Delta C \left[e^{j(\omega_p t - n\varphi_p)} + e^{-j(\omega_p t - n\varphi_p)} \right] \tag{6}$$

where $\Delta C = \frac{dC_{dc}}{dV}(V_p)_0$, provided $\Delta C \ll C_v$.

1.2 The Coupling between Signal and Idling Waves

This varying capacitance causes a coupling between signal and idling waves for which an expression must be found. For this purpose susceptance B is considered and a signal voltage $V_s \cdot e^{j\omega_s t}$ and an idling voltage $V_i \cdot e^{-j\omega_i t}$ are assumed to be applied to this susceptance B. When the currents and voltages are now calculated in the susceptance B, it is assumed that the time-varying part ΔC of the varicap is so small that a perturbation calculation is permitted and that second order terms of mixed currents and voltages can thus be neglected. The same assumption must be made later to solve equation (13).

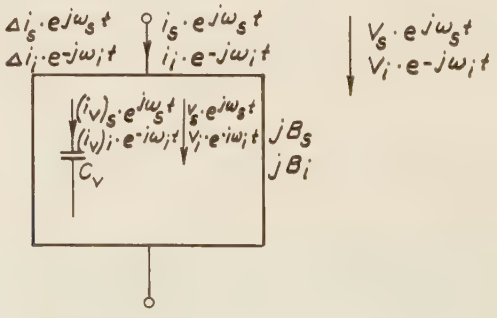

X 11051

Fig. 2. Susceptance B with coupled varicap.

The signal and idling voltages across susceptance B produce currents $(i_v)_s \cdot e^{j\omega_s t}$ and $(i_v)_i \cdot e^{-j\omega_i t}$ through the varicap, and these can be written

$$\begin{cases} (i_v)_s \cdot e^{j\omega_s t} = jb_s \cdot V_s \cdot e^{j\omega_s t} \\ (i_v)_i \cdot e^{-j\omega_i t} = -jb_i \cdot V_i \cdot e^{-j\omega_i t} \end{cases} \tag{7}$$

The terms b_s and b_i can be easily calculated if the circuitry of susceptance B is known. The signal and idling currents through the varicap are now mixed with the pump wave, and thus mixed currents are obtained that can be written

$$\begin{cases} \Delta(i_v)_s e^{j\omega_s t} = \dfrac{d}{dt}\left\{\Delta C\left[e^{j(\omega_p t - n\varphi_p)} + e^{-j(\omega_p t - n\varphi_p)}\right]\dfrac{1}{-j\omega_i C_v}(i_v)_i e^{-j\omega_i t}\right\} \\ \Delta(i_v)_i e^{-j\omega_i t} = \dfrac{d}{dt}\left\{\Delta C\left[e^{j(\omega_p t - n\varphi_p)} + e^{-j(\omega_p t - n\varphi_p)}\right]\dfrac{1}{j\omega_s C_v}(i_v)_s e^{j\omega_s t}\right\} \end{cases} \tag{8}$$

The mixed voltages $\Delta v_s \cdot e^{j\omega_s t}$ and $\Delta v_i \cdot e^{-j\omega_i t}$ across the varicap correspond to these mixed currents. According to $\Delta v = \dfrac{1}{j\omega C_v}\Delta(i_v)$, and introducing equations (7) and (8), these voltages can be written

$$\begin{cases} \Delta v_s \cdot e^{j\omega_s t} = \dfrac{\Delta C b_i}{\omega_i C_v^2} V_i e^{j\omega_s t} \cdot e^{-jn\varphi_p} \\ \Delta v_i \cdot e^{-j\omega_i t} = \dfrac{\Delta C b_s}{\omega_s C_v^2} V_s e^{-j\omega_i t} \cdot e^{jn\varphi_p} \end{cases} \tag{9}$$

The mixed voltages across the varicap generate the mixed currents $\Delta i_s \cdot e^{j\omega_s t}$ and $\Delta i_i \cdot e^{-j\omega_i t}$ through susceptance B, and these currents can be determined by means of the reciprocity theorem. According to equation (7), the currents generated through the varicap by the signal and idling voltages across the susceptance are known, and as the susceptance is contained in a closed network, the reciprocity theorem holds true. According to equation (7) the currents generated through the susceptance by the mixed voltages across the varicap are known and may be written

$$\begin{cases} \Delta i_s \cdot e^{j\omega_s t} = j\dfrac{b_s b_i \Delta C}{\omega_i C_v^2} V_i e^{j\omega_s t} \cdot e^{-jn\varphi_p} \\ \Delta i_i \cdot e^{-j\omega_i t} = -j\dfrac{b_s b_i \Delta C}{\omega_s C_v^2} V_s e^{-j\omega_i t} \cdot e^{jn\varphi_p} \end{cases} \tag{10}$$

According to equation (10), the coupling between signal and idling waves is known, and thus treatment of the wave propagation in the filter ladder may be proceeded with. Depending on the values of reactances and susceptances, different methods of calculation can be used; if $BX \ll 1$, the circuit can be treated as a homogeneous line, and if $0 \leqq BX \leq 4$, the circuit must be treated as a filter ladder with concentrated circuit elements.

1.3 Homogeneous Lines

Assume $BX \ll 1$, and the circuit can then be treated as a homogeneous line. The number of filter sections, n, from the circuit input will be used instead of the distance along a homogeneous line, and then the phase shift φ per section will replace the wave propagation constant for a homogeneous line. With these conditions, the equations below hold for the circuit.

$$\begin{aligned} \varphi_s &= \sqrt{B_s X_s} & (Z_0)_s &= \sqrt{\frac{X_s}{B_s}} \\ \varphi_i &= \sqrt{B_i X_i} & (Z_0)_i &= \sqrt{\frac{X_i}{B_i}} \\ \varphi_p &= \sqrt{B_p X_p} & (Z_0)_p &= \sqrt{\frac{X_p}{B_p}} \end{aligned} \tag{11}$$

Let $V_s(n)e^{j\omega_s t}$, $V_i(n)e^{-j\omega_i t}$, $I_s(n)e^{j\omega_s t}$, and $I_i(n)e^{-j\omega_i t}$ be the voltages and currents of the signal and idling waves in the circuit. Then

$$\begin{cases} \dfrac{dV_s(n)}{dn} = -jX_s I_s(n) \\ \dfrac{dI_s(n)}{dn} = -jB_s V_s(n) - j\dfrac{b_s b_i \Delta C}{\omega_i C_v^2} V_i(n) \cdot e^{-jn\varphi_p} \\ \dfrac{dV_i(n)}{dn} = jX_i I_i(n) \\ \dfrac{dI_i(n)}{dn} = jB_i V_i(n) + j\dfrac{b_s b_i \Delta C}{\omega_s C_v^2} V_s(n) \cdot e^{jn\varphi_p} \end{cases} \tag{12}$$

hold true.

Combination of the first equation with the second and the third with the fourth yields

$$\begin{cases} \dfrac{d^2 V_s(n)}{dn^2} = -B_s X_s V_s(n) - X_s \dfrac{b_s b_i \Delta C}{\omega_i C_v^2} V_i(n) \cdot e^{-jn\varphi_p} \\ \dfrac{d^2 V_i(n)}{dn^2} = -B_i X_i V_i(n) - X_i \dfrac{b_s b_i \Delta C}{\omega_s C_v^2} V_s(n) \cdot e^{jn\varphi_p} \end{cases} \tag{13}$$

Waves with the time dependence $e^{-j\omega_s t}$ and $e^{j\omega_i t}$ give the same equations, but with conjugate complex numbers.

Irrespective of the perturbation terms, equations (13) have the same form as the ordinary wave equations for homogeneous lines. Assuming $\dfrac{b_s b_i \Delta C}{\omega C_v^2} \ll B$, the equations can be treated by means of a perturbation theory.

1.31 Coupling Conditions

In order to obtain parametric amplification, one of the following three phase conditions must be satisfied

$$\varphi_p = \varphi_s + \varphi_i \qquad \varphi_p = \varphi_s - \varphi_i \qquad \varphi_p = \varphi_i - \varphi_s \tag{14}$$

The phase shifts φ are assumed positive.

For each phase condition satisfied, a number of wave pairs coupled to each other are obtained.

When the phase condition $\varphi_p = \varphi_s + \varphi_i$ is fulfilled, the coupled wave pairs will be

$$\begin{cases} V_s(n,t) = A_s(n)\, e^{j(\omega_s t - n\varphi_s)} \\ V_i(n,t) = A_i^*(n) e^{-j(\omega_i t - n\varphi_i)} \end{cases} \qquad \begin{cases} V_s(n,t) = A_s^*(n) e^{-j(\omega_s t - n\varphi_s)} \\ V_i(n,t) = A_i(n) e^{j(\omega_i t - n\varphi_i)} \end{cases} \tag{15}$$

When the phase condition $\varphi_p = \varphi_s - \varphi_i$ is fulfilled, the coupled wave pairs will be

$$\begin{cases} V_s(n,t) = C_s(n) e^{j(\omega_s t - n\varphi_s)} \\ V_i(n,t) = C_i^*(n) e^{-j(\omega_i t + n\varphi_i)} \end{cases} \qquad \begin{cases} V_s(n,t) = C_s^*(n) e^{-j(\omega_s t - n\varphi_s)} \\ V_i(n,t) = C_i(n) e^{j(\omega_i t + n\varphi_i)} \end{cases} \tag{16}$$

When the phase condition $\varphi_p = \varphi_i - \varphi_s$ is fulfilled, the coupled wave pairs will be

$$\begin{cases} V_s(n,t) = D_s(n) e^{j(\omega_s t + n\varphi_s)} \\ V_i(n,t) = D_i^*(n) e^{-j(\omega_i t - n\varphi_i)} \end{cases} \qquad \begin{cases} V_s(n,t) = D_s^*(n) e^{-j(\omega_s t + n\varphi_s)} \\ V_i(n,t) = D_i(n) e^{j(\omega_i t - n\varphi_i)} \end{cases} \tag{17}$$

The disposition of the wave pairs shows that there is amplification in only one direction, and thus a signal reflected due to mismatch is not amplified when returning.

In determining the coupled wave pairs in (15), (16) and (17), the phase conditions in (14) are assumed to be satisfied for the signal and idling frequencies, since if one of the phase conditions (14) is met with for higher mixed frequencies, new coupled wave pairs will be obtained at these frequencies, and these coupled wave pairs absorb pump power. This has been shown by G M Roe and M R Boyd[4] for a zero-dispersion line, where all the mixed frequencies meet the first phase condition in (14), thus forming coupled wave pairs. In such a line, the amplification of the signal wave will be negligible, and the pump power is converted into a whole spectrum of mixed frequencies. However, this assumption of the range of validity for the phase conditions does not limit to any large extent the validity of the calculations.

1.32 Calculation of the Amplification

The first wave pair in equation (15) is introduced into equation (13). Since the perturbation terms are small $\frac{d^2A}{dn^2}$ can be neglected compared to $\varphi \frac{dA}{dn}$, and the following are obtained

$$\begin{cases} -2j\varphi_s \dfrac{dA_s(n)}{dn} = -X_s \dfrac{b_s b_i \Delta C}{\omega_i C_v^2} A_i^*(n) \\ 2j\varphi_i \dfrac{dA_i^*(n)}{dn} = -X_i \dfrac{b_s b_i \Delta C}{\omega_s C_v^2} A_s(n) \end{cases} \tag{18}$$

These equations are combined and yield

$$\begin{cases} \dfrac{d^2A_s(n)}{dn^2} = \dfrac{1}{4} \dfrac{X_s X_i}{\varphi_s \varphi_i \omega_s \omega_i} \left(\dfrac{b_s b_i \Delta C}{C_v^2} \right)^2 A_s(n) \\ \dfrac{d^2A_i^*(n)}{dn^2} = \dfrac{1}{4} \dfrac{X_s X_i}{\varphi_s \varphi_i \omega_s \omega_i} \left(\dfrac{b_s b_i \Delta C}{C_v^2} \right)^2 A_i^*(n) \end{cases} \tag{19}$$

The remaining wave pairs can be treated in the same way and the results will be,

if the phase condition $\varphi_p = \varphi_s + \varphi_i$ is satisfied, differential equations according to (19) are obtained for the wave pairs in (15),

if the phase condition $\varphi_p = \varphi_s - \varphi_i$ is satisfied, the following differential equations are obtained for the wave pairs in (16)

$$\begin{cases} \dfrac{d^2C_s(n)}{dn^2} = -\dfrac{1}{4} \dfrac{X_s X_i}{\varphi_s \varphi_i \omega_s \omega_i} \left(\dfrac{b_s b_i \Delta C}{C_v^2} \right) C_s(n) \\ \dfrac{d^2C_i^*(n)}{dn^2} = -\dfrac{1}{4} \dfrac{X_s X_i}{\varphi_s \varphi_i \omega_s \omega_i} \left(\dfrac{b_s b_i \Delta C}{C_v^2} \right) C_i^*(n) \end{cases} \tag{20}$$

and if the phase condition $\varphi_p = \varphi_i - \varphi_s$ is satisfied, differential equations according to (20) are obtained for the wave pairs in (17).

The solutions of differential equations (19) and (20) become exponential or periodic functions due to the signs of X_s and X_i. The periodic solutions lead to parametric backward-wave amplification, where signal and idling waves have group velocities with opposite directions, and according to P K Tien[2], this amplification is unstable and principally narrow-banded. In this paper, interest lies only in wide-band parametric amplification, and thus only circuits leading to exponential solutions of differential equations (19) and (20) will be dealt with. In fulfilling the phase condition $\varphi_p = \varphi_s + \varphi_i$, exponential solutions are obtained when X_s and X_i have the same sign, and in fulfilling one of the two remaining phase conditions, exponential solutions are obtained when X_s and X_i have different signs.

Exponential solutions of the following type are obtained for the wave pairs in (15)

$$e^{\pm\frac{1}{2}\frac{b_s b_i \Delta C}{C_v^2}\sqrt{\frac{X_s X_i}{\varphi_s \varphi_i \omega_s \omega_i}}\cdot n} \tag{21}$$

Consider the boundary conditions at the filter ladder input

$$\begin{cases} V_s(n=0,t) = V_0 \cdot e^{j(\omega_s t+\Theta)} \\ V_i(n=0,t) = 0 \end{cases} \tag{22}$$

and by means of (18) the following solutions are obtained

$$\begin{cases} V_s(n,t) = V_0 \cosh\left[\frac{1}{2}\frac{b_s b_i \Delta C}{C_v^2}\sqrt{\frac{X_s X_i}{\varphi_s \varphi_i \omega_s \omega_i}}n\right] e^{j(\omega_s t - n\varphi_s+\Theta)} \\ V_i(n,t) = jV_0\sqrt{\frac{\omega_i Z_i}{\omega_s Z_s}}\sinh\left[\frac{1}{2}\frac{b_s b_i \Delta C}{C_v^2}\sqrt{\frac{X_s X_i}{\varphi_s \varphi_i \omega_s \omega_i}}n\right] e^{-j(\omega_i t - n\varphi_i-\Theta)} \end{cases} \tag{23}$$

From the expressions for the signal and idling voltages in (23) it is seen that MANLEY-ROWE[5] power relations are fulfilled, and for signal power P_s and idling power P_i

$$\frac{P_s - (P_s)_{in}}{\omega_s} = \frac{P_i}{\omega_i} \tag{24}$$

holds true.

If the circuit has a length of N filter sections, the amplification F expressed in db for the signal wave will be

$$F = 20 \log\cosh\left[\frac{1}{2}\frac{b_s b_i \Delta C}{C_v^2}\sqrt{\frac{X_s X_i}{\varphi_s \varphi_i \omega_s \omega_i}}N\right] \tag{25}$$

The remaining wave pairs in (16) and (17) are treated in the same way, and similar solutions and expressions are obtained for the amplification.

1.33 The Bandwidth

In order to obtain wide-band amplification, the phase condition in (14) should be satisfied within the largest possible frequency range. Assume the pump frequency to be fixed, and let the signal and idling frequencies vary. In this way the following wide-band conditions are obtained.

If the phase condition $\varphi_p = \varphi_s + \varphi_i$ is satisfied,

$$\left(\frac{d\varphi}{d\omega}\right)_s - \left(\frac{d\varphi}{d\omega}\right)_i = 0 \tag{26}$$

holds for the phase angles.

If one of the phase conditions $\varphi_p = \varphi_s - \varphi_i$ and $\varphi_p = \varphi_i - \varphi_s$ is satisfied,

$$\left(\frac{d\varphi}{d\omega}\right)_s + \left(\frac{d\varphi}{d\omega}\right)_i = 0 \tag{27}$$

holds true for the phase angles.

Equations (26) and (27) imply that the signal and idling waves have the same group velocity.

In order to calculate the bandwidth of the amplifier, expressions for the amplification are necessary when the phase conditions in (14) are not exactly fulfilled, but can be written

$$\varphi_p = \varphi_s + \varphi_i + \Delta\varphi;\ \ \varphi_p = \varphi_s - \varphi_i + \Delta\varphi;\ \ \varphi_p = \varphi_i - \varphi_s + \Delta\varphi_i \tag{28}$$

Assume $\Delta\varphi \ll \varphi$. The coupled wave pairs will then be the same as those in (15), (16) and (17). It is decided to treat the first wave pair in (15) and introduce the corrected phase angles

$$\varphi_s' = \varphi_s + k_s\Delta\varphi;\ \ \varphi_i' = \varphi_i + k_i\Delta\varphi;\ \ k_s + k_i = 1 \quad \varphi_p = \varphi_s' + \varphi_i' \tag{29}$$

According to P K Tien,[2] $k_s = k_i = \frac{1}{2}$, and introduction of the first wave pair in (15) into equation (13) then yields (provided that the perturbation terms are small so that $\frac{d^2A}{dn^2}$ can be neglected compared with $\varphi \frac{dA}{dn}$ and with $\Delta\varphi \ll \varphi$)

$$\begin{cases} -\varphi_s\Delta\varphi A_s(n) - 2j\varphi_s \dfrac{dA_s(n)}{dn} = -X_s \dfrac{b_s b_i \Delta C}{\omega_i C_v^2} A_i^*(n) \\ -\varphi_i\Delta\varphi A_i^*(n) + 2j\varphi_i \dfrac{dA_i^*(n)}{dn} = -X_i \dfrac{b_s b_i \Delta C}{\omega_s C_v^2} A_s(n) \end{cases} \tag{30}$$

These equations are combined and give

$$\begin{cases} \dfrac{d^2A_s(n)}{dn^2} = \dfrac{1}{4}\left[\dfrac{X_s X_i}{\varphi_s\varphi_i\omega_s\omega_i}\left(\dfrac{b_s b_i \Delta C}{C_v^2}\right)^2 - (\Delta\varphi)^2\right] A_s(n) \\ \dfrac{d^2A_i^*(n)}{dn^2} = \dfrac{1}{4}\left[\dfrac{X_s X_i}{\varphi_s\varphi_i\omega_s\omega_i}\left(\dfrac{b_s b_i \Delta C}{C_v^2}\right)^2 - (\Delta\varphi)^2\right] A_i^*(n) \end{cases} \tag{31}$$

Interest only lies in the decrease of the amplification given by a divergence from the phase conditions in (14), and thus only the exponential solutions are considered where

$$(\Delta\varphi)^2 \leqq \left| \frac{X_s X_i}{\varphi_s \varphi_i \omega_s \omega_i} \right| \left(\frac{b_s b_i C}{C_v^2} \right)^2 \tag{32}$$

For the wave pairs in (15), solutions are obtained of the type

$$e^{\pm \frac{1}{2} \sqrt{\frac{X_s X_i}{\varphi_s \varphi_i \omega_s \omega_i} \left(\frac{b_s b_i \Delta C}{C_v^2} \right)^2 - (\Delta\varphi)^2}\, n} \tag{33}$$

The boundary conditions (22) are considered at the filter ladder input and by means of (30) the following solutions are obtained

$$\begin{cases} V_s(n,t) = V_0 \left[\cosh\left(\frac{1}{2}\xi n\right) + j \frac{\Delta\varphi}{\xi} \sinh\left(\frac{1}{2}\xi n\right) \right] e^{j(\omega_s t - n\varphi_s + \Theta)} \\ V_i(n,t) = j V_0 \frac{\frac{X_i}{\varphi_i \omega_s} \frac{b_s b_i \Delta C}{C_v^2}}{\xi} \sinh\left(\frac{1}{2}\xi n\right) e^{-j(\omega_i t - n\varphi_i - \Theta)} \end{cases} \tag{34}$$

where $\xi = \sqrt{\frac{X_s X_i}{\varphi_s \varphi_i \omega_s \omega_i} \left(\frac{b_s b_i \Delta C}{C_v^2} \right)^2 - (\Delta\varphi)^2}$

From the expressions in (34) is evident that MANLEY-ROWE[5] power relations according to equation (24) are satisfied.

The circuit has a length of a number of filter sections N, and then the amplification F of the signal wave expressed in db will be

$$F = 10 \cdot \log \left[\cosh^2\left(\frac{1}{2}\xi N\right) + \frac{(\Delta\varphi)^2}{\xi^2} \sinh^2\left(\frac{1}{2}\xi N\right) \right] \tag{35}$$

The remaining wave pairs in (16) and (17) can be treated in the same way and give similar solutions and expressions for the amplification.

1.4 Circuits with Concentrated Elements

The treatment will now proceed to consider parametric travelling-wave amplifiers where the reactances and susceptances inserted in the filter ladder have such large values that the approximation to a homogeneous line is not permissible. The frequencies lie within the transmission range of the filter ladder, where $0 < BX < 4$ holds true, and the calculations are made by using filter theory. The filter ladder consists of π- or T-sections built up according to *fig. 3.*

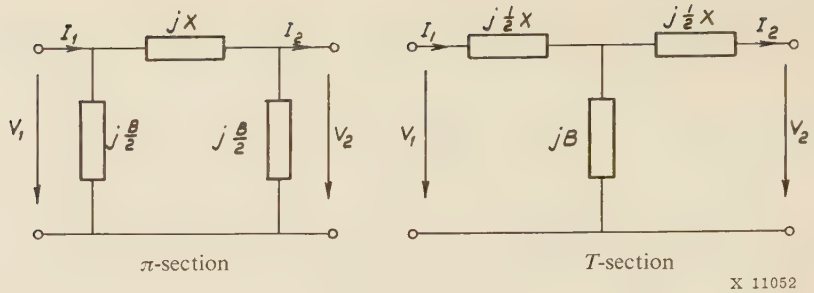

Fig. 3. π or T-section inserted in the filter ladder.

For the characteristic impedance and phase shift per section of the filter ladder at the actual frequencies, the following equations hold true:

For a ladder composed of π-sections, the following equations are obtained

$$\begin{cases} (Z_0)_s = \sqrt{\dfrac{X_s}{B_s}} \dfrac{1}{\sqrt{1 - \dfrac{1}{4} B_s X_s}} \\ (Z_0)_i = \sqrt{\dfrac{X_i}{B_i}} \dfrac{1}{\sqrt{1 - \dfrac{1}{4} B_i X_i}} \\ (Z_0)_p = \sqrt{\dfrac{X_p}{B_p}} \dfrac{1}{\sqrt{1 - \dfrac{1}{4} B_p X_p}} \end{cases} \tag{36}$$

For a ladder composed of T-sections, the following apply

$$\begin{cases} (Z_0)_s = \sqrt{\dfrac{X_s}{B_s} \left(1 - \dfrac{1}{4} B_s X_s\right)} \\ (Z_0)_i = \sqrt{\dfrac{X_i}{B_i} \left(1 - \dfrac{1}{4} B_i X_i\right)} \\ (Z_0)_p = \sqrt{\dfrac{X_p}{B_p} \left(1 - \dfrac{1}{4} B_p X_p\right)} \end{cases} \tag{37}$$

For a ladder composed of π-or T- sections, the equations below are obtained:

$$\begin{cases} \sin \varphi_s = \sqrt{B_s X_s \left(1 - \frac{1}{4} B_s X_s\right)} \\ \sin \varphi_i = \sqrt{B_i X_i \left(1 - \frac{1}{4} B_i X_i\right)} \\ \sin \varphi_p = \sqrt{B_p X_p \left(1 - \frac{1}{4} B_p X_p\right)} \end{cases} \tag{38}$$

According to equation (10), and knowing the coupling between the signal and idling waves, expressions can be found for the amplification. From the coupling terms (10), it follows that the condition for obtaining parametric amplification is that one of the phase conditions in (14) is satisfied, and then the coupled wave pairs will be the same as those contained in equations (15), (16) and (17).

It is decided to treat the first wave pair in (15), where $\varphi_s + \varphi_i = \varphi_p$. A ladder of T-sections is assumed, and in order to calculate the amplification, a filter section is investigated where the voltages and currents at the input are $(V_s)_1 e^{j\omega_s t}$, $(V_i)_1 e^{-j\omega_i t}$, $(I_s)_1 e^{j\omega_s t}$, and $(I_i)_1 e^{-j\omega_i t}$, and at the output $(V_s)_2 e^{j\omega_s t}$, $(V_i)_2 e^{-j\omega_i t}$, $(I_s)_2 e^{j\omega_s t}$, and $(I_i)_2 e^{-j\omega_i t}$.

After introducing the coupling between signal and idling waves, the following relations between voltages and currents are obtained:

$$\begin{cases} (V_s)_2 = (V_s)_1 \left[1 - \frac{1}{2} B_s X_s\right] - (I_s)_1 j X_s \left[1 - \frac{1}{4} B_s X_s\right] - (V_i)_1 \frac{1}{2} \delta_s X_s - (I_i)_1 j \frac{1}{4} \delta_s X_s X_i \\ (I_s)_2 = (I_s)_1 \left[1 - \frac{1}{2} B_s X_s\right] - (V_s)_1 j B_s + (I_i)_1 \frac{1}{2} \delta_s X_i - (V_i)_1 j \delta_s \\ (V_i)_2 = (V_i)_1 \left[1 - \frac{1}{2} B_i X_i\right] + (I_i)_1 j X_i \left[1 - \frac{1}{4} B_i X_i\right] - (V_s)_1 \frac{1}{2} \delta_i X_i + (I_s)_1 j \frac{1}{4} \delta_i X_s X_i \\ (I_i)_2 = (I_i)_1 \left[1 - \frac{1}{2} B_i X_i\right] + (V_i)_1 j B_i + (I_s)_1 \frac{1}{2} \delta_i X_s + (V_s)_1 j \delta_i \end{cases} \tag{39}$$

where

$$\begin{cases} \delta_s = \dfrac{b_s b_i \Delta C}{\omega_i C_v^2} \\ \delta_i = \dfrac{b_s b_i \Delta C}{\omega_s C_v^2} \end{cases} \tag{40}$$

1.41 Calculation of the Amplification

To be able to calculate the amplification some simplifying assumptions are made. Assume the filter section to lie midway along a filter ladder of infinite length, and to be matched in both directions. The following can then be written

$$\begin{cases} (Z_0)_s = \dfrac{(V_s)_2}{(I_s)_2} = \dfrac{(V_s)_1}{(I_s)_1} \\ (Z_0)_i = \dfrac{(V_i)_2}{(I_i)_2} = \dfrac{(V_i)_1}{(I_i)_1} \end{cases} \tag{41}$$

Furthermore, assume that the signal and idling waves have been coupled to each other by an infinite number of filter sections, so that a state of equilibrium between these waves has been reached, and thus

$$K = \frac{(V_s)_1}{(V_i)_1} = \left| \frac{(V_s)_2}{(V_i)_2} \right|$$

and since, at the same time, the phase condition $\varphi_s + \varphi_i = \varphi_p$ must be fulfilled,

$$K = \frac{(V_s)_1}{(V_i)_1} = \frac{(V_s)_2}{(V_i)_2} \cdot e^{j\varphi_p} \tag{42}$$

holds true.

For the calculation of the amplification a perturbation calculation is applied and all the perturbation terms of second order neglected. Introduce K according to equation (42) into equation (39) and assume the characteristic impedances $(Z_0)_s$ and $(Z_0)_i$ to contain perturbation terms compared with the impedances for the uncoupled line,

$$\begin{cases} (Z_0)_s = \sqrt{\dfrac{X_s}{B_s}\left(1 - \dfrac{1}{4} B_s X_s\right)}\,[1 + \Delta_s] \\ (Z_0)_i = \sqrt{\dfrac{X_i}{B_i}\left(1 - \dfrac{1}{4} B_i X_i\right)}\,[1 + \Delta_i] \end{cases} \tag{43}$$

that are introduced into equations (39) and yield

$$\begin{cases} (V_s)_2 = (V_s)_1 e^{-j\varphi_s} \left\{ 1 + j\Delta_s \sin\varphi_s e^{j\varphi_s} - \frac{1}{2} \frac{\delta_s X_s}{\cos\frac{1}{2}\varphi_i} \frac{1}{K} e^{j\frac{1}{2}\varphi_i} \cdot e^{j\varphi_s} \right\} \\ (I_s)_2 = (I_s)_1 e^{-j\varphi_s} \left\{ 1 - j\Delta_s \sin\varphi_s e^{j\varphi_s} - j\frac{1}{2} \frac{\delta_s X_s}{\cos\frac{1}{2}\varphi_i} \frac{\cos\frac{1}{2}\varphi_s}{\sin\frac{1}{2}\varphi_s} \frac{1}{K} e^{j\frac{1}{2}\varphi_i} \cdot e^{j\varphi_s} \right\} \\ (V_i)_2 = (V_i)_1 e^{j\varphi_i} \left\{ 1 - j\Delta_i \sin\varphi_i e^{-j\varphi_i} - \frac{1}{2} \frac{\delta_i X_i}{\cos\frac{1}{2}\varphi_s} K e^{-j\frac{1}{2}\varphi_s} \cdot e^{-j\varphi_i} \right\} \\ (I_i)_2 = (I_i)_1 e^{j\varphi_i} \left\{ 1 + j\Delta_i \sin\varphi_i e^{-j\varphi_i} + j\frac{1}{2} \frac{\delta_i X_i}{\cos\frac{1}{2}\varphi_s} \frac{\cos\frac{1}{2}\varphi_i}{\sin\frac{1}{2}\varphi_i} K e^{-j\frac{1}{2}\varphi_s} \cdot e^{-j\varphi_i} \right\} \end{cases} \tag{44}$$

Considering the assumption in (41) for equations (44), Δ_s and Δ_i can be expressed in terms of K as follows

$$\begin{cases} \Delta_s = -\frac{1}{4} \frac{\delta_s X_s}{\cos\frac{1}{2}\varphi_i} \frac{e^{j\frac{1}{2}(\varphi_s+\varphi_i)}}{\sin\varphi_s \sin\frac{1}{2}\varphi_s} \frac{1}{K} \\ \Delta_i = -\frac{1}{4} \frac{\delta_i X_i}{\cos\frac{1}{4}\varphi_s} \frac{e^{-j\frac{1}{2}(\varphi_s+\varphi_i)}}{\sin\varphi_i \sin\frac{1}{2}\varphi_i} K \end{cases} \tag{45}$$

which, when introduced into (44) yield

$$\begin{cases} (V_s)_2 = (V_s)_1 e^{-j\varphi_s} \left\{ 1 - j\frac{1}{4} \frac{\delta_s X_s}{\cos\frac{1}{2}\varphi_i} \frac{e^{j\frac{1}{2}(\varphi_s+\varphi_i)}}{\sin\frac{1}{2}\varphi_s} \frac{1}{K} \right\} \\ (V_i)_2 = (V_i)_1 e^{j\varphi_i} \left\{ 1 + j\frac{1}{4} \frac{\delta_i X_i}{\cos\frac{1}{2}\varphi_s} \frac{e^{-j\frac{1}{2}(\varphi_s+\varphi_i)}}{\sin\frac{1}{2}\varphi_i} K \right\} \end{cases} \tag{46}$$

Now consider also the assumption in (42), and K can then be solved from (46).

$$K = \pm j \sqrt{\frac{\delta_s \sqrt{\frac{X_s}{B_s}\left(1 - \frac{1}{4} B_s X_s\right)}}{\delta_i \sqrt{\frac{X_i}{B_i}\left(1 - \frac{1}{4} B_i X_i\right)}}} e^{j\frac{1}{2}(\varphi_s+\varphi_i)} \tag{47}$$

It is evident from expression (47) for K that for the filter section, MANLEY-ROWE[5] power relations are satisfied and can be written

$$\frac{(V_s)_2 (I_s)_2^* - (V_s)_1 (I_s)_1^*}{\omega_s} = \frac{(V_i)_2 (I_i)_2^* - (V_i)_2 (I_i)_1^*}{\omega_i} \tag{48}$$

Equation (47) for K is introduced into equations (46) and yields

$$\begin{cases} (V_s)_2 = (V_s)_1 e^{-j\varphi_s} \left\{ 1 \mp \frac{1}{2} \sqrt{\frac{\delta_s \delta_i X_s X_i}{\sin\varphi_s \sin\varphi_i}} \right\} \\ (V_i)_2 = (V_i)_1 e^{j\varphi_i} \left\{ 1 \mp \frac{1}{2} \sqrt{\frac{\delta_s \delta_i X_s X_i}{\sin\varphi_s \sin\varphi_i}} \right\} \end{cases} \tag{49}$$

In the case of homogeneous lines there was only interest in exponential solutions of differential equations (19) and (20), and for circuits with concentrated elements this corresponds to the fact that the expressions within the brackets in equation (49) are real, which is realized on the same conditions that are required for exponential solutions in a homogeneous line. Thus solution (49) corresponds to the exponential solution (21) for a homogeneous line, and if the boundary conditions (22) are considered, the following solutions are obtained by means of expression (47) for K.

$$\begin{cases} V_s(n,t) = V_0 \dfrac{\overset{n}{\underset{0}{\pi}} \left(1 + \frac{1}{2} \sqrt{\frac{\delta_s \delta_i X_s X_i}{\sin\varphi_s \sin\varphi_i}} \right) + \overset{n}{\underset{0}{\pi}} \left(1 - \frac{1}{2} \sqrt{\frac{\delta_s \delta_i X_s X_i}{\sin\varphi_s \sin\varphi_i}} \right)}{2} e^{j(\omega_s t - n\varphi_s + \Theta)} \\ V_i(n,t) = jV_0 \sqrt{\frac{\delta_i Z_i}{\delta_s Z_s}} \dfrac{\overset{n}{\underset{0}{\pi}} \left(1 + \frac{1}{2} \sqrt{\frac{\delta_s \delta_i X_s X_i}{\sin\varphi_s \sin\varphi_i}} \right) - \overset{n}{\underset{0}{\pi}} \left(1 - \frac{1}{2} \sqrt{\frac{\delta_s \delta_i X_s X_i}{\sin\varphi_s \sin\varphi_i}} \right)}{2} \end{cases} \tag{50}$$

$$e^{-j(\omega_i t - n\varphi_i - \Theta)} \cdot e^{-j\frac{1}{2}(\varphi_s + \varphi_i)}$$

The circuit has a length of N filter sections, and amplification F for the signal wave will be

$$F = 20 \log \frac{1}{2} \left\{ \overset{N}{\underset{0}{\pi}} \left(1 + \frac{1}{2} \sqrt{\frac{\delta_s \delta_i X_s X_i}{\sin\varphi_s \sin\varphi_i}} \right) + \overset{N}{\underset{0}{\pi}} \left(1 - \frac{1}{2} \sqrt{\frac{\delta_s \delta_i X_s X_i}{\sin\varphi_s \sin\varphi_i}} \right) \right\} \tag{51}$$

The remaining wave pairs in (16) and (17) are treated in the same way, and similar solutions and expressions for the amplification are obtained.

1.42 The Bandwidth

In order to obtain wide-band amplification, the phase condition in (14) should be satisfied within the largest possible frequency range and these wide-band conditions are expressed in equations (26) and (27) and hold also for circuits with concentrated elements.

In order to determine the bandwidth, the amplification must be calculated when phase conditions (14) are not exactly fulfilled, but can be written according to (28). The phase divergence is assumed to be so small that the coupled wave pairs will be the same as before. Now restrict the treatment to the first wave pair in (15), introduce the same assumptions used when the phase condition was satisfied, and follow the same sequence of calculation as far as to equation (46). Corrected phase angles,

$$\varphi_s' = \varphi_s + \frac{1}{2}\Delta\varphi \qquad \varphi_i' = \varphi_i + \frac{1}{2}\Delta\varphi \qquad \varphi_s' + \varphi_i = \varphi_p$$

are now introduced into equation (46) and the following obtained

$$\left\{\begin{array}{l} (V_s)_2 = (V_s)_1 e^{-j\varphi_s'}\left\{1 + j\frac{1}{2}\Delta\varphi - j\frac{1}{4}\frac{\delta_s X_s}{\cos\frac{1}{2}\varphi_i}\frac{e^{j\frac{1}{2}(\varphi_s+\varphi_i)}}{\sin\frac{1}{2}\varphi_s}\frac{1}{K}\right\} \\ (V_i)_2 = (V_i)_1 e^{j\varphi_i'}\left\{1 - j\frac{1}{2}\Delta\varphi + j\frac{1}{4}\frac{\delta_i X_i}{\cos\frac{1}{2}\varphi_s}\frac{e^{-j\frac{1}{2}(\varphi_s+\varphi_i)}}{\sin\frac{1}{2}\varphi_i}K\right\} \end{array}\right. \tag{52}$$

By means of the assumption in (42), K can be solved from (52) and becomes

$$K = 2\frac{\cos\frac{1}{2}\varphi_s \sin\frac{1}{2}\varphi_i}{\delta_i X_i}\left\{\Delta\varphi \pm j\sqrt{\frac{\delta_s\delta_i X_s X_i}{\sin\varphi_s\sin\varphi_i} - (\Delta\varphi)^2}\right\}e^{j\frac{1}{2}(\varphi_s+\varphi_i)} \tag{53}$$

From the expression for K it is evident that MANLEY-ROWE[5] power relations according to (48) are satisfied.

Expression (53) for K is introduced into equations (52) and yields

$$\left\{\begin{array}{l} (V_s)_2 = (V_s)_1 e^{-j\varphi_s'}\left\{1 \mp \frac{1}{2}\sqrt{\frac{\delta_s\delta_i X_s X_i}{\sin\varphi_s\sin\varphi_i} - (\Delta\varphi)^2}\right\} \\ (V_i)_2 = (V_i)_1 e^{j\varphi_i'}\left\{1 \mp \frac{1}{2}\sqrt{\frac{\delta_s\delta_i X_s X_i}{\sin\varphi_s\sin\varphi_i} - (\Delta\varphi)^2}\right\} \end{array}\right. \tag{54}$$

Solution (54) corresponds to the exponential solution (33) for the homogeneous line, and as there is only interest in the decrease of amplification given by the divergence from the phase condition,

$$(\Delta\varphi)^2 \leqq \left| \frac{\delta_s \delta_i X_s X_i}{\sin\varphi_s \sin\varphi_i} \right| \tag{55}$$

holds true.

In taking into consideration the boundary conditions (22), by means of expression (54) for K, the following solutions are obtained

$$\begin{cases} V_s(n,t) = V_0 \underbrace{\left\{ \frac{\overset{n}{\underset{0}{\pi}}\left(1+\frac{1}{2}\xi\right) + \overset{n}{\underset{0}{\pi}}\left(1-\frac{1}{2}\xi\right)}{2} + j\frac{\Delta\varphi}{\xi}\frac{\overset{n}{\underset{0}{\pi}}\left(1+\frac{1}{2}\xi\right) - \overset{n}{\underset{0}{\pi}}\left(1-\frac{1}{2}\xi\right)}{2} \right\}}_{e^{j(\omega_s t - n\varphi_s' + \Theta)}} \\ V_i(n,t) = jV_0 \underbrace{\frac{\delta_i X_i}{\xi\sqrt{X_i B_i\left(1-\frac{1}{4}B_s X_s\right)}}\frac{\overset{n}{\underset{0}{\pi}}\left(1+\frac{1}{2}\xi\right) - \overset{n}{\underset{0}{\pi}}\left(1-\frac{1}{2}\xi\right)}{2}}_{e^{-j(\omega_i t - n\varphi_i' + \Theta)} \cdot e^{-j\frac{1}{2}(\varphi_s + \varphi_i)}} \end{cases} \tag{56}$$

where

$$\xi = \sqrt{\frac{\delta_s \delta_i X_s X_i}{\sin\varphi_s \sin\varphi_i} - (\Delta\varphi)^2}$$

The circuit has a length of N filter sections, and amplification F for the signal wave becomes

$$F = 10\log\frac{1}{4}\left\{\left[\overset{N}{\underset{0}{\pi}}\left(1+\frac{1}{2}\xi\right) + \overset{N}{\underset{0}{\pi}}\left(1-\frac{1}{2}\xi\right)\right]^2 + \frac{(\Delta\varphi)^2}{\xi^2}\left[\overset{N}{\underset{0}{\pi}}\left(1+\frac{1}{2}\xi\right) - \overset{N}{\underset{0}{\pi}}\left(1-\frac{1}{2}\xi\right)\right]^2\right\} \tag{57}$$

The remaining wave pairs in (16) and (17) are treated in the same way, and similar solutions and expressions for the amplification are obtained.

1.5 Summary of the Results

The theoretical results will now be summarized and formulas proposed that are essential in constructing a parametric travelling-wave amplifier.

In order to obtain parametric travelling-wave amplification, the frequency condition $\omega_s + \omega_i = \omega_p$ and one of the following three phase conditions must be satisfied

1) $\varphi_s + \varphi_i = \varphi_p$ 2) $\varphi_s - \varphi_i = \varphi_p$ 3) $\varphi_i - \varphi_s = \varphi_p$

The first phase condition is written for a homogeneous line

$$\sqrt{B_s X_s} + \sqrt{B_i X_i} = \sqrt{B_p X_p} \tag{58}$$

and for a circuit with concentrated elements

$$\left(1 - \frac{1}{2} B_i X_i\right) \sqrt{B_s X_s \left(1 - \frac{1}{4} B_s X_s\right)} + \left(1 - \frac{1}{2} B_s X_s\right) \sqrt{B_i X_i \left(1 - \frac{1}{4} B_i X_i\right)} = \\ = \sqrt{B_p X_p \left(1 - \frac{1}{4} B_p X_p\right)} \tag{59}$$

The second phase condition is written for a homogeneous line

$$\sqrt{B_s X_s} - \sqrt{B_i X_i} = \sqrt{B_p X_p} \tag{60}$$

and for a circuit with concentrated elements

$$\left(1 - \frac{1}{2} B_i X_i\right) \sqrt{B_s X_s \left(1 - \frac{1}{4} B_s X_s\right)} - \left(1 - \frac{1}{2} B_s X_s\right) \sqrt{B_i X_i \left(1 - \frac{1}{4} B_i X_i\right)} = \\ = \sqrt{B_p X_p \left(1 - \frac{1}{4} B_p X_p\right)} \tag{61}$$

The third phase condition is written for a homogeneous line

$$\sqrt{B_i X_i} - \sqrt{B_s X_s} = \sqrt{B_p X_p} \tag{62}$$

and for a circuit with concentrated elements

$$\left(1 - \frac{1}{2} B_s X_s\right) \sqrt{B_i X_i \left(1 - \frac{1}{4} B_i X_i\right)} - \left(1 - \frac{1}{2} B_i X_i\right) \sqrt{B_s X_s \left(1 - \frac{1}{4} B_s X_s\right)} = \\ = \sqrt{B_p X_p \left(1 - \frac{1}{4} B_p X_p\right)} \tag{63}$$

When the first phase condition is fulfilled, a stable forward-wave amplification is obtained when X_s and X_i have the same sign, and the amplification for the signal wave can be written:

for a homogeneous line

$$F = 20 \log \cosh \left[\frac{1}{2} \frac{b_s b_i \Delta C}{C_v^2} \sqrt{\frac{X_s X_i}{\varphi_s \varphi_i \omega_s \omega_i}} N \right] \tag{64}$$

for a circuit with concentrated elements

$$F = 20 \log \frac{1}{2} \left\{ \pi_0^N \left(1 + \frac{1}{2} \sqrt{\frac{\delta_s \delta_i X_s X_i}{\sin \varphi_s \sin \varphi_i}} \right) + \pi_0^N \left(1 - \frac{1}{2} \sqrt{\frac{\delta_s \delta_i X_s X_i}{\sin \varphi_s \sin \varphi_i}} \right) \right\} \tag{65}$$

When the second or third phase condition is fulfilled, a stable forward-wave amplification is obtained when X_s and X_i have different signs, and the amplification for the signal wave can be written:

for a homogeneous line

$$F = 20 \log \cosh \left[\frac{1}{2} \frac{b_s b_i \Delta C}{C_v^2} \sqrt{\frac{X_s X_i}{\varphi_s \varphi_i \omega_s \omega_i}} N \right] \tag{66}$$

for a circuit with concentrated elements

$$F = 20 \log \frac{1}{2} \left\{ \pi_0^N \left(1 + \frac{1}{2} \sqrt{-\frac{\delta_s \delta_i X_s X_i}{\sin \varphi_s \sin \varphi_i}} \right) + \pi_0^N \left(1 - \frac{1}{2} \sqrt{-\frac{\delta_s \delta_i X_s X_i}{\sin \varphi_s \sin \varphi_i}} \right) \right\} \tag{67}$$

In order to obtain wide-band amplification, the phase conditions should be satisfied within the largest possible frequency range, and this will lead to the fact that the phase angles should fulfil the following wide-band conditions.

When the first phase condition is satisfied, equation (26) should hold true, and can be written:

for a homogeneous line

$$\frac{d}{d\omega_s} \left(\sqrt{B_s X_s} \right) - \frac{d}{d\omega_i} \left(\sqrt{B_i X_i} \right) = 0 \tag{68}$$

for a circuit with concentrated elements

$$\frac{\frac{d}{d\omega_s} (B_s X_s)}{\sqrt{B_s X_s \left(1 - \frac{1}{4} B_s X_s \right)}} - \frac{\frac{d}{d\omega_i} (B_i X_i)}{\sqrt{B_i X_i \left(1 - \frac{1}{4} B_i X_i \right)}} = 0 \tag{69}$$

When the second or third phase condition is satisfied, equation (27) should hold true, and this equation can be written:

for a homogeneous line

$$\frac{d}{d\omega_s}\left(\sqrt{B_sX_s}\right)+\frac{d}{d\omega_i}\left(\sqrt{B_iX_i}\right)=0 \tag{70}$$

for a circuit with concentrated elements

$$\frac{\frac{d}{d\omega_s}(B_sX_s)}{\sqrt{B_sX_s\left(1-\frac{1}{4}B_sX_s\right)}}+\frac{\frac{d}{d\omega_i}(B_iX_i)}{\sqrt{B_iX_i\left(1-\frac{1}{4}B_iX_i\right)}}=0 \tag{71}$$

The wide-band conditions imply that the signal and idling waves have the same group velocity.

In order to determine the bandwidth of the amplifier, it should be possible to calculate the amplification at the band edges, where the phase conditions are not exactly fulfilled, but can be written according to equation (28).

When the first phase condition is almost satisfied, the amplification for the signal wave can be written:

for a homogeneous line

$$F=10\log\left[\cosh^2\left(\frac{1}{2}\xi N\right)+\frac{(\Delta\varphi)^2}{2}\sinh^2\left(\frac{1}{2}\xi N\right)\right] \tag{72}$$

where

$$\xi=\sqrt{\frac{X_sX_i}{\varphi_s\varphi_i\omega_s\omega_i}\left(\frac{b_sb_i\Delta C}{C_v^2}\right)^2-(\Delta\varphi)^2}$$

for a circuit with concentrated elements

$$F=10\log\frac{1}{4}\left\{\left[\underset{0}{\overset{N}{\pi}}\left(1+\frac{1}{2}\xi\right)+\underset{0}{\overset{N}{\pi}}\left(1-\frac{1}{2}\xi\right)\right]^2+\frac{(\Delta\varphi)^2}{\xi^2}\left[\underset{0}{\overset{N}{\pi}}\left(1+\frac{1}{2}\xi\right)-\underset{0}{\overset{N}{\pi}}\left(1-\frac{1}{2}\xi\right)\right]^2\right\} \tag{73}$$

where

$$\xi=\sqrt{\frac{\delta_s\delta_iX_sX_i}{\sin\varphi_s\sin\varphi_i}-(\Delta\varphi)^2}$$

When the second or the third phase condition is almost satisfied, the amplification of the signal wave for a homogeneous line is calculated from equation (72), but with

$$\xi = \sqrt{-\frac{X_s X_i}{\varphi_s \varphi_i \omega_s \omega_i}\left(\frac{b_s b_i \Delta C}{C_v^2}\right)^2 - (\Delta\varphi)^2}$$

and for a circuit with concentrated elements from equation (73), but with

$$\xi = \sqrt{-\frac{\delta_s \delta_i X_s X_i}{\sin\varphi_s \sin\varphi_i} - (\Delta\varphi)^2}$$

The parametric travelling-wave amplifier should also be matched to its external circuits at signal, idling and pump frequencies. The external circuits have the impedances $(Z_{ext})_s$ $(Z_{ext})_i$ and $(Z_{ext})_p$ at these frequencies, and hence the following matching conditions are obtained:

$$\begin{cases} (Z_0)_s = (Z_{ext})_s \\ (Z_0)_i = (Z_{ext})_i \\ (Z_0)_p = (Z_{ext})_p \end{cases} \tag{74}$$

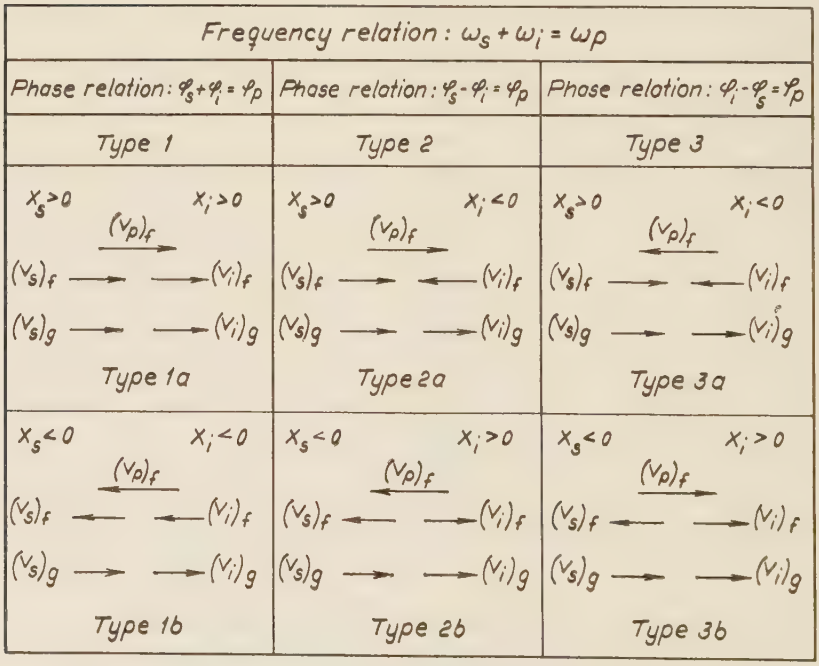

X 11053

Fig. 4. Table showing different types of parametric forward-wave amplifiers.

The characteristic impedances for a homogeneous line are obtained from equation (11), and for a circuit with concentrated elements from equation (36) or (37), due to whether the circuit is built up of π or T-sections.

It is known that, within the transmission range, $0 \leq BX \leq 4$ holds true for a filter ladder, and thus B and X have the same sign. If B and X are positive, the phase and group velocities of the circuit have the same direction. If B and X are negative, the phase and group velocities of the circuit have opposite directions. Now different types of parametric travelling-wave amplifiers can be classified according to the phase condition fulfilled, and the phase and group velocities of the different waves scheduled. In *fig. 4*, index f indicates phase velocity, and index g group velocity.

CHAPTER 2

Circuits Composed of LC-Circuits

For the construction of travelling-wave amplifiers for lower frequencies, the reactances and susceptances inserted in the filter ladder can be composed of coils and capacitors, *LC*-circuits. In order to obtain a survey of the different types of filters that can be built, the reactances that can be built from *LC*-circuits will first be systemized.

2.1 Classification of Reactance Elements

The reactances that are inductive at low frequency ≈ 0, are to be classified among inductive elements, and the reactances that are capacitive at low frequency ≈ 0, among capacitive elements. Inductive elements are written $L_{()}$ and capacitive elements are denoted $C_{()}$. The index figure of $L_{()}$ and $C_{()}$ indicates the order of the element. Now the synthesis made by R M Foster[6] will be followed, and then the following dispositions of inductive and capacitive elements obtained.

The dispositions in *fig. 5* and *6* show the simplest construction of an element of a certain order. It is schematically shown in the dispositions how the reactance and susceptance of the elements vary with frequency.

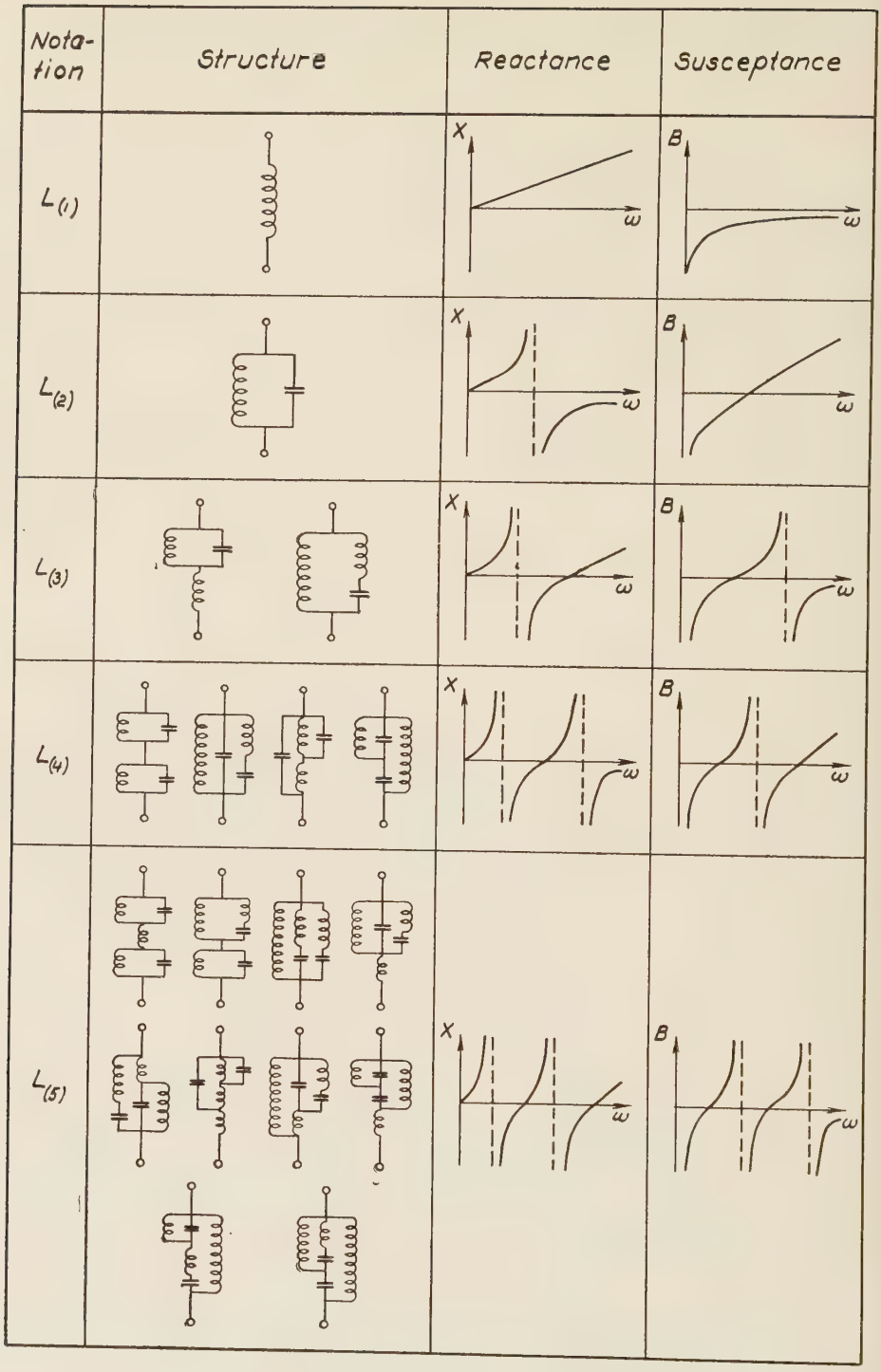

Fig. 5. Arrangement of inductive elements.

X 11054

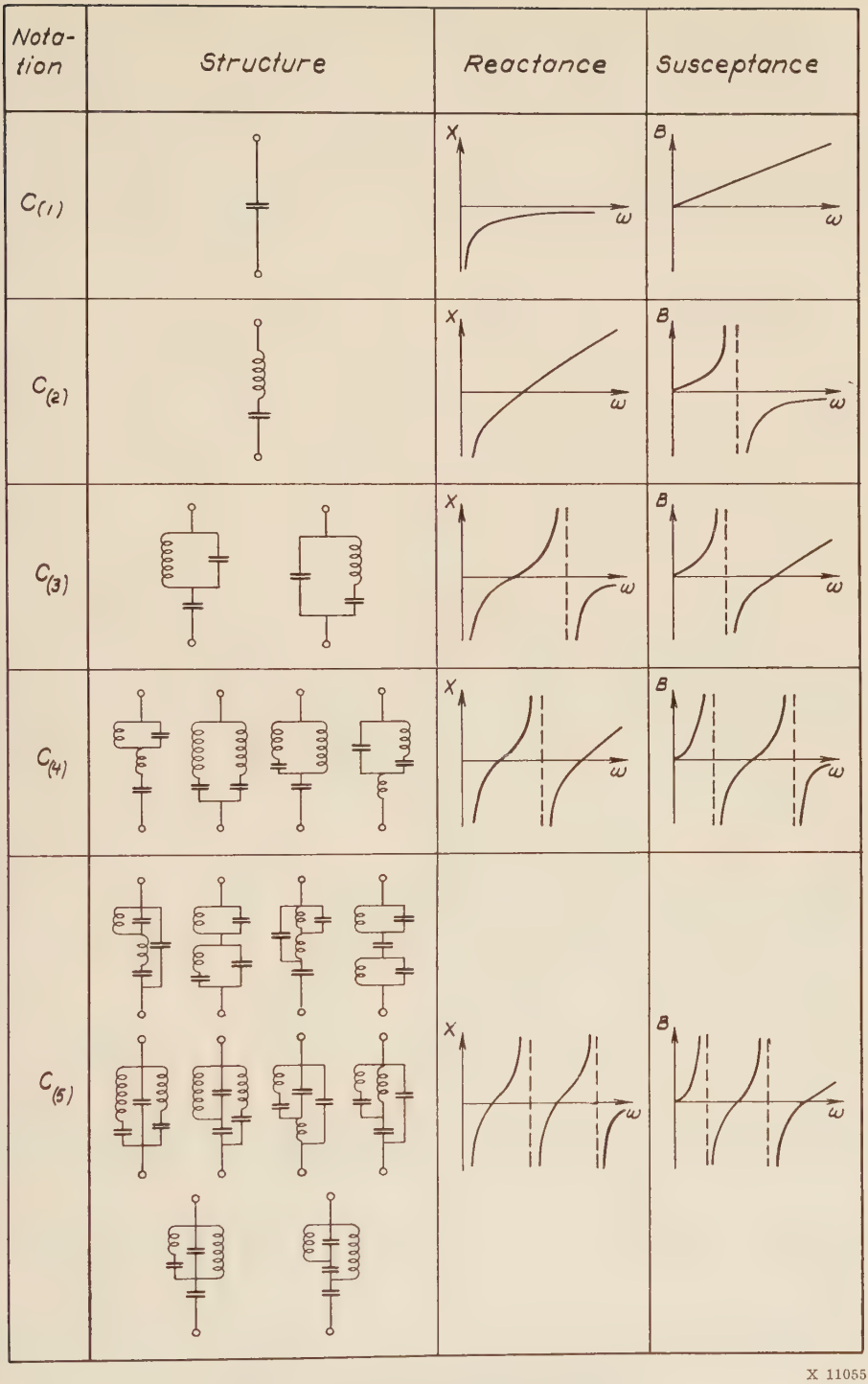

X 11055

Fig. 6. Arrangement of capacitive elements.

2.2 Different Filter Types

After systematization of the different reactance elements, opinion can be formed on the filter types required to realize the different types of parametric amplifiers. The filter ladder consists of π- or T-sections (see example in *fig. 7*) where the same φ-ω-diagram is to be obtained.

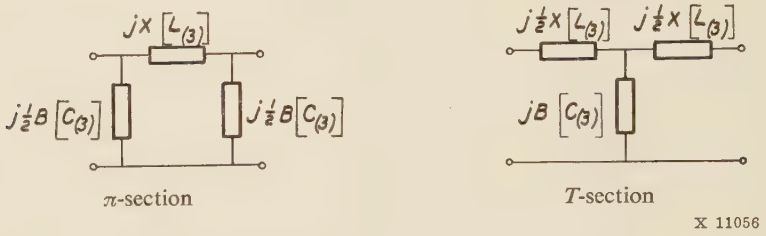

Fig. 7. Example of filter sections for parametric amplifier.

In the following, a filter section according to *fig. 7* will be written schematically $\underline{L_{(3)}}$ / $C_{(3)}$.

Knowing the variation with frequency of reactances and susceptances, the φ-ω-diagram of the filter is obtained. It is then assumed that the series reactance and parallel susceptance cross zero at the same frequency. A small divergence from this gives a narrow attenuating band around $\varphi = 0$. The signal, idling, and pump frequencies are drawn in the φ-ω-diagrams and the circuits can be classified into four groups according to the distribution of frequencies in the pass-bands of the circuits.

From the schedule showing different filter types, it is evident how the signal and pump sources should be connected to the circuit. In this

$\boxed{S}$ = signal source

$\boxed{P}$ = pump source

hold true.

The filters shown are of simplest possible design, and can also be built from reactance elements of a higher order. This may be necessary to obtain the desired filter characteristics.

2.21 Signal, Idling, and Pump Frequencies within the same Pass-band

In this type of circuit, operation is within the linear part of the φ-ω-diagram, where the phase and wide-band conditions are automatically satisfied, and the amplification can be calculated as for a homogeneous line. The filter ladder must also be matched to external

circuits, and the characteristic impedance is then equal at all three frequencies. It is important that the φ-ω-characteristic diverges when $\omega > \omega_p$, since otherwise, according to G M Roe and M R Boyd,[4] power-absorbing coupled wave-pairs at higher frequencies would be obtained. In this type of circuit, a very large bandwidth is obtained. At 12 db amplification, the bandwidth will be 100 percent, but in return a great number of filter sections must be used to attain adequate amplification. With this type of filter ladder, the parametric travelling-wave amplifier may be directly transformed into the degenerated two-frequency amplifier, where $\omega_s = \omega_i$. (See *table 1*).

2.22 Signal and Idling Frequencies within the same Pass-band

With this design of the filter ladder, the amplifier can be directly transformed into the degenerated two-frequency amplifier, where $\omega_s = \omega_i$. The signal and idling frequencies are to be found on either side of $\frac{1}{2}\omega_p$, and if the condition where $2(\varphi)_{\omega_{p/2}} = \varphi_p$ is satisfied, the phase and wide-band conditions will be automatically met with, and there only remains the mismatching of the filter ladder to external circuits. (See *table 2*).

2.23 Idling and Pump Frequencies within the same Pass-band

In these circuits signal and idling frequencies are definitely separated, and in dimensioning the circuits, five conditions, i.e. one phase condition, one wide-band condition and three matching conditions must be satisfied. (See *table 3*).

2.24 Signal, Idling, and Pump Frequencies within Different Pass-bands

In these circuits, all the frequencies are definitely separated, and in dimensioning the circuits, five conditions, i.e. one phase condition, one wide-band condition, and three matching conditions should be satisfied. When the frequencies are chosen, five relations between the reactances and susceptances of the filter are obtained from these conditions.

The relation obtained by means of the phase condition is derived, for amplifiers type 1, from equation (59), for amplifier type 2 from equation (61), and for amplifier type 3 from equation (63).

The relation obtained by means of the wide-band condition is derived, for amplifiers type 1 from equation (69), and for amplifier type 2 or 3 from equation (71).

For all types of amplifiers, three more conditions are obtained by means of the matching conditions (74).

From these five relations, the inductances and capacitances to be inserted in the filter can be determined. Knowing the filter design, the amplification from equation (65) or (66) and the bandwidth by means of equation (73) can be determined. (See *table 4*).

Type	Structure	φ-ω-diagram	Connection
1a	$L_{(1)}$ / $C_{(1)}$	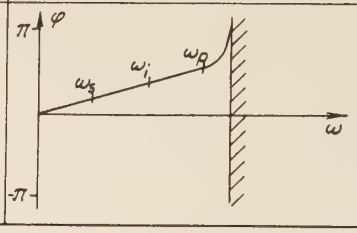	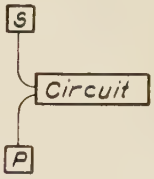

X 11072

Table 1. Signal, Idling, and Pump Frequencies within the same Pass-band.

Type	Structure	φ-ω-diagram	Connection
1a	$L_{(2)}$ / $C_{(2)}$	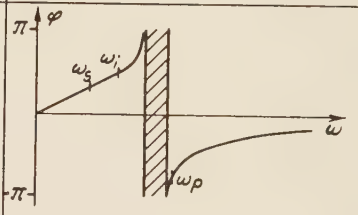	
	$L_{(3)}$ / $C_{(3)}$	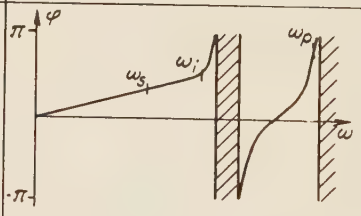	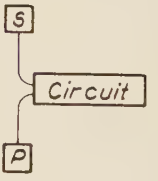
1b	$C_{(2)}$ / $L_{(2)}$	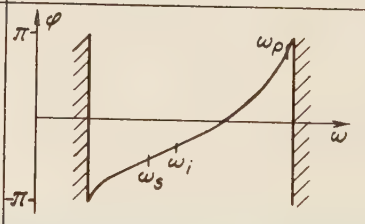	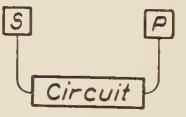
	$C_{(3)}$ / $L_{(3)}$	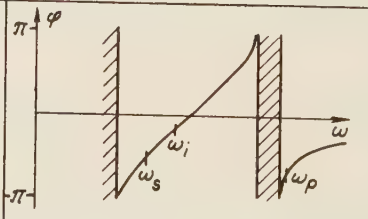	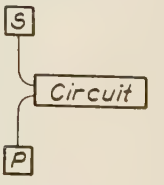

X 11073

Table 2. Signal and Idling Frequencies within the same Pass-band.

Type	Structure	φ-ω-diagram	Connection
1a	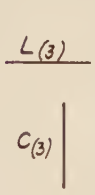	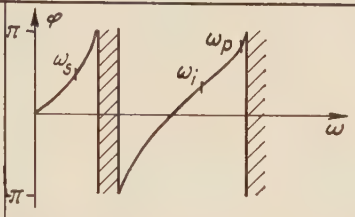	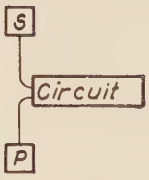
2a	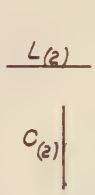	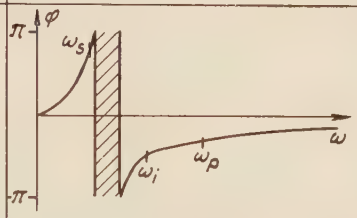	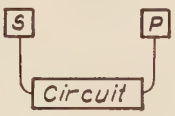
2b	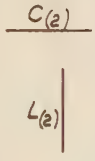	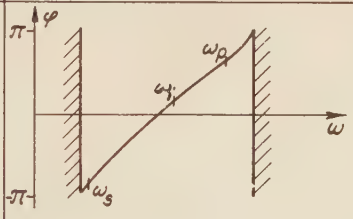	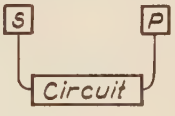
3a	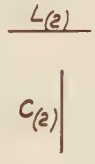	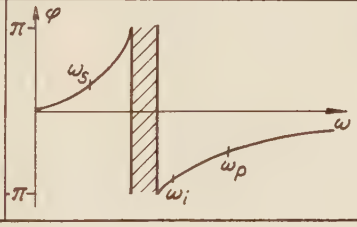	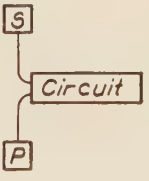

X 11074

Table 3. Idling and Pump Frequencies within the same Pass-band.

Type	Structure	φ-ω-diagram	Connection
1a	L(4) / C(4)	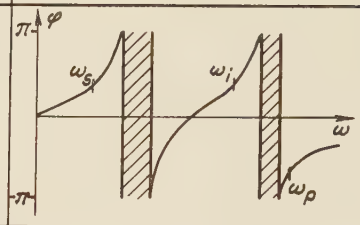	
	L(5) / C(5)	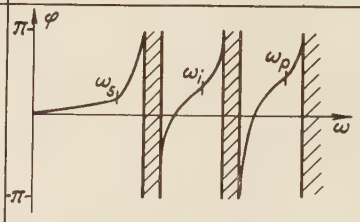	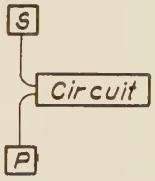
1b	C(4) / L(4)	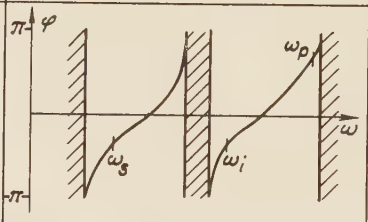	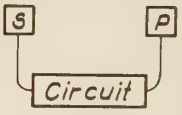
	C(5) / L(5)	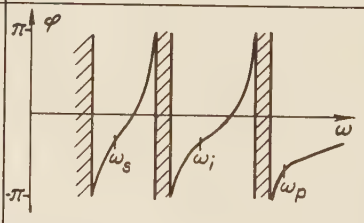	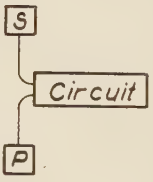
2a	L(3) / C(3)	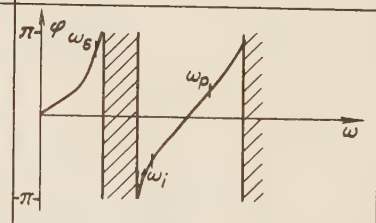	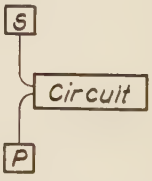
	L(4) / C(4)	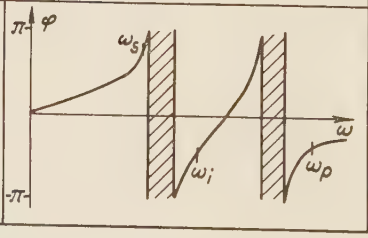	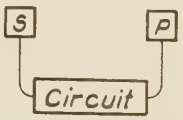

X 11075

Table 4. Signal, Idling, and Pump Frequencies within Different Pass-bands.

Type	Structure	φ-ω-diagram	Connection
2b	$C_{(3)}$ / $L_{(3)}$	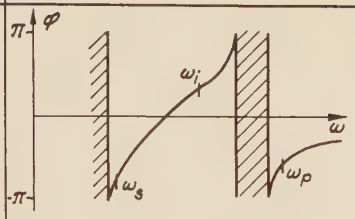	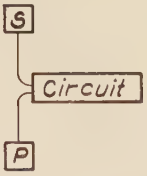
	$C_{(4)}$ / $L_{(4)}$	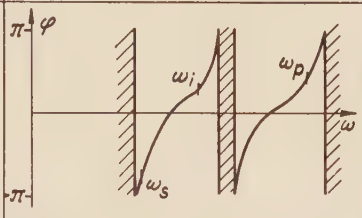	
3a	$L_{(3)}$ / $C_{(3)}$	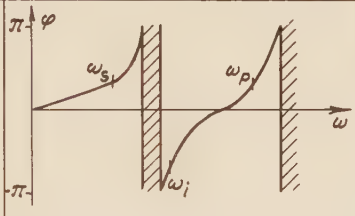	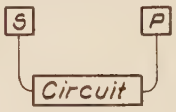
	$L_{(4)}$ / $C_{(4)}$	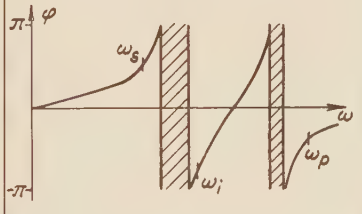	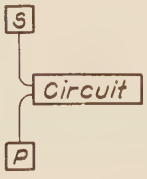
3b	$C_{(3)}$ / $L_{(3)}$	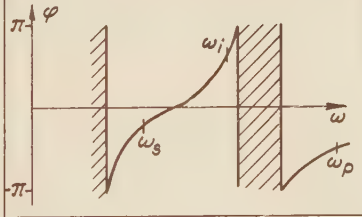	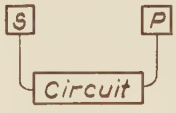
	$C_{(4)}$ / $L_{(4)}$	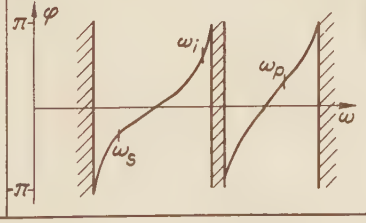	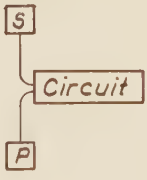

X 11076

Table 4. Signal, Idling, and Pump Frequencies within Different Pass-bands.

CHAPTER 3

Circuits Composed of Transmission Lines

3.1 Different Filter Types

In the design of parametric travelling-wave amplifiers for higher frequencies, it will be difficult to build adequate filters of *LC*-circuits. This is due to the fact that the low inductances and capacitances needed will be more and more difficult to manufacture and that at higher frequencies, inductances in connecting leads play an ever-increasing role. In order to avoid these difficulties, filters are constructed where parts of open or short-circuited transmission lines, e.g. coaxial lines, lecher-lines or strip-lines form the basic element. An excellent review by TH J WEIJERS[7] treats different methods used to construct filters from coaxial lines, and among these methods, the following ones seem applicable in the design of filters for parametric travelling-wave amplifiers.

a) Filters composed of transmission lines of equal lengths. These filters can be considered as *LC*-filters, where all the inductances have been replaced by short-circuited lines and all the capacitances, except for the coupled varicaps, have been replaced by open-circuited lines.

b) Filters composed of transmission lines of different lengths. These filters are built up in the same way as those in a) above, but one or more series circuits consisting of one inductance and one capacitance have been replaced by an open line of electrical length $\lambda/4$ at the resonant frequency, and one or several parallel circuits consisting of one inductance and one capacitance have been replaced by a short-circuited line of electrical length $\lambda/4$ at the resonant frequency.

c) Filters composed of transmission lines and capacitances. These filters are built up in the same way as those in a) or b) above, but several capacitances have been retained from the equivalent *LC*-filter.

d) Filters consisting of a transmission line loaded in parallel by impedances consisting of transmission lines and varicaps.

3.2 Filters of Substituted *LC*-Type

Filters built according to methods a), b), and c) are of similar kind, and to understand them, the impedances that can be formed by means of transmission lines will first be considered. For a transmission line with characteristic impedance Z_0, length l, and wave propagation constant β, and with currents and voltages according to *fig. 8*.

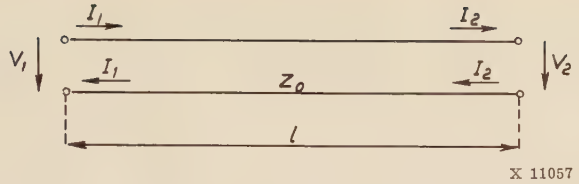

Fig. 8. Currents and voltages in a transmission line.

$$\begin{cases} V_2 = V_1 \cdot \cos \beta l - jI_1 Z_0 \cdot \sin \beta l \\ I_2 = I_1 \cdot \cos \beta l - jV_1 \dfrac{1}{Z_0} \cdot \sin \beta l \end{cases} \tag{75}$$

hold true.

If the transmission line is short-circuited at its right-hand end, $V_2 = 0$, and the input impedance can then be calculated.

$$Z = \frac{V_1}{I_1} = jZ_0 \cdot \tan \beta l \tag{76}$$

If the transmission line is open at its right-hand end, $I_2 = 0$, and the input impedance can be calculated.

$$Z = \frac{V_1}{I_1} = -jZ_0 \cdot \cot \beta l \tag{77}$$

These impedances are drawn in diagrams as a function of βl, and the equivalent LC-circuit is shown at the respective values of βl.

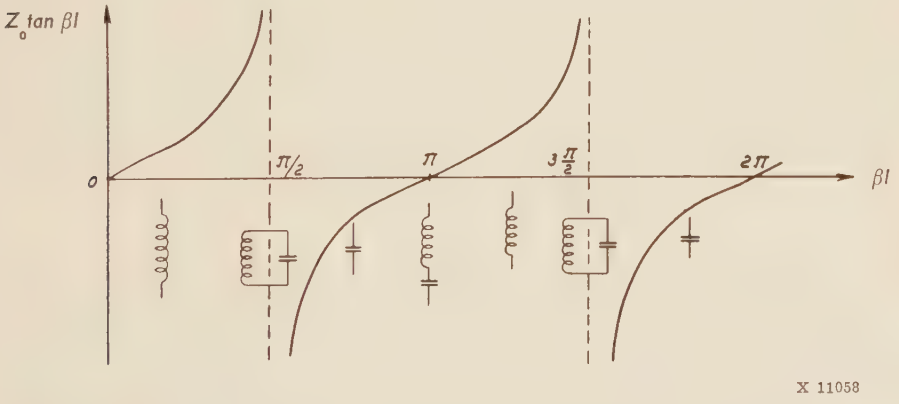

Fig. 9. Impedance and equivalent LC-circuit for a short-circuited transmission line.

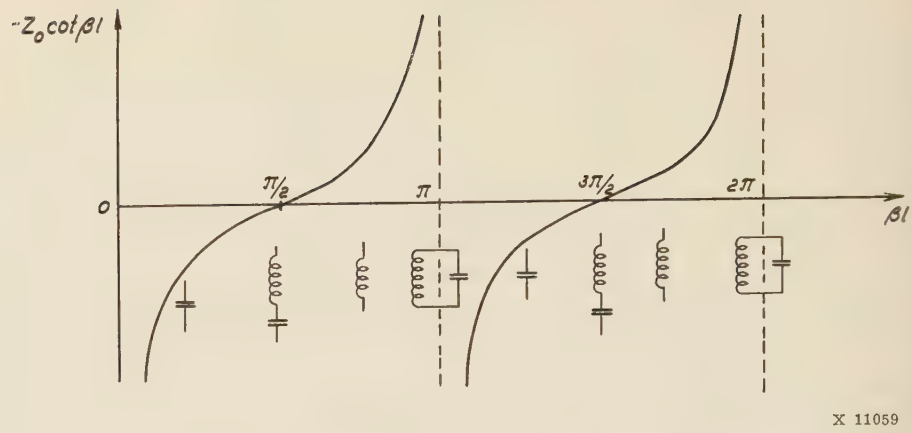

Fig. 10. Impedance and equivalent LC-circuit for open-circuited transmission line.

The values of the equivalent LC-circuits will now be calculated. For $\beta l < \pi/2, \omega L = Z_0 \cdot \tan \beta l$ holds for a short-circuited line, and $\omega C = \frac{1}{Z_0} \cdot \tan \beta l$ holds for an open-circuited line. From these equations, equivalent values of L and C are calculated, and the equations show that the smaller the value of βl, the more tan βl approaches a straight line, and the better the approximation to an inductance and a capacitance, respectively.

For $\beta l \approx \pi/2$, a short-circuited line can be approximated to a parallel circuit composed of an inductance (L) and a capacitance (C), and an open-circuited line can be approximated to a series circuit of an inductance (L) and a capacitance (C). L and C are chosen such that the resonant frequency of the LC-circuit is equal to the frequency where the electrical length of the line is $\lambda/4$, and that the derivative of the impedance with respect to frequency, at resonant frequency, is equal for the LC-circuit and the line.

With $\beta = \omega/v$, where v is the phase velocity of the line, the following conditions are obtained: for the short-circuited line $LC = \frac{4}{\pi^2}\left(\frac{l}{v}\right)^2$; $L = Z_0 \frac{\pi}{4} \frac{1}{\omega}$, and for the open-circuited line $LC = \frac{4}{\pi^2}\left(\frac{l}{v}\right)^2$; $C = \frac{1}{Z_0} \frac{\pi}{4} \frac{1}{\omega}$.

After having investigated which impedances can be obtained by means of open and short-circuited transmission lines, an opinion can be formed of the filters that can be built according to methods a), b), and c). These investigations are based on the calculations and the classification made earlier for LC-filters.

3.21 Possible Filter Structures

By means of method a), all the filters on the list of different LC-filters can be built. In this list of LC-filters all the inductances are replaced by short-circuited transmission lines, and all the capacitances, except for the coupled varicaps, by open-circuited transmission lines. Within the whole frequency range where the filter is to be used, the electrical length of the lines must be less than $\lambda/4$. If within the whole frequency range the fact holds that $\tan \beta l \approx \beta l$, calculations made for LC-filters can be used directly and an inductance L can be replaced by a short-circuited line with characteristic impedance $Z_0 = L \cdot \frac{v}{l}$, and a capacitance is replaced by an open-circuited line with impedance $Z_0 = \frac{1}{C} \cdot \frac{l}{v}$. If this approximation does not hold, the reactance $jZ_0 \tan \beta l$ for a short-circuited line and with the reactance $-jZ_0 \cot \beta l$ for an open-circuited line must be reckoned with. These reactances are introduced into the equations obtained from the phase condition, wide-band condition, and the three matching conditions. In this case, the electrical lengths of the lines can be considered as known, and the equations can be solved with respect to the characteristic impedances Z_0 of the lines. The method of calculation followed is given in the text after the disposition of LC-filters belonging to section 2.24.

Also by means of method b), all the filters on the list of different LC-filters can be built. With the same procedure as in method a), inductances are replaced by short-circuited lines, and capacitances by open-circuited lines, but in addition one or several parallel circuits consisting of an inductance and a capacitance are replaced by a short-circuited line of electrical length $\lambda/4$ at the resonant frequency of the LC-circuit, and one or several series circuits consisting of an inductance and a capacitance are replaced by an open-circuited line of electrical length $\lambda/4$ at the resonant frequency of the LC-circuit. In this case, it is necessary to note that the resonant frequency of the LC-circuit must lie within the upper half of the frequency range within which the filter is to be used, since otherwise the line would cause a non-desired parallel or series resonance within the frequency range. In calculating filters built according to method b), the reactance $jZ_0 \tan \beta l$ for a short-circuited line, and the reactance $-jZ_0 \cot \beta l$ for an open-circuited line must be reckoned with, for it is only within a small frequency range around the resonant frequency that it is possible to approximate a short-circuited line to a parallel circuit, and an open-circuited line to a series circuit. These reactances are introduced into equations obtained from the phase condition, the wide-band condition and the three matching conditions, and in the same way as with method a), the equations with respect to the characteristic impedances Z_0 of the lines are solved.

Filters built according to method c) do not contain anything essentially new in addition to what is known about filters built according to methods a) and b). In filters built according to method c), the difference is that some capacitances from the equivalent LC-filter have not been replaced by open-circuited lines. The same sequence of calculation is followed and the same properties as for filters built according to methods a) and b) may be expected. Some

band-pass filters built from coaxial lines and capacitances have been treated by RAGAN[8] and COHN,[9] and filters for parametric travelling-wave amplifiers can possibly be built in a similar way.

3.3 Periodically Loaded Transmission Line as Parametric Circuit

Filters built according to method d) consist of a transmission line which is loaded with shunt impedances z at equidistant points. The distance between the points is $2\,l_0$, the characteristic impedance of the transmission line is z_0, and its wave propagation constant is β_0 $\left(\beta_0 = \frac{\omega}{v}\right.$, where v = the phase velocity of the line$\left.\right)$. Impedance z is built of transmission lines and contains a varicap. A filter section is shown in *fig. 11*.

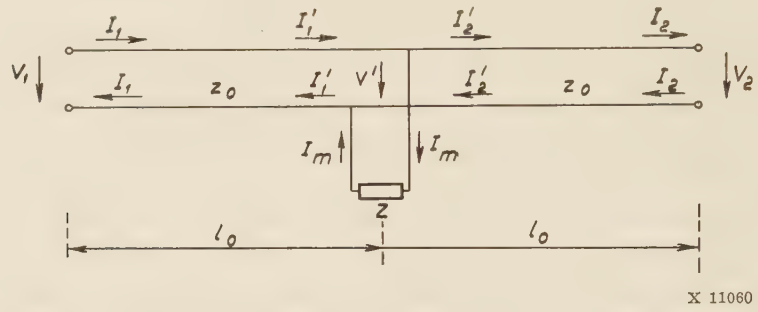

Fig. 11. Currents and voltages in a transmission line loaded with impedance z.

With the symbols according to *fig. 11*,

$$\begin{cases} V' = V_1 \cos\beta_0 l_0 - jI_1 z_0 \sin\beta_0 l_0 \\ I_1' = I_1 \cos\beta_0 l_0 - jV_1 \dfrac{1}{z_0} \sin\beta_0 l_0 \\ V_2 = V' \cos\beta_0 l_0 - jI_2' z_0 \sin\beta_0 l_0 \\ I_2 = I_2' \cos\beta_0 l_0 - jV' \dfrac{1}{z_0} \sin\beta_0 l_0 \\ I_1' = I_2' + I_m \\ I_m = V'/z \end{cases} \tag{78}$$

hold true.

By eliminating V', I_1', I_2', and I_m, the following equation is obtained.

$$\begin{cases} V_2 = V_1(\cos 2\beta_0 l_0 + q \sin 2\beta_0 l_0) - jI_1 z_0 (\sin 2\beta_0 l_0 + 2q \sin^2 \beta_0 l_0) \\ I_2 = I_1(\cos 2\beta_0 l_0 + q \sin 2\beta_0 l_0) - jV_1 \dfrac{1}{z_0} (\sin 2\beta_0 l_0 - 2q \cos^2 \beta_0 l_0) \end{cases} \tag{79}$$

where

$$q = j \frac{1}{2} \frac{z_0}{z} \tag{80}$$

Since z is imaginary, q always is real.

These equations are now compared to corresponding equations (81) for a filter section with the characteristic impedance Z_0 and the phase shift φ

$$\begin{cases} V_2 = V_1 \cos\varphi - jI_1 Z_0 \sin\varphi \\ I_2 = I_1 \cos\varphi - jV_1 \dfrac{1}{Z_0} \sin\varphi \end{cases} \tag{81}$$

After simplification of the expressions, this comparison gives

$$Z_0 = z_0 \sqrt{\frac{1 + q \tan\beta_0 l_0}{1 - q \cot\beta_0 l_0}} \tag{82}$$

$$\cos\varphi = \cos 2\beta_0 l_0 + q \sin 2\beta_0 l_0 = 1 + (q - \tan\beta_0 l_0) \sin 2\beta_0 l_0 = -1 + (q + \cot\beta_0 l_0) \sin 2\beta_0 l_0 \tag{83}$$

$$\sin\varphi = \sqrt{(1 + q \tan\beta_0 l_0)(1 - q \cot\beta_0 l_0)} \cdot \sin 2\beta_0 l_0 \tag{84}$$

Z_0 is real within the pass-bands of the filter, and hence

$$(1 + q \tan\beta_0 l_0)(1 - q \cot\beta_0 l_0) \geq 0 \tag{85}$$

holds within the pass-bands.

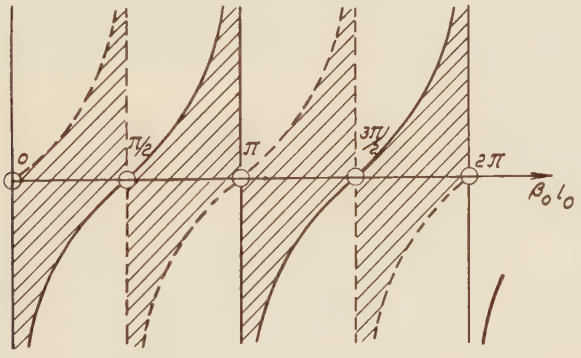

X 11061

Fig. 12. $\tan\beta_0 l_0$ (dotted) and $-\cot\beta_0 l_0$ (solid) as a function of $\beta_0 l_0$. When q lies within the shaded area, the filter is transmitting. When q intersects solid boundary curves, $Z_0 = 0$, and when q intersects dotted boundary curves, $Z_0 = \infty$.

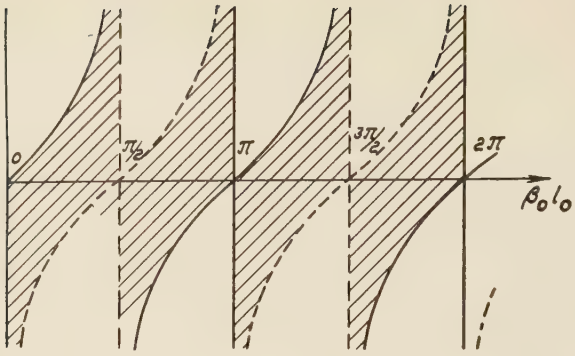

X 11062

Fig. 13. $\tan \beta_0 l_0$ (solid) and $-\cot \beta_0 l_0$ (dotted) as a function of $\beta_0 l_0$. When q lies within the shaded area, the filter is transmitting. When q intersects solid boundary curves, $\varphi = 0$, and when q intersects dotted boundary curves, $\varphi = \pm \pi$.

From (85) it is evident that at the cut-off frequencies, the expression in (85) is zero or infinite so that $q = \tan \beta_0 l_0$, $q = -\cot \beta_0 l_0$, $\tan \beta_0 l_0 = 0$ or $\cot \beta_0 l_0 = 0$. Within the pass-bands, q consequently lies between $\tan \beta_0 l_0$ and $-\cot \beta_0 l_0$. In the diagrams of *figures 12* and *13*, $\tan \beta_0 l_0$ and $-\cot \beta_0 l_0$ are now drawn as functions of $\beta_0 l_0$. Now when q lies within the shaded area between these curves, the filter is transmitting, and by applying equations (82) and (83), Z_0 and φ, when q intersects the boundary curves can be determined.

By means of expressions (82), (83), and (84) for Z_0, $\cos \varphi$ and $\sin \varphi$, the properties of filters built according to method d) can be determined. The signal, idling or pump frequencies are introduced into (82), (83), and (84), and then the characteristic impedance and phase shift of the filter at these frequencies can be calculated. By means of these values of Z_0 and φ, it is now possible to check that the phase condition, the wide-band condition and the three matching conditions are satisfied.

The phase condition can now be written,

for amplifier type 1 $$\sin \varphi_s \cdot \cos \varphi_i + \cos \varphi_s \sin \varphi_i = \sin \varphi_p \tag{86}$$

for amplifier type 2 $$\sin \varphi_s \cos \varphi_i - \cos \varphi_s \cdot \sin \varphi_i = \sin \varphi_p \tag{87}$$

and for amplifier type 3 $$\sin \varphi_i \cos \varphi_s - \cos \varphi_i \sin \varphi_s = \sin \varphi_p \tag{88}$$

The wide-band condition can be written, for amplifier type 1

$$\frac{\frac{d}{d\omega_s}(\cos \varphi_s)}{\sin \varphi_s} - \frac{\frac{d}{d\omega_i}(\cos \varphi_i)}{\sin \varphi_i} = 0 \tag{89}$$

and for amplifier types 2 and 3

$$\frac{\frac{d}{d\omega_s}(\cos\varphi_s)}{\sin\varphi_s} + \frac{\frac{d}{d\omega_i}(\cos\varphi_i)}{\sin\varphi_i} = 0 \tag{90}$$

In order to match the filter to external circuits, equations (74) should be satisfied, and the characteristic impedances are obtained from equation (82).

From the equations for the five conditions given above, the characteristic impedance of the transmission line z_0, the distance $2l_0$ between the parallel impedances and the parallel impedance z as a function of frequency is calculated. If the equations lead to a mathematically intricate system, the filter can be designed by means of a cut-and-try method, where the φ-ω-characteristic is calculated for different parameters. When the filter is designed, the amplification is determined by equation (65) or (67), and the bandwidth is calculated by means of equation (73). Note that, irrespective of impedance z, the first passband in these filters always have positive dispersion. This will lead to the fact that only parametric travelling-wave amplifiers of types 1a), 2a), and 3a) would suitably be realized by means of these filters.

3.31 Possible Filter Structures

Using the diagrams in *figures 12* and *13*, a rough estimate can be made of the filter properties and a decision made as to which impedances z should be chosen to obtain a certain type of filter. Some examples are given below of suitable impedances z for different filters, and the types of parametric amplifiers that can be realized by means of these filters are indicated. The approximate φ-ω- and Z_0-ω-characteristics of the filters are shown.

In a circuit shown in *fig. 14*, the signal, idling, and pump frequencies lie within the first passband, and operation is along the linear part of the φ-ω-characteristic. In order to avoid

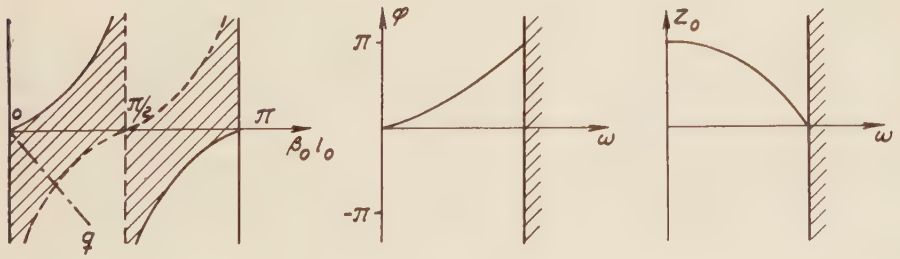

X 11063

Fig. 14. Characteristics of filters according to method d) where the parallel impedance z is a varicap.

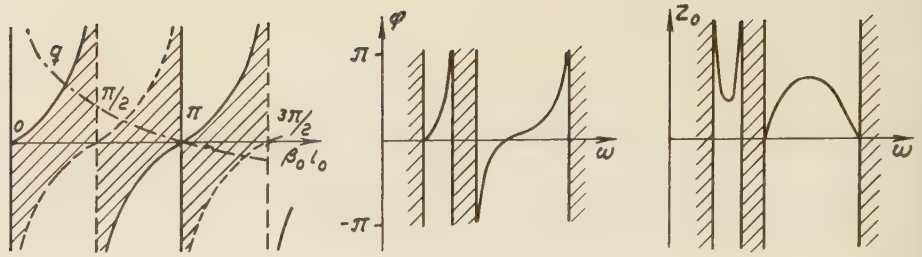

X 11064

Fig. 15. Characteristics of filters according to method d) where the parallel impedance z is a varicap coupled in parallel with a short-circuited transmission line.

power-absorbing coupled wave pair, it is essential, according to above statement, that the φ-ω-characteristic bends immediately after the pump frequency. An amplifier type 1a) with large bandwidth is obtained, but in return the amplification per section will be small.

From circuits according to *fig. 15*, different types of parametric travelling-wave amplifiers can be built. If the signal and idling frequencies are placed within the same pass-band, amplifiers type 1a) can be built; if the idling and pump frequencies are placed within the same pass-band, amplifiers types 2a) and 3a) can be built; and if signal, idling, and pump frequencies are each placed within its own pass-band, amplifiers types 2a) and 3a) can be built.

A filter built according to *fig. 16* has properties similar to those built according to *fig. 15*, and amplifiers of the same type can be built.

Even other, more complicated forms of parallel impedance z can be used when forming an impedance with a certain frequency dependence.

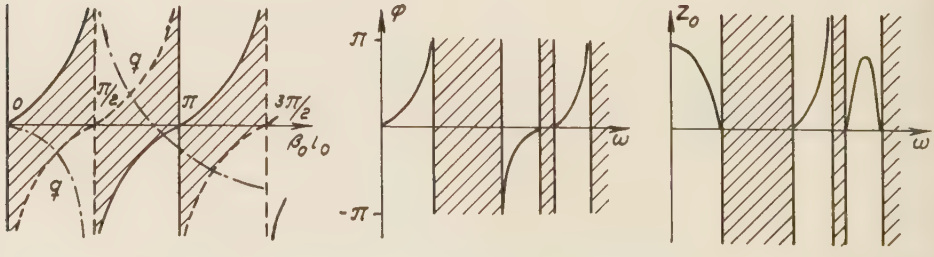

X 11065

Fig. 16. Characteristics of filters according to method d) where the parallel impedance z is a varicap coupled in parallel with an open-circuited transmission line.

CHAPTER 4

Circuits Composed of Slow-Wave Structures

4.1 Introductory Remarks

In the design of parametric travelling-wave amplifiers with filters built of transmission lines, certain difficulties arise with increasing frequency. With shorter wavelengths, the different transmission lines will be inconveniently short, and it is also difficult to manufacture transmission lines with the extremely low or high characteristic impedances needed to form suitable reactance elements. With higher frequencies, parametric travelling-wave amplifiers must consequently be built by means of different types of periodic slow-wave structures. Different microwave filters with capacitive and inductive windows and chains of coupled resonators are also included in slow-wave structures.

Great difficulties arise when theoretically designing parametric travelling-wave amplifiers built of slow-wave structures. The dispersion curve of the slow-wave structures is calculated by means of MAXWELL's equations, and in those equations the varicaps cannot be introduced as reactance elements. It is known that slow-wave structures contain a spectrum of pass-bands, and dispersion curves are obtained, the general nature of which is shown in *fig. 17*, where β_0 is the wave-propagation constant of the fundamental wave, and s the periodicity of the slow-wave structure.

In most slow-wave structures, the first pass-band has positive dispersion, which implies that only parametric travelling-wave amplifiers types 1a), 2a), and 3a) can suitably be built of slow-wave structures. The different pass-bands can be used in the same way as in the case of LC-filters. If the first pass-band of the slow-wave structure is a low-pass band, the signal,

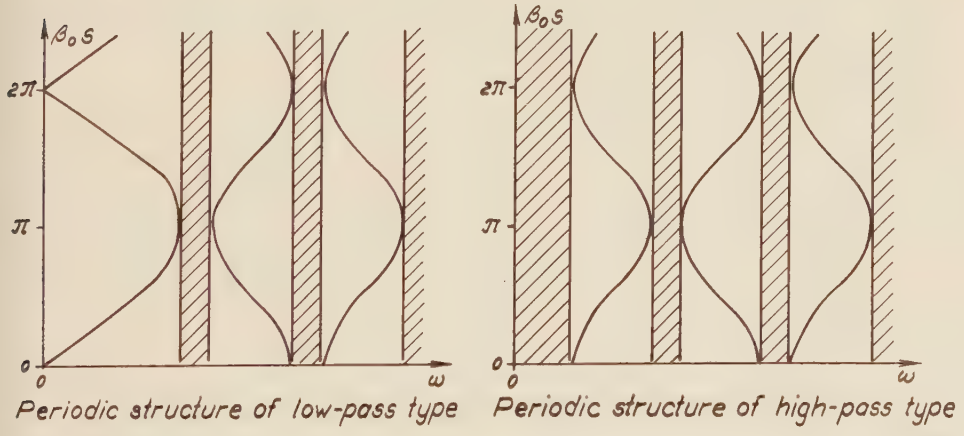

Fig. 17. Dispersion curves for periodic slow-wave structures.

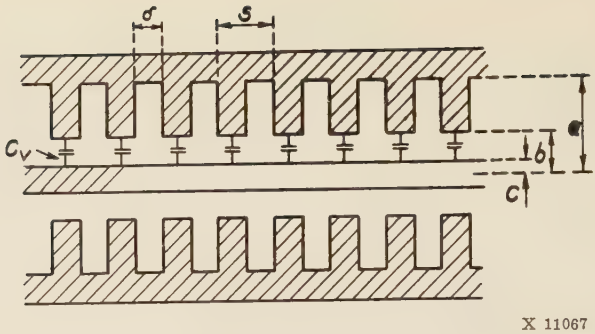

Fig. 18. Disk-loaded waveguide with coupled varicaps.

idling, and pump frequencies can be placed within this band, and if operation is within the linear part of the $\beta_0 s$-ω-characteristic, a very wide-band parametric travelling-wave amplifier type 1a) will be obtained. In the following a calculation method for designing parametric amplifiers will be outlined.

4.2 Design of Parametric Slow-Wave Structures

The disk-loaded waveguide with centre conductor is a slow-wave structure, the lowest pass-band of which is of low-pass type. In order to obtain a parametric travelling-wave amplifier, voltage-dependent varicaps are placed between the centre conductor and the flanges protruding from the outer conductor.

The disk-loaded wave-guide has been treated earlier by the author,[10] and the dispersion curve is known at different circuit parameters. To be able to design the amplifier, the slow-wave structure without coupled varicaps will first be treated, and by means of the dispersion curve the equivalent filter chain will be calculated.

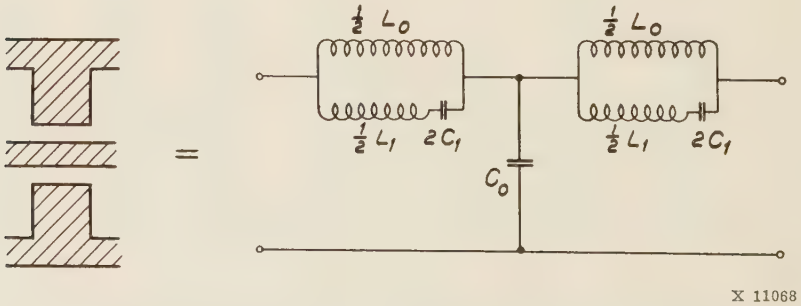

Fig. 19. Equivalent filter section for a segment of a slow-wave structure.

According to the paper[10],

$$\beta_0 s = \omega\sqrt{\mu_0\varepsilon_0}s\sqrt{1+\frac{\delta}{s}\frac{\ln(a/b)}{\ln(b/c)}} \tag{91}$$

and

$$Z_0 = \sqrt{\frac{\mu_0}{\varepsilon_0}}\frac{\ln(b/c)}{2\pi}\sqrt{1+\frac{\delta}{s}\frac{\ln(a/b)}{\ln(b/c)}} \tag{92}$$

hold true for a disk-loaded waveguide with centre conductor at very low frequencies.

From these equations, L_0 and C_0 can be obtained which wholly determine the filter properties at low frequencies.

$$L_0 = \frac{\mu_0}{2\pi}\left[s\ln(b/c) + \delta\ln(a/b)\right] \tag{93}$$

$$C_0 = \varepsilon_0 2\pi s\frac{1}{\ln(b/c)} \tag{94}$$

Now it is noted that L_0 consists of an inductance $\frac{\mu_0}{2\pi}s\ln(b/c)$ which applies to a non-corrugated coaxial line, and an inductance $\frac{\mu_0}{2\pi}\delta\ln(a/b)$ which is the inductance of the groove, and C_0 corresponds to a cylindrical capacitor of the length s. The values of L_1 and C_1 are calculated from the cut-off frequency, and the value of ω at $\beta_0 s = \frac{\pi}{2}$.

Knowing the equivalent filter ladder of the slow-wave structure, varicap C_v can be considered to be coupled in parallel with C_0, and amplification and bandwidth calculated in the same way as for LC-filters. However, it must be remembered that when using the equivalent filter ladder the space harmonics are neglected. This must be considered when calculating the amplification.

The same method of calculation can also be used in connection with other types of periodic slow-wave structures, and can further be applied when using more than one of the pass-bands of the slow-wave structure. In complex slow-wave structures, however, this method will lead to calculations difficult to survey, and a pure experimental evaluation of slow-wave structures would be preferable in this case.

CHAPTER 5

The Effect of Losses in a Parametric Travelling-Wave Amplifier

5.1 Parametric Circuit

It is to be expected that losses in a parametric travelling-wave circuit will cause a decrease of the amplification, and it is of interest to calculate this decrease. In the calculations a filter ladder with series impedance $r + jX$ and parallel admittance $g + jB$ is assumed. As before, a signal and pump wave are applied to the circuit, and the frequency relation $\omega_s + \omega_i = \omega_p$ is always satisfied.

The impedances and admittances of the circuit can be written:

$$\text{at frequency } \omega_s \begin{cases} r + jX = r_s + jX_s \\ g + jB = g_s + jB_s \end{cases} \tag{95}$$

$$\text{at frequency } \omega_i \begin{cases} r + jX = r_i + jX_i \\ g + jB = g_i + jB_i \end{cases} \tag{96}$$

$$\text{at frequency } \omega_p \begin{cases} r + jX = jX_p \\ g + jB = jB_p \end{cases} \tag{97}$$

Thus the losses at pump frequency are neglected in the following calculations:

φ_s is the signal wave phase shift per section
φ_i is the idling wave phase shift per section
φ_p is the pump wave phase shift per section
$(Z_0)_s$ is the characteristic impedance of the circuit at signal frequency
$(Z_0)_i$ is the characteristic impedance of the circuit at idling frequency
$(Z_0)_p$ is the characteristic impedance of the circuit at pump frequency

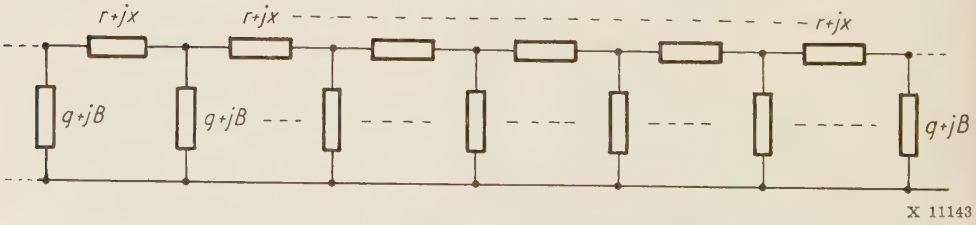

Fig. 20. Equivalent scheme for a parametric travelling-wave circuit.

The losses in the circuit cause an exponential damping of the propagation waves.

α_s is the exponential damping of the signal wave

α_i is the exponential damping of the idling wave

The coupling between the signal and idling waves is determined according to equations (10) and (40) and can be written:

$$\begin{cases} \Delta i_s \cdot e^{j\omega_s t} = j\delta_s V_i e^{j\omega_s t} \cdot e^{-jn\varphi_p} \\ \Delta i_i \cdot e^{-j\omega_i t} = -j\delta_i V_s e^{-j\omega_i t} \cdot e^{jn\varphi_p} \end{cases} \tag{98}$$

The wave propagation in the circuit will now be treated for the cases: $BX \ll 1$, where the circuit can be treated as a homogeneous line, and $0 \leq BX \leq 4$, where the circuit must be treated as a filter ladder with concentrated circuit elements.

5.2 Homogeneous Lines

Assume $BX \ll 1$, and the circuit can then be treated as a homogeneous line. On the assumption that the losses are small, so that $r \ll |X|$ and $g \ll |B|$, the equations below hold for the circuit.

$$\begin{aligned} (Z_0)_s &= \sqrt{\frac{X_s}{B_s}} & \varphi_s &= \sqrt{B_s X_s} & \alpha_s &= \frac{\varphi_s}{2}\left(\frac{g_s}{B_s} + \frac{r_s}{X_s}\right) \\ (Z_0)_i &= \sqrt{\frac{X_i}{B_i}} & \varphi_i &= \sqrt{B_i X_i} & \alpha_i &= \frac{\varphi_i}{2}\left(\frac{g_i}{B_i} + \frac{r_i}{X_i}\right) \\ (Z_0)_p &= \sqrt{\frac{X_p}{B_p}} & \varphi_p &= \sqrt{B_p X_p} \end{aligned} \tag{99}$$

Let $V_s(n)e^{j\omega_s t}$, $V_i(n)e^{-j\omega_i t}$, $I_s(n)e^{j\omega_s t}$ and $I_i(n)e^{-j\omega_i t}$ be the voltages and currents of the signal and idling waves in the circuit. The following are then obtained.

$$\begin{cases} \dfrac{dV_s(n)}{dn} = -(jX_s + r_s)\, I_s(n) \\ \dfrac{dI_s(n)}{dn} = -(jB_s + g_s)\, V_s(n) - j\delta_s V_i(n) e^{-jn\varphi_p} \\ \dfrac{dV_i(n)}{dn} = (jX_i - r_i)\, I_i(n) \\ \dfrac{dI_i(n)}{dn} = (jB_i - g_i)\, V_i(n) + j\delta_i V_s(n) e^{jn\varphi_p} \end{cases} \tag{100}$$

On the assumption $\delta \ll B$, $g \ll B$ and $r \ll X$, combination of the first equation with the second and the third with the fourth yields

$$\begin{cases} \dfrac{d^2V_s(n)}{dn^2} = -B_sX_s\left[1 - j2\dfrac{\alpha_s}{\varphi_s}\right]V_s(n) - X_s\delta_sV_i(n)e^{-jn\varphi_p} \\ \dfrac{d^2V_i(n)}{dn^2} = -B_iX_i\left[1 + j2\dfrac{\alpha_i}{\varphi_i}\right]V_i(n) - X_i\delta_iV_s(n)e^{jn\varphi_p} \end{cases} \tag{101}$$

Waves with the time dependence $e^{-j\omega_s t}$ and $e^{j\omega_i t}$, give the same equations, but with conjugate complex numbers.

Irrespective of the perturbation terms, equations (101) have the same form as the ordinary wave equations for homogeneous lines. As it has been assumed that $\delta \ll B$, the equations can be treated by means of perturbation theory.

In order to get parametric amplification one of the phase conditions (14) must be satisfied. The coupled wave pairs are given by equations (15), (16), and (17).

Now interest lies in calculating how the wave propagation is changed by the losses in the circuit. It can be concluded at once that the phase and wide-band conditions are unaffected, and calculation is restricted to determining how much the amplification is decreased. It is decided to treat the first wave pair in (15), and the phase condition can be written:

$$\varphi_p = \varphi_s + \varphi_i + \Delta\varphi$$

Assume $\Delta\varphi \ll \varphi$ and introduce the complex phase angles

$$\varphi_s' - j\frac{1}{2}(\alpha_s + \alpha_i) \qquad \varphi_i' + j\frac{1}{2}(\alpha_s + \alpha_i)$$

where

$$\varphi_s' = \varphi_s + \frac{1}{2}\Delta\varphi \qquad \varphi_i' = \varphi_i + \frac{1}{2}\Delta\varphi \qquad \varphi_s' + \varphi_i' = \varphi_p$$

Now the first wave pair in (15) can be written

$$\begin{cases} V_s(n) = A_s(n)e^{-\frac{1}{2}(\alpha_s+\alpha_i)}e^{j(\omega_s t - n\varphi_s')} \\ V_i(n) = A_i^*(n)e^{-\frac{1}{2}(\alpha_s+\alpha_i)}e^{-j(\omega_i t - n\varphi_i')} \end{cases} \tag{102}$$

This wave pair is introduced in equation (101), and assuming that the perturbation terms are small, so that $\frac{d^2A}{dn^2}$ can be neglected compared to $\varphi \frac{dA}{dn}$, the following equations are obtained.

$$\begin{cases} -\varphi_s [\Delta\varphi + j(\alpha_s - \alpha_i)] A_s(n) - 2j\varphi_s \dfrac{dA_s(n)}{dn} = -X_s\delta_s A_i^*(n) \\ -\varphi_i [\Delta\varphi + j(\alpha_s - \alpha_i)] A_i^*(n) + 2j\varphi_i \dfrac{dA_i^*(n)}{dn} = -X_i\delta_i A_s(n) \end{cases} \tag{103}$$

These equations are combined and give

$$\begin{cases} \dfrac{d^2A_s(n)}{dn^2} = \dfrac{1}{4}\left\{ \dfrac{X_sX_i\delta_s\delta_i}{\varphi_s\varphi_i} - [\Delta\varphi + j(\alpha_s - \alpha_i)]^2 \right\} A_s(n) \\ \dfrac{d^2A_i^*(n)}{dn^2} = \dfrac{1}{4}\left\{ \dfrac{X_sX_i\delta_s\delta_i}{\varphi_s\varphi_i} - [\Delta\varphi + j(\alpha_s - \alpha_i)]^2 \right\} A_i^*(n) \end{cases} \tag{104}$$

For the wave pair in (102) solutions of the type

$$e^{\pm\frac{1}{2}\xi_r n} \cdot e^{\pm j\xi_i n} \tag{105}$$

are obtained, where

$$\begin{cases} \xi_r = R_e\left[\sqrt{\dfrac{X_sX_i\delta_s\delta_i}{\varphi_s\varphi_i} - [\Delta\varphi + j(\alpha_s - \alpha_i)]^2}\right] \\ \xi_i = I_m\left[\sqrt{\dfrac{X_sX_i\delta_s\delta_i}{\varphi_s\varphi_i} - [\Delta\varphi + j(\alpha_s - \alpha_i)]^2}\right] \\ \xi = \xi_r + j\xi_i \end{cases} \tag{106}$$

Consider the boundary conditions (22) at the filter ladder input and by means of (103) the following solutions are obtained

$$\begin{cases} V_s(n,t) = V_0\left[\cosh\left(\dfrac{1}{2}\xi n\right) + j\dfrac{\Delta\varphi + j(\alpha_s - \alpha_i)}{\xi}\sinh\left(\dfrac{1}{2}\xi n\right)\right] e^{-\frac{1}{2}(\alpha_s+\alpha_i)n} \cdot e^{j(\omega_s t - n\varphi_s' + \Theta)} \\ V_i(n,t) = jV_0\dfrac{\delta_i X_i}{\xi\varphi_i}\sinh\left(\dfrac{1}{2}\xi n\right) e^{-\frac{1}{2}(\alpha_s+\alpha_i)n} \cdot e^{-j(\omega_i t - n\varphi_i' - \Theta)} \end{cases} \tag{107}$$

If $\Delta\varphi = 0$, equation (107) can be written

$$\begin{cases} V_s(n,t) = V_0\left\{\cosh\left(\frac{1}{2}\sqrt{\frac{\delta_s\delta_i X_s X_i}{\varphi_s\varphi_i} + (\alpha_s - \alpha_i)^2 n}\right) - \right. \\ \left. - \frac{\alpha_s - \alpha_i}{\xi}\sinh\left(\frac{1}{2}\sqrt{\frac{\delta_s\delta_i X_s X_i}{\varphi_s\varphi_i} + (\alpha_s - \alpha_i)^2 n}\right)\right\} \cdot e^{-\frac{1}{2}(\alpha_s+\alpha_i)n} \cdot e^{j(\omega_s t - n\varphi_s' + \Theta)} \\ V_i(n,t) = jV_0\frac{\delta_i X_i}{\xi\varphi_i}\sinh\left(\frac{1}{2}\sqrt{\frac{\delta_s\delta_i X_s X_i}{\varphi_s\varphi_i} + (\alpha_s - \alpha_i)^2 n}\right) e^{-\frac{1}{2}(\alpha_s+\alpha_i)n} e^{-j(\omega_i t - n\varphi_i' - \Theta)} \end{cases} \quad (108)$$

From the equations (107) and (108), the way in which the amplification is affected by the losses in the circuit can be determined. The circuit has a length of N filter sections, and provided $\alpha_s = \alpha_i$, the amplification F of the signal wave expressed in db will be

$$F = 10\log\left[\cosh^2\left(\frac{1}{2}\xi N\right) + \frac{(\Delta\varphi)^2}{\xi^2}\sinh^2\left(\frac{1}{2}\xi N\right)\right] - 4.3\ (\alpha_s + \alpha_i)N \quad (109)$$

The remaining wave pairs in (16) and (17) can be treated in the same way and give similar solutions and expressions for the amplification.

5.3 Circuits with Concentrated Elements

Now the wave propagation in circuits will be treated for the case where $0 \leq BX \leq 4$, and thus the approximation to a homogeneous line is not permissible. The filter ladder consists of a chain of π- or T-sections built up according to *fig. 21.*

As before, the losses at pump frequency are neglected and it is assumed that the losses at signal and idling frequency are so small, that $r \ll X$ and $g \ll B$. With these assumptions the characteristic impedance and phase shift per section of the filter chain at the actual frequencies are given by the equations (36), (37) and (38).

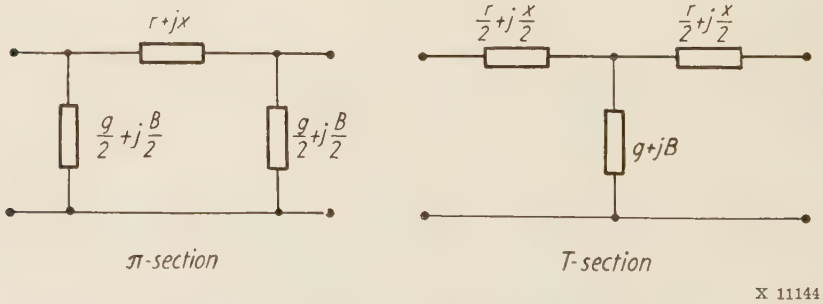

Fig. 21. π- or T-section inserted in the filter ladder.

In chapter 1.4 the wave propagation and amplification in loss-free circuits with concentrated elements have been calculated. Now interest lies in investigating how the losses affect the wave propagation and amplification in the circuit. As the phase and wide-band condition are unaffected, it is sufficient to determine to what extent the amplification is decreased by the losses.

As in chapter 1.4 it is decided to treat the first wave pair in (15), and the phase condition can be written

$$\varphi_p = \varphi_s + \varphi_i + \Delta\varphi$$

Assume a ladder of T-sections, and in order to calculate the amplification, a filter section is investigated where the voltages and currents at the input are $(V_s)_1 e^{j\omega_s t}$, $(V_i)_1 e^{-j\omega_i t}$, $(I_s)_1 e^{j\omega_s t}$ and $(I_i)_1 e^{-j\omega_i t}$ and at the output $(V_s)_2 e^{j\omega_s t}$, $(V_i)_2 e^{-j\omega_i t}$, $(I_s)_2 e^{j\omega_s t}$ and $(I_i)_2 e^{-j\omega_i t}$.

The coupling between the signal and idling waves according to equation (98) is introduced. Assuming $\delta \ll B$, a perturbation calculation can be applied and the same sequence of calculation followed as in chapter 1.4. As before, it is assumed that the filter section is matched in both directions, and that there is a state of equilibrium between the signal and idling waves. Thus the equations (41) and (42) are fulfilled.

However the exponential damping caused by the losses in the circuit must be considered. The exponential damping can be written

$$\begin{cases} \alpha_s = \dfrac{1}{2} \dfrac{B_s X_s \left(\dfrac{r_s}{X_s} + \dfrac{g_s}{B_s} \right)}{\sqrt{B_s X_s \left(1 - \dfrac{1}{4} B_s X_s \right)}} \\ \alpha_i = \dfrac{1}{2} - \dfrac{B_i X_i \left(\dfrac{r_i}{X_i} + \dfrac{g_i}{B_i} \right)}{\sqrt{B_i X_i \left(1 - \dfrac{1}{4} B_i X_i \right)}} \end{cases} \tag{110}$$

Now introducing the complex phase angles

$$\varphi_s' - j\frac{1}{2}(\alpha_s + \alpha_i) \qquad \varphi_i' + j\frac{1}{2}(\alpha_s + \alpha_i)$$

where

$$\varphi_s' = \varphi_s + \frac{1}{2}\Delta\varphi \qquad \varphi_i' = \varphi_i + \frac{1}{2}\Delta\varphi \qquad \varphi_s' + \varphi_i' = \varphi_p$$

into equation (52), the following are obtained.

$$\left\{\begin{array}{l}(V_s)_2=(V_s)_1 e^{-j\varphi_s'}\left\{1+j\frac{1}{2}[\Delta\varphi+j(\alpha_s-\alpha_i)]-j\frac{1}{4}\frac{\delta_s X_s}{\frac{1}{\cos\frac{1}{2}\varphi_i}}\frac{e^{j\frac{1}{2}(\varphi_s+\varphi_i)}1}{\frac{1}{\sin\frac{1}{2}\varphi_s}K}\right\}e^{-\frac{1}{2}(\alpha_s+\alpha_i)}\\ (V_i)_2=(V_i)_1 e^{j\varphi_i'}\left\{1-j\frac{1}{2}[\Delta\varphi+j(\alpha_s-\alpha_i)]+j\frac{1}{4}\frac{\delta_i X_i}{\frac{1}{\cos\frac{1}{2}\varphi_s}}\frac{e^{-j\frac{1}{2}(\varphi_s+\varphi_i)}}{\sin\frac{1}{2}\varphi_i}K\right\}e^{-\frac{1}{2}(\alpha_s+\alpha_i)}\end{array}\right. \tag{111}$$

By means of equation (42), K can be solved from (111). This expression for K is reintroduced into equations (111) and yields

$$\left\{\begin{array}{l}(V_s)_2=(V_s)_1 e^{-j\varphi_s'}\left\{1\mp\frac{1}{2}\sqrt{\frac{\delta_s\delta_i X_s X_i}{\sin\varphi_s\sin\varphi_i}-[\Delta\varphi+j(\alpha_s-\alpha_i)]^2}\right\}e^{-\frac{1}{2}(\alpha_s+\alpha_i)}\\ (V_i)_2=(V_i)_1 e^{j\varphi_i'}\left\{1\mp\frac{1}{2}\sqrt{\frac{\delta_s\delta_i X_s X_i}{\sin\varphi_s\sin\varphi_i}-[\Delta\varphi+j(\alpha_s-\alpha_i)]^2}\right\}e^{-\frac{1}{2}(\alpha_s+\alpha_i)}\end{array}\right. \tag{112}$$

By taking into account the boundary conditions (22) and by means of the expression for K, the following solution from (112) is obtained.

$$\left\{\begin{array}{l}V_s(n,t)=V_0\left\{\frac{\overset{n}{\underset{0}{\pi}}\left(1+\frac{1}{2}\xi\right)+\overset{n}{\underset{0}{\pi}}\left(1-\frac{1}{2}\xi\right)}{2}+j\frac{\Delta\varphi+j(\alpha_s-\alpha_i)}{\xi}\frac{\overset{n}{\underset{0}{\pi}}\left(1+\frac{1}{2}\xi\right)-\overset{n}{\underset{0}{\pi}}\left(1-\frac{1}{2}\xi\right)}{2}\right\}\\ \qquad e^{-\frac{1}{2}(\alpha_s+\alpha_i)n}\cdot e^{j(\omega_s t-n\varphi'+\Theta)}\\ V_i(n,t)=jV_0\frac{\delta_i X_i}{\xi\sqrt{B_i X_i\left(1-\frac{1}{4}B_s X_s\right)}}\frac{\overset{n}{\underset{0}{\pi}}\left(1+\frac{1}{2}\xi\right)-\overset{n}{\underset{0}{\pi}}\left(1-\frac{1}{2}\xi\right)}{2}e^{-\frac{1}{2}(\alpha_s+\alpha_i)n}\cdot\\ \qquad\cdot e^{-j(\omega_i t-n\varphi_i'-\Theta)}\cdot e^{-j\frac{1}{2}(\varphi_s+\varphi_i)}\end{array}\right. \tag{113}$$

From the equations (113), the way in which the amplification is affected by the losses in the circuit can be determined. The circuit has a length of N filter sections, and provided $\alpha_s = \alpha_i$, the amplification F of the signal wave will be

$$F=10\log\frac{1}{4}\left\{\left[\overset{N}{\underset{0}{\pi}}\left(1+\frac{1}{2}\xi\right)+\overset{N}{\underset{0}{\pi}}\left(1-\frac{1}{2}\xi\right)\right]^2+\frac{(\Delta\varphi)^2}{\xi^2}\left[\overset{N}{\underset{0}{\pi}}\left(1+\frac{1}{2}\xi\right)-\overset{N}{\underset{0}{\pi}}\left(1-\frac{1}{2}\xi\right)\right]^2\right\}-$$
$$-4.3(\alpha_s+\alpha_i)N \tag{114}$$

The remaining wave pairs in (16) and (17) can be treated in the same way and give similar solutions and expressions for the amplification.

5.4 Discussion of the Results

Inspection of the equations (107), (108), (109), (113) and (114) shows that the amplification of the signal wave is decreased by losses in both signal and idling circuits. This result is in agreement with results obtained for single parametric amplifiers. A closer examination, especially of equations (108) shows that losses in the signal circuit have a more unfavourable effect on the signal amplification than that due to losses in the idling circuit. This means that to some extent idling frequency losses are compensated by increased signal amplification.

In the calculations the losses at pump frequency have been neglected. A consideration of the pump losses would complicate the problem considerably. A pump voltage with varying amplitude will cause the characteristic impedance to vary along the line and it will no longer be possible to assume that the individual filter sections are matched. A rough estimation of the effect of pump losses can be obtained if the coupling terms δ are changed to $\delta_0 e^{-\alpha_p n}$, where α_p is the exponential damping of the pump wave.

CHAPTER 6

Noise

6.1 Origin of Noise

Now it is required to investigate how noise is generated in a parametric travelling-wave amplifier and to calculate its noise figure. It has been shown by A Uhlir[11] and by H Heffner and G Wade,[12] that the shot noise originating from the varicaps and the noise generated by the pump generator can be neglected compared to the thermal noise at signal and idling frequencies. Thus there remains only thermal noise which is generated, partly by the input circuit, and partly by the loss resistances within the filter ladder. When calculating the noise figure, it is assumed that the filter ladder is completely matched, so that no backward travelling noise is reflected at the input or within the filter ladder.

6.2 Distribution of Power within the Circuit

To be able to calculate the noise figure, it is necessary to investigate how signal and idling power applied at the input is transformed into signal power at the output. This transformation is expressed in the general equation.

$$(P_s)_{\text{out}} = (P_s)_{\text{in}} F_s(\omega_s, n) \cdot e^{-(\alpha_s+\alpha_i)n} + (P_i)_{\text{in}} \frac{\omega_s}{\omega_i} F_i(\omega_s, n)\, e^{-(\alpha_s+\alpha_i)n} \qquad (115)$$

The expressions $F_s(\omega_s, n)$ and $F_i(\omega_s, n)$ can be determined from the equations (107), (108) and (113). The treatment is restricted to calculating the noise figure in the middle of the band, where $\Delta\varphi = 0$. Thus the expressions $F_s(\omega_s, n)$ and $F_i(\omega_s, n)$ can be written

For a homogeneous line

$$\begin{cases} F_s(\omega_s, n) = \left\{\cosh\left(\frac{1}{2}\xi n\right) + \frac{\alpha_i - \alpha_s}{\xi}\sinh\left(\frac{1}{2}\xi n\right)\right\}^2 \\ F_i(\omega_s, n) = \frac{\xi^2 - (\alpha_s - \alpha_i)^2}{\xi^2}\sinh^2\left(\frac{1}{2}\xi n\right) \end{cases} \tag{116}$$

where

$$\xi = \sqrt{\frac{\delta_s \delta_i X_s X_i}{\varphi_s \varphi_i} + (\alpha_s - \alpha_i)^2}$$

For a circuit with concentrated elements

$$\begin{cases} F_s(\omega_s, n) = \left\{\frac{\overset{n}{\underset{0}{\pi}}\left(1 + \frac{1}{2}\xi\right) + \overset{n}{\underset{0}{\pi}}\left(1 - \frac{1}{2}\xi\right)}{2} + \frac{\alpha_i - \alpha_s}{\xi}\,\frac{\overset{n}{\underset{0}{\pi}}\left(1 + \frac{1}{2}\xi\right) - \overset{n}{\underset{0}{\pi}}\left(1 - \frac{1}{2}\xi\right)}{2}\right\}^2 \\ F_i(\omega_s, n) = \frac{\xi^2 - (\alpha_s - \alpha_i)^2}{\xi^2}\left[\frac{\overset{n}{\underset{0}{\pi}}\left(1 + \frac{1}{2}\xi\right) - \overset{n}{\underset{0}{\pi}}\left(1 - \frac{1}{2}\xi\right)}{2}\right]^2 \end{cases} \tag{117}$$

where

$$\xi = \sqrt{\frac{\delta_s \delta_i X_s X_i}{\sin\varphi_s \sin\varphi_i} + (\alpha_i - \alpha_s)^2}$$

6.3 Generation and Distribution of Thermal Noise

The available thermal noise power NP_{av} from a resistance R with the absolute temperature T can be written

$$(NP)_{av} = kT\Delta f \tag{118}$$

where k = BOLTZMAN constant and Δf = frequency interval. This corresponds to a noise source with the internal resistance R and the noise voltage ε

$$\varepsilon^2 = 4RkT\Delta f \tag{119}$$

Now the following notations are introduced

T_a = antenna temperature
T_i = idling input temperature
T_0 = filter ladder temperature

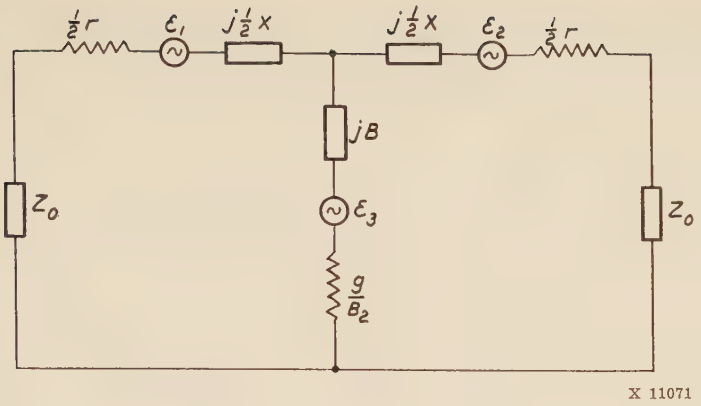

Fig. 22. Noise sources in a filter section.

The antenna and idling input are matched to the filter ladder, but can be separated from each other by use of filters. In that case T_a and T_i are different, and a low idling input temperature can be obtained by separate cooling of the idling input circuit. The noise powers received by the filter ladder are

$$\begin{cases} (NP_s)_{\text{in}} = k\,T_a\,\Delta f \\ (NP_i)_{\text{in}} = k\,T_i\,\Delta f \end{cases} \tag{120}$$

It now remains to determine how the noise generated by a filter section is distributed within the filter ladder. A start is made from a T-section matched in both directions and with noise sources according to *fig. 22*.

According to equation (119) the noise voltages can be written

$$\begin{cases} (\varepsilon_1)_s^2 = (\varepsilon_2)_s^2 = 2r_s k T_0 \Delta f \\ (\varepsilon_3)_s^2 = 4\,\dfrac{g_s}{B_s^2}\,k T_0 \Delta f \\ (\varepsilon_1)_i^2 = (\varepsilon_2)_i^2 = 2r_i k T_0 \Delta f \\ (\varepsilon_3)_i^2 = 4\,\dfrac{g_i}{B_i^2}\,k T_0 \Delta f \end{cases} \tag{121}$$

All noise sources are uncorrelated and thus can be superposed.

As before it is assumed that $\delta \ll B$, $r \ll X$ and $g \ll B$ and thus the losses and the coupling between noise of signal and idling frequencies can be neglected, when determining the distribution of noise in *fig. 22*.

It is seen from *fig. 22* that the filter section is emitting equal noise powers backwards and forwards. In the forward direction the noise powers $d(NP_s)_{\text{circuit}}$ and $d(NP_i)_{\text{circuit}}$ are emitted. These noise powers can easily be determined from *fig. 22* and thus

$$\begin{cases} d(NP_s)_{\text{circuit}} = \dfrac{B_s X_s \left(\dfrac{r_s}{X_s} + \dfrac{g_s}{B_s} \right)}{\sqrt{B_s X_s \left(1 - \dfrac{1}{4} B_s X_s \right)}} kT_0 \Delta f \\ d(NP_i)_{\text{circuit}} = \dfrac{B_i X_i \left(\dfrac{r_i}{X_i} + \dfrac{g_i}{B_i} \right)}{\sqrt{B_i X_i \left(1 - \dfrac{1}{4} B_i X_i \right)}} kT_0 \Delta f \end{cases} \tag{122}$$

Introducing the exponential damping according to (110) the equations (122) can be written

$$\begin{aligned} d(NP_s)_{\text{circuit}} &= 2\alpha_s kT_0 \Delta f \\ d(NP_i)_{\text{circuit}} &= 2\alpha_i kT_0 \Delta f \end{aligned} \tag{123}$$

The formulas (123) are valid both for homogeneous lines and circuits with concentrated elements.

6.4 Noise Figure of Parametric Travelling-Wave Amplifier

The noise powers applied to and generated in the filter ladder are known from the equations (120) and (123). By means of the power relations in (115) the noise power $(NP_s)_{\text{out}}$ of signal frequency at the output of a parametric circuit with N filter sections can be determined. In this case

$$\begin{aligned} (NP_s)_{\text{out}} = {} & kT_a \Delta f \cdot F_s(\omega_s, N) + kT_i \Delta f \frac{\omega_s}{\omega_i} F_i(\omega_s, N) + \\ & + 2\alpha_s kT_0 \Delta f \sum_{n=0}^{N-1} F_s(\omega_s, n) + 2\alpha_i kT_0 \Delta f \frac{\omega_s}{\omega_i} \sum_{n=0}^{N-1} F_i(\omega_s, n) \end{aligned} \tag{124}$$

The noise figure NF of a parametric travelling-wave amplifier is defined by

$$NF = \frac{(NP_s)_{\text{out}}}{kT_a \Delta f F_s(\omega_s, N)} \tag{125}$$

The expressions (116) or (117) are introduced into (124) and (125) and the noise figure of different parametric circuits can be determined. As an example it is decided to determine the noise figure of a homogeneous parametric circuit, where $\Delta\varphi = 0$ and $\alpha_s = \alpha_i$. In this case

$$NF = 1 + \frac{\omega_s}{\omega_i}\frac{T_i}{T_a}\tanh^2\left(\frac{1}{2}\xi N\right) + 2\alpha_s\frac{T_0}{T_a}\int_0^{N-1}\frac{\cosh^2\left(\frac{1}{2}\xi n\right)}{\cosh^2\left(\frac{1}{2}\xi N\right)}e^{(\alpha_s+\alpha_i)(N-n)}dn + \\ + 2\alpha_i\frac{\omega_s}{\omega_i}\frac{T_0}{T_a}\int_0^{N-1}\frac{\sinh^2\left(\frac{1}{2}\xi n\right)}{\cosh^2\left(\frac{1}{2}\xi N\right)}e^{(\alpha_s+\alpha_i)(N-n)}dn \tag{126}$$

If the damping in the circuit can be neglected, the familiar expression for the noise figure below is obtained

$$NF \approx 1 + \frac{\omega_s}{\omega_i}\cdot\frac{T_i}{T_a} \tag{127}$$

6.5 Measures to Minimize the Noise Figure

The measures that should be taken to obtain a low noise figure can be concluded from the noise figures in (126) and (127). First of all the signal frequency should be lower than the idling frequency, and the difference between them should be as wide as possible, thus making it more difficult for the idling noise to be transformed into signal noise. Secondly, the antenna and idling input should be separated by filters, and the idling input circuit separately cooled, thus minimizing the idling input noise power. Thirdly, losses and temperature in the filter ladder should be kept as low as possible, thus avoiding additional thermal noise.

CHAPTER 7

Discussion

The theoretical treatment has shown that parametric travelling-wave amplification is obtained when certain phase conditions are fulfilled. When the group velocities of the signal and idling waves are equal, wide-band amplification is obtained, and this is the principal advantage of the travelling-wave amplifier over the single parametric amplifier. To this is added the advantage of the unidirectional, stable gain in the wide-band parametric travelling-wave amplifier.

However, the greatest advantage of parametric amplifiers is still the possibility of obtaining amplifiers with a low noise figure. The principal ways of minimizing the noise figure are wide separation of signal and idling frequencies whereby the signal frequency is lower and separate cooling of the idling input circuit. From practical reasons wide separation of signal and idling frequencies is preferred.

In the literature some practical parametric travelling-wave amplifiers developed by R. S. Engelbrecht[13] have been described. These amplifiers have amplified signal frequencies up to 650 Mc/s, and have given considerable bandwidths. The circuits used have been of low-pass type.

If consideration is now made of the desirability of wide separation of signal and idling frequencies, low-pass structures have certain drawbacks. It can be shown that if the signal or idling phase shift is decreased the amplification is also decreased. Thus it follows that in a low-pass structure the signal and idling frequencies can be widely separated only with considerable sacrifice of gain. This leads to the possibility of using band-pass structures where the signal and idling frequencies can be separated without sacrifice of gain. The layout of band-pass structures will be determined by the desired amplification, bandwidth and noise figure.

When predicting future development in parametric travelling-wave amplifiers, it can be noted that varicaps available are already applicable to parametric amplification up to frequencies of about 10 kMc/s. Thus the basic components are available, and it can be supposed that future work on parametric travelling-wave amplification will be concerned with the development of various parametric filter structures usable at higher frequencies and giving low noise figures.

Acknowledgement

The investigation described has been carried out in Sweden at the Research Institute of National Defence. Their permission to publish the paper is much appreciated.

Bibliography

1. Tien, P K & Suhl, H: *A Traveling-Wave Ferromagnetic Amplifier.* Proc. IRE *46*(1958): 4, pp. 700—706.
2. Tien, P K: *Parametric Amplification and Frequency Mixing in Propagating Circuits.* J. appl. Phys. *29*(1958): 9, 1347—1357.
3. Louisell, W H & Quate, C F: *Parametric Amplification of Space Charge Waves.* Proc. IRE *46* (1958): 4, pp. 707—716.
4. Roe, G M & Boyd, M R: *Parametric Energy Conversion in Distributed Systems.* Proc. IRE *47* (1959): 7, pp. 1213—1218.
5. Manley, J M & Rowe, H E: *Some General Properties of Nonlinear Elements*—Part I. *General Energy Relations.* Proc. IRE *44*(1956): 7, pp. 904—913.
6. Foster, R M: *A Reactance Theorem.* Bell Syst. tech. J. *3*(1924): 2, pp. 259—267.
7. Weijers, Th J: *Filters Built from Coaxial Conductors.* Philips Telecomm. Rev. *18*(1957): 4, pp. 186—206; *19*(1958): 1, pp. 23—54.
8. Ragan, C L: *Microwave Transmission Circuits.* New York 1948. (Radiation Laboratory Series 9.)
9. Cohn, S B: *Principles of Transmission-Line Filter Design.* New York 1947. (Radio Research Laboratory Staff, Very High-Frequency Techniques.)
10. Henoch, B T: *Investigations of the Disk-Loaded and Helical Waveguide.* Trans. Roy. Inst. Technol. Stockholm 1958: 129.
11. Uhlir, Jr, A: *The Potential of Semiconductor Diodes in High-Frequency Communications.* Proc. IRE *46*(1958): 6, pp. 1099—1115.
12. Heffner, H & Wade, G: *Gain, Band Width, and Noise Characteristics of the Variable-Parameter Amplifier.* J. appl. Phys. *29*(1958): 9, pp. 1321—1331.
13. Engelbrecht, R S: *Nonlinear-Reactance (Parametric) Traveling-Wave Amplifiers for UHF.* 1959 Solid-State Circuits Conference. Digest of Technical Papers. Philadelphia 1959.

Manuscript received by the editors January 1960.

Transient Electromagnetic Waves around a Cylindrical Transmitting Antenna

BY

PER-OLOF BRUNDELL*

UDC 621.371
621.396.67
LME 764,765

The purpose of the present article is to determine theoretically the electromagnetic field generated by a cylindrical transmitting antenna, which is fed by a voltage of given, non-sinusoidal timevariation. The mathematical formulation chosen yields a certain type of mixed wave equation problem. By considering a combined EMF and current generator feeding method related to an infinite antenna it is shown that the field can be considered as built from an infinite set of elementary travelling waves being reflected at the antenna ends. These waves are determined exactly and their relationship to the travelling wave antenna theory of Hallén is demonstrated.

* Division of Theoretical Electrical Engineering, Royal Institute of Technology, Stockholm.

Introduction

The theory of the cylindrical antenna was developed by HALLÉN (see the bibliography) and his followers. Out of a great many papers published in this range only two (as far as the author has been able to discover) contain serious attacks on non-stationary, non-homogeneous problems.

In HALLÉN (1939) the absorption of unperiodic radiation is treated by means of HALLÉN's linearization method. SCHMITT (SCHMITT 1959) has investigated the properties of transient communication between two antennas theoretically and experimentally. His paper, however, provides no essential contribution to the theoretical aspects of the problem.

The successful travelling wave antenna theory created by HALLÉN (HALLÉN 1948 a, b, 1953, 1955, 1956) hints a natural approach to transient antenna problems. In the present paper the travelling wave structure of the electromagnetic field around a cylindrical transmitting antenna is investigated theoretically.

CHAPTER 1

General Electromagnetic Considerations

We first state the following theorem.

Any electromagnetic field due to electric charges and currents continuously distributed along a closed surface S is uniquely determined by the prescription at each point on S of

a) either the tangential component of the electric field strength

b) or the electric surface current density $= n\,x$ the jump, $\boldsymbol{H}_e - \boldsymbol{H}_i$, of the $\boldsymbol{H}$-vector at the surface

and at each point of space of

c) the values at some instant t_0 of all the electromagnetic field components.

The statement is an immediate consequence of POYNTING's theorem and a slight variation of a well-known uniqueness theorem of electromagnetic theory (cf. STRATTON 1941, p. 486). The difference between any two solutions of MAXWELL's equations describing a physical situation as above and satisfying conditions a – c has a POYNTING vector the normal component of which at any point of S is either continuous and zero (condition a) or at least continuous (condition b). Thus the total field energy rate of increase throughout space (inside and outside S) will always be zero. As the energy at t_0 is zero it will remain zero. Hence the corresponding electromagnetic field vanishes which establishes the theorem.

Incidentally, from a mathematical point of view, the above result is equivalent to a uniqueness theorem on a certain class of mixed vector wave equation problems. The corresponding mixed scalar problem prescribes CAUCHY values at $t = t_0$ and either the functional value jump by a continuous normal derivative or the normal derivative jump by a continuous functional value at any point of S (cf. PETROWSKI 1955, p. 122). We now apply these results to a straight cylindrical antenna, consisting of a thin metal tube of negligible resistivity and

being operated in a TM-manner. Suppose that at some instant when the antenna is electrically dead a distributed longitudinal, axial-symmetric surface EMF is applied to some parts of the antenna and that a likewise longitudinal, axial-symmetric surface current is injected along other parts (where the antenna may then be considered as removed). Then this determines mathematically and physically a unique electromagnetic field inside and outside the antenna.

The HERTZIAN vector of any electromagnetic field in free space, due to charges and currents and having its origin at a time t_0 not infinitely remote, could be defined

$$\boldsymbol{\Pi}(x, y, z, t) = c^2 \int_{t_0}^{t} \boldsymbol{A}(x, y, z, \tau)\, d\tau \tag{1.01}$$

where $\boldsymbol{A}$ is the vector potential. This gives

$$\boldsymbol{\Pi}(x, y, z, t) = \frac{1}{4\pi\varepsilon_0} \iiint \frac{\boldsymbol{P}\left(\xi, \eta, \zeta, t - \frac{r}{c}\right)}{r}\, dv \tag{1.02}$$

where

$$\boldsymbol{P}(t) = \int_{t_0}^{t} \boldsymbol{J}(\tau)\, d\tau \tag{1.03}$$

$\boldsymbol{J}$ being the current density vector. $\boldsymbol{P}$ has the same dimension as a dipole moment per unit volume. Incidentally, it is clear from simple considerations that an electric polarization according to Eq. (1.03) yields the same electromagnetic field — but not the same $\boldsymbol{D}$-vector — as the actual current-charge distribution. With V denoting the scalar potential one immediately gets the well-known relations

$$\boldsymbol{A} = \frac{1}{c^2} \frac{\partial \boldsymbol{\Pi}}{\partial t} \tag{1.04}$$

$$V = -\operatorname{div} \boldsymbol{\Pi} \tag{1.05}$$

and, finally, for the electromagnetic field

$$\boldsymbol{E} = \operatorname{curl} \operatorname{curl} \boldsymbol{\Pi} - \frac{\boldsymbol{P}}{\varepsilon_0} \tag{1.06}$$

$$\boldsymbol{B} = \frac{1}{c^2} \operatorname{curl} \frac{\partial \boldsymbol{\Pi}}{\partial t} \tag{1.07}$$

If our antenna is operating as described above the antenna current will everywhere be longitudinal and the $\boldsymbol{\Pi}$-vector will have but one cartesian component with suitable orientation of the coordinate system. As in stationary theory the complete determination of the electromagnetic field corresponding to a TM mode of operation is reduced to the finding of one single scalar quantity.

CHAPTER 2

Formulation of the Problem

A voltage $2V_0(t)$ being zero when $t < 0$ is maintained across an infinitesimally small gap between two straight, circularly cylindrical thin metal tubes of radius a, lengths l_1 and l_2 and negligible resistivity (see fig. 1). The function $V_0(t)$ is assumed to be infinitely continuously differentiable (even at $t = 0$; step and pulse voltages are treated as limiting forms, see below).

The magnitude $\Pi(r, z, t)$ of the corresponding HERTZIAN vector will then form a continuous function satisfying the following conditions.

a)
$$\Box \Pi = \frac{1}{r}\frac{\partial}{\partial r}\left(r\frac{\partial \Pi}{\partial r}\right) + \frac{\partial^2 \Pi}{\partial z^2} - \frac{1}{c^2}\cdot\frac{\partial^2 \Pi}{\partial t^2} = 0 \tag{2.01}$$

when $r \neq a$

b)
$$\Pi = \frac{\partial \Pi}{\partial t} = 0 \quad \text{at} \quad t = 0 \tag{2.02}$$

c) at $r = a$

$$\frac{1}{r}\frac{\partial}{\partial r}\left(r\frac{\partial \Pi}{\partial r}\right) = 2V_0(t)\,\delta(z) \quad \text{when} \quad -l_2 < z < l_1 \tag{2.03}$$

d)
$$I(z, t) = -2\pi\varepsilon_0 a\left(\frac{\partial^2 \Pi_e}{\partial r \partial t} - \frac{\partial^2 \Pi_i}{\partial r \partial t}\right)_{r=a} = 0 \tag{2.04}$$

when $z > l_1$
$z < -l_2$

With respect to Eq. (2.01) condition c) is equivalent to the statement that along the antenna Π forms a set of undistorted waves travelling with velocity c (cf. HALLÉN e.g. 1953, p. 403 – 404).

In condition d) the indices e and i refer to the external and internal field respectively.

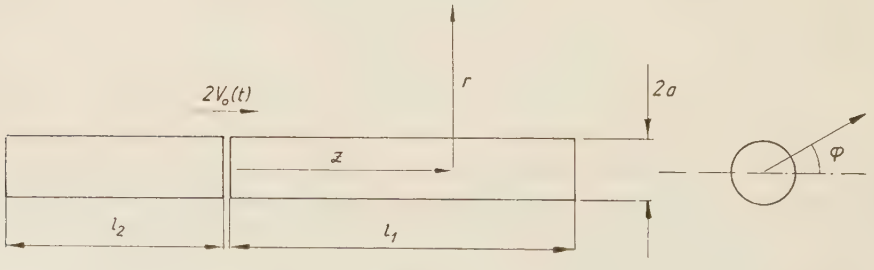

X 11043

Fig. 1.

When applying the uniqueness theorem of Chapter 1 to the problem just stated it must be remembered that our field is bound to have singularities at $r = a$; $z = -l_2, 0, l_1$.

Yet by considering these singularities as the result of a limiting process containing continuously differentiable functions the theorem may still be applied. One may also, when applying POYNTING's theorem to a solution difference, exclude three tori of radius ε containing the critical circles. The character of the singularity near the feeding gap is described by a pure electrostatic field (see Chapter 5), known in advance. Further the magnetic field near the antenna ends will be bounded whilst the electric field increases as $\varepsilon^{-1/2}$. Hence the contribution from the ring surfaces will tend to zero with ε and our theorem holds.

In any boundary problem of electromagnetic theory a given boundary value will not affect the solution in a point at a distance d until a time $\frac{d}{c}$ has elapsed. Our feeding voltage $2V_0(t)$ will thus generate a field being zero outside the expanding wave front $(r-a)^2+z^2=c^2t^2$. Denote by $\boldsymbol{\Pi}_0$ the HERTZIAN vector in the case of an infinite antenna. Then $\boldsymbol{\Pi}_0=\boldsymbol{\Pi}$ when $t<\frac{l_1}{c}$, $t<\frac{l_2}{c}$. We now define $\boldsymbol{\Pi}_{1,1}$ as describing the field generated by a current $-I_0(z,t)$ — I_0 being the current, corresponding to $\boldsymbol{\Pi}_0$ — injected into an infinite antenna in the region $z>l_1$. $\boldsymbol{\Pi}_{1,1}$ will then be zero until $t=\frac{l_1}{c}$ and the corresponding field will thereafter expand outwards, its wave front being $(r-a)^2+(z-l_1)^2=c^2\left(t-\frac{l_1}{c}\right)^2$. $\boldsymbol{\Pi}_0+\boldsymbol{\Pi}_{1,1}$ will then – because of identical boundary values – describe the actual electromagnetic field in any point until the first reflection at $z=-l_2$ starts influencing it. We further analogously define $\boldsymbol{\Pi}_{2,1}$ as characterizing the field generated by $-I_0$ injected in the region $z<-l_2$ of an infinite antenna. Generally each elementary field $\boldsymbol{\Pi}_{1,n}$ and $\boldsymbol{\Pi}_{2,n}$ is defined as generated by a current cancelling the current of the preceding one as soon as it reaches outside the limit of our finite antenna. Thus with $p>0$:

$$\left.\begin{aligned} E_{1,2p+1}&=0\\ E_{2,2p}&=0 \end{aligned}\right\}\ \text{when } z<l_1 \qquad \left.\begin{aligned} I_{1,2p+1}&=-I_{1,2p}\\ I_{2,2p}&=-I_{2,2p-1} \end{aligned}\right\}\ \text{when } z>l_1 \tag{2.05}$$

$$\left.\begin{aligned} E_{1,2p}&=0\\ E_{2,2p+1}&=0 \end{aligned}\right\}\ \text{when } z>-l_2 \qquad \left.\begin{aligned} I_{1,2p}&=-I_{1,2p-1}\\ I_{2,2p+1}&=-I_{2,2p} \end{aligned}\right\}\ \text{when } z<-l_2 \tag{2.06}$$

the letter E everywhere denoting the z-component of the electric force at the surface.

Obviously

$$\Pi=\Pi_0+\sum_{n=1}^{\infty}(\Pi_{1,n}+\Pi_{2,n}) \tag{2.07}$$

as the boundary conditions of the left and right members of this equation—described by Eq:s (2.03—2.04) and (2.05—2.06) plus the above discussions, respectively—are identical. Each term in the right member of Eq. 2.07 has the character of an elementary travelling wave generated by an infinite antenna. The wave $\Pi_{1,\,2p}$ describes, for instance, a field generated after $2p$ antenna end reflections, being zero when $t < \dfrac{2pl_1 + (2p-1)l_2}{c}$ and outside

$$(r-a)^2 + (z+l_2)^2 = c^2\left(t - \frac{2pl_1 + (2p-1)l_2}{c}\right)^2$$

Its value will obviously depend on the pre-history of the total field ($2p$, l_1, l_2 etc.) but not on forthcoming reflections. The close relationship of these waves to those of HALLÉN's theory will be demonstrated in Chapter 7.

CHAPTER 3

Calculation of the Outgoing Wave

We now proceed to calculate the outgoing wave Π_0. Thereby condition d) of the preceding section is eliminated and Eq. (2.03) is valid for all z-values. For the sake of brevity we drop index zero in the following.

The substitution

$$\left.\begin{aligned} x &= \frac{1}{2}(ct - z) \\ y &= \frac{1}{2}(ct + z) \end{aligned}\right\} \tag{3.01}$$

yields

$$\frac{1}{r}\frac{\partial}{\partial r}\left(r\frac{\partial \Pi}{\partial r}\right) - \frac{\partial^2 \Pi}{\partial x\,\partial y} = 0 \tag{3.02}$$

We now dissolve Π into a double LAPLACE-integral

$$\Pi = -\frac{1}{4\pi^2}\int_{\Gamma_{s_x}}\int_{\Gamma_{s_y}} \Pi_L(r, s_x, s_y)\, e^{s_x x + s_y y}\, ds_x\, ds_y \tag{3.03}$$

where Γ_{s_x} and Γ_{s_y} are vertical paths in the right semi-planes and

$$\Pi_L = \int_0^\infty\int_0^\infty \Pi(r, \xi, \eta)\, e^{-s_x\xi - s_y\eta}\, d\xi\, d\eta \tag{3.04}$$

With respect to Eq. (2.02) a LAPLACE-transformation of Eq. (3.02) gives

$$\frac{1}{r}\frac{\partial}{\partial r}\left(r\frac{\partial \Pi_L}{\partial r}\right) - s_x s_y \Pi_L = 0 \tag{3.05}$$

Thus Π_L must be a BESSEL-function of order zero and argument $r\sqrt{-s_x s_y}$. As Π_L is necessarily bounded when $r \to \infty$ and when $r \to 0$ we get

$$\Pi_L = \left.\begin{array}{ll} A(s_x, s_y)\dfrac{K_0\left(r\sqrt{s_x s_y}\right)}{K_0\left(a\sqrt{s_x s_y}\right)} & \text{when } r > a \\ A(s_x, s_y)\dfrac{I_0\left(r\sqrt{s_x s_y}\right)}{I_0\left(a\sqrt{s_x s_y}\right)} & \text{when } r < a \end{array}\right\} \tag{3.06}$$

where $Re\ \sqrt{s_x s_y} > 0$, I_0 and K_0 are defined according to (WATSON 1944, p. 77—78) and $A(s_x, s_y)$ is to be determined.

LAPLACE-transforming Eq. (2.03) and substituting the results of Eq:s (3.05—3.06) we obtain

$$A(s_x, s_y) = \frac{c}{s_x s_y}\int_0^\infty V_0(\tau) e^{-\frac{c}{2}(s_x+s_y)\tau}\, d\tau$$

and, finally, after changing the order of integration and introducing x, y according to Eq. (3.01)

$$\Pi_e = \int_0^\infty V_0(\tau)\, d\tau \int_{\Gamma_{s_x}}\int_{\Gamma_{s_y}} -\frac{c}{4\pi^2} e^{\frac{c}{2}(t-\tau)(s_x+s_y) - \frac{z}{2}(s_x-s_y)} \frac{K_0\left(r\sqrt{s_x s_y}\right)}{K_0\left(a\sqrt{s_x s_y}\right)} \frac{ds_x\, ds_y}{s_x s_y} \tag{3.07}$$

valid when $r > a$

Making the substitution

$$\left.\begin{array}{l} \dfrac{c}{2}(t-\tau)(s_x+s_y) - \dfrac{z}{2}(s_x - s_y) = \alpha \\ \sqrt{s_x s_y} = w \end{array}\right\} \tag{3.08}$$

one has

$$\left.\begin{array}{l} s_x = \dfrac{\alpha + \sqrt{\alpha^2 - [c^2(t-\tau)^2 - z^2]w^2}}{c(t-\tau) - z} \\ s_y = \dfrac{\alpha - \sqrt{\alpha^2 - [c^2(t-\tau)^2 - z^2]w^2}}{c(t-\tau) + z} \end{array}\right\} \tag{3.09}$$

and the Jacobian

$$\frac{\partial(s_x, s_y)}{\partial(\alpha, w)} = \frac{2w}{\sqrt{\alpha^2 - [c^2(t-\tau)^2 - z^2]w^2}} \tag{3.10}$$

We will now discuss the inner double integral ϕ_e of Eq. (3.07) by performing the substitution of Eq. (3.08) in steps. Denoting the original integrand $F(s_x, s_y)$, $G(s_x, \alpha)$ and $H(w, \alpha)$ respectively, one has

$$\phi_e = \int_{\Gamma_{s_x}} ds_x \int_{\Gamma_{s_y}} F(s_x, s_y)\, ds_y = \int_{\Gamma_{s_x}} ds_x \int_{\Gamma_\alpha} G(s_x, \alpha)\, \frac{d\alpha}{\frac{\partial \alpha}{\partial s_y}} \tag{3.11}$$

where Γ_α is a vertical contour in the α-plane. As Γ_α is independent of s_x, we may invert the order of integration and get

$$\phi_e = \int_{\Gamma_\alpha} d\alpha \int_{\Gamma_{s_x}} G(s_x, \alpha)\, \frac{ds_x}{\frac{\partial \alpha}{\partial s_y}}$$

Here, in the inner integral $d\alpha = 0$. Consequently

$$ds_x = -\frac{\frac{\partial \alpha}{\partial s_y}}{\frac{\partial(\alpha, w)}{\partial(s_x, s_y)}}\, dw$$

and our double integral finally becomes

$$\phi_e = -\int_{\Gamma_\alpha} d\alpha \int_{\Gamma_w(\alpha)} H(\alpha, w)\, \frac{\partial(s_x, s_y)}{\partial(\alpha, w)}\, dw =$$

$$= \frac{c}{2\pi^2} \int_{\Gamma_\alpha} e^{\alpha}\, d\alpha \int_{\Gamma_w(\alpha)} \frac{K_0(rw)}{K_0(aw)}\, \frac{dw}{w\sqrt{\alpha^2 - [c^2(t-\tau)^2 - z^2]\, w^2}} \tag{3.12}$$

As Π_e vanishes when $t - \tau < 0$ and as it is further an even function of z we only consider the case $t - \tau > 0$, $z > 0$. The properties of $\Gamma_w(\alpha)$ are easily discussed since the corresponding contours in the w^2-plane are parabolas.

Figs. 2 and 3 show the character of $\Gamma_w(\alpha)$ when $c(t-\tau) > z$ and $c(t-\tau) < z$ respectively. The signs of the square root at distant parts of the contour as well as the branch cuts of the analytic function integrated are also demonstrated. Thus when $c(t-\tau) < z$ the inner integrand is regular to the right of the branch cut – K_0 has no zeros – and of asymptotic behaviour $\frac{e^{-(r-a)w}}{w^2}$ in the right semi-plane. Consequently, the inner integral is then zero. Similarly, when $c(t-\tau) > z$, $\Gamma_w(\alpha)$ may be deformed into a vertical contour Γ_w, having

$$0 < Re\, w < \frac{Re\, \alpha}{\sqrt{c^2(t-\tau)^2 - z^2}}$$

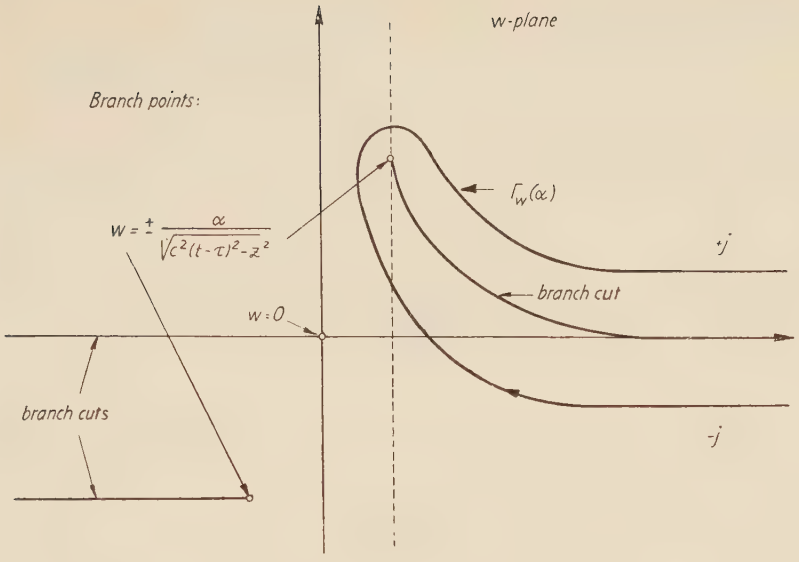

Fig. 2. $c(t-\tau) > z$

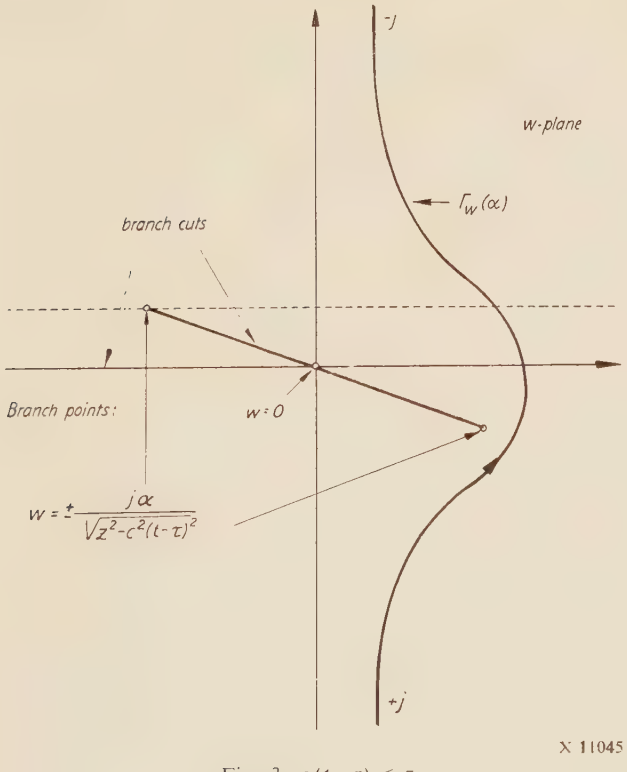

Fig. 3. $c(t-z) < z$

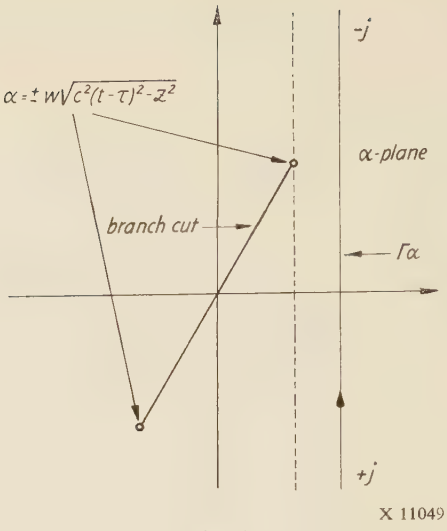

Fig. 4.

As Γ_w is independent of α, we may again invert the order of integration, and get

$$\phi_e = \frac{c}{2\pi^2} \int_{\Gamma_w} \frac{K_0(rw)}{K_0(aw)} \frac{dw}{w} \int_{\Gamma_\alpha} \frac{e^{\alpha}\, d\alpha}{\sqrt{\alpha^2 - [c^2(t-\tau)^2 - z^2]\, w^2}}$$

The character of Γ_α, the signs of the square root, and the corresponding branch cut are demonstrated in fig. 4. Deforming Γ_α into a closed contour encircling the branch cut we determine the α-integral to $-2\pi j I_0(\sqrt{c^2(t-\tau)^2 - z^2}\, w)$. Finally, as $I_0(z)$ is asymptotically $\sim \frac{e^z}{\sqrt{z}}$ in the right semi-plane it is clear by contour deformation that $\phi_e = 0$ whenever $r - a > \sqrt{c^2(t-\tau)^2 - z^2}$ that is when $\tau > t - \frac{\sqrt{(r-a)^2 + z^2}}{c}$

We have thus arrived at the following final expression of the HERTZIAN vector

$$\Pi_e(r, z, t) = \int_0^{t - \frac{\sqrt{(r-a)^2 + z^2}}{c}} V_0(\tau)\, \phi_e(r, z, t-\tau)\, d\tau \tag{3.13}$$

where

$$\phi_e(r, z, t) = \frac{c}{j\pi} \int_{\Gamma_w} \frac{K_0(rw)}{K_0(aw)}\, I_0\left(\sqrt{c^2 t^2 - z^2}\, w\right) \frac{dw}{w} \tag{3.14}$$

valid when $r > a$.

By considering Eq. (3.06) and the steps of the following integration process it becomes clear that the internal electromagnetic field is obtained by exchanging K_0 for I_0 in Eq. (3.14). Thus when $r < a$

$$\Pi_i(r, z, t) = \int_0^{t - \frac{\sqrt{(a-r)^2 + z^2}}{c}} V_0(\tau) \phi_i(r, z, t - \tau) d\tau \tag{3.15}$$

where

$$\phi_i(r, z, t) = \frac{c}{j\pi} \int_{\Gamma_w} \frac{I_0(rw)}{I_0(aw)} I_0\left(\sqrt{c^2 t^2 - z^2}\, w\right) \frac{dw}{w} \tag{3.16}$$

By means of the substitution $w \to -w$ the integral of Eq. (3.16) may be evaluated as a sum of residues, namely

$$\phi_i(r, z, t) = c \left\{ 1 - 2 \sum_{m=1}^{\infty} \frac{J_0\left(\frac{\xi_{0m}}{a} r\right)}{\xi_{0m} J_1(\xi_{0m})} J_0\left(\frac{\xi_{0m}}{a} \sqrt{c^2 t^2 - z^2}\right) \right\} \tag{3.17}$$

where ξ_{0m} are the zeros of $J_0(x)$. Eq:s (3.15) and (3.17) express the internal electromagnetic field as a sum of transient TM wave-guide waves.

Of course the integration process leading up to Eq:s (3.13—3.16) can be stringently justified. For some physical reasons it is, however, interesting to demonstrate directly that our solution has indeed the properties a)—c) of Chapter 2. As some of the results of the next section will be needed in that discussion we postpone it for the moment.

CHAPTER 4

The Response of a Unit Pulse Voltage

Eq:s (3.13) and (3.15) have a distinct physical meaning. They express the electromagnetic disturbance as superimposed by the influence of a set of unit pulse voltages occurring at instants τ. Thereby ϕ is the influence (GREEN'S) function, or, physically speaking, the HERTZIAN vector response of a unit pulse voltage. Because of Eq. (1.04), ϕ is also c^2 times the vector potential response of a unit step voltage. The upper integration limit expresses the wave front shape—or, rather, the latest instant at which a disturbance travelling with the velocity c must emanate from the feeding gap in order to have reached a given point r, z at a given instant t.

10*—910127

Introducing in Eq. (3.14) the new quantities

$$\left.\begin{aligned} u &= \frac{r}{a} \\ v &= \frac{\sqrt{c^2 t^2 - z^2}}{a} \end{aligned}\right\} \tag{4.01}$$

the relation takes the form

$$\phi_e = \frac{c}{j\pi} \int_{\Gamma_w} \frac{K_0(uw)}{K_0(w)} I_0(vw) \frac{dw}{w} \tag{4.02}$$

that is, contrary to what might be expected, ϕ_e is a function of only two independent variables.

Similarly we have

$$\phi_i = \frac{c}{j\pi} \int_{\Gamma_w} \frac{I_0(uw)}{I_0(w)} I_0(vw) \frac{dw}{w} \tag{4.03}$$

ϕ is singular at the wave front. However, writing when $u \neq 1$

$$\phi = \sqrt{v^2 - (u-1)^2}\, \psi(u, v) \tag{4.04}$$

ψ can be shown—as a consequence of the asymptotic properties of K_0 and I_0—to be infinitely continuously differentiable at the wave front $v = |u-1|$. We calculate the corresponding leading term

$$\phi_e \approx \frac{c}{j\pi} \sqrt{\frac{1}{2\pi uv}} \int_{\Gamma_w} \frac{e^{(v-u+1)w}}{w^{3/2}}\, dw = \sqrt{\frac{8\, c^2 (v-u+1)}{\pi^2 uv}}$$

Similarly

$$\phi_i \approx \sqrt{\frac{8\, c^2 (v-1+u)}{\pi^2 uv}}$$

Thus at a point in the wave front—with $v = u-1$ — we have

$$\left.\begin{aligned} \psi_e &= \frac{2c}{\pi} \frac{1}{(u-1)\sqrt{u}} \\ \psi_i &= \frac{2c}{\pi} \frac{1}{(1-u)\sqrt{u}} \end{aligned}\right\} \tag{4.05}$$

Generally, the wave equation can be reduced into an ordinary differential equation describing the distribution of a discontinuity along a characteristic surface—or, physically speaking, the wave front character during propagation (cf. COURANT-HILBERT 1937, p.

360—364). Thus, inserting Eq. (4.04) in the wave equation, we can—except for the numerical factor—state Eq. (4.05) directly, using the mere fact that ψ and its derivatives are finite at the wave front.

To discuss the character of the wave front at the antenna itself—where ϕ is constant—we form

$$\left(\frac{\partial \phi_e}{\partial u}\right)_{u=1} = -\frac{c}{j\pi v} \int_{\Gamma_w} \frac{K_1\left(\frac{w}{v}\right)}{K_0\left(\frac{w}{v}\right)} I_0(w)\, dw$$

When v is small $\frac{K_1}{K_0} \approx 1$, and further $\int_{\Gamma_w} I_0(w)\, dw = 2j$. Similar relations hold for $\frac{\partial \phi}{\partial u}$. Thus with

$$\left(\frac{\partial \phi}{\partial u}\right)_{u=1} = \frac{\psi_1}{v} \tag{4.06}$$

we have

$$\left.\begin{aligned} [\psi_{1e}]_{v=0} &= -\frac{2c}{\pi} \\ [\psi_{1i}]_{v=0} &= \frac{2c}{\pi} \end{aligned}\right\} \tag{4.07}$$

Eq:s (4.04—4.05) and (4.06—4.07) can be related by a geometric study of the wave front. They have the following physical meaning. If the antenna is fed by a pulse voltage, the electromagnetic field forces will tend to infinity in the vicinity of the wave front. The character of this singularity will be $\delta^{-3/2}$ where δ is the distance to the wave front. This statement being true at the antenna itself, we conclude that the antenna current and surface charge density show the same $\delta^{-3/2}$-behaviour near the wave front.

Turning to Eq. (4.02) we want to express ϕ_e as an outwardly real integral. This could be done immediately by letting Γ_w be the imaginary axis, indented at the origin, and exchanging K_0, I_0 for H_0, J_0 with a real argument. In order to get an integral with exponentially decreasing integrand we keep, however, the functions K_0, I_0 and transform Eq. (4.02), making use of the relations

$$K_0(ze^{\pm j\pi}) = K_0(z) \mp j\pi I_0(z) \tag{4.08}$$

derived from the formula

$$K_0(z) = -I_0(z)\left(\log\frac{z}{2} + \gamma\right) + k(z) \tag{4.09}$$

where γ is EULER's constant and $k(z)$ is regular and zero when $z=0$.

According to Eq. (4.09) the indentation integral mentioned above equals c and we get

$$\frac{1}{c}\phi_e = 1 -$$

$$-\frac{1}{\pi^2}\int_{j\varepsilon}^{j\infty}\frac{K_0(uw)}{K_0(w)}\left[K_0(vwe^{-j\pi}) - K_0(vw)\right]\frac{dw}{w} -$$

$$-\frac{1}{\pi^2}\int_{-j\infty}^{-j\varepsilon}\frac{K_0(uw)}{K_0(w)}\left[K_0(vw) - K_0(vwe^{j\pi})\right]\frac{dw}{w} = \tag{4.10}$$

$$= 1 -$$

$$-\frac{1}{\pi^2}\int_{j\varepsilon}^{j\infty}K_0(vw)\left[-\frac{K_0(uw)}{K_0(w)} + \frac{K_0(uw) + j\pi I_0(uw)}{K_0(w) + j\pi I_0(w)}\right]\frac{dw}{w} -$$

$$-\frac{1}{\pi^2}\int_{-j\varepsilon}^{-j\infty}K_0(vw)\left[-\frac{K_0(uw)}{K_0(w)} + \frac{K_0(uw) - j\pi I_0(uw)}{K_0(w) - j\pi I_0(w)}\right]\frac{dw}{w}$$

Now according to Eq. (4.09) indentation integrals corresponding to the last two integrands tend to zero as $\varepsilon \to 0$. Consequently deforming the integration paths into the positive real axis, we obtain

$$\phi_e = c - 2c\int_0^{\infty}\frac{I_0(w)K_0(vw)\left[I_0(uw)K_0(w) - I_0(w)K_0(uw)\right]}{wK_0(w)\left[K_0^2(w) + \pi^2 I_0^2(w)\right]}dw \tag{4.11}$$

valid when $v > u - 1 > 0$. Because of the exponentially decreasing integrand of Eq. (4.11), an arbitrary number of differentiations of ϕ_e with respect to u and v may be performed in the integrand directly. (Eq. 4.02 may only be formally differentiated once.)

The quantity $\left(\frac{\partial\phi}{\partial u}\right)_{u=1}$ is fundamental in calculations of the antenna current, the surface charge density and the energy radiation (see below). The antenna current by a unit step feeding voltage, $-2\pi\varepsilon_0\left(\frac{\partial\phi_e}{\partial u} - \frac{\partial\phi_i}{\partial u}\right)^{u=1}_{v=\frac{1}{a}\sqrt{c^2t^2-z^2}}$, is a function of one variable only.

Since

$$I_0(z)K_1(z) + I_1(z)K_0(z) = \frac{1}{z} \tag{4.12}$$

we have, according to Eq. (4.11)

$$\left(\frac{\partial\phi_e}{\partial u}\right)_{u=1} = -2c\int_0^{\infty}\frac{I_0(w)K_0(vw)}{wK_0(w)\left[K_0^2(w) + \pi^2 I_0^2(w)\right]}dw \tag{4.13}$$

Because of the monotonic character of the integrands, the tabulation of ϕ_e according to Eq. (4.11) and of $\left(\frac{\partial \phi_e}{\partial u}\right)_{u=1}$ according to Eq. (4.13) should be comparatively easy. The outer electromagnetic field at a given point due to a given feeding voltage is determined by Eq:s (1.06—1.07) and (3.14). It seems likely that even such field values—and certainly the antenna current—could be numerically estimated from such tables without too much computation work.

We now turn back to demonstrate that the function Π defined according to Eq:s (3.13—3.17) has the properties a)—c) of Chapter 2.

As Π is zero outside the wave front condition b) is obviously satisfied. We further have

$$\phi(a, z, t) = \begin{matrix} c & \text{when } |z| < ct \\ 0 & \text{when } |z| > ct \end{matrix}$$

Relation (2.03) is then easily established as soon as Eq. (2.01) is verified.

The upper integration limits of Eq:s (3.13) and (3.15) may be chosen to infinity. The natural way to establish the relation $\Box \Pi = 0$ would then be to differentiate these equations under the integration sign. As ϕ is singular at the wave front, this cannot, however, be done directly. On the other hand ϕ represents a true electromagnetic field having—in a physical sense—the properties b), c) and even a). The difficulty mentioned above is thus only formal and can be mathematically overcome in a way, closely related to the above physical ideas.

We first state, that ϕ is a "weak solution" (cf. SCHWARTZ 1957) of the wave equation throughout free r, z, t-space, i.e. that the integral throughout space $\iiint\int \phi \, \Box u \, dv\,dt$ vanishes for any infinitely differentiable function u being zero at points sufficiently remote. To prove this we note that ϕ satisfies the wave equations inside the wave front. This can be shown by formal differentiation of Eq. (4.11) and by proving that $\Box R_n \to 0$ where R_n is the remainder of Eq. (3.17). Further, applying GREEN's generalized integral theorem to a region slightly inside the characteristic cone $c^2t^2 - (r-a)^2 - z^2 = 0$—note the resemblance to the integration method of HADAMARD—we find that

$$\iiint\int \phi \, \Box u \, dv\,dt = 0 \quad \text{if} \quad \frac{\partial \phi}{\partial n} + \frac{1}{c} \cdot \frac{\partial \phi}{\partial t} \to 0$$

when the point in question approaches the wave front. This condition—meaning that the wave front slope, though infinitely steep, remains stationary—is easily established by means of Eq. (4.04).

Secondly, as a consequence of definitions it follows immediately from Eq:s (3.13) and (3.15) that Π is then also a weak solution of the wave equation.

Now any twice continuously differentiable, weak solution of the wave equation is also a "strong" solution – i.e. a solution in the ordinary sense—a fact which is easily demonstrated by means of GREEN's theorem. As Π is twice continuously differentiable—again as a consequence of Eq. (4.04)—the relation $\Box \Pi = 0$ is established.

Solution Character Near the Feeding Gap. Energy Radiation

In the vicinity of the feeding gap the surface charge density must be essentially electrostatically distributed. Consider a thin plane metal sheet placed in the yz-plane, cut along the y-axis and with a voltage $2V_0$ applied between its two parts. This situation is physically equivalent to our gap problem which should then on each side of the antenna have a surface charge distribution with a leading term $\frac{2\varepsilon_0 V_0}{\pi z}$ for small z-values.

The external antenna surface charge density is given by

$$q_e(z, t) = \varepsilon_0 \left(\frac{\partial^2 \Pi_e}{\partial r \partial z} \right)_{r=a} \tag{5.01}$$

We have

$$\frac{\partial \Pi_e}{\partial r} = a \int_{\frac{r}{a}-1}^{\frac{\sqrt{c^2 t^2 - z^2}}{a}} V_0 \left(t - \frac{\sqrt{a^2 v^2 + z^2}}{c} \right) \frac{\partial \phi_e}{\partial u} \frac{v dv}{c\sqrt{a^2 v^2 + z^2}} \tag{5.02}$$

and

$$q_e(z, t) = -\varepsilon_0 a \int_0^{\frac{\sqrt{c^2 t^2 - z^2}}{a}} V_0 \left(t - \frac{\sqrt{a^2 v^2 + z^2}}{c} \right) \left(\frac{\partial \phi_e}{\partial u} \right)_{u=1} \frac{z v dv}{c(a^2 v^2 + z^2)^{3/2}} -$$

$$- \varepsilon_0 a \int_0^{\frac{\sqrt{c^2 t^2 - z^2}}{a}} V_0' \left(t - \frac{\sqrt{a^2 v^2 + z^2}}{c} \right) \left(\frac{\partial \phi_e}{\partial u} \right)_{u=1} \frac{z v dv}{c^2 (a^2 v^2 + z^2)} \tag{5.03}$$

Using Eq:s (4.06—4.07) we find by means of the substitution $\frac{av}{z} = \zeta$ the leading term of Eq. (5.03) when z is small

$$q_e(z, t) =$$

$$= -\varepsilon_0 a V_0(t) \int_0^{\infty} -\frac{2ca}{\pi z \zeta} \frac{\zeta d\zeta}{ca^2 (\zeta^2 + 1)^{3/2}} + 0(1)$$

$$= \frac{2\varepsilon_0 V_0}{\pi z} + 0(1) \tag{5.04}$$

as was predicted. Similarly the external antenna current can be written

$$I_e(z,t) = -2\pi\varepsilon_0 a \left[\frac{\partial^2 \Pi_e}{\partial r \partial t}\right]_{r=a} =$$

$$= -2\pi\varepsilon_0 a^2 \int_0^{\frac{\sqrt{c^2t^2-z^2}}{a}} V_0'\left(t - \frac{\sqrt{a^2v^2+z^2}}{c}\right)\left(\frac{\partial \phi_e}{\partial u}\right)_{u=1} \frac{v\,dv}{c\sqrt{a^2v^2+z^2}} \tag{5.05}$$

that is

$$I_e(z,t) = -4\varepsilon_0 a V_0'(t) \log\frac{|z|}{a} + 0(1) \tag{5.06}$$

where the leading term expresses a capacitive current charging the region around the feeding gap electrostatically.

We thus recognize the fact, well-known in antenna theory (see HALLÉN 1953, p. 417) that an idealized feeding gap represents an infinite parallel capacitance and that the electromagnetic field energy will, consequently, be infinite whenever the feeding voltage differs from zero.

Regard for the moment the antenna as being of finite but small thickness. Consider further a surface S generated by the lines of electric force and bounded by a simple closed curve C according to fig. 5. We apply STOKE's theorem to MAXWELL's equation

$$\text{curl } H = J + \frac{\partial D}{\partial t}$$

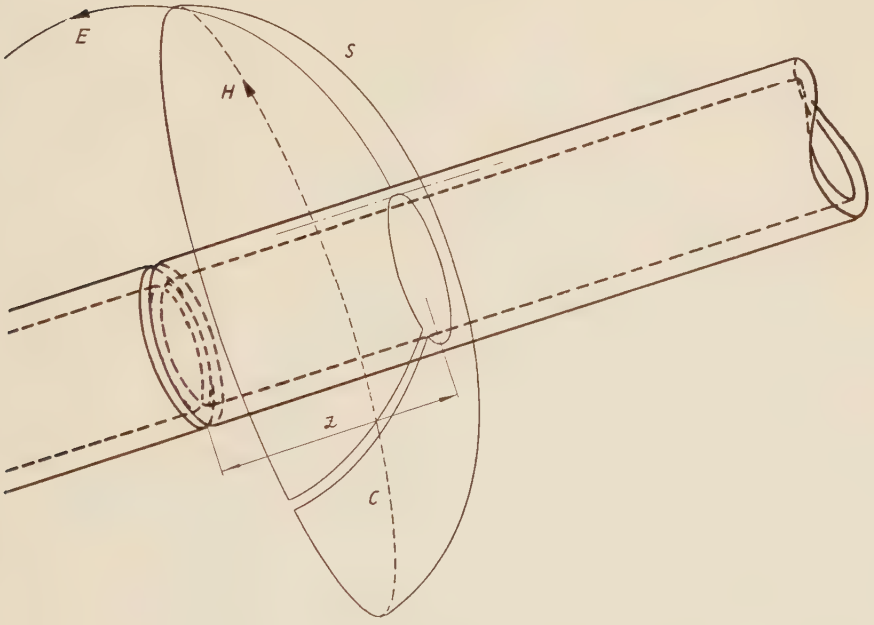

X 11047

Fig. 5.

and the surface S. Thereby the displacement current through S will tend to zero as $z \to 0$. (Note that the lines of electric force are essentially stationary.) Thus

$$\oint H ds = I_e(z) + 0(z)$$

the circulation integral taken around the outer circle of C. This result can, of course, be computed directly from Eq. (5.02).

Further

$$\int E ds = 2V_0 + 0(z)$$

along any line of force connecting the two antennas. With respect to Eq. (5.06) we thus find the rate of energy flow into a region outside the antenna and outside the surface S extended to both antenna halves

$$P = 2V_0 I_e(z) + o(1) \tag{5.07}$$

Eq. (5.07) contains a term $-8\varepsilon_0 a V_0 V_0' \log \frac{|z|}{a}$, singular at $z=0$ and expressing a purely electrostatic power transfer. Its time-integral, expressing an electrostatic energy, vanishes if $V_0=0$. We thus find the total energy W radiated from an antenna whose driving voltage is of finite time-duration

$$W = \lim_{z \to 0} \int_0^\infty 2V_0(\tau) I_e(z, \tau) d\tau \tag{5.08}$$

as could be expected. By introducing Eq. (5.05) and inverting the order of integration we find for an infinite antenna

$$W = -4\pi\varepsilon_0 a \int_0^\infty \frac{1}{c} \left(\frac{\partial \phi_e}{\partial u}\right)_{u=1} dv \int_{\frac{av}{c}}^\infty V_0(\tau) V_0' \left(\tau - \frac{av}{c}\right) d\tau \tag{5.09}$$

the convergence of the outer integral being assured by the fact that the inner integral tends to zero at least as v when $v \to 0$.

For physical reasons W must obviously be a positive quantity. To show that this is indeed the case we make some transformations.

After integration by parts and the substitution $\tau - \frac{av}{c} \to \tau$, the inner integral of Eq. (5.09) becomes

$$-\int_0^\infty V_0' \left(\tau + \frac{av}{c}\right) V_0(\tau) d\tau$$

Integrating now the outer integral by parts, we obtain

$$W = \frac{4\pi}{Z_0} \int_0^\infty \frac{1}{c} \left(\frac{\partial^2 \phi_e}{\partial u \partial v} \right)_{u=1} dv \tag{5.10}$$

$$\int_0^\infty V_0(\tau) \left[V_0(\tau) - V_0\left(\tau + \frac{av}{c}\right) \right] d\tau$$

the inner integral tending to zero at least as v^2 as $v \to 0$. Now the inner integral of Eq. (5.10) can be written

$$\frac{1}{2} \int_0^\infty \left[V_0(\tau) - V_0\left(\tau + \frac{av}{c}\right) \right]^2 d\tau + \frac{1}{2} \int_0^{\frac{av}{c}} V_0^2(\tau) d\tau$$

and is hence positive. As $\left(\frac{\partial \phi_e}{\partial u} \right)_{u=1}$ is an increasing function of v —see Eq. (4.13)— we have shown that $W > 0$ for any $V_0(t)$, which was to be proved.

CHAPTER 6

Reflected Waves

The determination of the reflected, transient, waves defined in Chapter 2 is, of course, a more involved problem than the calculation of Π_0. The essential difficulty lies in the more complicated boundary condition, prescribing one functional property, $-\frac{1}{r} \frac{\partial}{\partial r} \left(r \frac{\partial \Pi}{\partial r} \right)$, along one, semi-infinite part of the antenna, and another, $-2\pi\varepsilon_0 a \left(\frac{\partial^2 \Pi_e}{\partial r \partial t} - \frac{\partial^2 \Pi_i}{\partial r \partial t} \right)$, along the rest. The increasing number of independent parameters by repeated reflections is, on the other hand, only a trivial complication. As is done by HALLÉN, we will remove it by making some natural simplifications.

Consider the current distribution of an elementary wave in a region near the end at which it is reflected. Suppose further that the antenna radius as well as the distances to the antenna end from the points within the region and from the wave front of the wave in question are all small compared to l_1 and l_2. It seems likely that the current distribution can then be approximated as an undamped, undistorted travelling wave. As to the outgoing wave Π_0 this can be confirmed directly by means of Eq. (5.05). (The internal field is supposed to be damped out as the frequency spectrum of $V_0(t)$ will normally be essentially within the cut-off region of the wave guide formed by the antenna.)

When determining the elementary wave generated by the above wave at its reflection we are thus led to the following problem.

Find a continuous function $\Pi(r, z, t)$ such that

$$\Box \Pi = 0 \qquad \text{when } r \neq a \tag{6.01}$$

$$\Pi = \frac{\partial \Pi}{\partial t} = 0 \quad \text{at} \quad t = 0 \tag{6.02}$$

$$E_z(a, z, t) = -\frac{1}{r}\frac{\partial}{\partial r}\left(r\frac{\partial \Pi}{\partial r}\right) = 0 \text{ when } z > 0 \tag{6.03}$$

$$I(z, t) = -2\pi\varepsilon_0 a\left[\frac{\partial^2 \Pi_e}{\partial r \partial t} - \frac{\partial^2 \Pi_i}{\partial r \partial t}\right]_{r=a} = I_0\left(t + \frac{z}{c}\right) \text{ when } z < 0 \tag{6.04}$$

As in Chapter 3 we put

$$\left.\begin{aligned} x &= \frac{1}{2}(ct - z) \\ y &= \frac{1}{2}(ct + z) \end{aligned}\right\} \tag{6.05}$$

and get

$$\Pi = -\frac{1}{4\pi^2}\int_{\Gamma_{s_x}}\int_{\Gamma_{s_y}} \Pi_L(r, s_x, s_y) e^{s_x x + s_y y}\, ds_x ds_y \tag{6.06}$$

where

$$\Pi_L(r, s_x, s_y) = \left\{\begin{aligned} &B(s_x, s_y)\frac{K_0(r\sqrt{s_x s_y})}{K_0(a\sqrt{s_x s_y})} && \text{when } r > a \\ &B(s_x, s_y)\frac{I_0(r\sqrt{s_x s_y})}{I_0(a\sqrt{s_x s_y})} && \text{when } r < a \end{aligned}\right. \tag{6.07}$$

Laplace-transformation of Eq. (6.03) yields

$$-s_x s_y B(s_x, s_y) = (E_z)_L^- \tag{6.08}$$

where

$$(E_z)_L^- = \int_0^\infty e^{-(s_x + s_y)\eta}\, d\eta \int_\eta^\infty E_z(a, \xi, \eta) e^{-s_x(\xi - \eta)}\, d\xi \tag{6.09}$$

With respect to Eq. (4.12) we similarly deduce from Eq. (6.05)

$$\frac{\pi}{Z_0}\frac{s_x + s_y}{K_0 I_0(a\sqrt{s_x s_y})} B(s_x, s_y) = \frac{c}{2 s_x}\int_0^\infty I_0(\tau) e^{-\frac{c}{2}(s_x + s_y)\tau} d\tau + I_L^+ \tag{6.10}$$

where

$$I_L^+ = \int_0^\infty e^{-(s_x+s_y)\xi}\, d\xi \int_\xi^\infty I(\xi,\eta) e^{-s_y(\eta-\xi)}\, d\eta \tag{6.11}$$

$B(s_x, s_y)$ can be determined from Eq:s (6.08—6.11) by means of a discussion analogous to the HOPF-WIENER solution method of certain integral equations with semi-infinite integration interval (see TITCHMARSH 1937 p. 339).

According to Eq. (6.09), $(E_z)_L^-$ must be expected to be regular when $Re\,(s_x+s_y) > 0$, $Re\, s_x > 0$. Similarly, by Eq. (6.11), I_L^+ will be regular when $Re\,(s_x+s_y) > 0$, $Re\, s_y > 0$. Further, the quantity $2K_0I_0\,(a\sqrt{s_x s_y})$ can—see HALLÉN 1956—be written

$$2I_0K_0\,(a\sqrt{s_x s_y}) = \frac{\varphi_1\left(\frac{s_y-s_x}{2j}, \frac{s_y+s_x}{2j}\right)}{\varphi_2\left(\frac{s_y-s_x}{2j}, \frac{s_y+s_x}{2j}\right)} \tag{6.12}$$

where

$$\varphi_{1,2}(\alpha,\beta) = \exp \frac{1}{2\pi j} \int_{\mp j\delta-\infty}^{\mp j\delta+\infty} \frac{\log\left[2I_0K_0\left(a\sqrt{\zeta^2-\beta^2}\right)\right]}{\zeta-\alpha}\, d\zeta \tag{6.13}$$

The branch cuts run horizontally from the branch points $\pm\beta$ to infinity. The square root denotes that functional branch which for large real ζ-values equals $|\zeta|$ and the integral is to be interpreted as a CAUCHY principal value. Suppose that β is given and that $0 < \varepsilon < \delta < < -Im\,\beta$. Then in the region $Im\,\alpha > -\varepsilon$, $\varphi_1(\alpha)$ is regular and

$$k_1 < |\varphi_1(\alpha)|\sqrt{|\alpha-\beta|} < K_1$$

where k_1 and K_1 are fixed numbers. Similarly, in the region $Im\,\alpha < \varepsilon$, $\varphi_2(\alpha)$ is regular and

$$k_2 < \frac{|\varphi_2(\alpha)|}{\sqrt{|\alpha+\beta|}} < K_2$$

We now write Eq. (6.10)

$$\frac{2\pi}{Z_0}\,\frac{s_x+s_y}{\varphi_1}\, s_x s_y B(s_x,s_y) = \frac{1}{\varphi_2}\left[\frac{c}{2} s_y \int_0^\infty I_0(\tau) e^{-\frac{c}{2}(s_x+s_y)\tau}\, d\tau + s_x s_y I_L^+\right] \tag{6.14}$$

Consider for the moment s_x+s_y as constant. Then the left member of Eq. (6.14) is o $(|s_y - - s_x|)$ and regular if $Re\,(s_y-s_x) < 2\varepsilon$ whilst the right member is regular and o $(|s_y-s_x|)$ if $Re\,(s_y-s_x) > -2\varepsilon$. Hence by the principle of analytic continuation and LIOUVILLE's theorem

both members are equal to a constant throughout the $(s_y - s_x)$-plane. In other words, they are functions of $s_y + s_x$ only. Putting $s_x = 0$ in Eq. (6.14) one finds

$$B(s_x, s_y) = \frac{1}{4\pi\varepsilon_0} \frac{1}{s_x s_y} \frac{\varphi_1\left(\frac{s_y - s_x}{2j}, \frac{s_y + s_x}{2j}\right)}{\varphi_2\left(\frac{s_y + s_x}{2j}, \frac{s_y + s_x}{2j}\right)} \int_0^\infty I_0(\tau) e^{-\frac{c}{2}(s_x + s_y)\tau} d\tau \qquad (6.15)$$

Inserting this result in Eq. (6.06) and inverting the order of integration we finally obtain the reflected wave

$$\Pi(r, z, t) = \int_0^\infty I_0(\tau) \phi_r(r, z, t - \tau) d\tau \qquad (6.16)$$

where

$$\phi_r(r, z, t) = -\frac{1}{16\pi^3\varepsilon_0} \int_{\Gamma_{s_x}} \int_{\Gamma_{s_y}} \frac{1}{s_x s_y} \frac{K_0\left(r\sqrt{s_x s_y}\right)}{K_0\left(a\sqrt{s_x s_y}\right)}$$

$$\exp\left\{\frac{ct}{2}(s_x + s_y) - \frac{z}{2}(s_x - s_y) + \frac{1}{2\pi j} \int_{-j\delta-\infty}^{-j\delta+\infty} \frac{\log\left[2I_0 K_0\left(a\sqrt{\zeta^2 - \left(\frac{s_x + s_y}{2j}\right)^2}\right)\right]}{\zeta - \frac{s_y - s_x}{2j}} d\zeta - \right.$$

$$\left. - \frac{1}{2\pi j} \int_{j\delta-\infty}^{j\delta+\infty} \frac{\log\left[2I_0 K_0\left(a\sqrt{\zeta^2 - \left(\frac{s_x + s_y}{2j}\right)^2}\right)\right]}{\zeta - \frac{s_y + s_x}{2j}} d\zeta \right\} ds_x ds_y \qquad (6.17)$$

valid when $r > a$. The solution when $r < a$ is obtained by exchanging as before

$$\frac{K_0\left(r\sqrt{s_x s_y}\right)}{K_0\left(a\sqrt{s_x s_y}\right)} \text{ for } \frac{I_0\left(r\sqrt{s_x s_y}\right)}{I_0\left(a\sqrt{s_x s_y}\right)}$$

Finally by making in one of the Γ-integrals the substitution

$$\alpha = \frac{z}{2}(s_x + s_y) - \frac{ct}{2}(s_x - s_y)$$

and considering the analytic properties of $\varphi_{1,2}$ described above, it is easily proved that $\phi_r = 0$ if $c^2t^2 - (r-a)^2 - z^2 < 0$.

Obviously any elementary wave, defined according to Chapter 2, may be calculated by the above method.

CHAPTER 7

Comparison to HALLÉN'S Theory

If $V_0(t)$ is a sinusoidal voltage, each one of the elementary waves defined in Chapter 2 will approach stationary conditions meaning e.g.

$$F_{1,n}(t) = Re\,[e^{j\omega t} F^s_{1,n}] + F^f_{1,n}(t) \tag{7.01}$$

where F denotes any electromagnetic field component and $F^f_{1,n}$, corresponding to free oscillations of the antenna, tends to zero as $t \to \infty$.

The electromagnetic field around the antenna at any moment is built from a finite number of elementary waves according to Eq. (2.07). (The high-index waves have not yet started developing.) By choosing first $N(\varepsilon)$ sufficiently large we get

$$\left| \sum_N^\infty (F_{1,n} + F_{2,n}) \right| < \varepsilon \quad \text{and} \quad \left| \sum_N^\infty (F^s_{1,n} + F^s_{2,n}) \right| < \varepsilon$$

meaning that the corresponding waves are attenuated out because of a high number of reflections. But with $t > T(N, \varepsilon)$

$$\left| F^f_0 + \sum_1^{N-1} (F^f_{1,n} + F^f_{2,n}) \right| < \varepsilon$$

since the free oscillations tend to zero. This means that the stationary field may be thought of as an infinite sum of elementary waves having reached stationary equilibrium. Each one of these stationary waves must then be identical with a corresponding wave of HALLÉN's theory, a fact which will now be demonstrated.

The principle by which one wave is generated by its predecessor is identically the same as in HALLÉN's theory. The physical meaning of Eq:s (35.46—47) in HALLÉN (1953), for instance, could be put in the following way. The current generating the n^{th} wave exactly cancels the current of the $(n-1)^{\text{th}}$ on the far side of the reflection point. On the other side the E_z-field generated by the current vanishes.

This yields exactly the same boundary conditions as those stated in Chapter 2 which proves the identity predicted above. For the case of the outgoing wave the identity will now be shown directly from the solution calculated in Chapter 3.

Any electromagnetic quantity is uniquely determined by the total antenna current, which we will thus choose as characteristic property.

Putting $V_0(t) = V_0 e^{j\omega t}$ we get

$$I(z, t) = I^f(z, t) + V_0 \frac{4\pi}{Z_0} i(z)\, e^{j\omega t} \tag{7.02}$$

where

$$\beta = \frac{\omega}{c}$$

$$I^f(z,t) = V_0 \frac{4\pi}{Z_0} \frac{1}{2\pi j} \int_{\Gamma_w} \frac{I_0\left(\sqrt{c^2t^2 - z^2}\, w\right)}{I_0(aw) K_0(aw)} \frac{dw}{w} -$$

$$- V_0 \frac{4\pi}{Z_0} \frac{\beta}{2\pi} e^{j\omega t} \int_{ct}^{\infty} e^{-j\beta\zeta} d\zeta \int_{\Gamma_w} \frac{I_0\left(\sqrt{\zeta^2 - z^2}\, w\right)}{I_0(aw) K_0(aw)} \frac{dw}{w} \tag{7.03}$$

with

$$\lim_{t \to \infty} I^f(z,t) = 0$$

and

$$i(z) = \frac{\beta}{2\pi} \int_{|z|}^{\infty} e^{-j\beta\zeta} d\zeta \int_{\Gamma_w} \frac{I_0\left(\sqrt{\zeta^2 - z^2}\, w\right)}{I_0(aw) K_0(aw)} \frac{dw}{w} \tag{7.04}$$

Putting now $\beta = \beta_0 - j\delta$ (β_0 real, $\delta > 0$) and choosing $\Gamma_w : Re w = \varepsilon < \delta$ we may invert the order of integration getting

$$i(z) = \frac{\beta}{2\pi} \int_{\Gamma_w} \frac{dw}{w K_0(aw) I_0(aw)} \int_{|z|}^{\infty} I_0\left(\sqrt{\zeta^2 - z^2}\, w\right) e^{-j\beta\zeta} d\zeta \tag{7.05}$$

Now for any w on Γ_w

$$\int_{-j\delta - \infty}^{-j\delta + \infty} \frac{e^{(j\zeta u - |z|\sqrt{u^2 + w^2})}}{\sqrt{u^2 + w^2}} du = \int \frac{e^{jv}}{\sqrt{v^2 + w^2(\zeta^2 - z^2)}} dv = \begin{cases} 2\pi j I_0\left(\sqrt{\zeta^2 - z^2}\, w\right) & \text{when } \zeta > |z| \\ 0 & \text{when } \zeta < |z| \end{cases} \tag{7.06}$$

(In both integrals the branch cut connects the branch points and the square root denotes that functional branch which at distant points is equal to u and v respectively.)

It now follows from FOURIER's integral theorem

$$\int_{|z|}^{\infty} e^{-j\beta\zeta} I_0\left(\sqrt{\zeta^2 - z^2}\, w\right) d\zeta = \frac{e^{-j|z|\sqrt{\beta^2 + w^2}}}{j\sqrt{\beta^2 + w^2}} \tag{7.07}$$

and

$$i(z) = \frac{\beta}{2\pi j} \int_{\Gamma_w} \frac{e^{-j|z|\sqrt{\beta^2 + w^2}}}{w\sqrt{\beta^2 + w^2}\, I_0(aw) K_0(aw)} dw \tag{7.08}$$

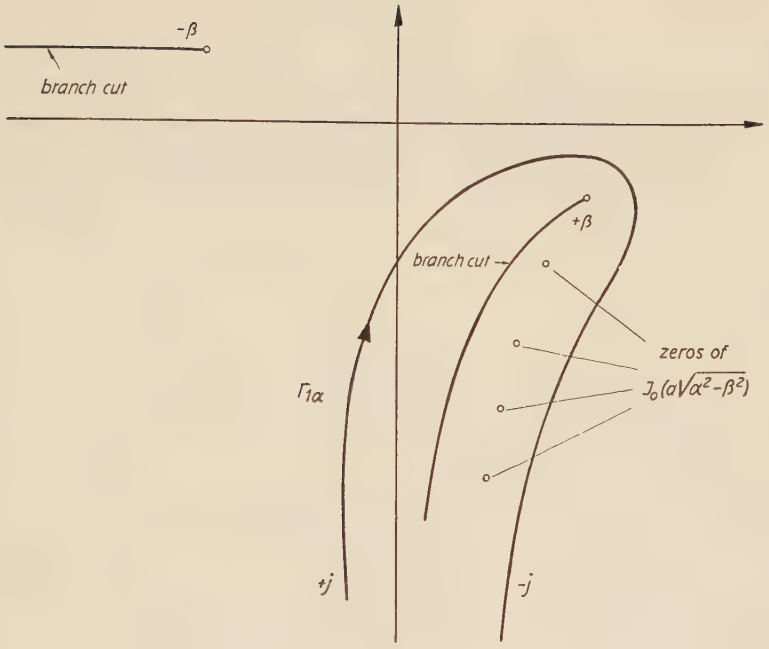

Fig. 6.

Finally making the substitution $\sqrt{\beta^2 + w^2} = \alpha$, we obtain

$$i(z) = \frac{j}{2\pi} \int_{\Gamma_{1\alpha}} \frac{\beta e^{-j\alpha|z|}}{(\alpha^2 - \beta^2) I_0 K_0 \left(a\sqrt{\alpha^2 - \beta^2}\right)} \, d\alpha \tag{7.09}$$

The character of $\Gamma_{1\alpha}$ as well as the branch cuts and the signs of the square root at distant parts of the contour are demonstrated in fig. 6.

Because of the exponential factor, $\Gamma_{1\alpha}$ may finally be deformed into the real axis whereby $i(z)$ takes the well-known form of the steady-state solution (cf. HALLÉN 1953, p. 409).

This paper thus has a strong connection to the HALLÉN theory. HALLÉN bases his investigation on integral equations, but this difference is only methodical and not essential. As is well-known, any boundary problem of the wave equation may be formulated as an integral equation connecting its boundary values and having a GREEN's function as a kernel and vice versa.

It may also be noted that while on one hand the waves of HALLÉN's theory represent the stationary equilibrium of $\Pi_{1,n}$ etc., it is hence possible to construct by means of FOURIER synthesis the transient waves from those of HALLÉN. Apart from the formal difference mentioned above the calculations of Chapter 6 are essentially such a synthesis. As none of the integrals could be transformed or evaluated this is obvious even from the outer appearance of the solution (cf. HALLÉN 1956, Eq. 57 a).

Acknowledgement

The investigations presented here were inspired by the travelling wave antenna theory of Professor Erik Hallén to whom the author wishes to express his gratitude for valuable ideas, kind interest and constant encouragement during the work. I also thank Civ.ing. J. Boman and Civ.ing. G. Petersson for several stimulating discussions on various parts of the subject. Financial support from the State Council of Technical Research is also gratefully admitted.

Bibliography

1. Courant-Hilbert: *Mathematische Physik*, Vol. 2. Berlin 1937, 549 pp.
2. Hallén, E: *Theoretical Investigations into the Transmitting and Receiving Qualities of Antennae*. Nova Acta Upsal. *11*(1938): 4, pp. 1—44.
3. Hallén, E: *Further Investigations into the Receiving Qualities of Antennae: The Absorbing of Transient Unperiodic Radiation*. Uppsala Univ. Årsskrift 1939: 4, pp. 1—39.
4. Hallén, E: *Travelling Waves and Unsymmetrically Fed Antennas*. Cruft Labor. Techn. Rep. No. 49, Cambridge, Mass. 1948, 48 pp.
5. Hallén, E: *Properties of Long Antennas*. Cruft Labor. Techn. Rep. No. 44, Cambridge, Mass. 1948, 16 pp.
6. Hallén, E: *Elektricitetslära* [Electromagnetic Theory]. Stockholm 1953, 556 pp.
7. Hallén, E: *Further Investigations into the Iterated Sine- and Cosineintegrals and their Amplitude Functions with Reference to Antenna Theory*. Trans. Roy. Inst. Techn. 1955: No. 89, 44 pp.
8. Hallén, E: *Exact Treatment of Antenna Current Wave Reflection at the End of a Tube-Shaped Cylindrical Antenna*. Trans IRE, AP-4, 1956: 3, pp. 479—491.
9. Petrowski, I G: *Partielle Differentialgleichungen*. Leipzig 1955, 293 pp.
10. Schmitt, H J: *Transients in Cylindrical Antennas*. Cruft Labor. Techn. Rep. No. 296, Cambridge, Mass. 1959, 28 pp.
11. Schwartz, L: *Théorie des distributions*, Tome 1. Paris 1950, 148 pp.
12. Stratton, J A: *Electromagnetic Theory*. New York 1941, 615 pp.
13. Titchmarsh, E C: *Fourier Integrals*. London 1937, 390 pp.
14. Watson, G N: *Bessel Functions*. Cambridge 1944, 804 pp.

Manuscript received by the editors November 1959.

Ericsson Technics

VOLUME 16 (1960) · No. 2

CONTENTS

TELEFONAKTIEBOLAGET L M ERICSSON
STOCKHOLM 32

ESSELTE AKTIEBOLAG
STOCKHOLM 1960
006819

Transmission Performance in Presence of Circuit Noise

A survey of work carried out in connection with noise questions entrusted to the 4th Study Group of the CCIF and the 12th Study Group of the CCITT.

BY

FREDRIK MARKMAN*

UDC. 621.391.822
LME 8402, 805

The transmission performance in presence of circuit noise of different types is a very important question. Comprehensive work has been done during the last decennium by Telephone Administrations, Recognized Private Operating Agencies, Industrial Organizations and the CCITT Laboratory in Geneva. The tests carried out in the CCITT Laboratory have been made using the AEN technique but according to the fact that this method suffers from many serious artificialities a new method, based on the opinions of ordinary telephone users, has been adopted by the International Telegraph and Telephone Consultative Committee, CCITT. This new method has been developed by Mr. D. L. Richards of the British Post Office Research Station. The new method has been used in other laboratories than the CCITT one. Results obtained from both methods are given.

The most extensive opinion tests have so far been carried out by the British Administration and the results obtained are the only ones that can be used for calculation of the transmission quality in presence of circuit noise. Therefore, only the British data are used in the present article.

Much work remains to be done ere all the noise questions raised by different Study Groups of the CCITT can be fully and finally treated.

* Telefonaktiebolaget LM Ericsson, Stockholm

Contents

CHAPTER 1

Introduction

The effect on transmission performance of circuit noise of different kinds belongs to some of the most important questions originally entrusted to Study Group 4 of the International Telephone Consultative Committee, CCIF, and later on (1956) to Study Group 12 of the International Telegraph and Telephone Consultative Committee, CCITT.

Two different test methods have so far been used for the determination of the reduction in transmission quality due to circuit noise, namely "articulation tests" using the AEN technique and "opinion tests" based on the opinions of typical telephone users. Articulation tests have been made in the CCIF-Laboratory in Geneva. The results obtained from these tests were studied by Study Group 4 at a meeting in Geneva 1954. It was then surmised that the impairment values obtained were too great, articulation tests suffering from many important artificialities, which will be mentioned in Chapter 3.

Therefore it was decided to use a new testing method, developed by Mr D. L. Richards of the British Post Office Research Station at Dollis Hill, London. Such tests, named opinion tests, are based on the opinions of a great number of typical telephone users and can not of explicable reasons be carried out at the CCITT-Laboratory.

Special attention is drawn to the article by D. L. Richards and J. Swaffield, "Assessment of Speech Communication Links". (See Bibliography).

Opinion tests have been made by a few Telephone Administrations and Private Operating Agencies besides the BPO. The BPO results are sufficiently extensive for direct application to problems connected with the effect of circuit noise on the transmission quality and are therefore the only ones which will be dealt with in the present article.

CHAPTER 2

Articulation Test Results

Three different types of commercial telephone systems have been used in the articulation tests carried out at the CCIF-Laboratory using the AEN technique, namely Dutch, Swedish and Swiss systems. A commercial telephone system consists of telephone instrument, local line and feeding bridge. The results for the Swiss set only will be shown because this set most typifies modern practice and only slightly different results have been obtained for the Dutch and Swedish sets.

In the present case the sending system of the "Articulation Reference System", SRAEN, with its 300—3400 Hz band pass filter has been used as sending system. The Swiss commercial telephone systems have been used as receiving system connected to the sending system through a 600 ohm variable distortionless attenuator. The injected circuit noise was measured at the distant local receiving system by means of a psophometer of the type recommended by CCIF, 1951, the reading expressed in db relative to 1 milliwatt of circuit noise, i.e. dbm, the commercial telephone system being replaced by a pure resistance of 600 ohms. A Hoth spectrum room noise of 50 db above 10^{-16} Watt/cm^2 was present in the listening room. The complete SRAEN-system with an injected room noise of 1.4 mV psophometric E.M.F. at the receiving end was used as a reference system.

The Swiss commercial telephone systems consisted of the following:

Telephone instrument type 1950.

Microphone type AW BV 53/2.

Receiver type Autophone TK 396 am/37.

Local line consisting of an artificial cable having a total loop resistance of 360 ohms and an image attenuation coefficient of 3.55 db at 1,500 Hz.

Feeding bridge 48 volts 350/350 ohms.

The reference equivalent of side-tone for 50 db Hoth spectrum room noise was about + 20 db and the receiving articulation reference equivalent was about + 1 db.

Curve *A* in *Fig. 1* shows the transmission impairment, *I*, due to circuit noise as a function of the psophometric reading, expressed in dbm, for the Swiss commercial telephone system.

This curve is of the form

$$I = 12 \log_{10} \left(1 + 10^{\frac{N+68}{12}}\right) \quad (1)$$

where I is the impairment in db

and N is the noise level in dbm at the distant local receiving exchange.

This relationship has been found to apply for the following types of circuit noise:

a. white noise,

b. white noise limited in frequency bandwidth to 300—3,400 Hz,

c. noise on a radio link,

d. noise on a 60-channel carrier system on balanced pair cable,

e. noise on a 12-channel carrier system on balanced pair cable,

f. noise on a 5-channel carrier system on a rural cable,

g. noise due to the reaction of rectifiers on the six-phase lines that feed them (the principal components of this noise had frequencies of 250, 350, 550, 650, 1,050, 1,350, 1,950, 2,050, 2,150, 2,350, 2,550, 2,950 and 3,050 Hz).

The noise by induction from the DC-side of a six-phase rectifier (frequency components $n \cdot 300$ Hz, n being integers) gave less impairment for the same psophometric noise level.

Curve B in *Fig. 1* shows the impairment, I, as a function of the circuit noise level, N, and is of the form:

$$I = 12 \log_{10} \left(1 + 10^{\frac{N+60}{12}}\right) \quad (2)$$

where I is the impairment in db

and N is the noise level in dbm at the distant local exchange.

Comparing these two equations, (1) and (2), it will be seen that six-phase rectifier noise of a level of N dbm gives the same impairment as white noise of a level of (N-8) dbm. This conclusion is believed to apply also when the impairment is assessed by opinions method, but has so far not been verified.

In the absence of circuit noise the speech volume under the test conditions in question, measured with the ARAEN volumeter at the point at which the noise level was measured, was -51 db relative to 1 volt. The difference between readings on the ARAEN volumeter and the vu-meter obtained with continuously spoken speech has been found to be

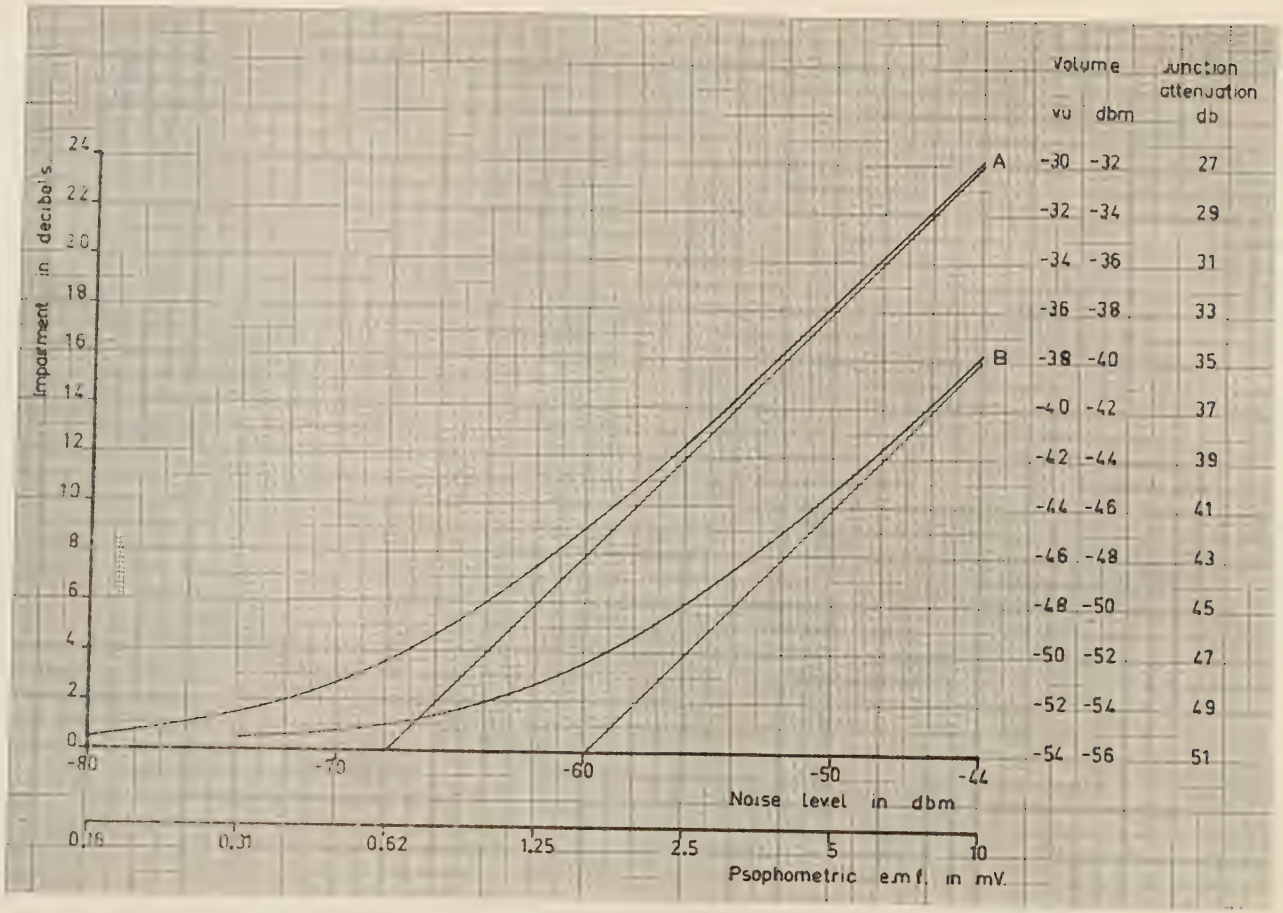

X 11145

Fig. 1. Impairment as a function of noise level.
Curve A. White noise.
Curve B. Noise by induction from the D.C. side of a six-phase rectifier.
Speech volume (at the point at which the noise level is measured) and junction loss (for 80 % sound articulation) as a function of noise level.

— 3 db. Thus a speech volume of – 51 db re 1 volt corresponds to – 54 vu. Furthermore — 54 vu corresponds to a mean power of – 56 dbm, i.e. db relative to 1 milliwatt.

The right hand ordinate scales in *Fig. 1* show the corresponding speech volume in vu and in dbm as well as the junction attenuation in db for 80 % sound articulation. If, for example, the noise level is – 60 dbm the corresponding impairment (curve *A*) is 9 db, the attenuation setting for 80 % sound articulation is 42 db and the volume is – 45 vu or — 47 dbm. Even if the impairment values obtained by articulation tests seem to be too high the AEN tests have given a valuable result regarding the classification of different types of circuit noise.

CHAPTER 3

Opinion Tests

Compared with articulation tests, which are one-way listening tests, opinion tests are more realistic for the following reasons. In articulation tests a highly trained crew of operators are used, the talking volume, the talking distance and the position of the hand-microtelephone are fixed and the speech material is meaningless Esperanto logatoms. Furthermore the speech volume at the distant local exchange is extremely low for 80 % sound articulation which plainly appears from the curves shown in *Fig. 1*. The operators consequently do not react to circuit degradations in the same way as ordinary telephone users. Opinion tests on the other hand are based on vigorous both-way conversation and the subjects participating in such a test are chosen from ordinary, untrained telephone users not directly concerned with speech studies and having no interest in the results of the experiments. The opinion tests are carried out under conditions which allow the participating persons the greatest possible freedom in their manner of using the telephone, thus approximating more closely to actual service conditions. Furthermore each person shall express his opinion once only within a test on any given circuit condition. If the subjects are used again on the same condition the results are to be analyzed as a separate replication.

The telephone circuit to be used for the determination of the fundamental data shall at each end consist of the following: Modern type subscriber's telephone sets, average subscriber's lines and feeding bridges, Hoth spectrum room noise at a level of 50 db.

The two local exchanges are connected together through two 600 ohm distortionless attenuators with means for injecting circuit noise at the point where these are joined together. By setting these attenuators to equal values, the same level of circuit noise will be

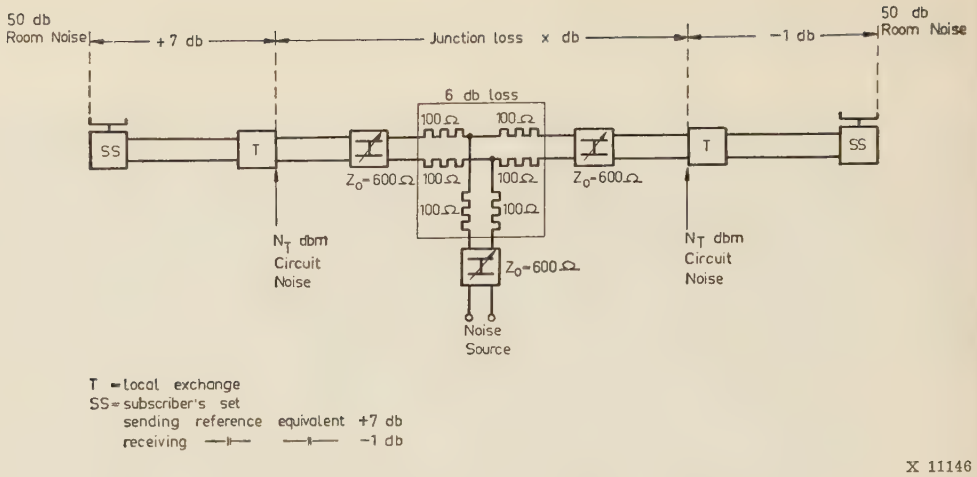

Fig. 2. Telephone connection used for determination of fundamental data.

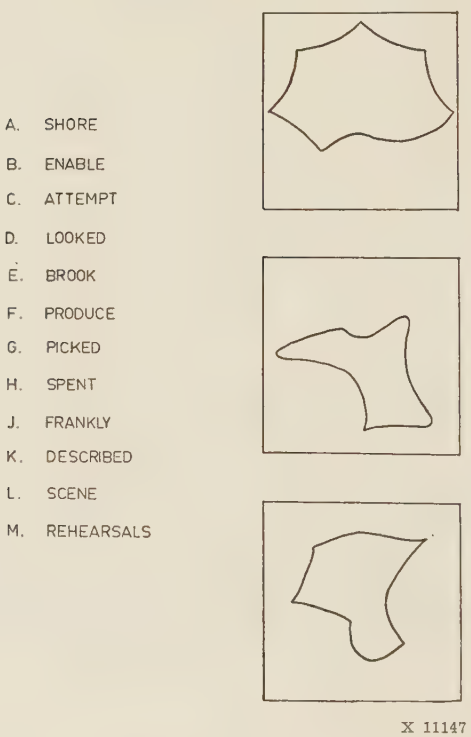

Fig. 3. Caller's sheet.

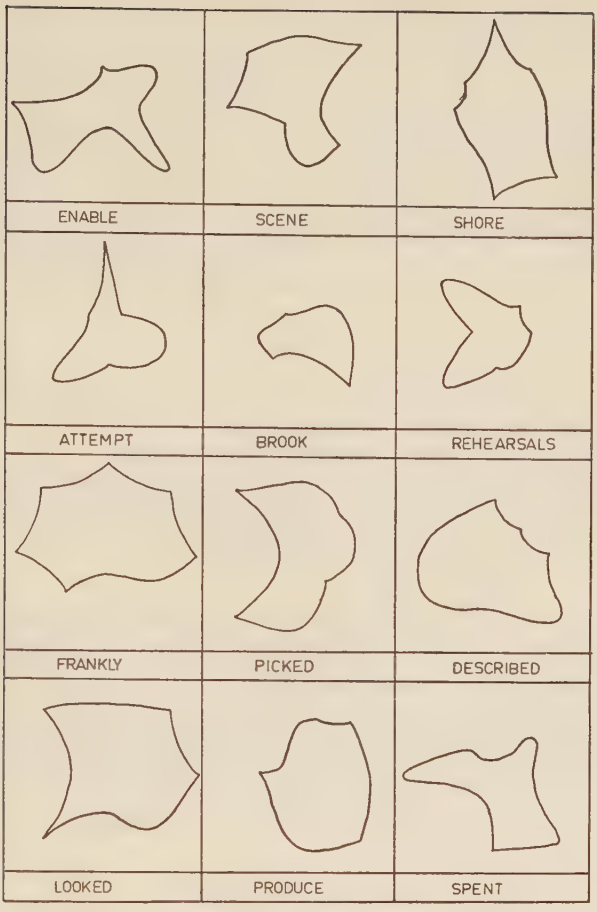

Fig. 4. Respondent's sheet.

heard at each end of the circuit. As circuit noise white noise, restricted in frequency bandwidth to 300—3,400 Hz, was used, expressed as decibels relative to 1 mW psophometric power, measured at either end of the junction, i.e. at the terminal exchange.

Fig. 2 shows the telephone connection used for the determination of the fundamental data.

The same type of telephone instruments has been used in the telephone connection shown in *Fig. 2*, and in the hypothetical overall connection shown in *Fig. 12*, namely 13—2 P—27.

Free conversation between the subjects is initiated by using random shaped figures, produced by plotting random numbers on a polar scale and drawing curves between the points. The figures are assembled on caller's (3 designs) and respondents' (12 designs) sheets each of which has an associated title and are selected at random. The procedure is for the caller to obtain the titles of his three shapes by giving to the respondent sufficient in-

formation to enable the latter to identify the figures. A caller's and a respondent's sheet are shown in *Figs. 3* and *4*. The caller describes thus the design in his own words and the respondent identifies the design, if necessary by questioning, and informs the caller of the word associated with that design. Then the caller writes down the code letter corresponding to the word. The subjects then exchange rôles and converse again. For each test condition twelve pairs of subjects are to be used. At the end of this procedure each subject expresses his opinion of the performance of the circuit on a copy of the form shown in *Table 1*.

Table 1. Opinion form 9.

When notified by the operator, will you please mark by a cross your opinion of the telephone call you have just had.
N.B. Please do not discuss your opinion with your companion.

Excellent	Good	Fair	Poor	Bad

The Mean Opinion Score, Y, is calculated by scoring the numbers of opinions in each category as follows:

4 for Excellent, E
3 for Good, G
2 for Fair, F
1 for Poor, P
0 for Bad, B

A family of curves showing mean opinion score, Y, as a function of junction loss, X db, with circuit noise level, N dbm, as parameter can now be plotted. The form of these curves is

$$Y = \alpha + \beta (X - \gamma)^2 \tag{3}$$

This family of curves enables the mean opinion score to be read off for any combination of values of X and N within the ranges covered by the test.

The final results are required in the form of percentages of users who express various classes of opinions for any combination of X and N, for example E, $E+G$, $E+G+F$, $E+G+F+P$.

The percentages of users who expressed the opinions E, $E+G$ and so on can be plotted against mean opinion score. However, it is more convenient to transform the percentage

into "probit" (equivalent number or fraction of standard deviations) and to plot probit against transformed mean opinion score, $\sqrt{4 - Y}$, the curve thus obtained being approximately a straight line over a useful range of Y.

Table I, page 264, in Probit Analysis by D. J. FINNEY, shows Transformation of Percentages to Probits.

Values taken from these lines may be restored to their original units and a table may be prepared for various classes of opinions.

CHAPTER 4

Data for Calculation of Transmission Performance in Presence of Circuit Noise

In order to obtain sufficient data for the final calculation of the transmission performance in presence of circuit noise BPO has carried out extensive opinion tests of two different types, namely *one-way listening tests*, where two different five-point scales were used, one based on preferred loudness (see *Table 2*) and the other on listening effort (see *Table 3*), *two-way conversational tests* the results of which are given in the form of percentages of subjects who vote for each of the five categories of an opinion scale (see *Table 1*) as functions of junction loss and circuit noise.

Table 2. Opinion Form 4.

Opinion Ratings based on Loudness Preference

Please express your opinion, when notified by the operator, by ticking the appropriate letter.

A	Much too loud	☐
B	Too loud	☐
C	O.K.	☐
D	Too quiet	☐
E	Much too quiet	☐

Table 3. Opinion Form 7.

Opinion Ratings based on Effort Required to Understand the Meanings of Sentences.
Please express your opinion, when notified by the operator, by ticking the appropriate letter.

A. Complete relaxation possible; no effort required.	☐
B. Attention necessary; no appreciable effort required.	☐
C. Moderate effort required.	☐
D. Considerable effort required.	☐
E. No meaning understood with any feasible effort.	☐

It has been found that a limited relationship exists between the results obtained from conversation tests and from one-way listening tests, probably valid for most speech links in ordinary telephone connections. This relationship depends upon the following two hypotheses.

1° Listening condition impairments can be used for conversational conditions provided that the corresponding junction loss is known for the latter, i.e. the loss which results in the same listening level.

2° The highest opinion score occurs at the same received level during conversation as during one-way listening.

The curve given in *Fig. 5* has been accepted as applying at a received level of —36 db relative to 1 volt in an one-way listening test corresponding to a mean opinion score of 2.5 or at the same received level in a conversational test which corresponds to a junction loss of 27 db.

The curve in *Fig. 5* is of the form

$$I = 20 \log_{10} \left(1 + 10^{\frac{N+53}{20}} \right) \tag{4}$$

where I is the impairment in db
and N is the circuit noise level in dbm.

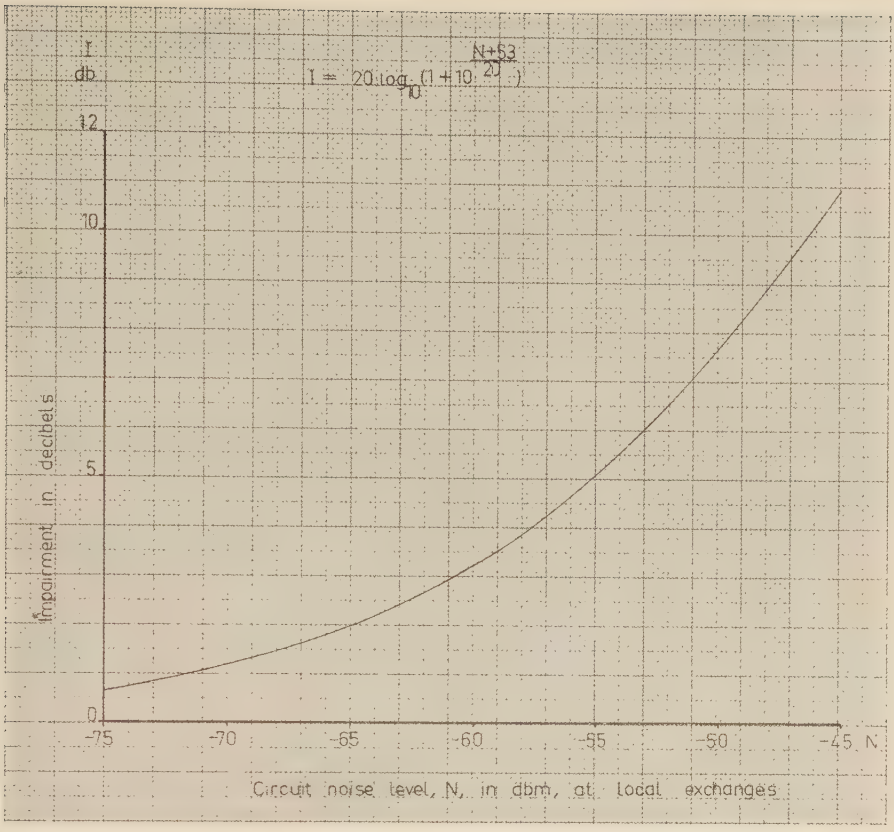

Fig. 5. Impairment as a function of noise level.

This equation, valid for a junction loss of 27 db, enables family of curves to be determined relating mean opinion scores to loss between terminal exchanges for any value of circuit noise using the parabola equation

$$Y = \alpha + \beta (X - \gamma)^2 \tag{3}$$

where Y is mean opinion score and X is junction loss in db. This equation (3) applies also to a curve of mean opinion score as a function of received level in which case X is the level in db relative to 1 volt.

For conversational tests using opinion form 9 the constants α and β are as follows:

$\alpha = 3.35$ (maximum mean opinion score independent of N for N not greater than — 45 dbm)

$\gamma = -2.5$ (junction loss at which this maximum is obtained)

If these values for α and β are inserted in equation (3) the fundamental equation (5) for the calculation of mean opinion score at different circuit noise levels is obtained.

$$\boxed{Y = 3.35 + \beta\,(X + 2.5)^2} \tag{5}$$

The value of β is depending on the noise level.

In absence of circuit noise a mean opinion score of $Y = 2.5$ occurs at a junction loss of $X = 25.5$ db. Thus the corresponding value of $\beta = \beta_0$ (no noise), using equation (5), becomes $\beta_0 = -0.00108$. The value of β for any circuit noise level can now be determined as follows:

If X_0 is the junction loss in absence of circuit noise, β_0 the corresponding value of β and β_1 is the value of β for that noise level N_1 which produces an impairment of I_1 db, the junction loss being X_1 db, then

$$Y = 3.35 + \beta_0\,(X_0 + 2.5)^2 = 3.35 + \beta_1\,(X_1 + 2.5)^2 \tag{6}$$

where Y is the mean opinion score for the two circuit noise conditions (without and with circuit noise).

Thus

$$X_1 = (X_0 + 2.5)\sqrt{\frac{\beta_0}{\beta_1}} - 2.5 \tag{7}$$

but the impairment I_1 is

$$I_1 = X_0 - X_1 \tag{8}$$

or

$$I_1 = X_0 - (X_0 + 2.5)\sqrt{\frac{\beta_0}{\beta_1}} + 2.5$$

and

$$\boxed{I_1 = (X_0 + 2.5)\left(1 - \sqrt{\frac{\beta_0}{\beta_1}}\right)} \tag{9}$$

Equations (4) and (9) give

$$\boxed{I_1 = (X_0 + 2.5)\left(1 - \sqrt{\frac{\beta_0}{\beta_1}}\right) = 20\log_{10}\left(1 + 10^{\frac{N+53}{20}}\right)} \tag{10}$$

By means of this equation (10) the value of β_1 can be calculated at different circuit noise levels N bearing in mind that $X_0 = 27$ db as mentioned before and $\beta_0 = -0.00108$.

It must be pointed out that X_0 always signifies the value of junction loss in absence of circuit noise. This value of X_0 must be reduced by the value of impairment in order to obtain that value of X, which in presence of a circuit noise with a level of N dbm gives the same mean opinion score as found in absence of circuit noise.

If, on the other hand, the circuit noise is present in that point, where the junction loss is X db, then this value of X must be increased by the value of the impairment to obtain the value of X_0.

Using equation (6)

$$(X_0 + 2.5)\sqrt{\beta_0} = (X_1 + 2.5)\sqrt{\beta_1} \tag{6}$$

Thus

$$X_0 = (X_1 + 2.5)\sqrt{\frac{\beta_1}{\beta_0}} - 2.5 \tag{11}$$

but the impairment I is

$$I = X_0 - X_1 \tag{8}$$

or

$$I = (X_1 + 2.5)\sqrt{\frac{\beta_1}{\beta_0}} - 2.5 - X_1$$

$$= X_1\sqrt{\frac{\beta_1}{\beta_0}} + 2.5\sqrt{\frac{\beta_1}{\beta_0}} - 2.5 - X_1$$

$$= X_1\left(\sqrt{\frac{\beta_1}{\beta_0}} - 1\right) + 2.5\left(\sqrt{\frac{\beta_1}{\beta_0}} - 1\right)$$

and finally

$$\boxed{I = (X_1 + 2.5)\left(\sqrt{\frac{\beta_1}{\beta_0}} - 1\right)} \tag{12}$$

Table 4 shows the following values calculated at different circuit noise levels, N_T, at the terminal exchanges.

Column 2. Impairment I at a junction loss of 27 db using equation (4).

Column 3. $\left(1 - \sqrt{\frac{\beta_0}{\beta}}\right)$ using equation (10).

Column 4. β

Column 5. $\left(\sqrt{\frac{\beta_1}{\beta_0}} - 1\right)$

Column 6. Mean opinion score at a junction loss of 23 db, using equation (5).

Column 7. Impairment I (23) at a junction loss of $X_0 = 23$ db, using equation (9).

Column 8. Mean opinion score at a junction loss of 28 db, using equation (5).

Column 9. Impairment I (28) at a junction loss of $X_0 = 28$ db, using equation (9).

Table 4.

Circuit Noise Level N_T dbm	Impairment $I(27)$ db	$1-\sqrt{\frac{\beta_0}{\beta}}$	β	$\sqrt{\frac{\beta_1}{\beta_0}}-1$	Junction Loss 23 db		Junction Loss 28 db	
					Mean Opinion Score Y	Impairment $X_0=23$ db $I(23)$ db	Mean Opinion Score Y	Impairment $X_0=28$ db $I(28)$ db
1	2	3	4	5	6	7	8	9
None	0	0	— 0.00108	0	2.65	0	2.35	0
— 75	0.66	0.0224	— 0.00113	0.0229	2.61	0.57	2.30	0.68
— 74	0.74	0.0251	— 0.001135	0.0258	2.61	0.64	2.29	0.77
— 73	0.83	0.0278	— 0.00114	0.0286	2.61	0.71	2.29	0.85
— 72	0.92	0.0312	— 0.00115	0.0323	2.60	0.80	2.28	0.95
— 71	1.03	0.0349	— 0.00116	0.0362	2.60	0.89	2.27	1.06
— 70	1.15	0.0389	— 0.00117	0.0405	2.59	0.99	2.26	1.19
— 69	1.28	0.0433	— 0.00118	0.0453	2.58	1.10	2.25	1.32
— 68	1.42	0.0482	— 0.00119	0.0506	2.58	1.23	2.24	1.47
— 67	1.58	0.0536	— 0.00120	0.0566	2.57	1.37	2.23	1.63
— 66	1.76	0.0595	— 0.00122	0.0633	2.56	1.52	2.22	1.81
— 65	1.95	0.0660	— 0.00124	0.0707	2.54	1.68	2.20	2.01
— 64	2.16	0.0731	— 0.00126	0.0789	2.53	1.86	2.18	2.23
— 63	2.39	0.0809	— 0.00128	0.0880	2.52	2.06	2.16	2.47
— 62	2.64	0.0894	— 0.00130	0.0982	2.505	2.28	2.14	2.73
— 61	2.91	0.0987	— 0.00133	0.1095	2.49	2.52	2.11	3.01
— 60	3.21	0.1087	— 0.00136	0.1220	2.47	2.77	2.08	3.32
— 59	3.53	0.1196	— 0.00139	0.1358	2.45	3.05	2.06	3.65
— 58	3.88	0.1314	— 0.00143	0.1513	2.42	3.35	2.02	4.01
— 57	4.25	0.1440	— 0.00147	0.1682	2.39	3.67	1.98	4.39
— 56	4.65	0.1576	— 0.00152	0.1871	2.36	4.02	1.94	4.81
— 55	5.08	0.1721	— 0.00158	0.2079	2.32	4.39	1.88	5.25
— 54	5.54	0.1876	— 0.00164	0.2309	2.28	4.78	1.82	5.72
— 53	6.02	0.2041	— 0.00171	0.2564	2.24	5.20	1.76	6.23
— 52	6.54	0.2216	— 0.00178	0.2847	2.19	5.65	1.69	6.76
— 51	7.08	0.2396	— 0.00187	0.3151	2.13	6.11	1.61	7.31
— 50	7.65	0.2593	— 0.00197	0.3501	2.07	6.61	1.52	7.91
— 49	8.25	0.2796	— 0.00208	0.3881	2.00	7.13	1.42	8.53
— 48	8.88	0.3009	— 0.00221	0.4304	1.91	7.67	1.29	9.18
— 47	9.53	0.3230	— 0.00236	0.4771	1.82	8.24	1.15	9.85
— 46	10.21	0.3460	— 0.00253	0.5291	1.70	8.82	1.00	10.55
— 45	10.91	0.3699	— 0.00272	0.5870	1.58	9.43	0.82	11.28

Table 5 shows percentage of opinions E, $E+G$ and so on for different values of mean opinion score as well as the corresponding probits.

Probits as a function of transformed mean opinion score for E, $E+G$, $E+G+F$, $E+G+F+P$ and $P+B$ are straight lines (see *Fig. 10*) and the equations for these lines are

$$E \qquad \text{Probit} = -2.87\sqrt{4-Y} + 7.10 \qquad (13)$$

$$E+G \qquad \text{Probit} = -3.53\sqrt{4-Y} + 9.34 \qquad (14)$$

$$E+G+F \qquad \text{Probit} = -4.31\sqrt{4-Y} + 11.74 \qquad (15)$$

$$E+G+F+P \qquad \text{Probit} = -4.41\sqrt{4-Y} + 13.09 \qquad (16)$$

$$P+B \qquad \text{Probit} = +4.31\sqrt{4-Y} - 1.74 \qquad (17)$$

Table 5. Percentage of opinions for different values of mean opinion score.

Mean Opinion Score	Transform. Mean Opinion Score	E		$E+G$		$E+G+F$		$E+G+F+P$		$P+B$	
Y	$\sqrt{4-Y}$	%	Probit	%	Probit	%	Probit	%	Probit	%	Probit
0.5	1.871			1.20	2.743	9.4	3.684	43.6	4.839	90.6	6.316
6	1.844			1.52	2.835	11.5	3.800	48.3	4.957	88.5	6.200
7	1.817			1.95	2.936	14.0	3.920	53.3	5.083	86.0	6.080
8	1.789			2.4	3.023	16.8	4.038	58.0	5.202	83.2	5.962
9	1.761	0.15	2.032	3.1	3.134	20.0	4.158	62.8	5.327	80.0	5.842
1.0	1.732	0.20	2.122	3.8	3.226	23.6	4.281	67.5	5.454	76.4	5.719
1	1.703	0.26	2.206	4.8	3.335	27.7	4.408	72.0	5.583	72.3	5.592
2	1.673	0.34	2.294	5.9	3.437	32.1	4.535	76.3	5.716	67.9	5.465
3	1.643	0.44	2.380	7.3	3.546	36.9	4.666	80.2	5.849	63.1	5.334
4	1.612	0.56	2.464	8.9	3.653	42.0	4.798	83.8	5.987	58.0	5.202
1.5	1.581	0.73	2.558	10.8	3.763	47.3	4.932	86.9	6.122	52.7	5.068
6	1.549	0.93	2.647	13.0	3.874	52.8	5.070	89.7	6.265	47.2	4.930
7	1.517	1.19	2.740	15.6	3.989	58.2	5.207	92.0	6.405	41.8	4.793
8	1.483	1.53	2.838	18.6	4.107	63.8	5.353	94.0	6.555	36.2	4.647
9	1.449	1.95	2.936	22.0	4.228	69.1	5.499	95.6	6.706	30.9	4.501
2.0	1.414	2.5	3.040	25.8	4.351	74.2	5.650	96.9	6.866	25.8	4.350
1	1.378	3.1	3.134	30.1	4.479	79.0	5.806	98.0	7.054	21.0	4.194
2	1.342	3.9	3.238	34.6	4.604	83.2	5.962	98.54	7.181	16.8	4.038
3	1.304	5.0	3.355	39.7	4.739	86.9	6.122	99.06	7.350	13.1	3.878
4	1.265	6.2	3.462	45.1	4.877	90.2	6.293	99.42	7.524	9.8	3.707
2.5	1.225	7.8	3.581	50.7	5.018	92.8	6.461	99.65	7.697	7.2	3.539
6	1.183	9.7	3.701	56.6	5.166	95.0	6.645	99.80	7.878	5.0	3.355
7	1.140	12.0	3.825	62.4	5.316	96.6	6.825			3.4	3.175
8	1.095	14.8	3.955	68.2	5.473	97.8	7.014			2.2	2.986
9	1.049	18.0	4.085	73.8	5.637	98.68	7.220			1.32	2.780
3.0	1.000	22.0	4.228	79.1	5.810	99.25	7.432			0.75	2.568
1	0.949	26.6	4.375	83.9	5.990	99.60	7.652			0.40	2.348
2	0.894	32.0	4.532	88.1	6.180	99.81	7.894			0.19	2.106
3	0.837	38.1	4.697	91.7	6.385						
4	0.775	45.0	4.874	94.5	6.598						
3.5	0.707	52.8	5.070	96.7	6.838						
6	0.632	61.2	5.285	98.24	7.106						
7	0.548	70.1	5.527	99.18	7.400						
8	0.447	79.3	5.817	99.71	7.759						
9	0.316	88.4	6.195								

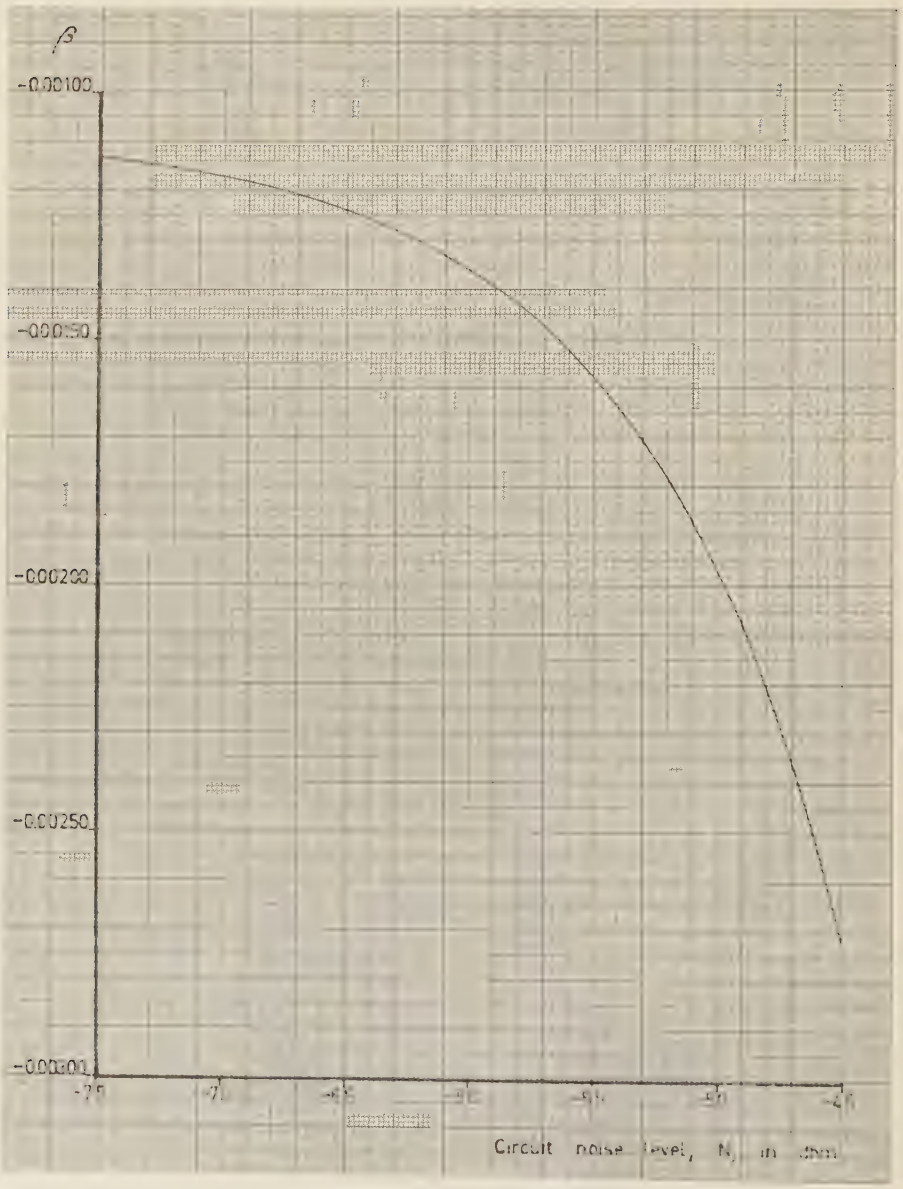

Fig. 6. β as a function of circuit noise level at terminal exchanges.

The results assembled in *Table 4* can be converted into curves showing the percentages of subjects who express opinions E, $E+G$ etc. by applying the relationships between percentages and mean opinion scores given in *Table 5*.

Fig. 6 shows β as a function of circuit noise level N.

Fig. 7 shows mean opinion score Y as a function of circuit noise level N_T (at local exchange) for 23 and 28 db junction losses.

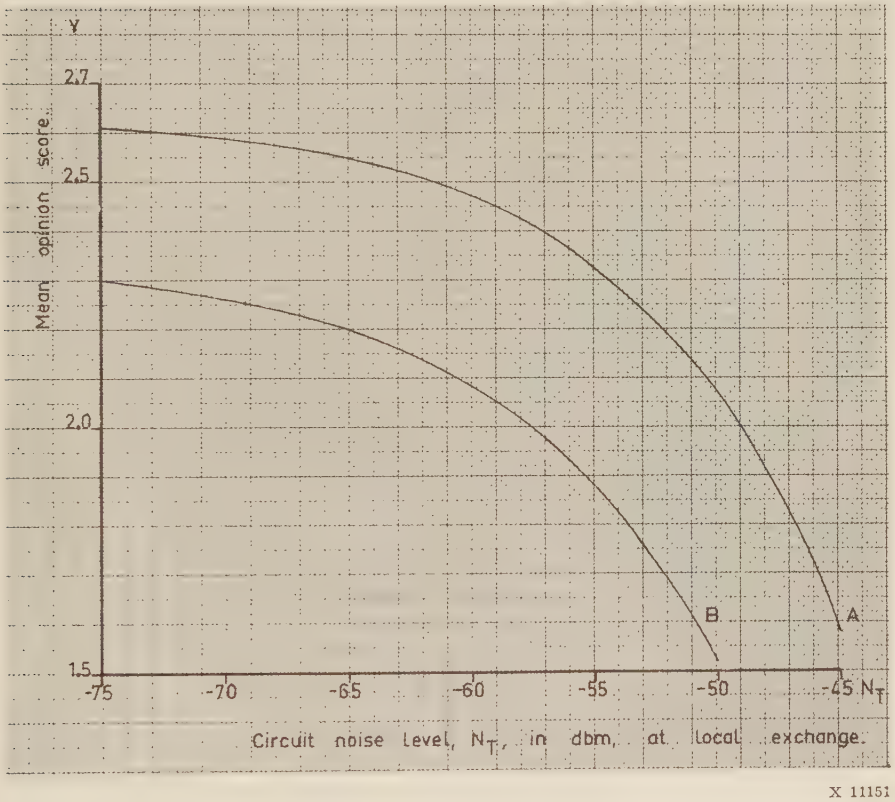

X 11151

Fig. 7. Mean opinion score as a function of circuit noise level at local exchanges.

Curve A. Junction loss 23 db.
Curve B. Junction loss 28 db.

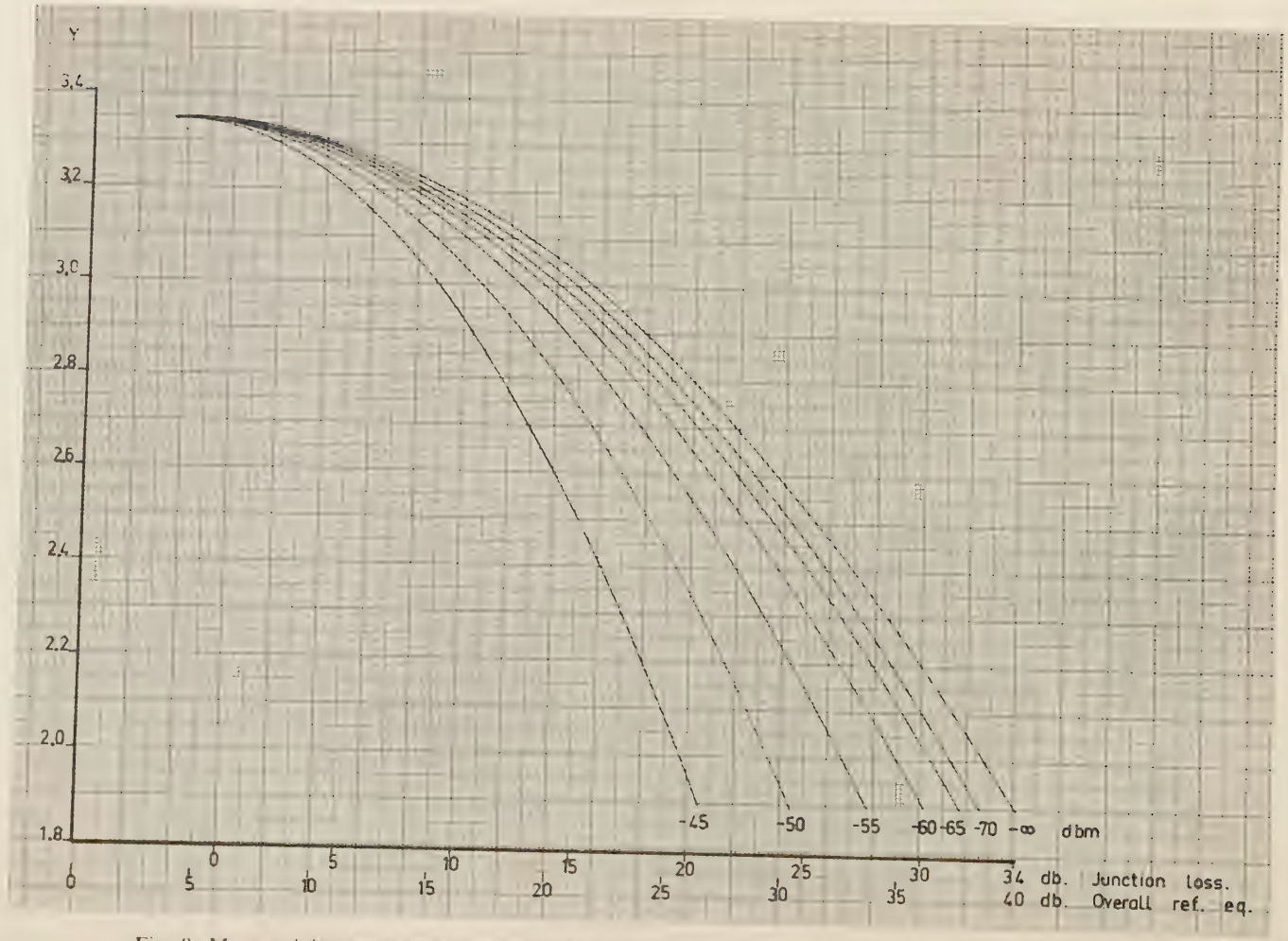

Fig. 8. Mean opinion score as a function of junction loss at different circuit noise levels at local exchanges.

X 11152

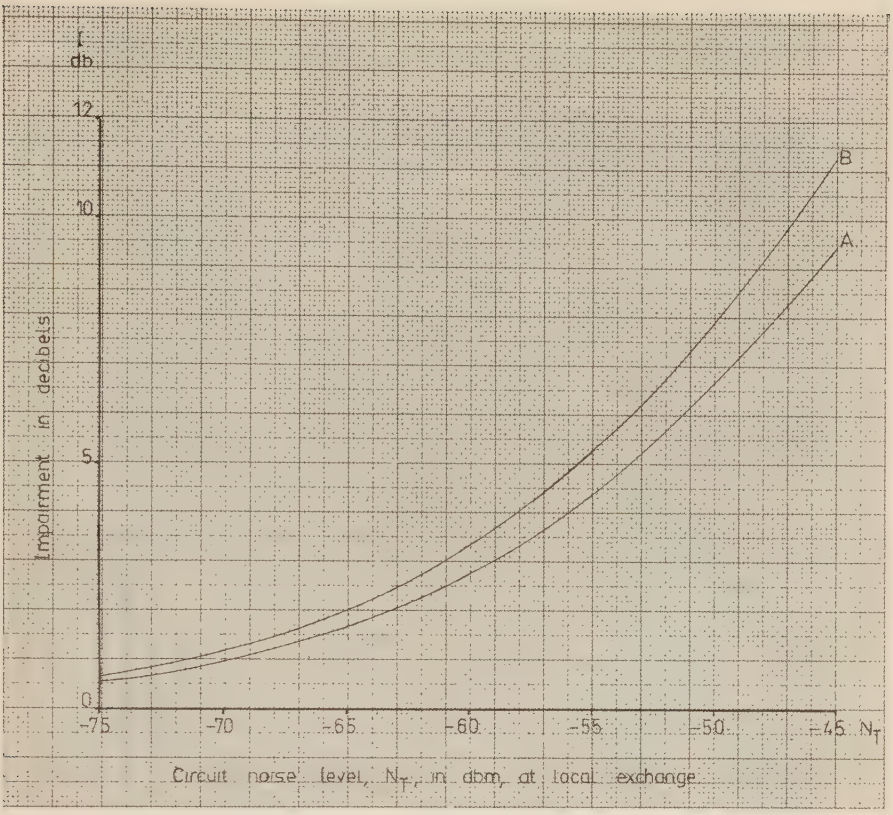

X 11153

Fig. 9. Impairment as a function of circuit noise level at local exchanges.
Curve A. Junction loss $X_0 = 23$ db.
Curve B. Junction loss $X_0 = 28$ db.

Fig. 8 shows mean opinion score Y as a function of junction loss and overall reference equivalent with circuit noise level N_T as parameter.

Fig. 9 shows impairment I as a function of circuit noise level N_T for 23 db and for 28 db junction losses.

Fig. 10 shows percentage of subjects, expressed as a probit, who give certain opinions as a function of transformed mean opinion score.

If the reference equivalents of the local systems do not correspond to those shown in the hypothetical overall connection, *Fig. 12*, a calculation of the transmission performance can be made by transfering the overall connection in question to the hypothetical one.

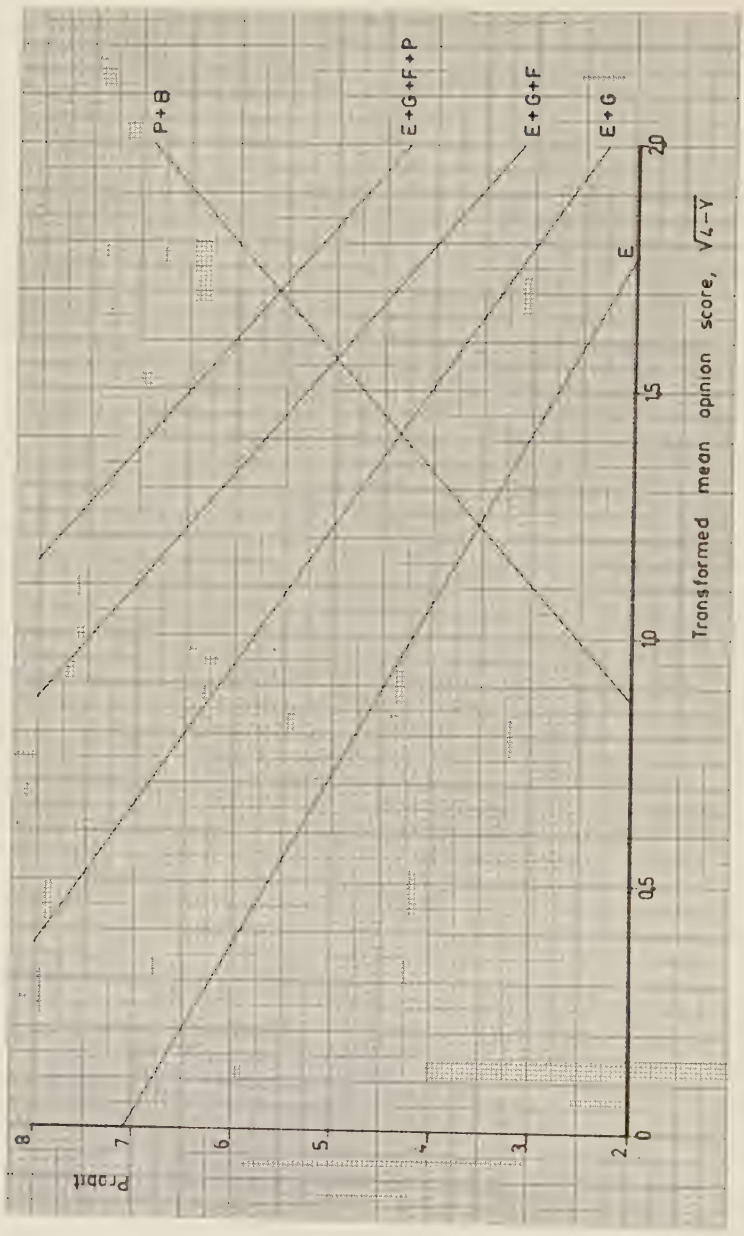

X 11154

Fig. 10. Probit as a function of transformed mean opinion score.

If for example the overall reference equivalent is 40 db, distributed as follows:

Sending local system $= +7 + \Delta_{S(ending)} = 10$ db

Junction loss $j = 28$ db

Receiving local system $= -1 + \Delta_{R(eceiving)} = 2$ db

then this connection transformed to the hypothetical one will be as follows:

Sending local system $= 7$ db

Junction loss $= j + \Delta_S + \Delta_R = 28 + 3 + 3 = 34$ db

Receiving local system $= -1$ db

Overall reference equivalent $= 40$ db

If, for example, the circuit noise level is – 50 dbm 0 at the zero relative level then the circuit noise level at the local exchanges is

$$N_T = -53.5 - \frac{28}{2} = -67.5 \text{ dbm} = N$$

for the connection in consideration.

After the transformation to the hypothetical connection N_T is

$$N_T = N - \Delta_R = -67.5 - 3 = -70.5 \text{ dbm}$$

the receiving system being 3 db worse than the average one. Thus it is assumed that a noise level of – 67.5 dbm in the first case will produce the same effect on the listener as – 70.5 dbm with an average line, the reference equivalent for receiving being 3 db worse as already mentioned. The transmission performance can now be easily calculated using the fundamental data given, bearing in mind that the junction loss is $X = 34$ db and that the circuit noise level is $N_T = -70.5$ dbm.

Table 6 shows mean opinion score as a function of junction loss and circuit noise level at terminal exchanges.

Table 7 shows impairment as a function of junction loss, X_0 db, and circuit noise level at terminal exchanges.

Table 8 shows impairment as a function of junction loss, X db, and circuit noise level at terminal exchanges.

Table 6. Mean Opinion Score as a function of junction loss and circuit noise level at terminal excha
Average subscribers' lines. Opinion form 9.

Noise Level N_T dbm	β	$Y(10)$	$Y(11)$	$Y(12)$	$Y(13)$	$Y(14)$	$Y(15)$	$Y(16)$	$Y(17)$	$Y(18)$	$Y(19)$	$Y(20)$	$Y(21)$	Y
None	— 0.00108	3.18	3.15	3.12	3.09	3.06	3.02	2.98	2.94	2.90	2.85	2.80	2.75	2
— 70	— 0.00117	3.17	3.14	3.10	3.07	3.03	2.99	2.95	2.91	2.86	2.81	2.76	2.70	2
— 69	— 0.00118	3.17	3.13	3.10	3.07	3.03	2.99	2.95	2.90	2.85	2.80	2.75	2.70	2
— 68	— 0.00119	3.16	3.13	3.10	3.06	3.03	2.99	2.94	2.90	2.85	2.80	2.75	2.69	2
— 67	— 0.00120	3.16	3.13	3.10	3.06	3.02	2.98	2.94	2.89	2.85	2.80	2.74	2.69	2
— 66	— 0.00122	3.16	3.13	3.09	3.06	3.02	2.98	2.93	2.89	2.84	2.79	2.73	2.68	2
— 65	— 0.00124	3.16	3.12	3.09	3.05	3.01	2.97	2.93	2.88	2.83	2.78	2.72	2.67	2
— 64	— 0.00126	3.15	3.12	3.09	3.05	3.01	2.96	2.92	2.87	2.82	2.77	2.71	2.65	2
— 63	— 0.00128	3.15	3.12	3.08	3.04	3.00	2.96	2.91	2.86	2.81	2.76	2.70	2.64	2
— 62	— 0.00130	3.15	3.11	3.08	3.04	3.00	2.95	2.91	2.86	2.80	2.75	2.69	2.63	2
— 61	— 0.00133	3.14	3.11	3.07	3.03	2.99	2.94	2.89	2.84	2.79	2.74	2.68	2.62	2
— 60	— 0.00136	3.14	3.10	3.06	3.02	2.98	2.93	2.88	2.83	2.78	2.72	2.66	2.60	2
— 59	— 0.00139	3.13	3.10	3.06	3.02	2.97	2.92	2.87	2.82	2.77	2.71	2.65	2.58	2
— 58	— 0.00143	3.13	3.09	3.05	3.01	2.96	2.91	2.86	2.81	2.75	2.69	2.63	2.56	2
— 57	— 0.00147	3.12	3.08	3.04	3.00	2.95	2.90	2.85	2.79	2.73	2.67	2.61	2.54	2
— 56	— 0.00152	3.11	3.07	3.03	2.98	2.94	2.88	2.83	2.77	2.71	2.65	2.58	2.51	2
— 55	— 0.00158	3.10	3.06	3.02	2.97	2.92	2.87	2.81	2.75	2.69	2.62	2.55	2.48	2
— 54	— 0.00164	3.09	3.05	3.01	2.96	2.90	2.85	2.79	2.73	2.66	2.59	2.52	2.44	2
— 53	— 0.00171	3.07	3.03	2.99	2.94	2.88	2.83	2.76	2.70	2.63	2.56	2.48	2.41	2
— 52	— 0.00178	3.07	3.03	2.98	2.92	2.87	2.80	2.74	2.67	2.60	2.53	2.45	2.37	2
— 51	— 0.00187	3.06	3.01	2.96	2.90	2.84	2.78	2.71	2.64	2.56	2.49	2.40	2.32	2
— 50	— 0.00197	3.04	2.99	2.94	2.88	2.81	2.75	2.68	2.60	2.52	2.44	2.35	2.26	2
— 49	— 0.00208	3.02	2.97	2.91	2.85	2.78	2.71	2.64	2.56	2.48	2.39	2.30	2.20	2
— 48	— 0.00221	3.00	2.95	2.89	2.82	2.75	2.67	2.59	2.51	2.42	2.33	2.23	2.13	2
— 47	— 0.00236	2.98	2.92	2.85	2.78	2.71	2.63	2.54	2.45	2.36	2.26	2.16	2.05	1
— 46	— 0.00253	2.95	2.89	2.82	2.74	2.66	2.58	2.48	2.39	2.29	2.18	2.07	1.95	1
— 45	— 0.00272	2.92	2.85	2.78	2.70	2.61	2.52	2.42	2.32	2.21	2.09	1.97	1.85	1

Table 6 (cont.)

Noise Level N_T dbm	β	$Y(23)$	$Y(24)$	$Y(25)$	$Y(26)$	$Y(27)$	$Y(28)$	$Y(29)$	$Y(30)$	$Y(31)$	$Y(32)$	$Y(33)$	$Y(34)$
None	— 0.00108	2.65	2.59	2.53	2.47	2.41	2.35	2.28	2.21	2.14	2.06	1.99	1.91
— 70	— 0.00117	2.59	2.53	2.47	2.40	2.33	2.26	2.19	2.11	2.04	1.96	1.88	1.79
— 69	— 0.00118	2.58	2.52	2.46	2.39	2.32	2.25	2.18	2.10	2.03	1.95	1.86	1.78
— 68	— 0.00119	2.58	2.51	2.45	2.38	2.31	2.24	2.17	2.09	2.01	1.93	1.85	1.76
— 67	— 0.00120	2.57	2.51	2.44	2.38	2.31	2.23	2.16	2.08	2.00	1.92	1.84	1.75
— 66	— 0.00122	2.56	2.49	2.43	2.36	2.29	2.22	2.14	2.06	1.98	1.90	1.81	1.72
— 65	— 0.00124	2.54	2.48	2.41	2.35	2.27	2.20	2.12	2.04	1.96	1.87	1.79	1.70
— 64	— 0.00126	2.53	2.47	2.40	2.33	2.25	2.18	2.10	2.02	1.94	1.85	1.76	1.67
— 63	— 0.00128	2.52	2.45	2.38	2.31	2.24	2.16	2.08	2.00	1.91	1.83	1.74	1.64
— 62	— 0.00130	2.50	2.44	2.37	2.29	2.22	2.14	2.06	1.98	1.89	1.80	1.71	1.62
— 61	— 0.00133	2.49	2.42	2.34	2.27	2.19	2.11	2.03	1.95	1.86	1.77	1.67	1.58
— 60	— 0.00136	2.47	2.39	2.32	2.25	2.17	2.08	2.00	1.91	1.82	1.73	1.64	1.54
— 59	— 0.00139	2.45	2.37	2.30	2.22	2.14	2.06	1.97	1.88	1.79	1.70	1.60	1.50
— 58	— 0.00143	2.42	2.35	2.27	2.19	2.11	2.02	1.93	1.84	1.75	1.65	1.55	1.44
— 57	— 0.00147	2.39	2.32	2.24	2.16	2.07	1.98	1.89	1.80	1.70	1.60	1.50	1.39
— 56	— 0.00152	2.36	2.28	2.20	2.12	2.03	1.94	1.84	1.74	1.64	1.54	1.43	1.32
— 55	— 0.00158	2.32	2.24	2.16	2.07	1.98	1.88	1.78	1.68	1.58	1.47	1.36	1.25
— 54	— 0.00164	2.28	2.20	2.11	2.02	1.92	1.82	1.72	1.62	1.51	1.40	1.28	1.17
— 53	— 0.00171	2.24	2.15	2.06	1.96	1.86	1.76	1.65	1.54	1.43	1.31	1.19	1.07
— 52	— 0.00178	2.19	2.10	2.00	1.90	1.80	1.69	1.58	1.47	1.35	1.23	1.11	0.98
— 51	— 0.00187	2.13	2.04	1.94	1.83	1.72	1.61	1.49	1.37	1.25	1.12	0.99	
— 50	— 0.00197	2.07	1.97	1.86	1.75	1.64	1.52	1.40	1.27	1.14	1.01		
— 49	— 0.00208	2.00	1.89	1.78	1.66	1.54	1.42	1.29	1.15	1.02			
— 48	— 0.00221	1.91	1.80	1.68	1.55	1.43	1.29	1.16	1.02				
— 47	— 0.00236	1.82	1.69	1.57	1.43	1.30	1.15	1.01					
— 46	— 0.00253	1.70	1.57	1.44	1.30	1.15	1.00						
— 45	— 0.00272	1.58	1.44	1.29	1.14	0.98							

Table 7. Impairment as a function of junction loss, X_0 db, and circuit noise level at terminal exchan
Average subscribers' lines. Opinion form 9.

Noise Level N_T dbm	$1-\sqrt{\frac{\beta_0}{\beta}}$	$I(10)$ db	$I(11)$ db	$I(12)$ db	$I(13)$ db	$I(14)$ db	$I(15)$ db	$I(16)$ db	$I(17)$ db	$I(18)$ db	$I(19)$ db	$I(20)$ db	$I(21)$ db	$I(2$ d
— 70	0.0389	0.49	0.52	0.56	0.60	0.64	0.68	0.72	0.76	0.80	0.84	0.88	0.91	0.9
— 69	0.0433	0.54	0.58	0.63	0.67	0.71	0.76	0.80	0.84	0.89	0.93	0.97	1.02	1.0
— 68	0.0482	0.60	0.65	0.70	0.75	0.80	0.84	0.89	0.94	0.99	1.04	1.08	1.13	1.1
— 67	0.0536	0.67	0.73	0.78	0.83	0.88	0.94	0.99	1.05	1.10	1.15	1.21	1.26	1.3
— 66	0.0595	0.74	0.80	0.86	0.92	0.98	1.04	1.10	1.16	1.22	1.28	1.34	1.40	1.4
— 65	0.0660	0.83	0.89	0.96	1.02	1.09	1.16	1.22	1.29	1.35	1.42	1.49	1.55	1.6
— 64	0.0731	0.91	0.99	1.06	1.13	1.21	1.28	1.35	1.43	1.50	1.57	1.64	1.72	1.7
— 63	0.0809	1.01	1.09	1.17	1.25	1.33	1.42	1.50	1.58	1.66	1.74	1.82	1.90	1.9
— 62	0.0894	1.12	1.21	1.30	1.39	1.48	1.56	1.65	1.74	1.83	1.92	2.01	2.10	2.1
— 61	0.0987	1.23	1.33	1.43	1.53	1.63	1.73	1.83	1.92	2.02	2.12	2.22	2.32	2.4
— 60	0.1087	1.36	1.47	1.58	1.68	1.79	1.90	2.01	2.12	2.23	2.34	2.45	2.55	2.6
— 59	0.1196	1.50	1.61	1.73	1.85	1.97	2.09	2.21	2.33	2.45	2.57	2.69	2.81	2.9
— 58	0.1314	1.64	1.77	1.91	2.04	2.17	2.30	2.43	2.56	2.69	2.83	2.96	3.09	3.2
— 57	0.1440	1.80	1.94	2.09	2.23	2.38	2.52	2.66	2.81	2.95	3.10	3.24	3.38	3.5
— 56	0.1576	1.97	2.13	2.29	2.44	2.60	2.76	2.91	3.07	3.23	3.39	3.55	3.70	3.8
— 55	0.1721	2.15	2.32	2.50	2.67	2.84	3.01	3.18	3.36	3.53	3.70	3.87	4.04	4.2
— 54	0.1876	2.35	2.53	2.72	2.91	3.10	3.28	3.47	3.66	3.85	4.03	4.22	4.41	4.6
— 53	0.2041	2.55	2.76	2.96	3.16	3.37	3.57	3.78	3.98	4.18	4.39	4.59	4.80	5.0
— 52	0.2216	2.77	2.99	3.21	3.43	3.66	3.88	4.10	4.32	4.54	4.76	4.99	5.21	5.4
— 51	0.2396	3.00	3.23	3.47	3.71	3.95	4.19	4.43	4.67	4.91	5.15	5.39	5.63	5.8
— 50	0.2593	3.24	3.50	3.76	4.02	4.28	4.54	4.80	5.06	5.32	5.57	5.83	6.09	6.3
— 49	0.2796	3.50	3.77	4.05	4.33	4.61	4.89	5.17	5.45	5.73	6.01	6.29	6.57	6.8
— 48	0.3009	3.76	4.06	4.36	4.66	4.96	5.27	5.57	5.87	6.17	6.47	6.77	7.07	7.3
— 47	0.3230	4.04	4.36	4.68	5.01	5.33	5.65	5.98	6.30	6.62	6.94	7.27	7.59	7.9
— 46	0.3460	4.33	4.67	5.02	5.36	5.71	6.06	6.40	6.75	7.09	7.44	7.79	8.13	8.4
— 45	0.3699	4.62	4.99	5.36	5.73	6.10	6.47	6.84	7.21	7.58	7.95	8.32	8.69	9.0

Table 7 (cont.)

Noise Level N_T dbm	$1-\sqrt{\frac{\beta_0}{\beta}}$	$I(23)$ db	$I(24)$ db	$I(25)$ db	$I(26)$ db	$I(27)$ db	$I(28)$ db	$I(29)$ db	$I(30)$ db	$I(31)$ db	$I(32)$ db	$I(33)$ db	$I(34)$ db
— 70	0.0389	0.99	1.03	1.07	1.11	1.15	1.19	1.23	1.26	1.30	1.34	1.38	1.42
— 69	0.0433	1.10	1.15	1.19	1.23	1.28	1.32	1.36	1.41	1.45	1.49	1.54	1.58
— 68	0.0482	1.23	1.28	1.33	1.37	1.42	1.47	1.52	1.57	1.61	1.66	1.71	1.76
— 67	0.0536	1.37	1.42	1.47	1.53	1.58	1.63	1.69	1.74	1.80	1.85	1.90	1.96
— 66	0.0595	1.52	1.58	1.64	1.70	1.76	1.81	1.87	1.93	1.99	2.05	2.11	2.17
— 65	0.0660	1.68	1.75	1.82	1.88	1.95	2.01	2.08	2.15	2.21	2.28	2.34	2.41
— 64	0.0731	1.86	1.94	2.01	2.08	2.16	2.23	2.30	2.38	2.45	2.52	2.60	2.67
— 63	0.0809	2.06	2.14	2.22	2.31	2.39	2.47	2.55	2.63	2.71	2.79	2.87	2.95
— 62	0.0894	2.28	2.37	2.45	2.55	2.64	2.73	2.82	2.91	2.99	3.08	3.17	3.26
— 61	0.0987	2.52	2.62	2.71	2.81	2.91	3.01	3.11	3.21	3.31	3.41	3.50	3.60
— 60	0.1087	2.77	2.88	2.99	3.10	3.21	3.32	3.42	3.53	3.64	3.75	3.86	3.97
— 59	0.1196	3.05	3.17	3.29	3.41	3.53	3.65	3.77	3.89	4.01	4.13	4.25	4.37
— 58	0.1314	3.35	3.48	3.61	3.74	3.88	4.01	4.14	4.27	4.40	4.53	4.66	4.80
— 57	0.1440	3.67	3.82	3.96	4.10	4.25	4.39	4.54	4.68	4.82	4.97	5.11	5.26
— 56	0.1576	4.02	4.18	4.33	4.49	4.65	4.81	4.96	5.12	5.28	5.44	5.59	5.75
— 55	0.1721	4.39	4.56	4.73	4.90	5.08	5.25	5.42	5.59	5.77	5.94	6.11	6.28
— 54	0.1876	4.78	4.97	5.16	5.35	5.53	5.72	5.91	6.10	6.28	6.47	6.66	6.85
— 53	0.2041	5.20	5.41	5.61	5.82	6.02	6.23	6.43	6.63	6.84	7.04	7.25	7.45
— 52	0.2216	5.65	5.87	6.09	6.32	6.54	6.76	6.98	7.20	7.42	7.65	7.87	8.09
— 51	0.2396	6.11	6.35	6.59	6.83	7.07	7.31	7.55	7.79	8.03	8.27	8.51	8.75
— 50	0.2593	6.61	6.87	7.13	7.39	7.65	7.91	8.17	8.43	8.69	8.95	9.21	9.47
— 49	0.2796	7.13	7.41	7.69	7.97	8.25	8.53	8.81	9.09	9.37	9.65	9.93	10.21
— 48	0.3009	7.67	7.97	8.27	8.58	8.88	9.18	9.48	9.78	10.08	10.38	10.68	
— 47	0.3230	8.24	8.56	8.88	9.21	9.53	9.85	10.17	10.50				
— 46	0.3460	8.82	9.17	9.52	9.86	10.21	10.55						
— 45	0.3699	9.43	9.80	10.17	10.54	10.91							

Table 8. Impairment as a function of junction loss, X db, and circuit noise level at terminal exchan
Average subscribers' lines. Opinion form 9.

Noise Level N_T dbm	$\sqrt{\frac{\beta}{\beta_0}} - 1$	$I(10)$ db	$I(11)$ db	$I(12)$ db	$I(13)$ db	$I(14)$ db	$I(15)$ db	$I(16)$ db	$I(17)$ db	$I(18)$ db	$I(19)$ db	$I(20)$ db	$I(21)$ db	$I(2$ d
— 70	0.0405	0.51	0.55	0.59	0.63	0.67	0.71	0.75	0.79	0.83	0.87	0.91	0.95	0.9
— 69	0.0453	0.57	0.61	0.66	0.70	0.75	0.79	0.84	0.88	0.93	0.97	1.02	1.06	1.1
— 68	0.0506	0.63	0.68	0.73	0.78	0.83	0.89	0.94	0.99	1.04	1.09	1.14	1.19	1.2
— 67	0.0566	0.71	0.76	0.82	0.88	0.93	0.99	1.05	1.10	1.16	1.22	1.27	1.33	1.3
— 66	0.0633	0.79	0.85	0.92	0.98	1.04	1.11	1.17	1.23	1.30	1.36	1.42	1.49	1.5
— 65	0.0707	0.88	0.95	1.03	1.10	1.17	1.24	1.31	1.38	1.45	1.52	1.59	1.66	1.7
— 64	0.0789	0.99	1.07	1.14	1.22	1.30	1.38	1.46	1.54	1.62	1.70	1.78	1.85	1.9
— 63	0.0880	1.10	1.19	1.28	1.36	1.45	1.54	1.63	1.72	1.80	1.89	1.98	2.07	2.1
— 62	0.0982	1.23	1.33	1.42	1.52	1.62	1.72	1.82	1.91	2.01	2.11	2.21	2.31	2.4
— 61	0.1095	1.37	1.48	1.59	1.70	1.81	1.92	2.03	2.14	2.24	2.35	2.46	2.57	2.6
— 60	0.1220	1.53	1.65	1.77	1.89	2.01	2.14	2.26	2.38	2.50	2.62	2.75	2.87	2.9
— 59	0.1358	1.70	1.83	1.97	2.10	2.24	2.38	2.51	2.65	2.78	2.92	3.06	3.19	3.3
— 58	0.1513	1.89	2.04	2.19	2.35	2.50	2.65	2.80	2.95	3.10	3.25	3.40	3.56	3.7
— 57	0.1682	2.10	2.27	2.44	2.61	2.78	2.94	3.11	3.28	3.45	3.62	3.78	3.95	4.1
— 56	0.1871	2.34	2.53	2.71	2.90	3.09	3.27	3.46	3.65	3.84	4.02	4.21	4.40	4.5
— 55	0.2079	2.60	2.81	3.01	3.22	3.43	3.64	3.85	4.05	4.26	4.47	4.68	4.89	5.0
— 54	0.2309	2.89	3.12	3.35	3.58	3.81	4.04	4.27	4.50	4.73	4.96	5.20	5.43	5.6
— 53	0.2564	3.21	3.46	3.72	3.97	4.23	4.49	4.74	5.00	5.26	5.51	5.77	6.03	6.2
— 52	0.2847	3.56	3.84	4.13	4.41	4.70	4.98	5.27	5.55	5.84	6.12	6.41	6.69	6.9
— 51	0.3151	3.94	4.25	4.57	4.88	5.20	5.51	5.83	6.14	6.46	6.77	7.09	7.40	7.7
— 50	0.3501	4.38	4.73	5.08	5.43	5.78	6.13	6.48	6.83	7.18	7.53	7.88	8.23	8.5
— 49	0.3881	4.85	5.24	5.63	6.02	6.40	6.79	7.18	7.57	7.96	8.34	8.73	9.12	9.51
— 48	0.4304	5.38	5.81	6.24	6.67	7.10	7.53	7.96	8.39	8.82	9.25	9.68	10.11	
— 47	0.4771	5.96	6.44	6.92	7.40	7.87	8.35	8.83	9.30	9.78	10.26			
— 46	0.5291	6.61	7.14	7.67	8.20	8.73	9.26	9.79	10.32					
— 45	0.5870	7.34	7.92	8.51	9.10	9.69	10.27							

Table 8 (cont.)

oise evel V_T bm	$\sqrt{\frac{\beta}{\beta_0}-1}$	$I(23)$ db	$I(24)$ db	$I(25)$ db	$I(26)$ db	$I(27)$ db	$I(28)$ db	$I(29)$ db	$I(30)$ db	$I(31)$ db	$I(32)$ db	$I(33)$ db	$I(34)$ db
- 70	0.0405	1.03	1.07	1.11	1.15	1.19	1.24	1.28	1.32	1.36	1.40	1.44	1.48
- 69	0.0453	1.16	1.20	1.25	1.29	1.34	1.38	1.43	1.47	1.52	1.56	1.61	1.65
- 68	0.0506	1.29	1.34	1.39	1.44	1.49	1.54	1.59	1.64	1.70	1.75	1.80	1.85
- 67	0.0566	1.44	1.50	1.56	1.61	1.67	1.73	1.78	1.84	1.90	1.95	2.01	2.07
- 66	0.0633	1.61	1.68	1.74	1.80	1.87	1.93	1.99	2.06	2.12	2.18	2.25	2.31
- 65	0.0707	1.80	1.87	1.94	2.01	2.09	2.16	2.23	2.30	2.37	2.44	2.51	2.58
- 64	0.0789	2.01	2.09	2.17	2.25	2.33	2.41	2.49	2.56	2.64	2.72	2.80	2.88
- 63	0.0880	2.24	2.33	2.42	2.51	2.60	2.68	2.77	2.86	2.95	3.04	3.12	3.21
- 62	0.0982	2.50	2.60	2.70	2.80	2.90	3.00	3.09	3.19	3.29	3.39	3.49	3.58
- 61	0.1095	2.79	2.90	3.01	3.12	3.23	3.34	3.45	3.56	3.67	3.78	3.89	4.00
- 60	0.1220	3.11	3.23	3.36	3.48	3.60	3.72	3.84	3.97	4.09	4.21	4.33	4.45
- 59	0.1358	3.46	3.60	3.73	3.87	4.01	4.14	4.28	4.41	4.55	4.69	4.82	4.96
- 58	0.1513	3.86	4.01	4.16	4.31	4.46	4.61	4.77	4.92	5.07	5.22	5.37	5.52
- 57	0.1682	4.29	4.46	4.63	4.79	4.96	5.13	5.30	5.47	5.63	5.80	5.97	6.14
- 56	0.1871	4.77	4.96	5.15	5.33	5.52	5.71	5.89	6.08	6.27	6.45	6.64	6.83
- 55	0.2079	5.30	5.51	5.72	5.93	6.13	6.34	6.55	6.76	6.96	7.17	7.38	7.59
- 54	0.2309	5.89	6.12	6.35	6.58	6.81	7.04	7.27	7.50	7.74	7.97	8.20	8.43
- 53	0.2564	6.54	6.79	7.05	7.31	7.56	7.82	8.08	8.33	8.59	8.85	9.10	9.36
- 52	0.2847	7.26	7.54	7.83	8.11	8.40	8.68	8.97	9.25	9.54	9.82	10.11	10.39
- 51	0.3151	8.04	8.35	8.67	8.98	9.30	9.61	9.93	10.24				
- 50	0.3501	8.93	9.28	9.63	9.98	10.33							
- 49	0.3881	9.90	10.28										
- 48	0.4304												
- 47	0.4771												
- 46	0.5291												
- 45	0.5870												

CHAPTER 5

Calculation of Transmission Performance, based on Opinion Tests, in Presence of Circuit Noise

Question 4. (Study Group 12 in cooperation with Study Group 1).

In the light of tests based on the opinions of typical telephone users what is the effect on transmission performance of the provisional noise limits adopted by the XVIIIth Plenary Assembly of the CCIF as proposed by the CCIF Study Group 3.

These provisional limits are:

a. For planning carrier systems on coaxial pairs.
The mean psophometric power at a point of zero relative level at the end of the hypothetical reference circuit on coaxial pairs, during any hour, is 10,000 picowatts.

b. For planning carrier systems on symmetrical pairs.
The mean psophometric power at a point of zero relative level at the end of the hypothetical reference circuit on symmetrical pairs, during any hour, is 10,000 picowatts.

c. It is desirable that the total circuit noise (including intermodulation crosstalk) measured at the end of a circuit with the CCIF psophometer shall not on an average exceed a value corresponding to an E.M.F. of 2 millivolts at a point of relative level – 0.8 neper or – 7 decibels.

Note. The mean value of psophometric power of 10,000 picowatts at a point of zero relative level, which serves as a design basis for planning carrier systems, corresponds to a psophometric E.M.F. of about 2.2 millivolts at a point of relative level – 0.8 neper or – 7 decibels.

Question 6. (Study Group 12 in cooperation with CCITT, Study Groups 1 and 3 and the CCIR).

What is the effect on transmission performance, as shown by the results of opinion tests (involving typical telephone users), of the various hypothetical distributions of noise level in radio relay systems submitted by the CCITT Study Groups 1 and 3?

Note. The distributions should take the form of curves indicating the proportions of intervals, each of one minute duration, for which the mean noise power, measured with

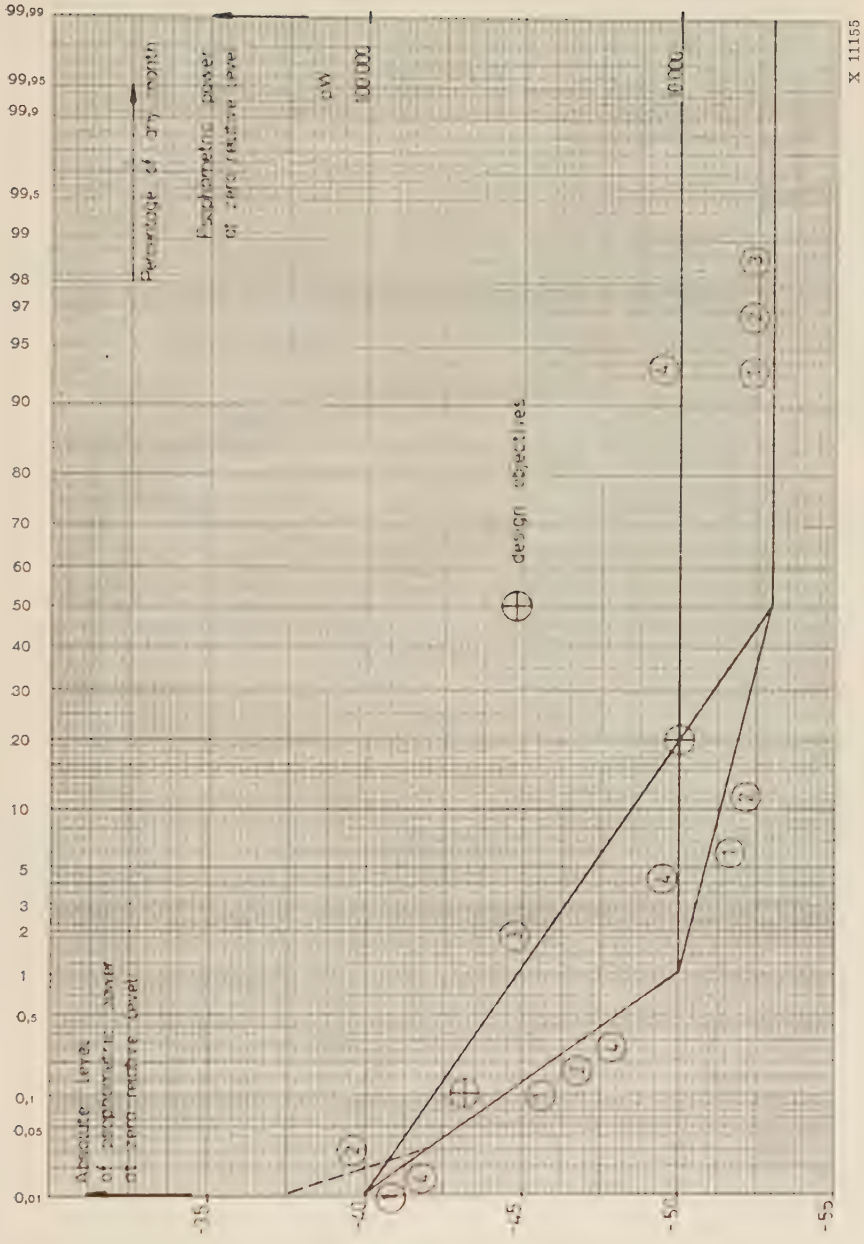

Fig. 11. Distribution curves, at the end of a 2,500 km circuit, submitted to the Study Group 12.

the psophometer specified by the CCIF for commercial telephone circuits, does not exceed each of a number of values. These curves should be determined by the method described in full in Annexe 4 to Question 7 of CCITT Study Group 1.

For the study of Question 6 the joint CCITT-CCIR Working Party on circuit noise has submitted four hypothetical noise distributing curves to the Study Group 12.

These curves are shown in *Fig. 11*. They are based on results of tests carried out in West Germany, France, Italy and Great Britain on existing radio relay links, and are referred to a circuit of 2,500 km.

The joint CCITT-CCIR Working Party has proposed to recommend as a design objective the following limits for the noise on any telephone channel of a wide band system measured in terms of the mean power over one minute, psophometrically weighted, and per cent of a month:

An absolute level of psophometric power of – 43 dbm at zero relative level, i.e. – 43 dbm 0, may not be exceeded 0.1 % of a month.

An absolute level of psophometric power of – 50 dbm at zero relative level, i.e. – 50 dbm 0, may not be exceeded 20 % of a month.

The circuit conditions used for answering both Questions 4 and 6 are shown in *Fig. 12*. They represent a fairly typical international connection of 29 db reference equivalent.

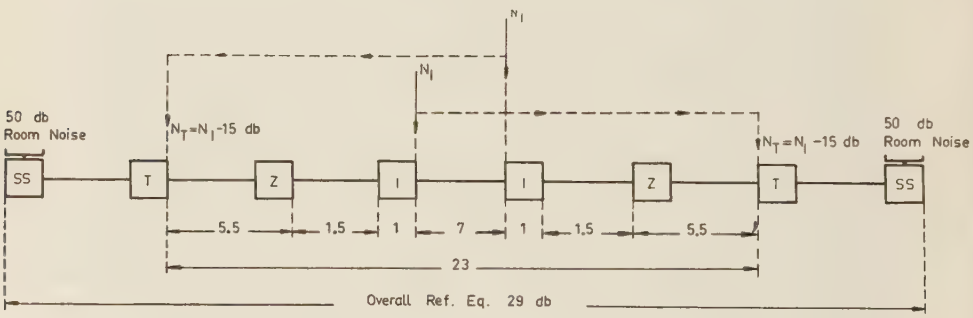

Notes. I = international exchange
Z = main national switching centre
T = local exchange
SS = subscriber's set
sending reference equivalent +7 db
receiving —||— —||— -1 db

X 11156

Fig. 12. Hypothetical overall connection for calculation of percentages of opinions.

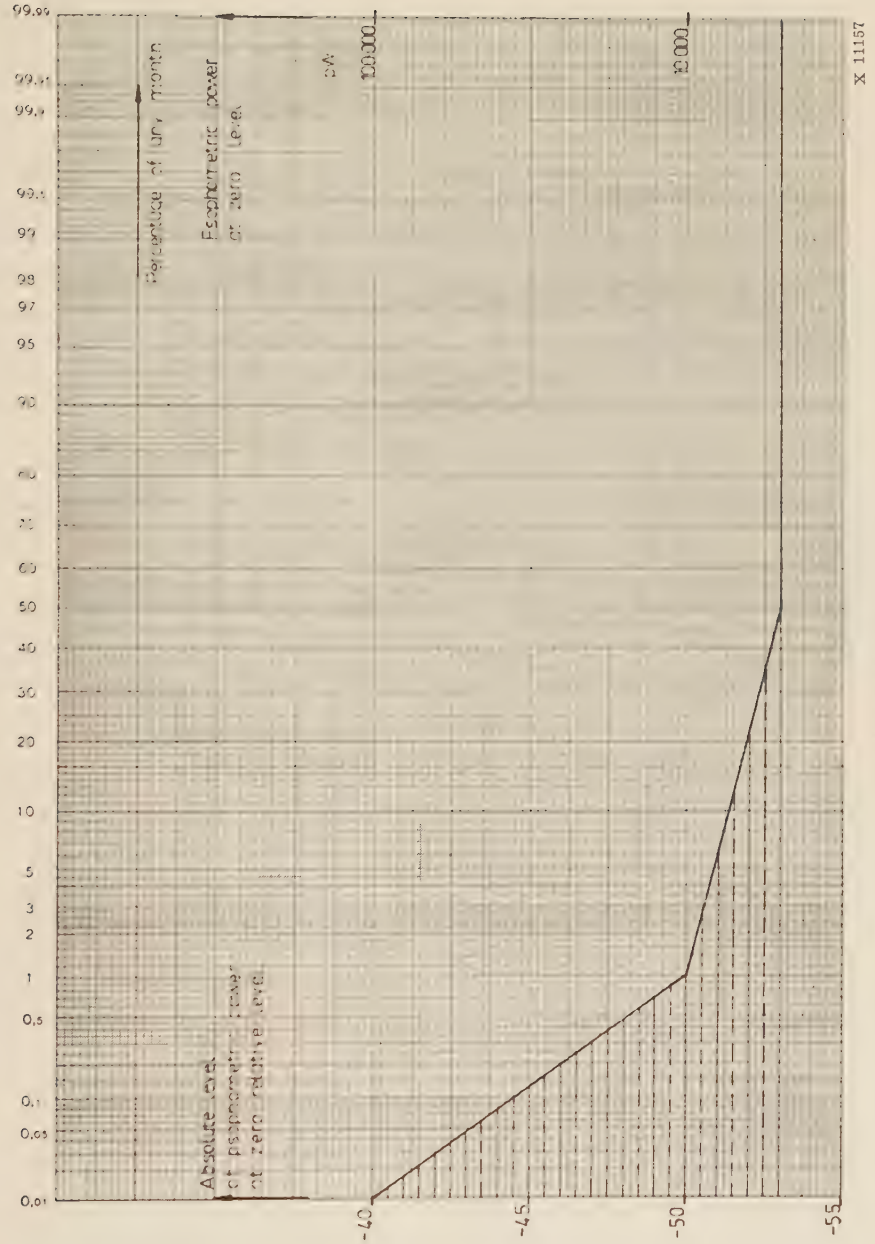

Fig. 13. Distribution curve 1 from *Fig. 11.*

Question 4

If the circuit noise level at zero relative level is − 50 dbm 0, corresponding to a psophometric power of 10,000 picowatts, then the noise level at the local exchange is $N_T = -50 - 15 = -65$ dbm and the mean opinion score is $Y = 3.35 - 0.00124\ (23 + 2.5)^2 = 2.55$ and the percentages of opinions (from *Table 5*) are those shown in *Table 11*.

Question 6

A calculation of the transmission performance for curve 1 of the four hypothetical noise distribution curves, shown in *Fig. 11*, will be performed. *Fig. 13* shows this particular curve. The percentage of calls, *f*, subject to each of a number of circuit noise levels at 1 db intervals are obtained from this curve. These figures are given in *Table 10*, column 3.

Table 9 shows mean opinion score *Y* and percentages of opinions for various levels of circuit noise, N_T, at the terminal exchanges for a junction loss of 23 db or an overall reference equivalent of 29 db.

Table 9. Mean opinion score and percentages of opinions at different circuit noise levels at local exchanges.

Circuit Noise Level N_T dbm	Mean Opinion Score	Percentages of Opinions			
	Y	*E*	*E*+*G*	*E*+*G*+*F*	*E*+*G*+*F*+*P*
1	2	3	4	5	6
$-\infty$	2.65	10.8	60.0	95.8	99.85
— 68	2.58	9.4	55.3	94.6	99.8
— 67	2.57	8.9	54.1	94.2	99.8
— 66	2.56	8.7	53.5	94.0	99.8
— 65	2.55	8.5	53.0	93.8	99.7
— 64	2.54	8.1	51.8	93.3	99.7
— 63	2.52	8.0	51.2	93.1	99.7
— 62	2.50	7.8	50.6	92.8	99.7
— 61	2.49	7.6	50.1	92.6	99.6
— 60	2.47	7.2	49.0	92.1	99.6
— 59	2.44	6.8	47.3	91.3	99.5
— 58	2.42	6.4	45.6	90.4	99.5
— 57	2.39	6.1	44.6	89.8	99.4
— 56	2.36	5.7	42.9	88.9	99.3
— 55	2.32	5.2	40.7	87.6	99.1
— 54	2.28	4.8	38.6	86.2	99.0
— 53	2.24	4.3	36.6	84.8	98.8

The percentages of opinions *E* (Excellent) taken from *Table 9*, column 3, are entered in column 4 of *Table 10*. The sum of the entries in column 5 of *Table 10* gives the total percentage of "Excellent" opinions for curve 1 in *Fig. 11*. Similar tables are drawn up for the other four opinions, i.e. "Good", "Fair" and "Poor". The same procedure is used for the

three remaining hypothetical noise distributing curves, shown in *Fig. 11*. The final results, thus obtained, are shown in *Table 11*.

Table 10.

Noise Level at zero Rel. Level N dbm 0	Noise Level at Terminal Exchanges N_T dbm	Percentage of Calls f %	Percentage of E Opinions X %	$\frac{fX}{100}$ %
1	2	3	4	5
— 53	— 68	100 — 34 = 66	9.4	6.204
— 52	— 67	34 — 12 = 22	8.9	1.958
— 51	— 66	12 — 2.5 = 9.5	8.7	0.826
— 50	— 65	2.5 — 0.8 = 1.7	8.5	0.144
— 49	— 64	0.8 — 0.53 = 0.27	8.1	0.0219
— 48	— 63	0.53 — 0.37 = 0.16	8.0	0.0128
— 47	— 62	0.37 — 0.24 = 0.13	7.8	0.0101
— 46	— 61	0.24 — 0.15 = 0.09	7.6	0.00684
— 45	— 60	0.15 — 0.10 = 0.05	7.2	0.00360
— 44	— 59	0.10 — 0.06 = 0.04	6.8	0.00272
— 43	— 58	0.06 — 0.04 = 0.02	6.4	0.00128
— 42	— 57	0.04 — 0.02 = 0.02	6.1	0.00122
— 41	— 56	0.02 — 0.01 = 0.01	5.7	0.00057
— 40	— 55	0.01	5.2	0.00052
	Sum	100.00	—	9.19 %

Table 11.

Curve No or Noise Level at zero Rel. Level	— 7 db point Psopho-metric E.M.F. mV	Percentages of Opinions				
		E %	G %	F %	P %	B %
1	2	3	4	5	6	7
Curve 1		9.19	45.60	39.64	5.37	0.20
Curve 2		9.19	45.60	39.64	5.37	0.20
Curve 3		8.98	45.18	40.01	5.60	0.23
Curve 4		8.49	44.49	40.81	5.91	0.30
— 50 dbm 0	2.19	8.50	44.50	40.80	5.90	0.30
— 43 dbm 0	4.9	6.40	39.20	44.80	9.10	0.50
No noise	0	10.80	49.20	35.80	4.05	0.15

The corresponding impairments can also be determined as follows. If the mean opinion score, Y, is calculated for curve 1, using the percentages of opinions given in *Table 11* a value of $Y = 2.58$ is obtained. From the curve A in *Fig. 7* as well as from *Table 6* it will be found that $Y = 2.58$ corresponds to a constant circuit noise level of $N_T = -69$ dbm at the local exchanges.

From the curve *A* in *Fig. 9* as well as from *Table 7* it will be found that the impairment $I(23) = 1.1$ db for a circuit noise level of – 69 dbm. The values so obtained are given in *Table 12*.

Table 12.

Curve No or Noise Level at zero Rel. Level	— 7 db point Psopho-metric E.M.F. mV	Mean Opinion Score Y	Circuit Noise Level at Local Exchanges N_T dbm	Impair-ment $I(23)$ db
1	2	3	4	5
Curve 1		2.58	— 69	1.1
Curve 2		2.58	— 69	1.1
Curve 3		2.57	— 67	1.4
Curve 4		2.55	— 65	1.7
— 50 dbm 0	2.19	2.55	— 65	1.7
— 43 dbm 0	4.9	2.42	— 58	3.4
No noise	0	2.65	— ∞	0

Conclusions

Question 4

Carrier systems on coaxial pairs or on symmetrical pairs have been planned for a long time to a circuit noise limit of – 50 dbm 0, corresponding to a mean psophometric power of 10,000 picowatts at a point of zero relative level, and their performance in service has been satisfactory. The final results do not show any need for a lower noise level limit than the provisional one adopted by CCIF.

Question 6

It will be seen from *Table 11* that the transmission performance given by a circuit (of the type shown in *Fig. 12*) subject to a distribution of circuit noise according to any one of the curves 1, 2, 3 and 4 in *Fig. 11* is not inferior to that obtained when a fixed noise of — 50 dbm 0 is present. Therefore, any one of these four curves is acceptable from the speech transmission point of view.

Question 2 of CCITT Study Group 1

Can a steady circuit noise characterized by a constant psophometric power of 100,000 picowatts (referred to the zero relative level point) be tolerated in an intercontinental communication? If not, what arrangements are to be recommended so that this noise level becomes tolerable?

In this case the calculation of the transmission performance has been carried out at a junction loss of 28 db between the two terminal exchanges and for average local systems

(see *Fig. 12*), approximately corresponding to an overall reference equivalent of 40 db when the local systems are at their limits.

The relative noise impairment, I_r, has been determined directly by means of the following graphical method.

If the noise level at the zero relative level point is – 50 dbm 0, corresponding to a psophometric power of 10,000 picowatts or about 5 mV psophometric E.M.F., which is the present design limit, then the noise level at the distant local exchanges is $N_T = -67.5$ dbm.

The mean opinion score is

$$Y = 3.35 + \beta\,(28 + 2.5)^2 \tag{5}$$

β is – 0.00120 for a noise level of N_T =—67.5 dbm (see *Fig. 6*).

Thus

$$Y = 3.35 - 1.12 = 2.23 \tag{5}$$

If (Poor + Bad) opinions are chosen as criterion for the transmission performance then the probit corresponding to a mean opinion score of $Y = 2.23$ is obtained by equation (17).

Thus $$\text{Probit} = 4.31\sqrt{4 - Y} - 1.74 = 3.99 \tag{17}$$

A Probit of 3.99 corresponds to a percentage of 15.7 (*Table I*, Probit Analysis by Finney). Thus the percentage of opinions ($P+B$) is 15.7.

A curve showing the noise level N_T as a function of the junction loss X for $Y = 2.23$ can now be plotted (see *Fig. 15*).

In this case

$$X = \left(\sqrt{\frac{-1.12}{\beta}} - 2.5\right) \text{db} \tag{5}$$

The values of β for different circuit noise levels are taken from *Table 4* and sufficient number of X values for determining the curve can be calculated (see *Table 13*).

Table 13.

Circuit Noise Level N_T dbm	β	X db
— 67.5	— 0.00120	28
— 65	— 0.00124	27.55
— 60	— 0.00136	26.2
— 55	— 0.00158	24.1
— 50	— 0.00197	21.3

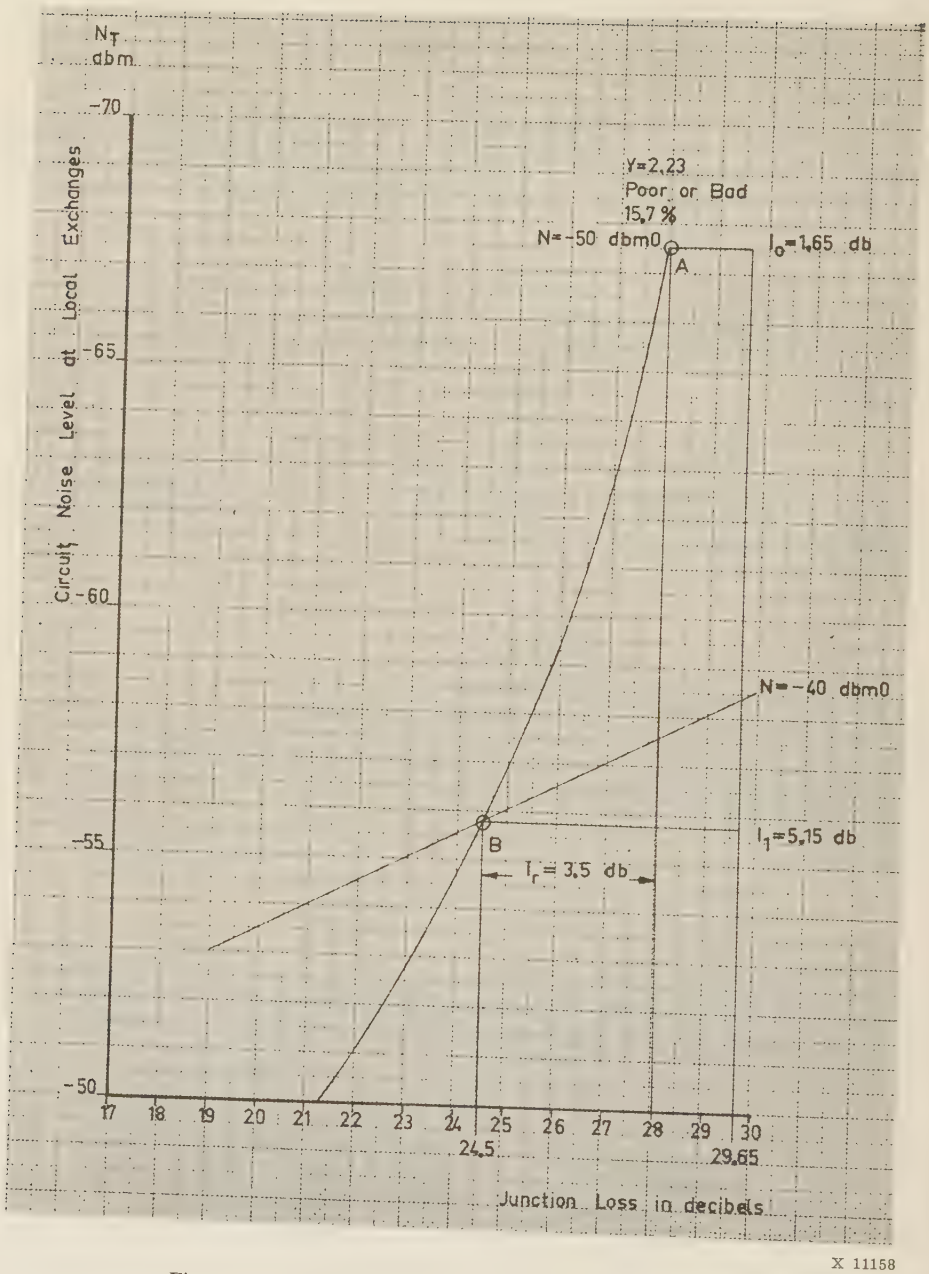

Fig. 14. Graphical construction of relative impairment.

The point A in *Fig. 14* represents the situation for a circuit noise level of – 50 dbm 0. For a circuit noise level of – 40 dbm 0, corresponding to a psophometric power of 100,000 picowatts at zero relative level, the junction loss has to be reduced to encounter the same mean opinion score. The curve showing the circuit noise level N_T as a function of the junction loss for a circuit noise level of – 40 dbm 0 at zero relative level is a straight line, the equation of which is

$$N_T = -43.5 - 0.5\ X \tag{18}$$

The point B is the intersection between this straight line and the curve $N_T = f(X)$ for $Y = 2.23$ (see *Fig. 14*).

The value of X for point B is

$$X = 24.5 \text{ db}$$

Therefore, the junction loss has to be reduced to 24.5 db to give the same percentage of "Poor" or "Bad" opinions, i.e. 15.7 %. Thus the relative impairment will be

$$I_r = 28 - 24.5 = 3.5 \text{ db}$$

The circuit noise level, N_T, for a junction loss of $X = 24.5$ db is

$$N_T = -43.5 - 0.5 \cdot 24.5 = -55.75 \text{ db} \tag{18}$$

and the corresponding value of β is

$$\beta = \frac{2.23 - 3.35}{(24.5 + 2.5)^2} = -0.00154 \tag{5}$$

If I_0 is the noise impairment, relative to the case where no circuit noise is present, corresponding to a noise level of – 50 dbm 0, i.e. a psophometric power of 10,000 picowatts at the zero relative level point, then

$$I_0 = (28 + 2.5)\left(\sqrt{\frac{\beta}{\beta_0}} - 1\right) = 1.65 \text{ db} \tag{12}$$

where $\beta = -0.00120$ and $\beta_0 = -0.00108$.

Thus $X_0 = 28 + 1.65 = 29.65$ db

If I_1 is the noise impairment, relative to the case where no circuit noise is present, corresponding to a noise level of – 40 dbm 0, i.e. a psophometric power of 100,000 picowatts at the zero relative level point, then

$$I_1 = (24.5 + 2.5)\left(\sqrt{\frac{\beta}{\beta_0}} - 1\right) = 5.15 \text{ db} \tag{12}$$

β being -0.00154, β_0 being -0.00108

and $$X_0 = 24.5 + 5.15 = 29.65 \text{ db}$$

Finally $$I_r = 5.15 - 1.65 = 3.5 \text{ db}$$

The mean opinion score for a junction loss of $X_0 = 29.65$ db is $Y = 2.23$ (See page 179).

In *Fig. 15* a family of curves are drawn, showing circuit noise level as a function of junction loss with percentage "Poor" or "Bad" opinions as parameter.

The straight lines

$$N_T = -53.5 - 0.5X \quad \text{valid for } N = -50 \text{ dbm } 0$$

and

$$N_T = -43.5 - 0.5X \quad \text{valid for } N = -40 \text{ dbm } 0$$

are also drawn. The points A and B are shown in the figure.

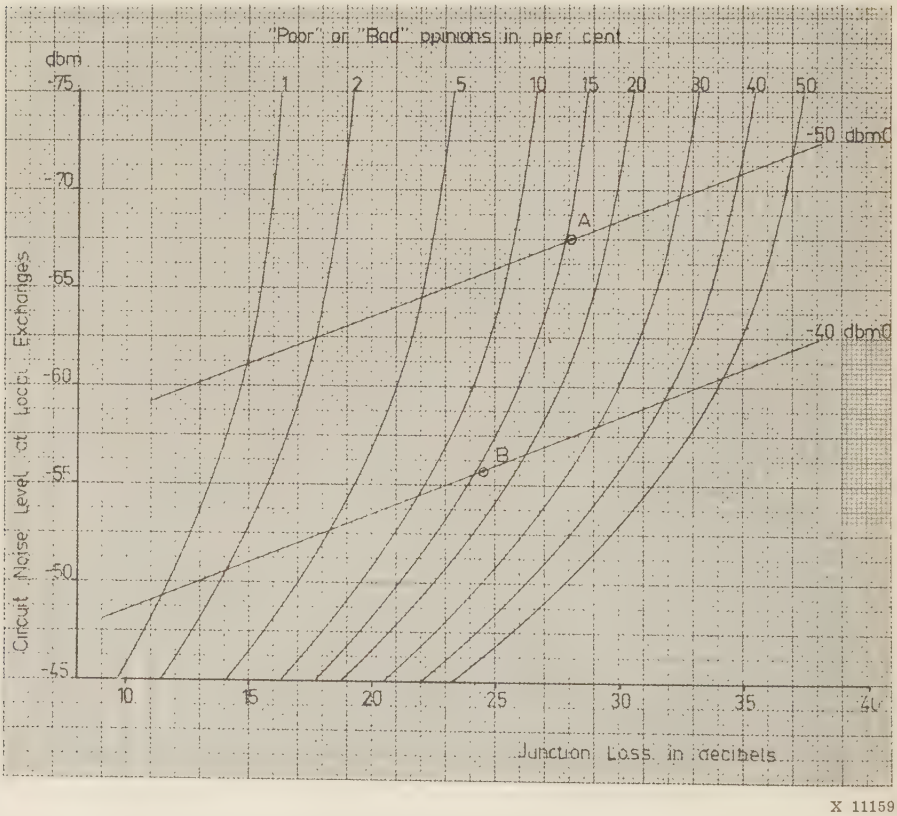

Fig. 15. Circuit noise level at local exchanges as a function of junction loss at different "Poor" or "Bad" opinions.

Reply to Question 2 of Study Group 1

The Study Group 12 of the CCITT considers that a circuit noise of – 40 dbm 0, corresponding to a psophometric power of 100,000 picowatts at zero level point, can be accepted in an intercontinental call if the overall reference equivalent of this call does not exceed 36 db, i.e. 4 db less than the present limit. This limit might be still further reduced in the event of considerable induced noise or an appreciable frequency distortion.

It should be pointed out that those circuits for which a circuit noise level of – 40 dbm 0 (at the zero relative level) can be expected will be extremely long circuits (i.e. 25,000 km) and will probably not be very numerous. Certain means can be used to render such an intense circuit noise tolerable, for example by introducing compandors, but the choice of such means should be settled by agreement between the Administrations concerned.

CHAPTER 6

General Conclusions

It is obvious that a test method based on the opinions of ordinary, untrained telephone users, where the participating persons are allowed the greatest freedom to use the telephone in their own manner, will give more accurate and reliable results than that using the AEN technique with its many artificialities.

The opinion method can of course be used not only for the determination of the transmission quality in presence of circuit noise but also be applicable to other problems regarding the transmission quality, for example the study of the influence of sidetone. New questions have been proposed by the 12th Study Group in connection with the effect of circuit noise on telephone calls and these questions have been submitted for approval by the IInd Plenary Assembly of the CCITT in New Delhi (December 1960). In this connection it has been anticipated to use the opinion test method. The method and the basic data given in this article for a hypothetical overall connection as shown in *Fig. 12* may still be used for the study of noise conditions including noises other than the continuous white noise if the potency of the other noise in relation to the continuous white noise is taken into account. The potency in db is defined as the difference between the mean psophometric power in dbm and that of white noise producing the same disturbance in the understanding of speech and can easily be measured by direct comparison listening tests. Then the percentages of calls, which are considered non-satisfactory (Poor + Bad), for any overall attenuation combination within practical limits can be calculated.

Acknowledgments

It is a pleasure for the writer to express his gratitude to Mr D. L. Richards of the British Post Office Research Station for his very kind elucidation of some of the problems involved and for having read the manuscript. Acknowledgment is made to the British Post Office for permission to make use of material contained in this paper. The author also is indebted to Mr A. Boeryd for having read the manuscript and thereby given valuable advice.

Bibliography

CCIF — 1952/1954 — 4ème CE — Document No 25. Compte rendu de la 11ème série d'expériences du Laboratoire du CCIF relative à la détermination de la réduction de qualité de transmission due au bruit de circuit.

CCIF — 1952/1954 — 4ème CE — Document No 25 bis. Compte rendu des essais complémentaires de la 11ème série d'expériences du Laboratoire du CCIF relative à la détermination de la réduction de qualité de transmission due au bruit de circuit.

CCIF — 1955/1956 — 4ème CE — Document No 2. Rapport technique No 241 du Laboratoire du CCIF. Compte rendu des résultats des essais de netteté relatifs à la détermination des »réductions de qualité de transmission» dues à divers types de bruits de circuit.

CCIF — 1955/1956 — 4ème CE — Document No 28. Rapport technique No 254 du Laboratoire du CCIF. Compte rendu des résultats des essais de netteté relatifs à la détermination des »réductions de qualité de transmission» dues à divers types de bruits de circuit (essais complémentaires de la 11ème série d'expériences du Laboratoire du CCIF).

CCIF — 1955/1956 — 4ème CE — Document No 31. Réponse de Teléfonos de México au point en suspens dans l'étude des questions Nos 5 et 6 de la 4ème Commission d'études du CCIF.

CCITT. Livre Rouge, Tome I. 1re Assemblée Plénière, Genève, 10—20 décembre 1956.

D. L. Richards and J. Swaffield: Assessment of Speech Communication Links. Proceedings of the Institution of Electrical Engineers, Vol. 106. Part B, No. 26, March 1959.

Post Office Engineering Department. Research Report No. 12970. A method of Generating Random Shapes for use as Material in the Message-Rate Method of Assessing Telephone Circuits.

CCITT — 1957/1960 — 12ème CE — Document No 2. Groupe de travail »Bruit» (M. Williams). Réunion de Genève 25 au 27 février 1957.

CCITT — 1957/1960 — 12ème CE — Document No 10. Groupe de travail mixte CCITT-CCIR des bruits de circuit. Compte rendu de la réunion de Genève 1er au 8 mai 1958.

CCITT — 1957/1960 — 12ème CE — Document No 13. Administration du Royaume-Uni. Assemblage et synthèse des données basées sur des opinions d'usagers du téléphone (contribution à l'étude des questions 4, 5 et 6 de la 12ème CE).

CCITT — 1957/1960 — 12ème CE — Document No 20. Administration du Royaume-Uni. Contribution à l'étude de diverses questions de la 12ème CE.

CCITT — 1957/1960 — 12ème CE — Document No 40. Secrétariat du CCITT. Compte rendu de la réunion de la 12éme Commission d'études du CCITT. (Genève 1er—9 octobre 1958).

CCITT — 1957/1960 — 12ème CE — Document No 42. Administration du Royaume-Uni. Effet du bruit de circuit sur la qualité de transmission des circuits internationaux et intercontinentaux (question 2 de la 1ère CE, questions 4, 5 et 6 de la 12ème CE).

CCITT — 1957/1960 — 12ème CE — Document No 44. France, République fédérale d'Allemagne, Royaume-Uni, Suède, Teléfonos de México. Effet du bruit de circuit sur la qualité de transmission des circuits internationaux et intercontinentaux.

CCITT — 1957/1960 — 12ème CE — Document No 46. Groupe de travail de la 12ème CE. Compte rendu de la réunion du Groupe de travail de la 12ème Commission d'études (Berne, 28 septembre—2 octobre 1959).

CCITT — 1957/1960 — 12ème CE — Document No 50. Groupe de travail mixte CCITT-CCIR des bruits de circuit (réunion de Genève, 4—10 novembre 1959). Bruit sur les circuits intercontinentaux; emploi de compresseurs — extenseurs.

CCITT — 1957/1960 — 12ème CE — Document No 67. Compte rendu de la réunion de Genève (19—25 mai 1960).

D. J. Finney: *Probit Analysis.* Second Edition, 1952.

Manuscript received by the editors August 1960.

Noise in a PCM Transmission System

BY

HENRY SCHEFTELOWITZ*

UDC 621.376.562
621.391.822.2
621.391.827
LME 8436,805

The different noise sources in a PCM transmission system have been evaluated and their impact on the overall signal-to-noise ratio calculated. Furthermore, formulae are given which show the signal-to-noise ratio in relation to repeater spacing.

*Research Department, Telefonaktiebolaget L M Ericsson, Stockholm

Contents

Introduction

It is one of the great advantages of a PCM transmission system that all amplification can be done by regeneration of the pulse shape. Non-linear devices such as blocking oscillators or multivibrators can perform this regeneration. This applies to all points within the system where the original analog signal has been converted into a binary-coded signal, i.e. in the repeaters, in the output amplifiers at the transmitter terminal or in the input amplifiers at the receiver terminal.

The blocking oscillator triggers when the sum of the instantaneous noise voltage and of any pulse voltage present exceeds the threshold. The regenerative repeater has two functions.

1. To detect the presence or absence of a pulse in the presence of noise.
2. To regenerate the pulse shape if a pulse has been detected.

It is to be noted that neither the amplitude, position or width of the pulse is critical.

Concerning the repeaters, we shall focus our interest on the following problems associated with the design of the PCM system:

1. How big a signal-to-noise ratio is necessary to get a "sufficient" certainty of triggering? The word "sufficient" must be considered in relation to the wanted characteristics of the system.
2. What noise sources are present and what is their impact on the signal-to-noise ratio?
3. In what manner does the signal-to-noise ratio depend on the spacing between repeaters?

It is well known that CCIF has specified certain characteristics concerning the performance of international telephone circuits. Those characteristics are related to a nominal maximum circuit with a length of 2 500 km. Most telecommunications administrations nowadays apply the same characteristics to their national long-distance telephone circuits.

Nothing similar exists for a short-haul system. Therefore we shall try to establish a nominal maximum circuit, and for this circuit specify such characteristics as seem reasonable for a PCM short-haul system working as an end-link.

CHAPTER 1

System Performance

1.1 System Configuration

Time-division multiplex:

A 24-channel time-division multiplex system with pulse-code modulation.

Nominal maximum circuit:

200 kilometres, divided into two 100-kilometre end-links (*Fig. 1*). The first part ES_1—FS_1 has analog-digital conversion in the terminal ES_1 and digital-analog conversion in the terminal FS_1. Somewhere in between we have the terminal KS_1 with digital-analog and analog-digital conversion. The same pattern applies to the second part FS_2—ES_2, but with the opposite sequence.

Transmission medium:

Four-wire circuit. Transmission in one direction is on a pair of paper-insulated wires (diameter 0.4 mm or 0.6 mm). Two pairs form a quad in a cable consisting of a large number of quads. It will be assumed initially that the length of a repeater section is 1800 metres.

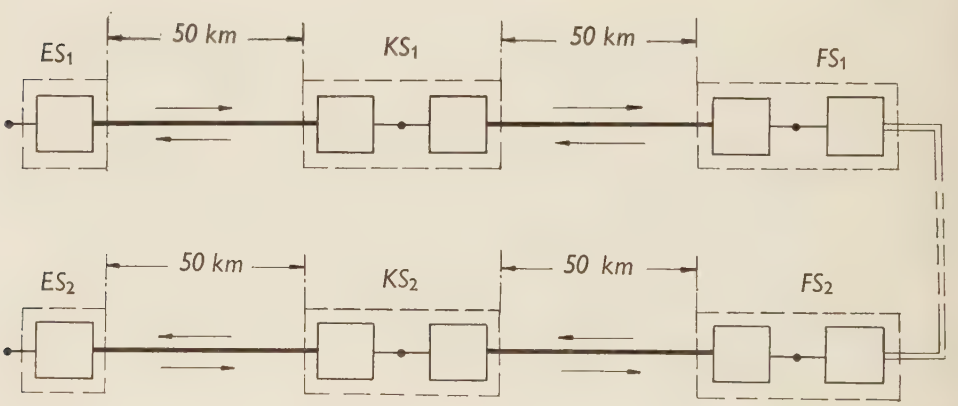

Fig. 1. Nominal maximum circuit for a PCM short-haul system.

═══ long distance carrier frequency path

━━━ PCM-path

—— voice frequency path

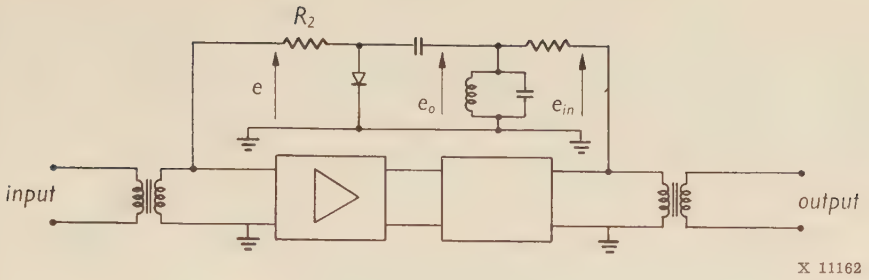

Fig. 2. Regenerative repeater.

Space multiplex:

We wish several PCM systems to operate in parallel within the same cable. This is called space multiplex.

Quantization:

Binary code, in which a positive pulse is "1" and no pulse is "0". Nominal pulse repetition frequency 1536 kc/s, i.e. the pulse repetition period is 0.65 μs.

Transmitter:

Blocking oscillator. Pulse amplitude $U_0 = 5—6$ volts.

Receiver:

A two-stage self-timed regenerative repeater. The first stage is an amplifier stage with a 2.4 Mc/s bandwidth. The second stage is a single shot blocking oscillator from which we get the output, the regenerated pulse (*Fig. 2*).

This type of repeater was invented by L. R. WRATHALL[1] of Bell Telephone Laboratories.

The following calculations and discussion are based on two assumptions:

1. If the pulse amplitude is U_m we adjust the triggering level to $U_m/2$.

2. The triggering instant is partially determined by the phase of the timing wave. The timing wave will be adjusted so that the triggering instant will fall within a small region around the maximum.

The timing wave is the response of the resonant circuit to the regenerated binary "on-off" pulse train. The voice-frequency signal has a random instantaneous voltage, and the traffic loading of the channels is random. However, the nominal pulse repetition frequency will always be contained in the spectrum of the pulse train, which we can regard as a random time series of discrete pulses[2]. So the response of the resonant circuit is a sine wave with the same frequency as the nominal pulse repetition frequency and with phase and amplitude dependent on the tuning of the circuit.

For different reasons, which will be examined later, the pulse appears at the receiver input with random timing deviations. The regenerated pulses will therefore not be uniformly spaced, but will rather have random deviations from the exact positions. Now, as the timing wave is derived from the regenerated pulses, it causes random phase deviations in the timing wave, and this in turn causes random deviations in the triggering instant.

1.2 Noise Limits

The maximum allowable noise power from the circuits FS_1—ES_1 at a zero level point is 1000 picowatts (~ -60 dbm0p), measured with a CCITT psophometer in a voice-frequency channel at ES_1, which has no signal input at FS_1.

Three components contribute to total noise power:

a) Thermal noise at the receiver input

b) Unintelligible crosstalk

c) Quantization noise

Unintelligible crosstalk is a function of the system's traffic load conditions and it appears in:

1. Space multiplex, as crosstalk from one time multiplex system to another, caused by unbalances in the cable.

2. Time multiplex, as intersymbol crosstalk which appears in unequalized cables or is caused by the random timing deviations in the self-timed regenerative repeaters.

Since adjacent pulses usually belong to the same channel, it will be appreciated that intersymbol crosstalk is not what is generally understood by crosstalk, but rather some kind of pulse interference.

The noise components a) and b) appear in the PCM side of the system, i.e. where we have four-wire digital transmission. b) might in addition appear on the analog side of the system, i.e. where we have PAM time-multiplex, as well as in parts where there are voice frequencies on two-wire lines.

Having regard to the technical difficulties, we have made the following division between the modulating equipments and the transmission line: 200 picowatts (~ -67 dbm0p) for every "half" terminal, where we have either digital-analog conversion or analog-digital conversion, and 200 picowatts for the digital transmission and all the associated intermediate repeaters.

The third component, quantization noise, appears merely when a signal is applied and may be conceived as some kind of distortion. This problem, however, will not be dealt with here.

1.3 Formulae Relating Signal/Noise Ratio at Input and Output of the Receiver

The received pulse train considered as a function of time is expressible by

$$u(t) = \sum_{n=-\infty}^{\infty} U_m g(t - nT) \tag{1.3.1}$$

and the timing wave can be expressed as

$$e(t) = E_m h(t) = -E_m \left\{ 1 - \cos\left(2\pi \frac{t}{T} - \psi \right) \right\} \tag{1.3.2}$$

The necessary condition for triggering the blocking oscillator is

$$u(t) + e(t) \geqq P_{\min} \tag{1.3.3}$$

The blocking oscillator is then adjusted so that its triggering level $P_{\min} = U_m/2$.

It is assumed that the total noise as well as the different noise components can be considered as random noise with a continuous and nearly constant spectral density, at least within the frequency band of interest in this connection. We further assume instantaneous noise values with gaussian distribution. Let n_{eff} and $n(t)$ (or simply n) be the r.m.s. value and the instantaneous value of noise. We then have the probability $p(n/n_{\text{eff}})$ that n exceeds $kn_{\text{eff}} (k > 1)$.

Table 1.

$n = 2.32\ n_{\text{eff}}$	$20 \log (n/n_{\text{eff}}) = 7.4$ db	$p\,(n/n_{\text{eff}}) = 10^{-2}$
$n = 3.72$ »	$= 11.4$ db	$= 10^{-4}$
$n = 4.76$ »	$= 13.6$ db	$= 10^{-6}$
$n = 5.60$ »	$= 15.0$ db	$= 10^{-8}$

At a time $t = t_n$ it might happen that

$$u(t_n) + e(t_n) + n(t_n) \geqq P_{\min} \tag{1.3.4}$$

when we actually should have

$$u(t_n) + e(t_n) < P_{\min} \tag{1.3.5}$$

which means that the blocking oscillator has added a "1" where, according to the digital signal, there should have been a "0". At another time $t = t_k$ the opposite might happen:

$$u(t_k) + e(t_k) + n(t_k) < P_{\min} \tag{1.3.6}$$

when we should have had

$$u(t_k) + e(t_k) \geqq P_{\min} \tag{1.3.7}$$

which means that we have a "0" when we should have had a "1". Errors may also arise under other circumstances not mentioned here, but are of minor importance[1].

In the first case $U_m/2$ is the tolerance to noise to provide against the insertion of a spurious pulse by positive noise peaks. In the second case $U_m/2$ is the tolerance to noise to provide against the omission of a signal pulse by negative noise peaks.

Between triggering points the timing wave assumes such negative values that, if E_m is sufficiently large, e.g. $E_m \simeq U_m$, it is impossible for a positive noise peak to insert a pulse. So the regenerative repeater is practically insensitive to any kind of impulses between triggering points.

It should be added that the blocking oscillator triggers only if the energy of the impulse exceeds an energy triggering level, e.g. for a normal junction transistor ($f_\alpha = 5$ Mc/s) we have

$$\int i_g \cdot u_g dt = \int (u_g^2/R_g) dt \geqq 3 \cdot 10^{-11} \text{ joule} \tag{1.3.8}$$

We assume that R_g is constant during the blocking oscillator's build-up time. Whether triggering takes place is then determined by the product of the square of the input voltage and the time during which the threshold value is exceeded. The above-mentioned transistor has a build-up time of 0.05 μs. Noise peaks generated by pulses in nearby cable pairs through capacity unbalance and/or mutual inductances cannot have rise or decay times shorter than those of the pulses by which they are generated, in this case about 0.25 μs. Let us take the first case, insertion of a pulse at a time when $u(t) = 0$ and $e(t) = 0$. The blocking oscillator triggers when (*Fig. 3*)

$$n(t) = \frac{1}{2} t_s \frac{U_m}{t_g} + \frac{1}{2} U_m \geqq 0.6\, U_m = 1.2\, P_{\min} \tag{1.3.9}$$

When we have thermal noise in a limited band the noise peaks ($n(t) \gg n_{\text{eff}}$) may reasonably have the appearance shown in *Fig. 3*. It is then obvious that either the instantaneous noise value exceeds the threshold of 1.2 $P_{\min}$ and we get an unwanted pulse in the digital signal, or it is below the threshold and is then without significance.

Now suppose that the instantaneous noise value n is always below a finite value, e.g. $n_{\max} = 2n_{\text{eff}}$; further, that the amplitude of the transmitted pulse is adjusted so that $0.6\, U_m > n_{\max}$, e.g. $U_m = 2n_{\max} = 4n_{\text{eff}}$. Then a signal-to-noise ratio, S/N, at the input of the regenerative repeater

$$10 \log_{10} \frac{S}{N} = 20 \log_{10} \frac{U_m}{n_{\text{eff}}} = 12 \text{ db} \tag{1.3.10}$$

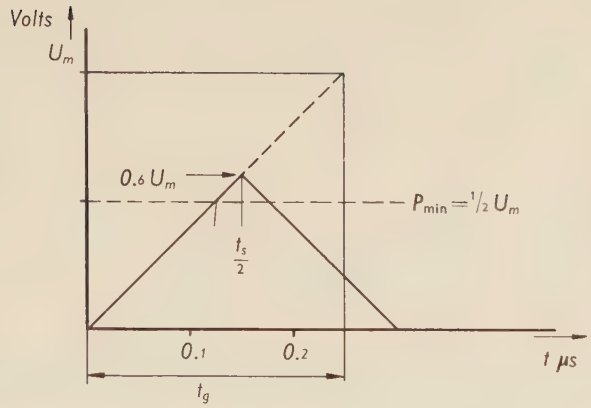

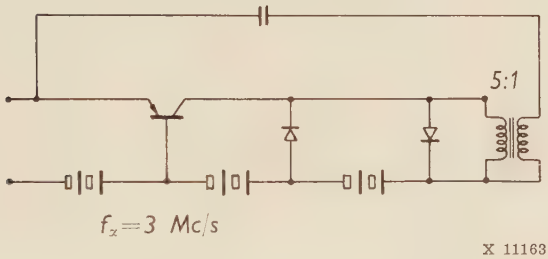

X 11163
X 11164

Fig. 3. Triggering level of blocking oscillator under conditions of disturbance of impulse character.

t_g = min. rise time for a pulse through a low pass channel

$$t_g = \frac{1}{2B} \cong \frac{1}{2 \times 2\ \text{Mc/s}} = 0.25\ \mu\text{s}$$

t_s = build-up time for alloyed pnp junction transistor in blocking oscillator coupling below.

would be represented by an infinite signal-to-noise ratio S^x/N^x at the output

$$10 \log_{10} \frac{S^x}{N^x} = \infty \tag{1.3.11}$$

However, the instantaneous noise voltage is the vector sum of an infinite number of sine waves (resolving each pulse into its corresponding fourier spectrum) which from all other channels are coupled to the non-loaded channel. These sine waves have finite but otherwise random amplitudes and random phase. We therefore presume a gaussian distribution of n, which means that there is no upper limit to n. So if $U_m = kn_{\text{eff}} (k > 1/0.6)$, then according to *table 1* there is always some possibility that n might exceed 0.6 U_m, i.e. a finite S/N value at

the input gives a finite S^x/N^x at the output. From [3] we quote the following relation between S^x/N^x and S/N:

$$\frac{S^x}{N_x} = \frac{\Phi^{2n}}{1 - \Phi^{2n}} \tag{1.3.12}$$

where

$$\Phi(\sqrt{S/N}) = \int_{-\sqrt{S/N}}^{\sqrt{S/N}} e^{-u^2/2} du \tag{1.3.13}$$

and n is the number of repeater sections. Inserting $n = 50$ and $10 \log (S^x/N^x) = 67$ db in the above expressions gives

$$\sqrt{\frac{S}{N}} = \frac{0.6 U_m}{n_{\text{eff}}} \cong 7 \tag{1.3.14}$$

so

$$U_m = 12\, n_{\text{eff}} \tag{1.3.15}$$

CHAPTER 2

PPM-Noise

2.1 Timing Deviations

Before it is possible to calculate the intersymbol crosstalk caused by random deviations of the triggering instant, it is necessary to determine the relationship between these deviations and the deviation of the timing wave and of the received pulses. The problem has been well covered by E. D. SUNDE in an article in the Bell System Technical Journal, July 1957, "Self-Timing Regenerative Repeaters"[4]. Here, therefore, we shall merely recapitulate some points of general interest together with the results necessary for the following calculations.

The digital message is assumed to be a random time series of discrete numbers. So the regenerated pulse train may have the appearance shown in *Fig. 4 a*. This pulse train may be resolved into components III and I + II, shown in *Fig. 4 b* and *c*. Component I + II may in turn be resolved into I and II (*Figs. 4 d* and *c*). This means that the original pulse train, which is random both in respect to the occurrence of the pulses and to the positions (deviations from the exact positions) of the pulses, has been resolved into three components with the following characteristics:

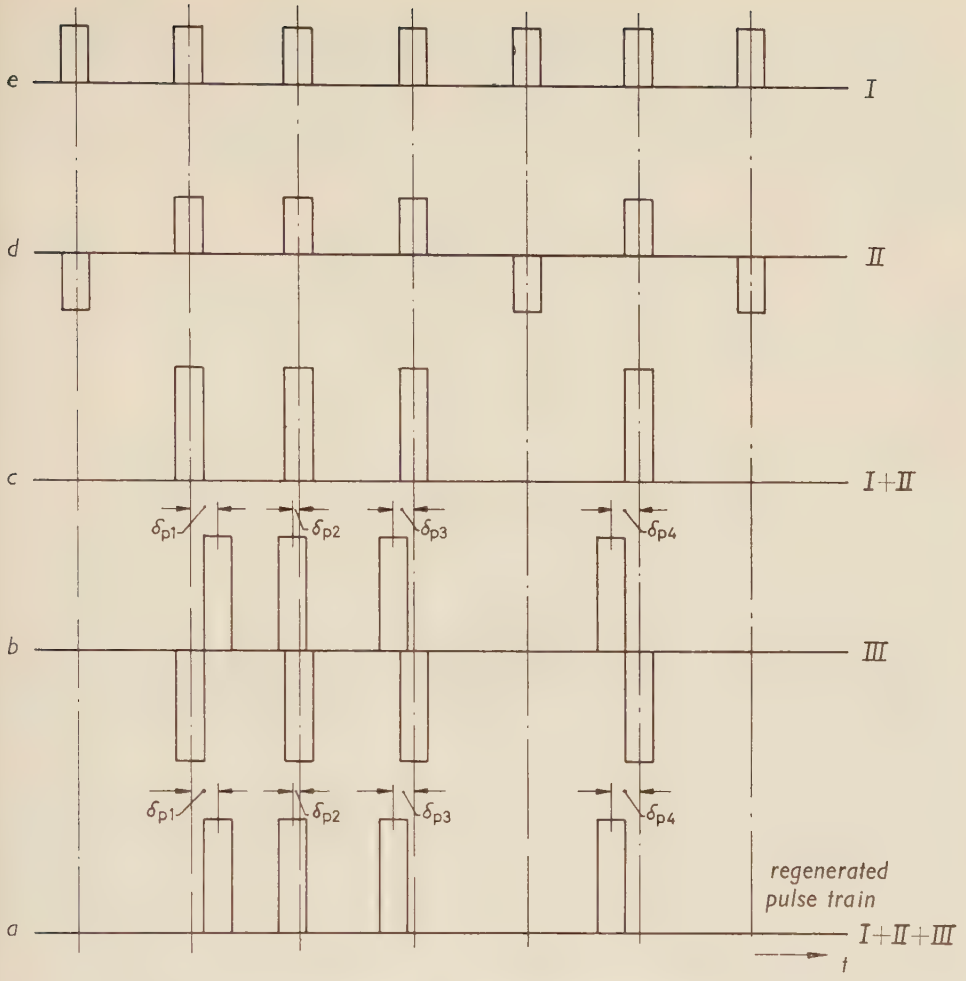

Fig. 4. The regenerated pulse train in Fig. 4 a resolved into components I, II and III, Figs. 4 e, 4 d and 4 b, respectively. (The Bell System Technical Journal, July 1957)

1. Component I is the steady state component consisting of an infinite sequence of positive pulses with period T. All pulses are in their correct positions and all have the same amplitude, equal to half the amplitude of the regenerated pulses.

2. Component II is a random component consisting of an infinite sequence of positive and negative pulses with random $\pm$ polarity. Amplitudes and positions of the pulses are the same as those of component I.

3. Component III is a random component consisting of an infinite sequence of dipulses which are pairs of negative and positive pulses in which all the negative pulses are in the exact positions whereas the positive pulses have random phases (*Fig. 4*). The

dipulses occur only in positions in which there are regenerated pulses, i.e. they occur at random. All amplitudes, both positive and negative, are equal to those of the regenerated pulses.

The resonant circuit in *Fig. 2* is considered as a four-terminal network, for which the input is the sum of three components and the output is the timing wave $e_0(t)$, which we express as

$$e_0(t) = e_0(t)_{\mathrm{I}} + e_0(t)_{\mathrm{II}} + e_0(t)_{\mathrm{III}} \tag{2.1.1}$$

With an input consisting only of component I, we get an output voltage

$$e_0(t)_{\mathrm{I}} = \cos\psi \cos(2\pi f t - \psi) \tag{2.1.2}$$

where

$$\tan\psi = Q\left(\frac{f}{f_0} - \frac{f_0}{f}\right) \cong 2Q\frac{\Delta f}{f} \tag{2.1.3}$$

Q is the loss constant of the resonant circuit and f is the pulse repetition frequency. f_0 is the resonant frequency and $\Delta f = f - f_0$ is the mistuning.

From equations (2.1.2) and (2.1.3) it can be seen that, with f and f_0 given, the output voltage — i.e. the timing wave — is a steady state sine wave with a constant amplitude $\cos\psi$ and a constant phase displacement ψ.

The response of the resonant circuit to component II is an output voltage which, as regards amplitude and phase, is a randomly fluctuating sine wave. We resolve this voltage into two components, one in phase and the other in quadrature with the steady state timing wave given by (2.1.2). We denote the r.m.s. values $e_0(t)'_{\mathrm{II\,eff}}$ and $e_0(t)''_{\mathrm{II\,eff}}$ respectively. We consider the steady state sine wave $e_0(t)_{\mathrm{I}}$ to be modulated by those fluctuating voltages of which $e_0(t)'_{\mathrm{II}}$ gives an amplitude modulation with the r.m.s. modulation index

$$\bar{m} = \frac{e_0(t)'_{\mathrm{II\,eff}}}{e_0(t)_{\mathrm{I}}} = \sqrt{\frac{\pi}{Q}}\frac{\sqrt{1 - \psi^2/2}}{\cos\psi} \tag{2.1.4}$$

and $e_0(t)''_{\mathrm{II}}$ gives a phase modulation with r.m.s. value

$$\bar{\varphi}_{k\,\mathrm{II}} \cong \tan\bar{\varphi}_{k\,\mathrm{II}} = \frac{e_0(t)''_{\mathrm{II\,eff}}}{e_0(t)_{\mathrm{I}}} = \sqrt{\frac{\pi}{Q}}\frac{|\psi|}{\cos\psi} \tag{2.1.5}$$

The r.m.s. value of the corresponding time deviation is given by

$$\delta_{k\,\mathrm{II}} = \frac{\sqrt{\frac{\pi}{Q}}\frac{|\psi|}{\cos\psi}}{2\pi} T \tag{2.1.6}$$

The response of the resonant circuit to component III is an output voltage $e_0(t)''_{III}$ which phase-modulates $e_0(t)_I$. Denoting the r.m.s. value of the fluctuating time deviations of the positive part of the dipulse by $\bar{\delta}_{p\,\mathrm{eff}}$, $e_0(t)_{III}$ gives the following phase modulation of $e(t)_I$:

$$\bar{\varphi}_{k\,III} = \frac{2\pi}{T}\sqrt{\frac{\bar{\pi}}{Q}}\,\delta_{p\,\mathrm{eff}} \tag{2.1.7}$$

The r.m.s. value of the corresponding time deviation is given by

$$\bar{\delta}_{k\,III} = \sqrt{\frac{\bar{\pi}}{Q}}\,\delta_{p\,\mathrm{eff}} \tag{2.1.8}$$

There is no correlation between the phase modulations caused by components II and III, so the total time deviation of the timing wave is given by

$$\bar{\tau}_k = \sqrt{\bar{\delta}^2_{k\,II} + \bar{\delta}^2_{k\,III}} \tag{2.1.9}$$

Equations (2.1.4), (2.1.6) and (2.1.8) show clearly that the amplitude and phase deviations of the timing wave caused by the random digital message (component II) and by the random time deviation in the regenerated pulse positions (component III) become smaller the bigger we make the Q of the resonant circuit. In practice, however, we always have to calculate with some mistuning Δf of the resonant circuit. A bigger Q then causes a decrease of the amplitude of $e_0(t)'_I$ (2.1.2), which in turn gives inferior definition of the triggering instant, i.e. of the position of the regenerated pulses. A Q of 50—100 is an appropriate compromise between the two opposing requirements for the resonant circuit.

If the received pulse has the shape of a cosine-squared pulse, then the individual pulse in the pulse train is given by

$$u(t) = (1 + m_p)\frac{U_m}{2}\left[1 + \cos\frac{\pi}{\eta}\,\frac{t + \tau_p}{T}\right] \tag{2.1.10}$$

where

$$-\pi \leq \frac{\pi}{\eta}\,\frac{t + \tau_p}{T} \leq \pi$$

m_p is an index of amplitude variation and τ_p is the time deviation.

Setting $\eta \ll 1$ gives a small pulse width, so that there will be little risk of pulse interference (intersymbol crosstalk). On the other hand a large bandwidth will be required both in the amplifiers and in the transmission circuit. $\eta = 1$ is the maximum allowable value, since $\eta > 1$ would make it very difficult to avoid serious pulse interference. Setting $\eta = 1$ in the following calculations will give us an upper limit for the pulse interference.

By suitable adjustment of R and R_2 (*Fig. 2*) the amplitude of the timing wave can, for $\psi=0$, be made equal to $U_m/2$. Then the timing wave can be expressed by

$$e(t) = -(1+m_k)\frac{U_m}{2}\cos\psi\left[1-\cos\left(2\pi\frac{t+\tau_k}{T}-\psi\right)\right] \tag{2.1.11}$$

The triggering instant is then determined by

$$e(t_0')+u(t_0') = (1+m_p)\frac{U_m}{2}\left[1+\cos\pi\frac{t_0'+\tau_p}{T}\right] -$$

$$-(1+m_k)\frac{U_m}{2}\cos\psi\left[1+\cos\left(2\pi\frac{t_0'+\tau_k}{T}-\psi\right)\right] = \frac{U_m}{2} \tag{2.1.12}$$

The steady state solution is obtained for $m_p=m_k=0$ and $\tau_p=\tau_k=0$, when t_0'/T can be determined as a function of ψ. Normally the variations of ψ are very slow compared with the amplitude variations or the time deviations. Therefore we consider ψ as a parameter and use equation (2.1.12) to investigate the dependence of the triggering instant on amplitude variations when $\tau_p=\tau_k=0$, and on time deviations when $m_p=m_k=0$. That has been done by SUNDE[4] and the results are given in *Table 2*. It is assumed that time deviations of the triggering instant caused by amplitude variations and by time deviations are uncorrelated, so the total r.m.s. value of the time deviation of the regenerated pulses is based on the root-sum-square addition.

Table 2

ψ	—60°	—30°	0	30°	60°
$\bar{\Delta}/T$	0.028	0.028	0.031	0.038	0.056
$\bar{\varphi}$	10°	10°	11°	13.5°	20°

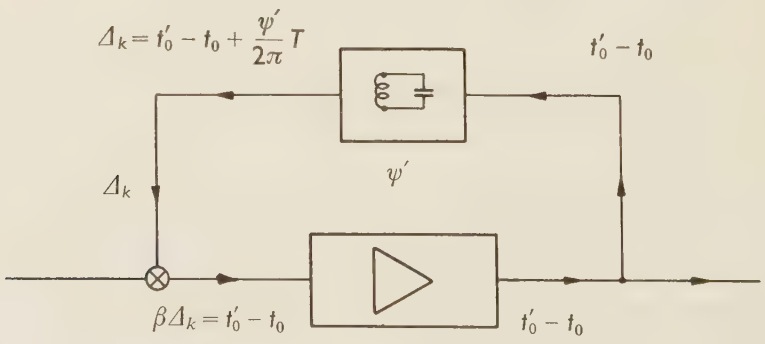

Fig. 5. Feedback of time deviation $t_0' - t_0$ of triggering point of a regenerative repeater.

To get a definite figure for φ it is necessary to estimate ψ. When the timing wave is derived from the regenerated pulses, the time deviation of the timing wave depends on the triggering instant. But the triggering instant depends on the timing wave. This means that we get some sort of timing feedback (*Fig. 5*). The relation between the deviation of the triggering instant and the timing wave can be expressed by

$$t_0' - t_0 = \beta \Delta_k \tag{2.1.13}$$

From *Fig. 5* we get

$$\Delta_k = t_0' - t_0 + \frac{\psi'}{2\pi} T \tag{2.1.14}$$

so

$$t_0' - t_0 = \frac{\frac{\psi'}{1-\beta}}{2\pi} = \frac{\psi}{2\pi} T \tag{2.1.15}$$

i.e. the feedback increases the phase displacement of the resonant circuit from ψ' to $\psi'/(1-\beta)$. By equation (2.1.12) it can be shown that $\beta_{\max} = 0.9$. Now, if the mistuning can be kept below 0.001 and we choose a loss constant $Q = 50$, then according to (2.1.3) $\psi' = 2 \times 50 \times \times 0.001 = 0.1$. This gives us a total displacement of $\psi = 60°$.

We shall now discuss some of the factors which might influence τ_k, τ_p, m_k and m_p. First we assume an ideal transmission circuit without any noise source. As shown in equations (2.1.4) and (2.1.5) a random digital message causes random time and amplitude deviations of the timing wave. That in turn gives a fluctuating triggering instant, i.e. the regenerated pulses show random time deviations from the exact positions. This means that all the succeeding regenerative repeaters will receive pulses with such deviations. However, the timing wave has to pass all the resonant circuits of those repeaters. But cascading a great number of resonant circuits with equal loss factors leads to a reduction of the bandwidth for the overall network. Hence the timing deviation will be reduced as well (see WRATHALL, page 1073, Bell Syst. tech. J *35*[1]).

Thermal noise and noise from crosstalk in the transmission circuit will impair the received pulses in respect of both amplitude and position. So we shall have fluctuating values of m_p and τ_p, and the regenerated pulses will have random time deviations. Now if only the pulse transmission on the first section is impaired, the deviations will be reduced for the same reason as mentioned above. However, it is most likely that all the repeater sections are nearly equally impaired by noise. We shall then get an accumulation of the random timing deviations from the various repeaters along the chain. At the end of the chain the total random timing deviation will be based on the root-sum-square addition. As a result of this accumulation the total timing deviation will be 20—30 % above the timing deviation of the individual section. In practice we shall disregard this accumulation.

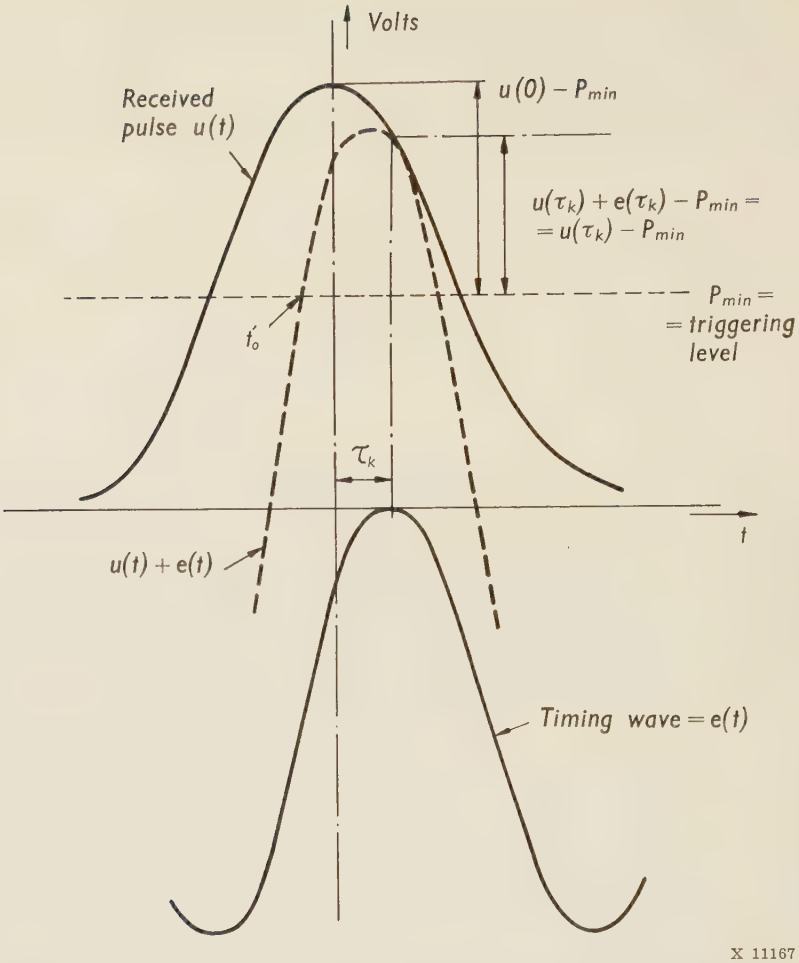

X 11167

Fig. 6. Tolerance to noise containing negative noise peaks. The timing wave is displaced by time τ_k in relation to the received pulse. The resulting reduction in tolerance to noise is

$$\mu = \frac{u(\tau_k) - P_{\min}}{u(0) - P_{\min}}$$

(The Bell System Technical Journal, July 1957)

The voltage at the triggering instant depends not only upon the voltage of the pulse present at that instant, but because of the timing deviation it also depends upon the voltage from adjacent pulses. The timing deviations are random, so the voltages from adjacent pulses appear as noise. But the timing deviation does not only cause noise, it also has the effect of reducing the tolerance to noise.

With no displacement the tolerance to noise with negative peaks at $t=0$ is $u_0(0)$—P (see *Fig. 6*). When for any of the reasons mentioned above the timing wave is displaced by τ_k, then the tolerance to noise is $u(\tau_k) - P$. So the tolerance to noise is reduced by the factor

$$\mu = \frac{u(\tau_k) - P_{\min}}{u(0) - P_{\min}} \tag{2.1.16}$$

Inserting (2.1.10) and $\psi = 70°$ gives $\mu = 0.8 \sim -2$ db.

2.2 Intersymbol Crosstalk

After determining in this way the r.m.s. value of the random time deviations from the correct pulse position, we can proceed directly to determine the resulting pulse interference which generates noise on triggering of the regenerative repeaters.

The signal occurs in the form of a binary code in the transmission circuit. We imagine that the transmission proceeds from $t = -\infty$ to $t = \infty$. This means that an infinitely long train of pulses of equal amplitude enters the regenerative repeater. Regarded as time function, the general expression for this pulse train will be

$$u(t) = \sum_{n=-\infty}^{\infty} U_m g(t - nT) \tag{2.2.1}$$

$U_m(n) = U_m$ if there is a "1" in the nth position

$U_m(n) = 0$ if there is a "0" in the nth position

$U_m(n)$ is thus a function of the random variations of the signal.

We start by assuming a pulse time $\tau \ll T$, the pulses being regarded as impulses (also called δ-pulses). In practice the pulses are neither short nor square. But the calculations are simpler and more readily understandable if based on these assumptions. Moreover, since δ-pulses give a higher noise level than any other pulse shape, this method is very useful for rough calculations.

With suitable equalizing and correction of attenuation, the cable will have the attenuation curve of *Fig. 7* which, together with the frequency characteristic for the input stage of the regenerative repeater, can be approximated to the transfer function of an ideal low pass filter:

$A(f) = 1$ for $f \leqq f_g$ and

$A(f) = 0$ for $f > f_g$

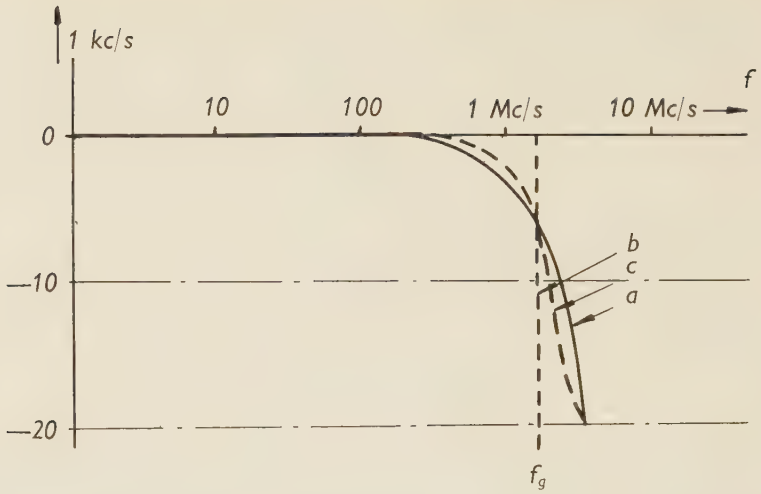

X 11168

Fig. 7. Transfer function for a) 1800 m two-wire equalized and matched cable compared with transfer function for b) ideal low pass filter, c) low pass filter with cosinusoidal transfer function.

As input signal to this ideal low pass filter we assume a δ-pulse, which occurs at time $t = 0$. The output signal is expressed by the time function

$$u_0(t) = \frac{1}{t_g} \frac{\sin \pi \frac{t}{t_g}}{\pi \frac{t}{t_g}} \tag{2.2.2}$$

where

$$t_g = \frac{1}{2f_g}$$

If the δ-pulse arrives, instead, at $t = nT$, we get

$$u_n(t) = \frac{1}{t_g} \frac{\sin \pi \frac{t - nT}{t_g}}{\pi \frac{t - nT}{t_g}} \tag{2.2.3}$$

According to the law of superposition, an infinite sequence of pulses within the time interval $-\infty$ to ∞ with pulse period T gives the voltage

$$u(t) = \sum_{n=-\infty}^{\infty} \frac{1}{t_g} \frac{\sin \pi \frac{t - nT}{t_g}}{\pi \frac{t - nT}{t_g}} \tag{2.2.4}$$

It is evident from eq. 2.2.4 that, at time $t=nT$, the nth pulse assumes its maximum voltage level equal to $\frac{1}{t_g}$ volt (*Fig. 8*), while all other pulses are at zero voltage. This means that, at $t=nT$, the triggering of the regenerative repeater will depend on the presence or absence of the nth pulse; all other pulses in the train are without significance at that point of time.

We make $U_m=1/t_g$ and obtain the following time function for the transmitted pulse train:

$$u(t)=\sum_{n=-\infty}^{\infty} U_m(n)\,\frac{\sin\frac{\pi}{t_g}(t-nT)}{\frac{\pi}{t_g}(t-nT)} \tag{2.2.5}$$

If the pulses lie in varying positions in relation to their correct positions, e.g. if the nth pulse comes at time $t=nT+\Delta_n$, we get

$$u(t)=\sum_{n=-\infty}^{\infty} U_m(n)\,\frac{\sin\frac{\pi}{t_g}(t-nT-\Delta_n)}{\frac{\pi}{t_g}(t-nT-\Delta_n)} \tag{2.2.6}$$

$\psi \cong 60°$ may be considered a reasonable value for a circuit in which $Q = 50$. From *Table II* we find $\overline{\Delta}/T \sim 20/360 = 1/18$. Initially we choose the smallest pulse period that is theoretically possible without the pulses becoming merged: $T = t_g = 1/2B$. We also assume that

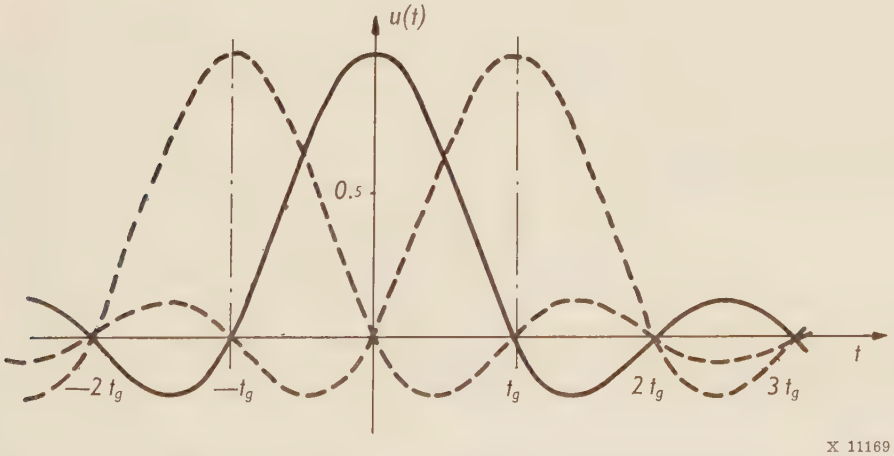

X 11169

Fig. 8. Three consecutive δ-pulses through an ideal low pass filter $t_g = 1/2f_g$. Pulse period $T = t_g$.

the 0th pulse is in the correct position and that triggering takes place at time $t=0$. The signal-to-noise ratio at this time is then

$$\frac{U_m}{n_{\text{eff}}} = \frac{U_m}{U_{PPM}} = -\frac{U_m(0)}{\sqrt{\sum_{n=-\infty}^{n=-1} U_m^2(n) \frac{\sin^2 \pi \frac{\Delta_n}{T}}{\pi^2 \left(\frac{nT+\Delta_n}{T}\right)^2} + \sum_{n=1}^{\infty} U_m^2(n) \frac{\sin^2 \pi \frac{\Delta_n}{T}}{\pi^2 \left(\frac{nT+\Delta_n}{T}\right)^2}}} \tag{2.2.7}$$

Since $\overline{\Delta}/T \ll 1$, we may make the following approximation:

$$\frac{nT+\overline{\Delta}}{T} \cong n$$

$$\sin \pi \frac{\overline{\Delta}}{T} \cong \pi \frac{\overline{\Delta}}{T} = \frac{\pi}{18} \tag{2.2.8}$$

Without considering the nature of the random variations in traffic load and in signal level or the relationship between analog and digital values, we assume an equal probability for "1" as for "0", i.e. that, on an average, "1" and "0" come in alternate positions. This gives

$$\frac{U_m}{U_{PPM}} = \frac{1}{\sqrt{\sum_{n=1}^{\infty} \frac{\pi^2 (\Delta_n/T)^2}{\pi^2 n^2}}} \tag{2.2.9}$$

Strictly speaking, Δ_n is a statistically distributed magnitude with respect to n; but since the number of n (pulses) is infinitely large, we can approximate Δ_n/T to $\overline{\Delta}/T$ = constant, which gives

$$\sum_{n=1}^{\infty} \frac{\left(\frac{\overline{\Delta}}{T}\right)^2}{n^2} = \frac{1}{18^2} \sum_{n-1}^{\infty} \frac{1}{n^2} = \frac{1}{18^2} \frac{\pi^2}{6} \tag{2.2.10}$$

So, with intersymbol crosstalk as the only noise source, we get the signal-to-noise ratio

$$\frac{U_m}{n_{\text{eff}}} = \frac{U_m}{U_{PPM}} = \frac{1}{\frac{1}{18} \frac{\pi}{\sqrt{6}}} = 14 \tag{2.2.11}$$

Assume that we had instead approximated the system (cable plus input stage) with a filter with cosinusoidal transfer function

$$A(f) = \frac{1}{2} + \frac{1}{2}\cos \pi \frac{f}{2f_g} \quad \text{for } f \leqq 2f_g$$
$$A(f) = 0 \quad \text{for } f > 2f_g \tag{2.2.12}$$

and in the same way as before let a δ-pulse appear at the input at time $t=0$ .We should then have obtained the output signal

$$u_0(t) = \frac{1}{t_g} \frac{\sin 2\pi \frac{t}{t_g}}{2\pi \frac{t}{t_g}} \frac{1}{1 - 4\left(\frac{t}{t_g}\right)^2} \tag{2.2.13}$$

In the same way as before, we assume an infinite train of pulses with the pulse period T:

$$u(t) = \sum_{n=-\infty}^{\infty} \frac{1}{t_g} \frac{\sin \frac{2\pi}{t_g}(t - nT)}{\frac{2\pi}{t_g}(t - nT)} \frac{1}{1 - 4\left(\frac{t - nT}{t_g}\right)^2} \tag{2.2.14}$$

We make $U_m = 1/t_g$ and choose the shortest possible pulse period $T = t_g = 1/2B$. Assuming also that the nth pulse arrives at time $t = nT + \Delta_n$, we get

$$u(t) = \sum_{n=-\infty}^{\infty} U_m(n) \frac{\sin \frac{2\pi}{T}(t - nT - \Delta_n)}{\frac{2\pi}{T}(t - nT - \Delta_n)} \frac{1}{1 - 4\left(\frac{t - nT - \Delta_n}{T}\right)^2} \tag{2.2.15}$$

We make the same approximations as before and, at time $t = 0$, obtain the signal-to-noise ratio

$$\frac{U_m}{n_{\text{eff}}} = \frac{U_m}{U_{PPM}} \frac{1}{\sqrt{\sum_{n=1}^{\infty} \frac{\left(2\pi \frac{\Delta_n}{T}\right)^2}{(2\pi n)^2} \frac{1}{(1 - 4n^2)^2}}} \tag{2.2.16}$$

But

$$\sum_{n=1}^{\infty} \frac{\left(\frac{\Delta}{T}\right)^2}{n^2} \frac{1}{(1 - 4n^2)^2} = \frac{1}{18^2}\left[\frac{1}{1}\frac{1}{3^2} + \frac{1}{2^2}\frac{1}{15^2} + \frac{1}{3^2}\frac{1}{99^2} + \ldots\ldots\right. \tag{2.2.17}$$

and, as this series converges very rapidly, we finally obtain

$$\frac{U_m}{n_{\text{eff}}} = \frac{U_m}{U_{PPM}} \cong \frac{1}{\frac{1}{18}\sqrt{\frac{1}{9}+\frac{1}{900}}} \cong 55 \tag{2.2.18}$$

CHAPTER 3

Crosstalk

In the following chapter we shall calculate the noise caused by unintelligible crosstalk between pairs of the same quad or between pairs in non-adjacent quads. We shall also make a distinction between near-end crosstalk and far-end crosstalk (*Figs. 9* and *11*).

3.1 Near-end Crosstalk

Starting with near-end crosstalk we assume the existence of both capacitive and inductive coupling between the pairs. We denote the capacity unbalance per metre k_1' (pair-pair) and the mutual inductance per metre m'. The total unbalance k_n' for near-end crosstalk can be expressed as

$$k_n' = k + \frac{m}{Z_1 Z_2}\,\text{pF/m} \tag{3.1.1}$$

where $k' = k_1'/4$.

The transmission circuit has the following characteristics:

0.4 mm paper insulated copper wire

Attenuation constant α in nepers/km

f:	100 kc/s	1.5 Mc/s	2.0 Mc/s
α:	1.0	4.0	4.4

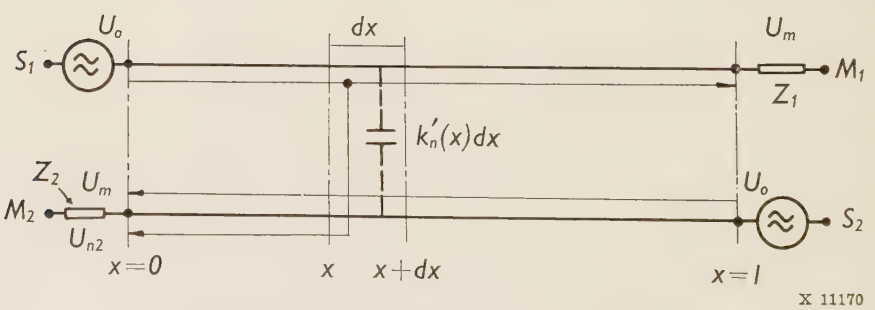

Fig. 9. Near-end crosstalk from circuit 1 to circuit 2.

Characteristic impedance $Z = Z_1 = Z_2 = 150\ \Omega$

$v = 2.5 \cdot 10^5$ km/s

$\gamma = \alpha + j\beta = \alpha + j\frac{\omega}{v}$.

Maximum unbalance (pair-pair of the same quad): $k_1 = 100$ pF per factory length ($s = 230$ m).

However k_n' is not constant along the cable. Fluctuating conditions in manufacture and the different mechanical strains imposed on cables make k_n' random along the cable. The fluctuating values of k_n' with respect to x have been taken into consideration by denoting it $k_n'(x)$. For the calculation of crosstalk it is therefore necessary to introduce the autocorrelation function and the corresponding power spectrum (H KADEN, "Das Nebensprechen in Kabeln bei nicht-stationären Vorgängen (Impulsen)", Arch. elektr. Übertragung 11[6]):

$$\varphi(\delta) = \lim_{L\to\infty} \frac{1}{2L} \frac{1}{\overline{k_n'^2}} \int_{-L}^{L} k_n'(x) k_n'(x+\delta)\, d\delta \tag{3.1.2}$$

$$\Phi\left(\frac{2\omega}{v}\right) = \int_{-\infty}^{\infty} \varphi(\delta) \exp\left(2\omega\delta/v\right) d\delta \tag{3.1.3}$$

In the following calculation we assume a distribution of the values of $k_n'(x)$ such that $\varphi(\delta)$ has the gaussian distribution:

$$\varphi(\delta) = \exp\left[-\frac{1}{2}(\delta/r)^2\right] \tag{3.1.4}$$

where r is defined as the correlation range. It is difficult to say anything definite concerning the length of r, but if we guess that the length of lay has some influence on r, we may expect r to be between 1 and 10 metres.

In M_2 we have the voltage dU_{n2} caused by the crosstalk in an infinitesimal length dx of the cable at distance x from M_2 (*Fig. 9*):

$$dU_{n2} = \frac{1}{2} \frac{U_0 e^{-2\gamma x}}{\frac{1}{j\omega k_n'(x)\, dx} + Z_2} \cong \frac{j\omega Z_2}{2} k_n'(x)\, U_0 e^{-2\gamma x} dx \tag{3.1.5}$$

The crosstalk factor for the whole cable length l is then

$$P(\omega) = \frac{U_{n2}}{U_0} = \frac{j\omega Z_2}{2} \int_{x=0}^{l} k_n'(x)\, e^{-2\gamma x} dx \tag{3.1.6}$$

which gives the near-end crosstalk attenuation

$$A_n = -10 \log_{10} \overline{|P(\omega)|^2} \text{ db} \tag{3.1.7}$$

where

$$\overline{|P(\omega)|^2} = \left(\frac{\omega Z_2}{4}\right)^2 \frac{1 - e^{-4\alpha l}}{\alpha} \Phi\left(\frac{2\omega}{v}\right) \overline{k_n'^2} \tag{3.1.8}$$

The relation between the r.m.s. value of the total unbalance per metre $k_n'^2$ and the r.m.s. value of the total unbalance of the whole cable length l is as follows[9]:

$$\overline{k_n'^2} = \frac{\overline{k_{nl}^2}}{l} \frac{1}{\sqrt{2\pi r}} \tag{3.1.9}$$

where

$$k_{nl}^2 = \frac{l}{s}\left(\frac{k_1}{4} + \frac{m}{Z_1 Z_2}\right)^2 = \frac{l}{s}\left(\frac{k_1}{4}\right)^2 = (140 \text{ pF})^2 \tag{3.1.10}$$

It is here assumed that we have a root-sum-square addition in M_2 of the crosstalk components from the various factory lengths of the cable, and that the mutual inductance coupling is equal to the capacity unbalance coupling.

Equation 3.1.8 holds good for a sinusoidal voltage. For a single pulse, which has a continuous spectrum, we have the formulae given below.

Now since a pulse consists of a continuous spectrum which, theoretically at least, is infinite, the voltage received at M_2 as a result of the near-end crosstalk will be

$$u_{n2}(t) = \frac{U_0 T_v}{2\pi} \int_{\omega=-\infty}^{\infty} F(\omega)\, P(\omega)\, e^{j\omega t}\, dt \tag{3.1.11}$$

where $U_0 T_v$ is pulse amplitude × pulse duration, and

$$F(\omega) = \int_{\tau=-\infty}^{\infty} \frac{u_0(\tau)}{U_0} e^{-j\omega\tau} d\left(\frac{\tau}{T_v}\right) = \begin{cases} \dfrac{\sin(\omega T_v/2)}{\omega T_v/2} & \text{for square pulse} \\ \dfrac{\sin(\omega T_v/2)}{\omega T_v/2} \dfrac{1}{1 - (\omega T_v/\pi)^2} & \text{for } \cos^2\text{-pulse} \end{cases} \tag{3.1.12}$$

$F(\omega)$, which is the Fourier spectrum of $u_0(t)$, is "weighted" against the crosstalk factor $P(\omega)$, after which, by integration, we obtain the converse Fourier transformation, i.e. the time function $u_{n2}(t)$ corresponding to $F(\omega)\, P(\omega)$.

Since, as appears from eq. 3.1.6, $P(\omega)$ is dependent on $k'(x)$, the same applies to $u_{n2}(t)$, from which it follows that $u_{n2}(t)$ has random values with respect to the distance travelled

by the pulse along the cable. What we are interested in, therefore, is the r.m.s. of $u_{n2}(t)$. To find this, we take the roundabout course of determining first the energy generated in M_2 within the time interval 0 to t, i.e. the time taken for the pulse to travel from M_2 to a distance $Z = vt/2$ and back again. For this purpose we use the proposition of Parsival, which from a physical point of view implies that the energy contained in the Fourier spectrum of a time function is equal to the energy of the time function:

$$w(t) = \int_{0}^{t=2x/v} \overline{u_{n2}^2(t)}\, dt = \frac{U_0^2 T_v^2}{2\pi} \int_{\omega=-\infty}^{\infty} |F(\omega)|\, \overline{|P(\omega)|^2}\, d\omega \tag{3.1.13}$$

We insert eq. 3.1.8 in 3.1.13 and differentiate $w(t)$ with respect to t, which leads after some calculations to

$$\overline{u_{n2}^2(t)} = \left(\frac{vZ_2}{4}\right)^2 U_0 \overline{k_n'^2}\, I^2 e^{-2\alpha v t} \tag{3.1.14}$$

where, if the autocorrelation function of $k_n'(x)$ follows the gaussian distribution as in the preceding section,

$$I^2 = \sqrt{\frac{2}{\pi}} \frac{r}{vT_v} \int_{\omega=-\infty}^{\infty} (\omega T_v)^2 |F(\omega)|^2 \exp\left(-2\omega^2 r^2/v^2\right) d(\omega T_v) \tag{3.1.15}$$

If the pulse shape has been established, $|F(\omega)|^2$ is also known (eq. 3.1.12). Since, moreover, the length of cable occupied by the pulse is given, viz.

$vT_v \simeq 2.5 \times 10^5$ km/sec $\times$ 0.4 μs = 100 m,

it is evident from eq. 6.17 that

$$I = f(r) \tag{3.1.16}$$

In *Fig. 11* this is shown both for cosine-squared pulse and square pulse.

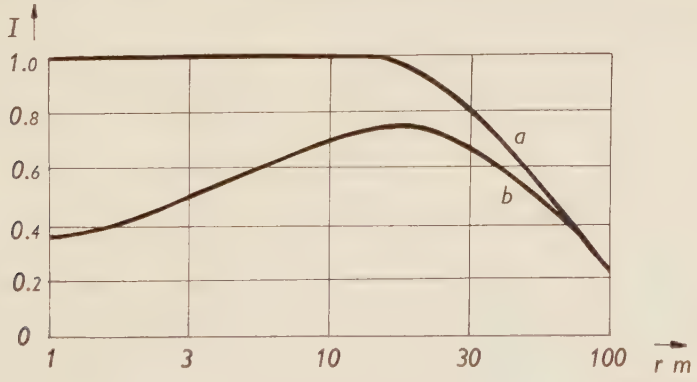

Fig. 10. $I = f(r)$.
a. square pulse
b. cosine-squared pulse

The number of simultaneous pulses on the circuit is

$$N = \frac{l}{vT} \quad (T \text{ is the pulse period}) \tag{3.1.17}$$

The voltage from these N pulses is summated in M_2:

$$U_{n2}^2 = \sum_{n=0}^{N} \overline{u_{n2}^2}(t) = \left(\frac{vZ_2}{4}\right)^2 U_0^2 \overline{k_n'^2} I^2 \sum_{n=0}^{N} e^{-2\alpha nT}$$
$$= \left(\frac{vZ_2}{4}\right)^2 U_0^2 \overline{k_n'^2} I^2 R^2 \tag{3.1.18}$$

where

$$R^2 = \frac{1 - e^{-2\alpha vNT}}{1 - e^{-2\alpha vT}} \tag{3.1.19}$$

and

$$\overline{k_n'^2} = \frac{\overline{k_{nl}^2}}{l\sqrt{2\pi r}} = \frac{140^2}{1.8\sqrt{2\pi r}} \text{ (pF)}^2/\text{km}^2 \tag{3.1.20}$$

If we now insert the given system data in eq. 3.1.18, we obtain the values of near-end crosstalk for the distance of 1 800 m between two regenerative repeaters:

Table 3

$A_n = 10 \log_{10} (U_0^2/U_{n2})$ db

r m	1	5	20
Square pulse	41	41	47
$\cos^2$-pulse	53	47	49

The attenuation between S_2 and M_2 (*Fig. 9*) is 1.8 km × 4.0 N/km × 8.68 = 63 db, i.e. the signal received at M_2 is (1/1400) U_0. According to *Table 3*, A_n is not greater than 53 db even in the most favourable case, which means that the noise level at M_2 due to near-end crosstalk is (1/450) U_0. The noise level is therefore three times as high as the signal level at M_2. Now it is obvious, of course, that there should never be two opposing circuits in the same quad. On the other hand it is conceivable that opposing circuits must be allowed in the same cable.

As is evident from eq. 3.1.18, if $\sqrt{\overline{k_{nl}^{x2}}}$ and $\sqrt{\overline{k_{nl}^{xx2}}}$ are the equivalent coupling capacitances between pair-pair circuits within the same quad and in two different quads, respectively, the relation between the corresponding near-end crosstalk attenuations will be

$$A_n^{xx} - A_n^{x} = 10 \log_{10} \frac{\overline{k_{nl}^{x2}}}{\overline{k_{nl}^{xx2}}} \text{ db} \tag{3.1.21}$$

As already mentioned, the maximum value of the unbalance per factory length of cable is 100 pF. The mean unbalance is 25—30 pF, and the unbalance between pair-pair circuits in different quads less than one-tenth, or about 2.5 pF. For couplings within the same quad we assumed that inductive and capacitive couplings were equally great and that the maximum inductive coupling coincided with the maximum capacitive coupling. For couplings between pairs in different quads the same regularity cannot be expected. We here assume, therefore, that the inductive and capacitive couplings are additive on a power basis, which gives

$$\sqrt{k_{nl}^{xx2}} = \frac{2.5}{4} \sqrt{\frac{1800}{230}} \sqrt{2} = 2.5 \text{ pF} \tag{3.1.22}$$

The improvement in signal-to-noise ratio will then be

$$A_n^{xx} - A_n^{x} = 20 \log_{10} \frac{140}{2.5} = 35 \text{ db} \tag{3.1.23}$$

According to *Table 3*, the U_2/U_{n2} ratio for a $\cos^2$-pulse with coupling within the same quad tends to vary between 47 and 53 db according to the magnitude of the correlation length. Assuming a mean value of 50 db, the U_0/U_{n2} ratio for coupling between side-circuits in different quads increases to 85 db. The signal-to-noise ratio is then

$$20 \log_{10} \frac{U_m}{n_{\text{eff}}} = 20 \log_{10} \frac{U_m}{U_{n2}} = (85 - 63) \text{ db or } \frac{U_m}{n_{\text{eff}}} = 13 \tag{3.1.24}$$

Comparing this value with eq. 1.3.15, it is found to suffice precisely. Everything would clearly be in order if there were no other noise components. Unfortunately there are, however, as is evident from the preceding as well as from the subsequent account.

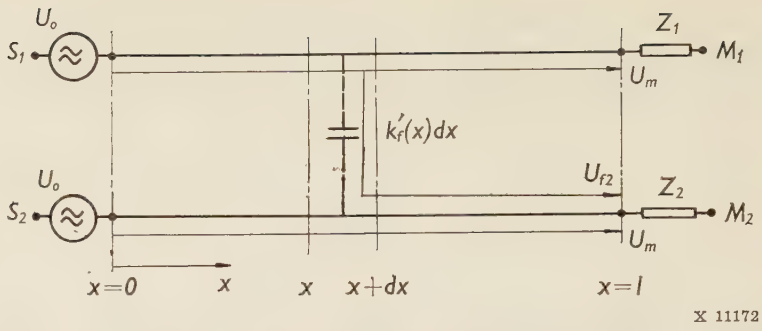

Fig. 11. Far-end crosstalk from circuit 1 to circuit 2.

3.2 Far-end Crosstalk

Far-end crosstalk is due to the coupling between two unidirectional circuits, i.e. with S_1, S_2 at one end and M_1, M_2 at the other end of section 1 (*Fig. 11*). We shall calculate the voltage generated by S_1 in M_2 consequent on the coupling k_f, where (cf. eq. 3.1.1):

$$k'_f = k - \frac{m}{Z_1 Z_2} \text{ pF/m} \tag{3.2.1}$$

We assume that two parallel unidirectional circuits can be carried on the same quad.

As before, there is some uncertainty as regards the inductive coupling. However, it is directly evident from eq. 3.2.1 that, for far-end crosstalk, the maximum coupling results when $m = 0$. We assume this and get

$$\overline{k_{fl}^2} = \frac{l}{s}\left(\frac{k_1}{4}\right) = \left\{\sqrt{\frac{1800}{230}\,\frac{100}{4}\text{ pF}}\right\} \tag{3.2.2}$$

Irrespective of where on the line the infinitesimal distance dx is situated, the voltage dU_{f2} generated in M_2 as a result of the coupling capacitance $k'_f(x)dx$ (*fig. 11*) will always have travelled the constant distance l. We thus get

$$Q(\omega) = \frac{U_{f2}}{U_0} = \frac{j\omega Z_2}{2}\, e^{-(\alpha+j\beta)l} \int_0^l k'_f(x)dx \tag{3.2.3}$$

from which is derived the r.m.s. value of the crosstalk factor

$$|Q(\omega)|^2 = \frac{\omega^2 Z_2}{4}\, e^{-2\alpha l}\, \overline{k_{fl}^2} \tag{3.2.4}$$

This formula is well known and holds good for a purely sinusoidal voltage.

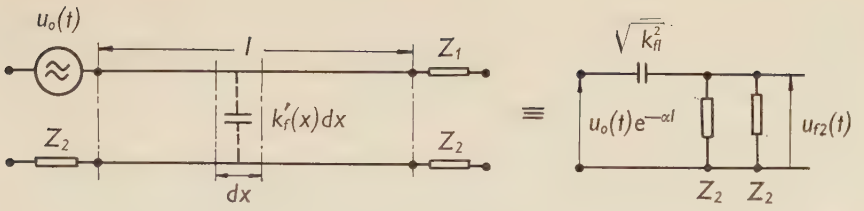

Fig. 12. Equivalent diagram for far-end crosstalk from circuit 1 to circuit 2.

As appears from eq. 3.2.3, the voltage U_{f2} is independent of x except with respect to the varying coupling capacitance $k'_f(x)$ along the cable. Since, according to the definition, $\overline{k''_{fl}}$ is the r.m.s. of the total coupling capacitance for the entire length l, use can be made of the equivalent current diagram shown in *Fig. 12*. From this we immediately see (disregarding the constant delay time $t_0 = l/v$ which is common to all pulses):

$$\sqrt{\overline{u''_{f2}(p)}} = \frac{Z_2/2}{(Z_2/2) + \left(1/p\sqrt{\overline{k''_{fl}}}\right)} u(p) \cong \frac{Z_2}{2} p\sqrt{\overline{k''_{fl}}} u(p) \tag{3.2.5}$$

i.e.

$$\sqrt{\overline{u''_{f2}(t)}} = \frac{Z_2}{2}\sqrt{\overline{k''_{fl}}} \frac{d\{u_0(t)\}}{dt} e^{-\alpha l} \tag{3.2.6}$$

The crosstalk voltage $\sqrt{\overline{u''_{f2}(t)}}$ is accordingly a time function which varies in proportion to the derivative of the pulse transmitted from S_1. The system must be designed for a sufficiently large signal-to-noise ratio even at the highest existing crosstalk voltage:

$$U_{f2} = \max\{u''_{f2}(t)\} \sim \left[\frac{d\{u_0(t)\}}{dt}\right]_{\max} \tag{3.2.7}$$

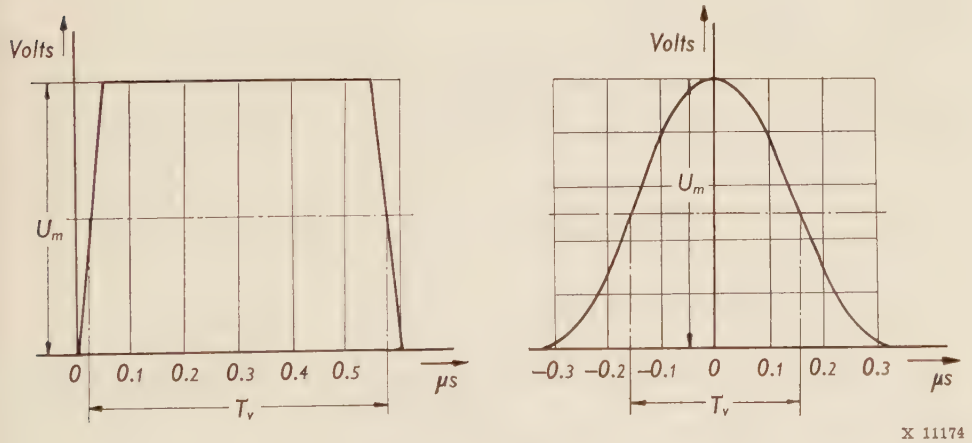

Fig. 13. Trapezoidal pulse and cosine-squared pulse.

It is seen that an ideal square pulse causes infinitely great crosstalk. This is of no importance, however, since such a pulse cannot be realized in practice. We instead calculate U_{fl} for the pulse shapes shown in *Fig. 13.*

a) Trapezoidal pulse

$$u_0(t)\,e^{-\alpha l} = u(t) = \frac{U_m}{t_g}\,t \quad \text{for} \quad 0 \leq t \leq 0.05\ \mu\text{s}$$

$$u(t) = U_m \quad \text{for} \quad 0.05 \leq t \leq 0.55\ \mu\text{s}$$

etc. etc.

which, inserted in eq. 3.2.7, yields

$$U_{f2} = \frac{Z_2}{2}\sqrt{\overline{\overline{k_{fl}^2}}}\,\frac{U_m}{t_g} \tag{3.2.8}$$

This gives the signal-to-noise ratio

$$\frac{U_m}{n_{\text{eff}}} = \frac{U_m}{U_{f2}} = \frac{2}{Z_2}\,\frac{1}{\sqrt{\overline{\overline{k_{fl}^2}}}}\,t_g \cong 10 \tag{3.2.9}$$

b) $\cos^2$-pulse

$$u_0(t)\,e^{-\alpha l} = u(t) = \frac{U_m}{2}\left(1 + \cos\pi\frac{t}{T}\right)$$

$$\pi \leq \pi\frac{t}{T} \leq \pi$$

which, inserted in eq. 3.2.7, yields

$$U_{f2} = \frac{Z_2}{2}\sqrt{\overline{\overline{k_{fl}^2}}}\,\frac{U_m}{2}\,\frac{\pi}{T} \tag{3.2.10}$$

This gives the signal-to-noise ratio

$$\frac{U_m}{n_{\text{eff}}} = \frac{U_m}{U_{f2}} = \frac{4}{Z_2}\,\frac{1}{\sqrt{\overline{\overline{k_{fl}^2}}}}\,\frac{\pi}{T} \cong 80$$

CHAPTER 4

Thermal Noise

The r.m.s. value of the thermal noise voltage at the input of the regenerative repeater is given by

$$e_N = \sqrt{4kTR_gF\Delta f} \cong 25\ \mu\text{V} \tag{4.1}$$

where

$4kT = 1.65 \times 10^{-20}$ joules ($T = 300°$ Kelvin)

$R_g = Z = 150\ \Omega$

F is the noise figure of the input stage, which is a transistor in common base coupling. F is under all circumstances below 20 db so long as the transistor is not broken.

Δf is the bandwidth, which according to the "Standards of PCM-Telemetry" has been set equal to 1.5 × pulse repetition frequency, so $\Delta f = 2.4$ Mc/s.

The received peak signal voltage is given by

$$U_m = U_0 e^{-\alpha l} = 5/1{,}400 \text{ V} \tag{4.2}$$

where

$\alpha = 4.0$ neper/km at 1.5 Mc/s and l has been tentatively set equal to 1.8 km. Inserting this value in (4.2) gives $U_m = 5/1{,}400$ V.

From this we calculate the signal-to-noise ratio for the case when only thermal noise is present:

$$\frac{U_m}{n_{\text{eff}}} = \frac{U_m}{e_N} = \frac{U_0 e^{-\alpha l}}{\sqrt{4kTR_g F \Delta f}}$$

CHAPTER 5

Conclusions

5.1 Summary of Noise Sources

In the following summary of the different noise components we shall investigate how the signal-to-noise ratio depends on the length of the repeater section, with the wire diameter and the pulse configuration as parameters.

5.1.1. *PPM noise* (cf. eq. 2.2.9 and 2.2.16)

$$U_{PPM}^2 = \sum_{n=1}^{\infty} \frac{(\Delta/T)}{n^2} U_m^2 = K_{1f} U_m^2 \text{ for square pulse} \tag{5.1.1}$$

$$U_{PPM}^2 = \sum_{n=1}^{\infty} \frac{(\Delta/T)^2}{n^2} \frac{1}{(1-4n^2)^2} U_m^2 = K_{1c} U_m^2 \text{ for } \cos^2\text{-pulse} \tag{5.1.2}$$

The PPM is thus proportional to the received pulse amplitude and independent of the length l of the circuit, but dependent on the pulse shape (K_{1f} and K_{1c}). As was stated on page 223, an equivalent phase displacement of 70° results in a lowering of the noise margin by 2 db. From eq. 3.1.15 it is seen that the signal-to-noise ratio on the receiver input U_m n_{eff} must be 12 ~ 21 db. Root-sum-square addition of the various noise components gives

$$\sqrt{N} = n_{\text{eff}} = \sqrt{e_N^2 + U_{PPM}^2 + U_{n2}^2 + U_{f2}^2} \tag{5.1.3}$$

To compensate for the 2 db reduction in the noise margin, the signal-to-noise ratio must be increased correspondingly, thus

$$10 \log_{10} \frac{U_m^2}{N} = 23 \text{ db} \qquad \text{i.e. } \frac{U}{\sqrt{N}} = 14 \tag{5.1.4}$$

5.1.2 *Near-end crosstalk* (cf. eq. 3.1.18—20)

$$U_{n2}^2 = \left(\frac{vZ_2}{4}\right)^2 \overline{k_n'^2} I_f^2 R^2 U_0^2 = K_{2f} f_n(l)\, U_0^2 \text{ for square pulse} \tag{5.1.5}$$

$$U_{n2}^2 = \left(\frac{vZ_2}{4}\right)^2 \overline{k_n'^2} I_f^2 R^2 U_0^2 = K_{2c} f_n(l)\, U_0^2 \text{ for } \cos^2\text{-pulse} \tag{5.1.6}$$

The near-end crosstalk level is proportional to the amplitude of the transmitted pulse and is also dependent on the length of the circuit ($f_n(l)$) and of the pulse shape (K_{2f} and K_{2c}). However, it is to be noted that its dependency on length is rather slight — an increase of 2 db for increase of l from 230 to 500 m. From there on the crosstalk level is nearly constant.

5.1.3 *Far-end Crosstalk* (cf. eq. 3.2.8 and 3.2.10)

$$U_{n2} = \frac{Z_2}{2} \frac{1}{t_g} \sqrt{\overline{k_{fl}^2}}\, U_m^2 = K_{3f} f_n(\sqrt{l})\, U_m^2 \text{ for square pulse} \tag{5.1.7}$$

$$U_{n2} = \frac{Z_2}{2} \frac{\pi}{2T} \sqrt{\overline{k_{fl}^2}}\, U_m^2 = K_{3c} f_n(\sqrt{l})\, U_m \text{ for } \cos^2\text{-pulse} \tag{5.1.8}$$

The far-end crosstalk is proportional to the amplitude of the received pulse and is dependent on the length of the circuit $f_n(\sqrt{l})$ and on the pulse shape (K_{3f} and K_{3c}).

5.1.4 *Thermal noise* (cf. eq. 4.1)

$$e_N^2 = 4kTR_gF\Delta f \tag{5.1.9}$$

The thermal noise is constant insofar as it is dependent only on the characteristics of the receiver.

5.2. Conclusions

If we look first at *Figs. 14* and *15*, which are noise level diagrams for square pulses through 0.4 mm and 0.6 mm cables, it is immediately apparent that the PPM and far-end crosstalk, which contribute almost equally to the total noise, each take up practically the entire noise margin. The consequence is that, if a square pulse is transmitted on the circuit, the circuit will be usable only over distances of less than 500 metres even under conditions of reduced quality of transmission.

If we now consider the longer sections of cable with $l > 1$ km (*Figs. 16* and *17*), we must be quite clear on two points:

1. Irrespective of the shape of the pulse at the time of transmission, the circuit, in consequence of its low pass filter characteristics (*Fig. 7*), tends to remove all sharp corners from the pulse with the result that the pulse becomes little different from a $\cos^2$-pulse.

2. One cannot make use of this circumstance and transmit square pulses unless certain precautions are taken, since the heavy far-end crosstalk, consequent on the differentiation of the pulse shape (eq. 3.2.7), has taken up a considerable portion of the margin after only a few hundred metres. The PPM noise is of no significance. It does not arise until triggering takes place and is therefore dependent exclusively on the pulse shape at the input of the regenerative repeater.

The diagrams in *Figs. 16* and *17* are intended to describe primarily the signal-to-noise ratio on distances above 1 kilometre. Only such curves are included, therefore, as describe $\cos^2$-pulses. The intersection between the maximum permissible noise level and the largest of the noise components gives the maximum permissible repeater spacing. *Fig. 16* is a noise level diagram for 0.4 mm cable. Wire of this small dimension is used mainly for subscriber's cable and hardly occurs in trunk cable. To complete the picture, however, curves are shown for 0.4 mm subscriber's and trunk cable. But the coupling capacitance of the subscriber's cable is 3.4 times that of the trunk cable, i.e. the crosstalk attenuation (eq. 3.1.21) in the subscriber's cable must be expected to be 10—11 db below that in the trunk cable. It is now seen that, in the subscriber's cable, the maximum permissible repeater spacing will be determined by the far-end and near-end crosstalk jointly, but in the trunk cable practically by the near-end crosstalk alone. The same applies to 0.6 mm trunk cable (*Fig. 17*).

In the two cases concerning trunk cables there are components from the PPM noise and from the far-end crosstalk, both of which are about 10 db ($\sim 1/3$) below the near-end crosstalk at the points of intersection under consideration, which, inserted in eq. 5.1.3, give

$$\sqrt{N} = \sqrt{1 + (1/9) + (1/9)}\, U_{n2}$$

The noise margin is thereby reduced by 1 db. Even if this reduction as such cannot be disregarded, yet, as appears from the diagrams, it can be compensated for by reducing the maximum permissible repeater spacing by only 100 metres.

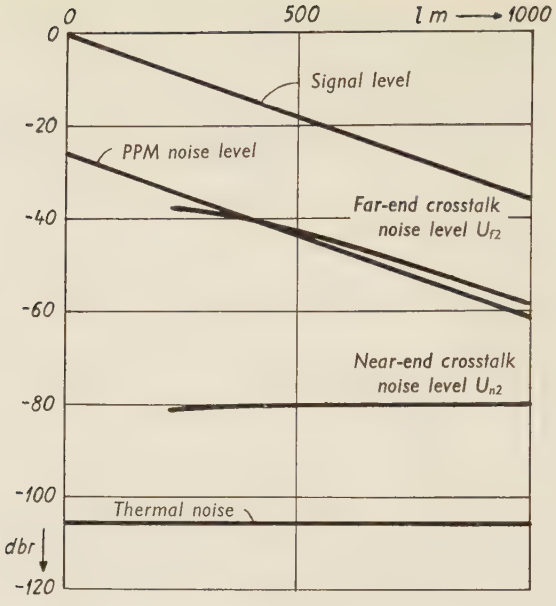

X 11175

Fig. 14. Noise level diagram: 0.4 mm cable. Square pulse ≅ trapezoidal pulse.

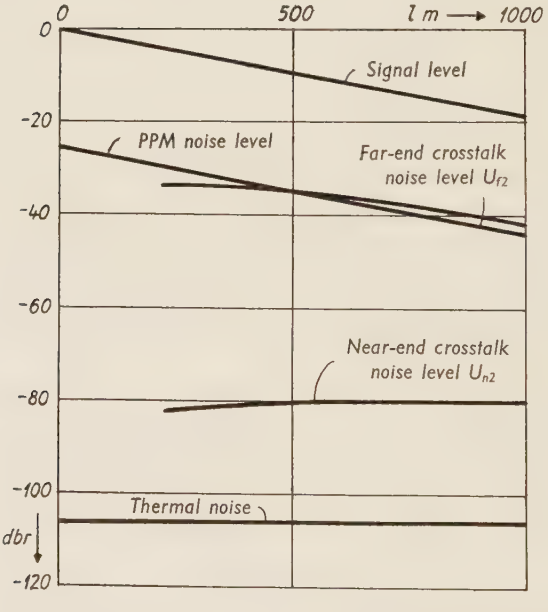

X 11176

Fig. 15. Noise level diagram: 0.6 mm cable. Square pulse ≅ trapezoidal pulse.

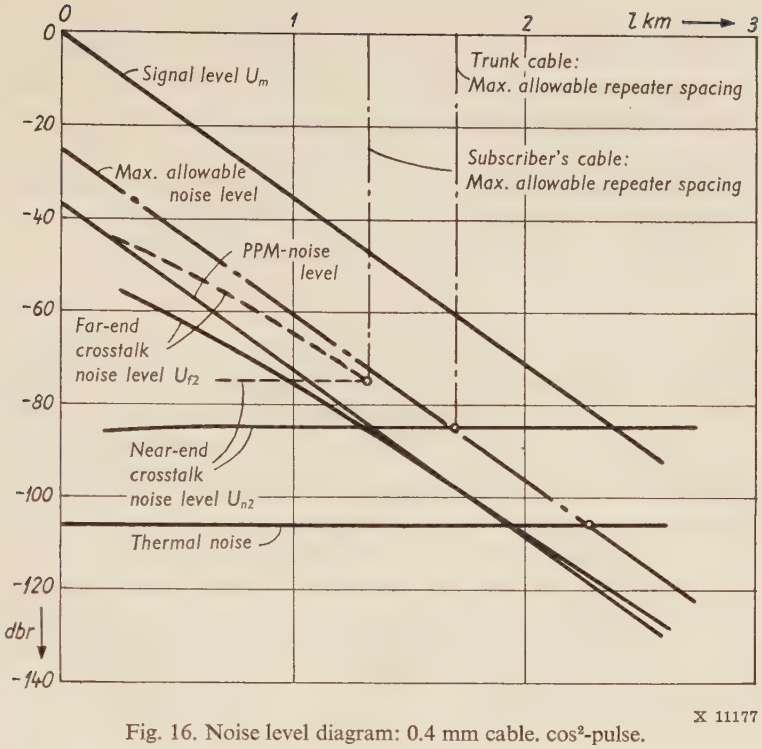

Fig. 16. Noise level diagram: 0.4 mm cable. cos²-pulse.
——— trunk cable
– – – – subscriber's cable

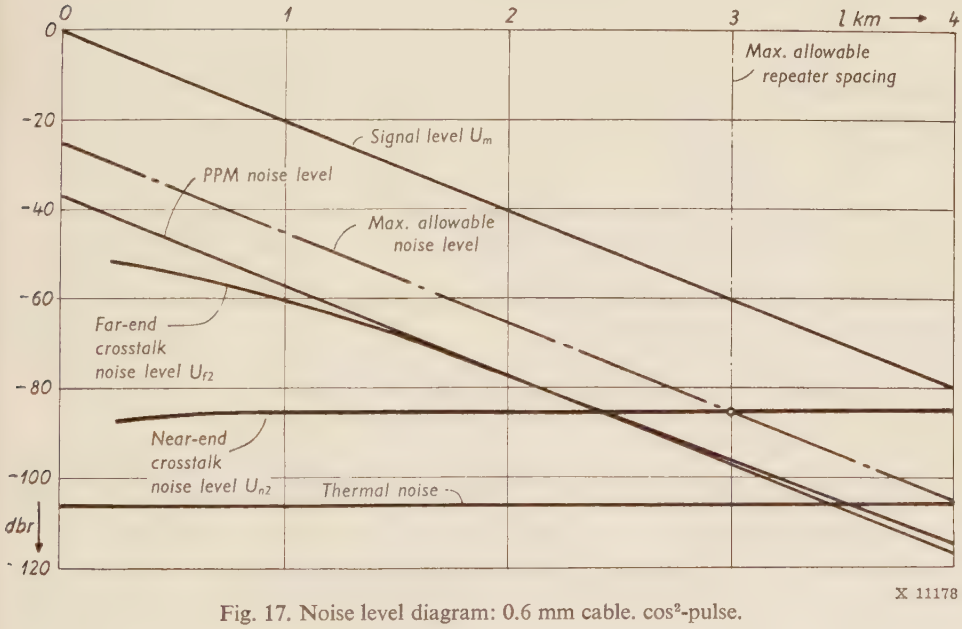

Fig. 17. Noise level diagram: 0.6 mm cable. cos²-pulse.

If two cables run in parallel over any section, each serving one direction of transmission, the near-end crosstalk disappears. *Figs. 16* and *17* then show that the maximum permissible repeater spacing is governed virtually by the thermal noise, and that the maximum allowable distance can be increased from 1.7 to 2.2, and from 3 to 4 km, for the two dimensions of cable.

Finally, it may be pointed out that, if the same cable carries both directions of traffic, the thermal noise is of no significance.

APPENDIX

We assume that we have a whole suite of infinite time series $u'(t),..,\ u''(t),.....,\ u^N(t),.....$ Each time series can be written under the form

$$u^N(t) = \sum_{n=-\infty}^{\infty} U_m(n) \frac{\sin \frac{\pi}{T}(t - nT - \Delta_n^N)}{\frac{\pi}{T}(t - nT - \Delta_n^N)}$$

To start with, we disregard the fact that $u''(t)$ represents a varying signal and, instead, assume that there is only one pulse, the kth:

$$u_k^N(t) = U_m \frac{\sin \frac{\pi}{T}(t - kT - \Delta_k^N)}{\frac{\pi}{T}(t - kT - \Delta_k^N)} \tag{A.2}$$

We investigate this signal at time $t = 0$ and introduce the approximations used in 2.2.8, so obtaining

$$U_k^N(0) = U_m \frac{\frac{\Delta_k^N}{T}}{k} \tag{A.3}$$

In relation to the time series, Δ_k^N/T is a varying magnitude which follows a certain distribution $p(\Delta_k^N/T)$, and consequently

$$p\left(u_k^N\right) = \frac{U_m}{k} p\left(\frac{\Delta_k^N}{T}\right)$$

This gives the following r.m.s. value for the noise voltage generated from the kth pulse, taken over all time series:

$$n_{\text{eff}} = \lim_{N\to\infty} \left\{ \sum_N \left(u_k^N\right)^2 p\left(u_k^N\right) \right\}^{\frac{1}{2}} = \left\{ \int_{-\infty}^{\infty} (u_k)^2 p(u_k)\, du_k \right\}^{\frac{1}{2}} \tag{A.4}$$

Assuming a gaussian distribution of the relative time deviation with an r.m.s. value $\sigma = \overline{\Delta}/T$, we get

$$n_{k\,\mathrm{eff}}^2 = \int_{-\infty}^{\infty} \frac{U_m^2}{k_2}\left(\frac{\Delta_k}{T}\right)^2 \frac{1}{\overline{\Delta}/T\sqrt{2\pi}} \exp\left[-\frac{1}{2}\frac{(\Delta_k/T)^2}{(\overline{\Delta}/T)^2}\right] d\left(\frac{\Delta_k}{T}\right)$$
$$= \frac{U_m^2}{k^2}\frac{1}{\overline{\Delta}/T\sqrt{2\pi}} \int_{-\infty}^{\infty} \left(\frac{\Delta_k}{T}\right)^2 \exp\left[-\frac{1}{2}\frac{(\Delta_k/T)^2}{(\overline{\Delta}/T)^2}\right] d\left(\frac{\Delta_k}{T}\right) \tag{A.5}$$

Eq. A.5 indicates the noise power from the kth pulse at time $t = 0$. We may also say that, from the infinitely many time series with varying Δ_k/T in the kth pulse position, we have formed a mean time series in which the noise component $n_{k\,\mathrm{eff}}^2$ comes from the kth pulse. On the assumption of the validity of the ergodic property, we can then determine the total noise from an arbitrary time series within the suite. We also assume an equally great probability for "1" as for "0". The noise power is then

$$n_{\mathrm{eff}}^2 = \frac{1}{\overline{\Delta}/T\sqrt{2\pi}} \sum_{n=1}^{\infty} \frac{U_m^2}{n^2} \int_{-\infty}^{\infty} \left(\frac{\Delta_n}{T}\right)^2 \exp\left[-\frac{1}{2}\frac{(\Delta_n/T)^2}{(\overline{\Delta}/T)^2}\right] d\left(\frac{\Delta_n}{T}\right) \tag{A.6}$$

It can be shown that

$$\int_0^{\infty} x^2 e^{-ax^2} dx = \frac{1}{4a}\sqrt{\frac{\pi}{a}} \tag{A.7}$$

We set

$$a = \frac{1}{2\sigma^2} = \frac{1}{2(\overline{\Delta}/T)^2} \quad \text{and} \quad x = \Delta_n/T \tag{A.8}$$

and get

$$\frac{1}{\sigma\sqrt{2\pi}} \int_{-\infty}^{\infty} x^2 \exp\left[-\frac{1}{2}\frac{x^2}{\sigma^2}\right] dx = \frac{1}{\sigma\sqrt{2\pi}}\, 2\, \frac{1}{4\frac{1}{2\sigma^2}} \sqrt{\frac{\pi}{\frac{1}{2\sigma^2}}} = \sigma^2 = (\overline{\Delta}/T)^2 \tag{A.9}$$

Therefore

$$n_{\mathrm{eff}}^2 = \sum_{n=1}^{\infty} \frac{U_m^2}{n^2}\left(\frac{\overline{\Delta}}{T}\right)^2 = U_m^2\left(\frac{\Delta}{T}\right)\frac{\pi^2}{6} \tag{A.10}$$

The signal-to-noise ratio at time $t = 0$ is then

$$\frac{U_m}{n_{\mathrm{eff}}} = \frac{U_m}{U_m \frac{\Delta}{T}\frac{\pi}{\sqrt{6}}} = \frac{T}{\overline{\Delta}}\frac{\sqrt{6}}{\pi} \tag{A.11}$$

This result is seen to be in full conformity with that for eq. 5.10 if we set $\overline{\Delta}/T = 1/18$. It must be pointed out, however, that the expression A.6 has a greater general validity than the value for n_{eff}° in eq. 5.9. Therefore we need no longer assume that $\Delta_n/T \ll 1$. For, if this is not the case,

$$n_{\text{eff}}^{\circ} \cong \frac{U_m^2}{\overline{\Delta}/T\sqrt{2\pi}} \left\{ \int_{-\infty}^{\infty} \frac{\sin^2 \pi \frac{\Delta_n}{T}}{\pi^2 (1 + \Delta_n/T)^2} \exp\left[-\frac{1}{2} \frac{(\Delta_n/T)^2}{(\overline{\Delta}/T)^2} \right] d\left(\frac{\Delta_n}{T}\right) + \right.$$

$$\left. + \sum_{n=2}^{\infty} \frac{1}{n^2} \int_{-\infty}^{\infty} \frac{\sin^2 \pi \frac{\Delta_n}{T}}{\pi^2} \exp\left[-\frac{1}{2} \frac{(\Delta_n/T)^2}{(\overline{\Delta}/T)^2} \right] d\left(\frac{\Delta_n}{T}\right) \right. \tag{A.12}$$

The first term can be suitably calculated by means of numerical integration. An analytical expression exists for the subsequent sum, since the integral

$$\int_{-\infty}^{\infty} e^{-ax^2} \sin^2 x dx$$

can be solved analytically.

Bibliography

1 Wrathall, L R: *Transistorized Binary Pulse Regenerators.* Bell Syst. tech. J *35*(1956): pp. 1059—1084.

2 Bennett, W R: *Statistics of Regenerative Digital Transmission.* Bell Syst. tech. J *37*(1958): pp. 1501—1542.

3 Mayer, H F: *Prinzipien der Pulse-Code-Modulation.* München 1954.

4 Sunde, E D: *Self-Timing Regenerative Repeaters.* Bell Syst. tech. J *36*(1957): pp. 891—937

5 Schütze, W: *Överhörning och dämpning på telefonikablar.* Stockholm 1960. (Telefonaktiebolaget L M Ericsson. [Report] Fx-18)

6 Kaden, H: *Das Nebensprechen in Kabeln bei nicht-stationären Vorgängen (Impulsen).* Arch. elektr. Übertragung *11*(1957): pp. 349—354.

7 Gugolz, M: *Överhörning vid pulsöverföring på kablar.* Stockholm 1960. (Telefonaktiebolaget L M Ericsson. [Report] T 684).

8 Rybner, J: *Teorien for elektriske kredsløb og ledninger. 1.* Copenhagen 1952, pp. 356—368.

9 Kaden, H: *Impulse und Schaltvorgänge in der Nachrichtentechnik.* München 1957.

10 Hölzler, E, & Holzwarth, H: *Theorie und Technik der Pulsmodulation.* Berlin, Göttingen & Heidelberg 1957, pp. 338—361 & 379—386.

11 *Standards for Pulse Code Modulation (PCM) Telemetry.* IRE Trans. Space Electronics and Telemetry. Dec. 1959, pp. 194—195.

Manuscript received by the editors September 1960.

Signal Injection in Time Division Multiplex Systems with Resonant Transfer

BY

WALTER JACOB*

UDC 621.395.345
621.395.38
LME 83024,831

This article gives information on some problems which arise in time division multiplex transmission systems with resonant transfer in connection with additional highway tuning.

Two examples of signal injection in a two-wire and four-wire system are worked out. Finally some methods for generating suitable sinusoidal or composite signals are described.

* Research Department, Telefonaktiebolaget L M Ericsson, Stockholm

General Considerations

For a better understanding of the problems associated with the injection of signals, such as ringing tone, busy tone or signals for tone ringing, into the common highway of a time division multiplex transmission system used for switching purposes in an electronic telephone exchange, it is advisable to give a brief summary of the development of transmission networks employing resonant transfer. [1, 2, 3]

The fundamental network is shown in *Fig. 1*. Each subscriber circuit consists essentially of a low-pass filter having a terminating condenser working as a store. This condenser may be charged or discharged in the interval between two transmission pulses. On the condensers C, which are parts of the low-pass filters, a charge is produced which is proportional to the subscriber speech voltage. During the time τ of a channel pulse, when two electronic subscriber contacts are closed simultaneously, the charges stored in the condensers C change place, provided that the pulse circuit between the subscribers has been tuned, by means of an inductance L, to a resonant frequency corresponding to $2\,\tau$. This gives the tuning condition:

$$\tau = \pi \sqrt{L \cdot C}$$

For the sake of simplicity we shall henceforth confine our study to the pulse part of the system, which lies between the dotted lines of *Fig. 1*.

With a large number of subscribers in such a system, stray capacitances in the contacts and in the common transmission medium pose certain problems. In order to eliminate them, a second tuning of the transmission system is introduced.[3, 4] By means of this "highway tuning", the stray capacitance of the transmission medium is artificially augmented to a value $C_{\text{tot}} = \dfrac{2\,C}{4\,n^2 - 1}$ as shown in *Fig. 1 a*, where n is an integer. With such a design the voltage on the highway at the beginning and end of the transmission pulse is theoretically zero and no energy is wasted. The highway tuning formula can be proved by the following reasoning: The voltages on the condensers C in *fig. 1 a* immediately before the

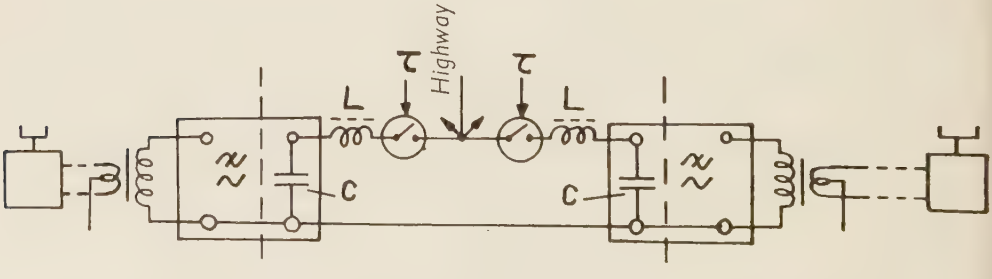

X 11179

Fig. 1. Basic bidirectional transmission PAM network with "resonant transfer".

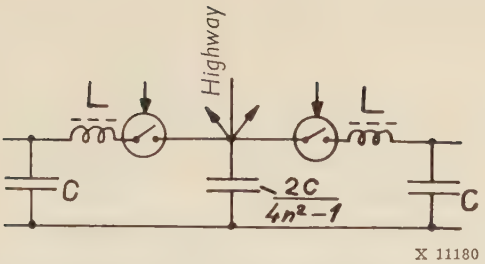

Fig. 1a. Highway tuning.

transmission pulse can be regarded as the sum of symmetrical and non-symmetrical components, i.e.

$$V_1 = V_a + V_s$$
$$V_2 = V_a - V_s$$

The transmission process can be regarded as a superposition of the two cases $V_a = 0$ and $V_s = 0$, In the first case, for reasons of symmetry, the voltage on the highway capacitance will be zero during the pulse, whereas the two charges will change places. In this case, therefore, the highway capacitance will not be noticeable. For $V_s = 0$, on the other hand, the current through the two contacts will be equal in magnitude and opposed in direction, so that the circuit may be conceived of as consisting of two symmetrical halves, each containing half the total highway capacitance. The current through the total highway capacitance during the pulse period will bé $2\,V_a/\omega L \cdot \sin \omega t$ and the voltage swing across the highway capacitance, due to the fact that it starts at zero, has the form $A \cdot (1 - \cos \omega t)$.

If we want the highway capacitance to be discharged again just at the breaking instant of the contacts $t = \alpha$, $\cos \omega\tau$ must be 1, and this is the case if the frequency of the oscillation is $f = \frac{\omega}{2} = \frac{2n}{2\tau}$, which is an even multiple of the frequency in the resonant transfer circuit. In order to obtain an even multiple the resulting capacitance in each half resonant circuit must be $\frac{C}{4n^2}$. This is the case if half the total highway capacitance is tuned to a value of $\frac{C}{4n^2 - 1}$.

The highway tuning and resonant transfer principles were discovered in different laboratories at about the same time. The first detailed description was given by K. W. Cattermole[3].

However, the capacitive highway tuning poses some new problems, which have to be solved if signal injection is to be established. This is because we wish the voltage on the highway tuning capacitance to be zero at the end of a transmission pulse even when signal

injection is in progress. According to the formula above, the maximum permissible highway capacitance is $C_{tot} = \frac{2C}{3}$, $(n = 1)$. However, we are at liberty to distribute this capacitance in a roughly arbitrary manner along the transmission path.

Signal Injection in 2-wire Systems

As an example, *Fig. 2* shows a transmission system which has four highways and thus contains three inter-highway contacts and two subscriber contacts in series. The tuning capacitances are distributed symmetrically with respect to the middle highway contact.

In this example, we can now study the problem of signal injection. As the system allows bidirectional transmission, the transmission path must, for signal injection, be broken by inhibiting one or several of the inter-highway contacts. The transmission path for signal injection will thus be shorter, which implies that the effective highway tuning capacitance would be too low. But we are now able to use the second solution of the tuning formula given above, that is, using $n = 2$. This gives us the value $\frac{2C}{15}$ for the effective highway tuning capacitance. This condition defines the point at which signal injection should take place. In the case under consideration it must take place directly on the subscriber highway, or at point A in *Fig. 2*. Thereafter the values of the B-highway capacitances, which are given both by the symmetry conditions of the transmission system and by the known sum $\frac{2C}{3}$ for all highway capacitances, will be $\frac{C}{5}$ as shown in *Fig. 2*.

For this case we have assumed that the elements of the signal injection circuit are the same as those for the subscriber pulse circuit. However, as the signal injector has to operate on a multiplex basis in an arbitrary number of pulse positions, a second pulse contact is necessary for charging the signal injector condenser, instead of the usual low-pass filter. This "charging contact" works in the intervals between the time slots, usually with a smaller pulse width τ', either before or after the time-channel carrying the signal. Because of the bidirec-

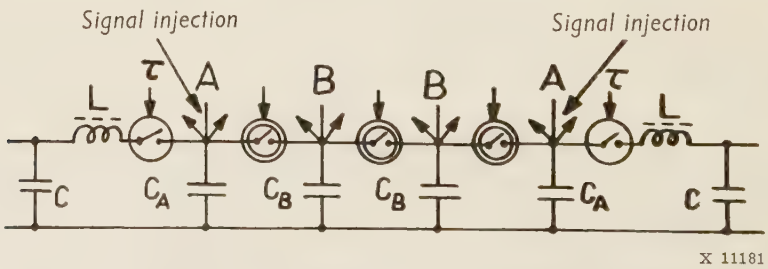

Fig. 2. Transmission over 4 highways with distributed highway tuning.

$$C_A = \frac{2C}{15} \qquad C_B = \frac{C}{5} \qquad 2C_A + 2C_B = \frac{2C}{3}$$

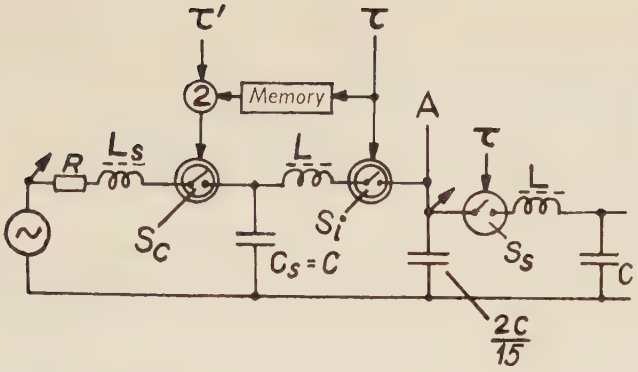

X 11182

Fig. 3. Signal injection circuit for the bidirectional system in Fig. 2.

tional transmission properties the following may now occur. The condenser C_s of the signal circuit in *Fig. 3* may be charged not only from the signal generator over the charging contact S_c, but also "backwards" over the transmission path by a subscriber speech pulse. If it is not possible to eliminate this charge component during the interval between channels, crosstalk between subscribers connected to the same signal injector in different pulse positions will ensue. This crosstalk, expressed in nepers, is equal to $\frac{R \cdot C_s}{\tau'}$, i.e. the ratio between the time constant of the charging circuit and the duration of the charging or discharging procedure. To eliminate this crosstalk, it would be necessary to reduce the time constant of the charging circuit to zero, which is hardly possible. However, we can adopt the stra-

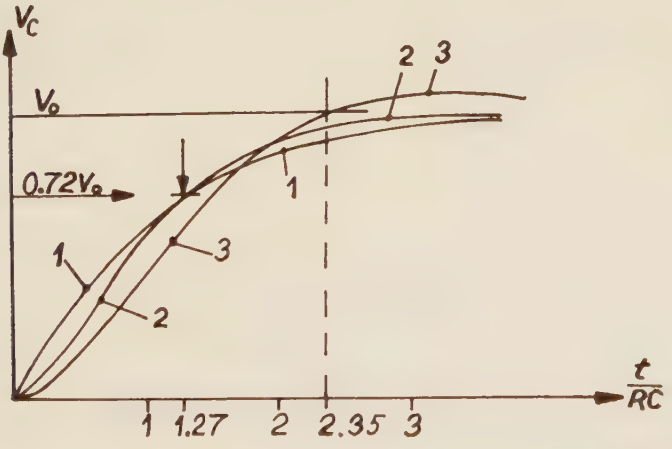

X 11183

Fig. 4. Charging of a capacitor via *RC*-circuit (1), critically damped resonant circuit (2) and undercritically damped ($L_s = 2L_{cr}$) resonant circuit (3).

tagem of tuning the charging circuit with the aid of a series inductance so as to form an undercritically damped resonant circuit. With such a circuit the voltage on the condenser passes the externally applied voltage after a certain time given by the circuit constants and independent of residual charges which may be present on the condenser at the start of the charging procedure. If the charging contact is broken at this instant, the condenser will be charged completely and the influence of an inversely transmitted speech pulse is eliminated.

For purposes of comparison, *Fig. 4* shows three different condenser charging functions with the same series resistance in the charging circuit. Curve 1 shows the pure RC charging function. Curve 2 shows the charging function in the case of critical damping with an inductance of $L_s = L_{cr} = \frac{R^2C}{4}$ in series. Curve 3, finally, shows an undercritically damped charging function with a series inductance equal to twice the value in the critical case:

$$L_s = 2L_{cr} = \frac{R^2C}{2}$$

The voltage V_0, externally applied to the circuit, is reached at the instant $\frac{t}{R \cdot C} = 2.35$.

For the mathematical treatment of the problem we can start from the equation for the damped oscillating circuit.

$$V_0 - V_t = V_0 \cdot e^{-\alpha t} \cdot \left(\cos \omega t + \frac{\alpha}{\omega} \sin \omega t \right) \tag{1}$$

where $\alpha = \frac{R}{2L_s}$ and $\omega = \sqrt{\frac{1}{L_s \cdot C} - \frac{R^2}{4L_s^2}}$

V_0 is the applied voltage and V_t the condenser voltage at the time t. Let us consider the time τ' for the first zero interception, where $V_0 - V_t = 0$. The condition for this is:

$$\cos \omega \tau' + \frac{\alpha}{\omega} \cdot \sin \omega \tau' = 0 \tag{2}$$

and we finally obtain:

$$\tau' = \frac{\pi - \operatorname{arc\,tg} \frac{\omega}{\alpha}}{\omega} \tag{3}$$

We introduce a new variable —a— as the ratio of the inductance in the undercritically to that in the critically damped case:

$$a = \frac{L_s}{L_{cr}} \tag{4}$$

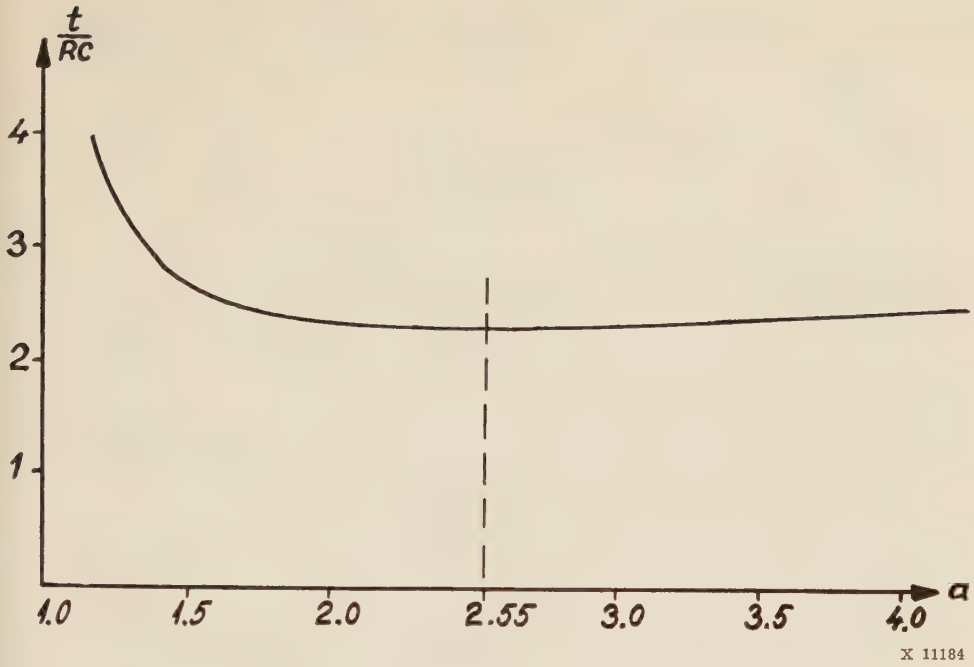

Fig. 5. Charging time τ' as a function of a.

With $L_{cr} = \frac{R^2 C}{4}$ we obtain $\omega = \frac{2}{R \cdot C \cdot a} \cdot \sqrt{a-1}$ and $\alpha = \frac{2}{R \cdot C \cdot a}$

Equation (3) then assumes the form

$$\tau' = \frac{R \cdot C \cdot a}{2 \cdot \sqrt{a-1}} \left(\pi - \text{arc tg} \sqrt{a-1}\right) \tag{5}$$

In *Fig. 5* this equation is shown in the form $\frac{\tau'}{R \cdot C}$ as a function of a. The function has a minimum at $a = 2.55$, i.e. with R and C constant in the charging circuit the fastest possible charging would take place using a series inductance equal to 2.55 times the inductance in the critical case. However, this case is not usable in practice, as the angle of intersection between the charging function and V_0 is too great, which would demand a charging contact with very good time precision. A measure of the angle of intersection is given by the current flowing in the circuit at the moment of breaking. In the inductance this current represents magnetic energy which must be destroyed before the next charging cycle starts, so as to avoid a new source of crosstalk on this account. This destruction takes place in the form of a

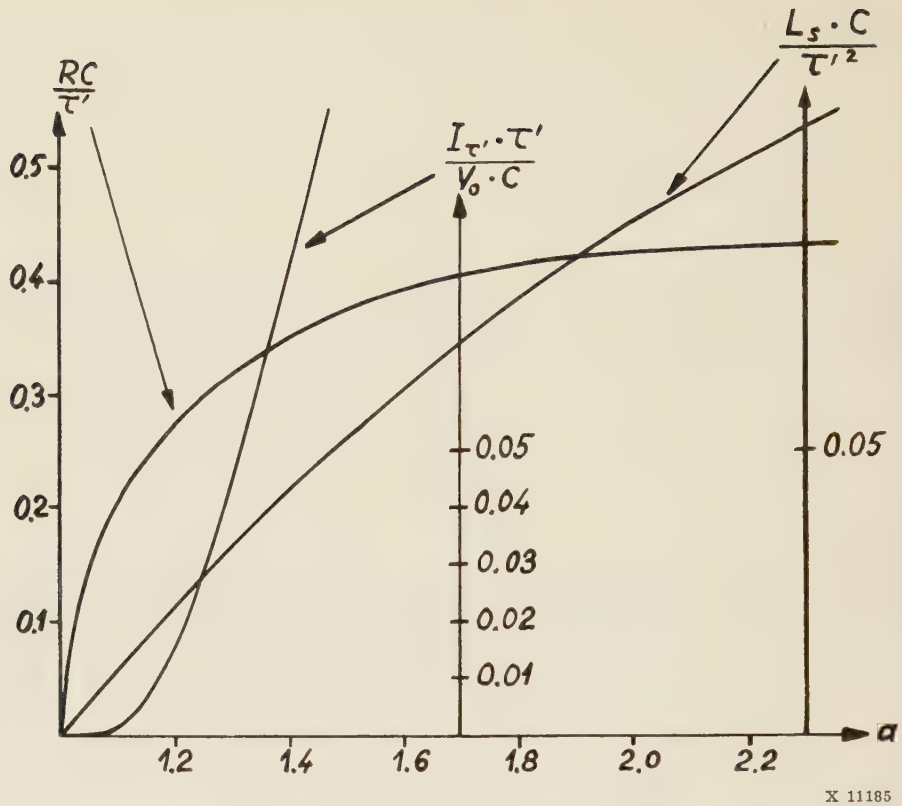

Fig. 6. R, L_s and $I_{\tau'}$ as function of a.

high-frequency oscillation, the frequency of which is given by the circuit stray capacitances. The peak amplitude of this oscillation must not exceed the permissible back-bias of the charging contact.

For the choice of a more advantageous design of the charging circuit we shall, for a given time τ', study the variation of the resistance R and of the series inductance L_s as functions of a. For R we obtain, after inverting eq. 5:

$$R = \frac{\tau'}{C} \cdot \frac{2 \cdot \sqrt{a-1}}{a \cdot (\pi - \operatorname{arc\,tg} \sqrt{a-1})} \tag{6}$$

and for L_s, keeping in mind the relationship between L_s and R,

$$L_s = a \cdot \frac{R^2 \cdot C}{4} = \frac{\tau'^2}{C} \cdot \frac{a-1}{a(\pi - \operatorname{arc\,tg} \sqrt{a-1})^2} \tag{7}$$

The two functions are shown in *Fig. 6*. Also, the current $I_{\tau'}$ at the moment of breaking $t = \tau'$ is shown in the same figure as a function of a. The equation is:

$$I_{\tau'} = \frac{V_0 \cdot C}{\tau'} \cdot \sqrt{a} \cdot \frac{\pi - \operatorname{arc\,tg} \sqrt{a-1}}{\sqrt{a-1}} \cdot e^{-\frac{(\pi - \operatorname{arc\,tg} \sqrt{a-1})}{\sqrt{a-1}}} \tag{8}$$

As we have already seen, large values of a would be unsuitable for the design, since the current at the instant of breaking is large and a considerable degree of time precision would be necessary for the charging contact. However, the current function inflects sharply in the region $1.1 < a < 1.15$. For $a = 1.1$ the current is almost negligible and the demands on time precision will be small. On the other hand, for values of a below 1.1 the circuit again becomes difficult to design because of the increasing resistance tolerance difficulties. The best compromise has therefore been found to exist for values of a between 1.1 and 1.2.

The charging contact is operated from a special pulse generator in the interval between channel time slots and under the additional condition that the injector contact has been operated in the preceding time slot as already mentioned. This additional condition may be fulfilled in many ways by means of a memory circuit as shown schematically in *Fig. 3*.

Signal Injection in 4-wire Systems

In 4-wire systems a simpler signal injection procedure may be used, provided that a separating amplifier is built in between the low-pass filter and the receiving subscriber. Since the transmission is unidirectional, no crosstalk problems of the kind mentioned above can arise.

It would seem natural to accomplish the signal injection in a form in which the functions of charging contact and injector contact are combined into one contact, closing synchronously with the subscriber contact, and in which the highway condenser takes over, in part, the function of the charging condenser. We shall study the problem in an example involving a system with two highways. We presume that the highway capacitance is distributed equally on both highways and that the inter-highway contact is inhibited when signal injection is taking place. We can therefore confine our study to the receiving highway, and we then obtain a circuit diagram as shown in *Fig. 7*. To the right of the highway lie, as usual, the subscriber circuit with the subscriber contact S_s, the pulse circuit with inductance L and capacitance C, the low-pass filter, in this case with resistive termination, and the terminating amplifier. To the left of the highway lies the injector contact S_i, which connects the signal source to the highway over an inductance L', which we shall specifically study later on.

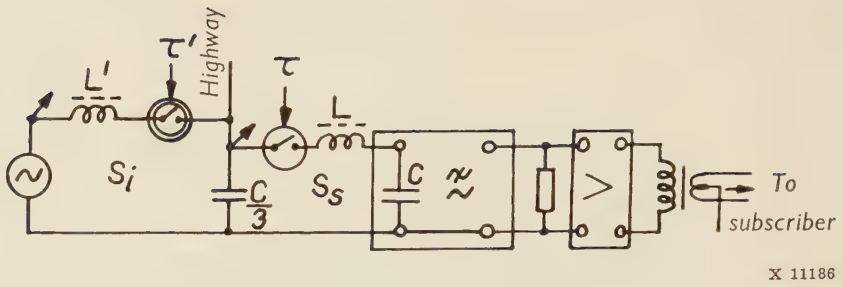

Fig. 7. Signal injection circuit for a unidirectional system.

For this circuit the following conditions are required:

1) The same transmission conditions should pertain for the subscriber circuit as in the case of speech transmission, i.e. at the instant $t = \tau$, when the subscriber contact breaks, the voltage on the subscriber condenser should have reached its maximum, while at the same time the current through the subscriber contact should pass zero.

2) At the time $t = \tau$ the voltage on the highway condenser should be a minimum at or near zero.

3) The current through the injector contact should be a minimum at or near zero when this contact breaks at the time $t = \tau'$.

The mathematical treatment of the problem is extremely difficult. By means of deductive reasoning, however, we shall reach the goal faster. We know that condition 1 is fulfilled if a voltage function, symmetrical with respect to $\frac{\tau}{2}$, is impressed on the highway, i.e. the input of the subscriber circuit. An example of such a function is the previously mentioned voltage swing with the form $A\ (1 - \cos \omega t)$ which for $\omega = \frac{2n}{\tau}$ assumes the form $A_{(n)} \cdot \left(1 - 2n \cdot \frac{t}{\tau}\right)$. Thus, we must find a pulse forming circuit that produces one of these functions under the given circumstances. This pulse generator must possess a small internal impedance so that the voltage function is not disturbed too much by the connected subscriber circuit. However, because of the limited permissible loading of the injector contact, this impedance cannot be chosen arbitrarily small. In our example the factor n will therefore hardly be greater than 2. If, across the given highway condenser of $\frac{C}{3}$, we wish to produce the function $1 - \cos 4\pi \cdot \frac{t}{\tau}$, the inductance L' – disregarding the influence of the subscriber circuit—must be chosen according to the equation below:

$$\tau = 4\pi \sqrt{L' \cdot \frac{C}{3}} = \pi \cdot \sqrt{LC} \tag{9}$$

For L' we obtain the value

$$L' = \frac{3L}{16}$$

If, synchronously, the subscriber circuit is now connected to the highway over its contact S_s, the voltage function on the highway will be altered in frequency and damped, so that the minima are no longer zero, since the subscriber circuit draws energy from the highway. The result of this will be a residual charge on the highway, which implies a distortion of the voltage function.

However, we can correct the function by quite simple means. This is done by breaking the injector contact earlier than the subscriber contact. The residual charge on the highway

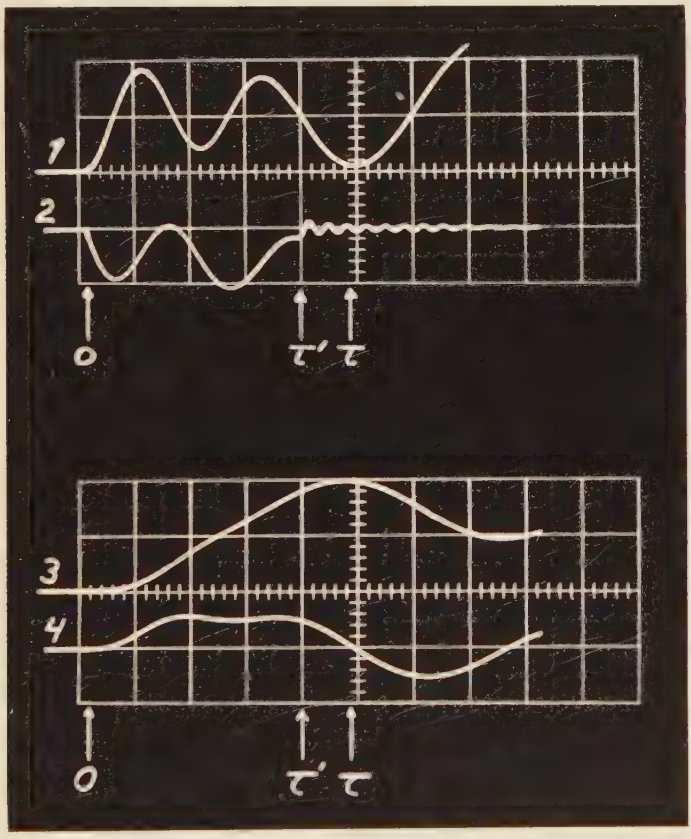

X 11187

Fig. 8. Significant waveforms concerning the circuit according to fig. 7.

1. Voltage on $C/3$
2. Current through S_i
3. Voltage on C
4. Current through S_s

condenser can then be drawn off during the residual time by the charging procedure in the subscriber circuit, which is still not completed. Thus, so to speak, the subscriber circuit itself corrects the voltage function which it has originally distorted. In order to reduce the current through the injector contact to a minimum at the breaking moment of this contact, the calculated value of L' must also be corrected. The optimal design of the injector circuit was tried out experimentally on a model circuit, in which a short circuit was substituted for the subscriber contact and a DC voltage source was used as signal source. By varying the inductance L' and the pulse time τ', while observing voltages and currents in subscriber and injector circuits at the relevant times, the correction could be trimmed in a simple manner.

Fig. 8 shows the oscillograms for this experiment.

We see that the highway voltage (curve 1) is almost zero at the time $t = \tau$. The breaking moment of the injector contact, as may be seen from the discontinuity of curve 2 (current), lies at $t = \frac{4\tau}{5}$. As we have specified, the current through the injector contact is a minimum near zero at this instant. Curve 3 shows the voltage on the subscriber condenser and curve 4 the current in the subscriber circuit. As specified, the voltage has a maximum at the time $t = \tau$, while the current has a zero intercept.

The curves shown are valid for a design of the injector circuit where

$$L' = \frac{L}{6.2} \qquad \tau' = \frac{4}{5}\tau$$

For this case the voltage maximum on the subscriber condenser is 1.8 times the voltage applied on the injector circuit.

Signal Generators

Signal generators common to the whole exchange and suitable for the injection processes mentioned must not only have a small low-frequency internal impedance, but also a negligible pulse impedance. Therefore, on the output of the signal generator a large shunt capacitance is necessary. This may suitably take the form of equally distributed capacitors on the inputs of all signal injector circuits. The capacitive low-frequency reactive current is compensated by a shunt inductance, which is designed as a transformer in order to permit adjustment of output level. *Fig. 9* shows the output stage of such a signal generator. The tuning capacitance is here distributed both to the primary and secondary windings of the

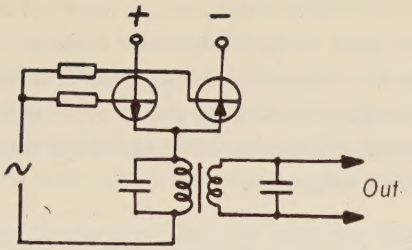

X 11188

Fig. 9. Power stage for a common sine-wave signal generator.

transformer. The power amplification is performed by a single-ended class B push-pull stage with two complementary transistors in an emitter follower circuit.

For signal generators with a higher power level and good efficiency, a circuit according to *Fig. 10* may be used.

For the sake of simplicity the transformer in the tuned circuit has been omitted here. As a power stage a transistor switch combination is used, which, by periodically switching between a positive and a negative voltage, delivers a square wave. If a sine-wave output signal is desired, the fundamental frequency of the square-wave is extracted by means of a series resonant circuit L_1C_1, which is tuned to the fundamental frequency. As we know, with such a filter system we get two resonance peaks, one above and one below the natural frequency of the two circuits.

The distance between the two peaks depends on the mutual coupling between the two circuits, given by the ratio between the inductances $\frac{L_2}{L_1 + L_2}$. When designing the filter, it is

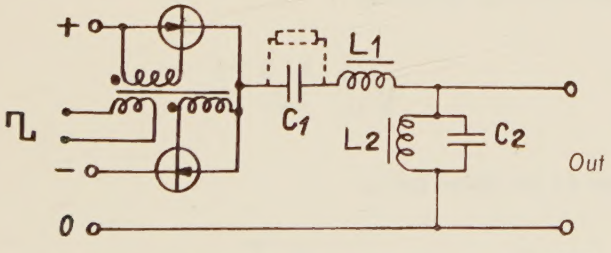

X 11189

Fig. 10. Signal generator for sinewave or composite signal.

therefore necessary to bear in mind that the coupling must not be chosen too loose, so that the resonance peaks get too close to the fundamental frequency, which would mean that a small change in the square-wave frequency would result in a change in output amplitude. On the other hand, with too tight coupling the danger arises that the upper resonance peak will be in the neighbourhood of the third harmonic of the square wave. In this case the output would no longer be a sine wave.

This fact, on the other hand, gives us the opportunity to design a signal generator which delivers a signal composed of the fundamental frequency and the third harmonic. Such a signal may be used to advantage as a dialling tone.

For the design of a filter of this type the following conditions apply:

$$(L_1 + L_2)\, C_1 = C_2 L_2 = \frac{1}{4\pi^2 \cdot f_0^2} \tag{10}$$

i.e. the series resonant circuit consisting of C_1 and $L_1 + L_2$ and the parallel circuit consisting of C_2 and L_2 must be tuned to the same resonant frequency f_0, which lies somewhere between the fundamental frequency and the third harmonic of the square-wave. f_0 is given by the condition for the two resonant frequencies of the filter

$$f_{1,2} = \frac{f_0}{\sqrt{1 \pm \sqrt{\frac{C_1}{C_2}}}} \tag{11}$$

By dividing $\frac{f_1}{f_2}$ we can determine $\sqrt{\frac{C_1}{C_2}}$ and we obtain:

$$\sqrt{\frac{C_1}{C_2}} = \frac{f_2^2 - f_1^2}{f_2^2 + f_1^2} \tag{12}$$

For our case, where $f_2 = 3f_1$, we obtain:

$$\sqrt{\frac{C_1}{C_2}} = \frac{9-1}{9+1} = \frac{4}{5} \tag{12a}$$

Inserting 12a into 11 we obtain for f_0:

$$f_0 = f_1 \cdot \sqrt{1 + \frac{4}{5}} = \frac{3f_1}{\sqrt{5}} = 1.34 \cdot f_1$$

For a tonality of 425 c/s the circuits should thus be tuned to a natural frequency of $1.34 \cdot 425 = 570$ c/s. The ratio between the amplitudes of fundamental frequency and third harmonic is 3 : 1 in accordance with the spectral distribution in the square wave. If a stronger emphasis on the third harmonic is desired, this can be simply accomplished by placing f_1 somewhat higher than the fundamental frequency of the square wave. Thus the fundamental frequency lies on the slope of the filter curve and is more attenuated.

The calculations for the 2-frequency filter are valid for undamped resonant circuits. The error introduced through the connected external load is, however, negligible, as experience has shown. In order to achieve an almost constant output level for variable loads, the series circuit must also be damped. This is preferably done by means of a resistance connected in parallel with the condenser C_1. The damping of the series circuit should be about the same as that of the parallel circuit for an average load.

Bibliography

1. Håård, H. B. & Svala, C. G.: U.S. Patent No. 2 718 621.
2. Svala, G. & Jacob, W.: *Electronic Telephone Exchanges.* Ericsson Rev. *33*(1956):1, pp. 2—14.
3. Cattermole, K. W. & Price, J. C.: *Efficiency and Reciprocity in Pulse-Amplitude Modulation;* Part I: *Principles*; Part II: *Testing and Applications.* Proc. Instn elec. Engrs. 105 (1958) B, pp. 449 & 463, Paper 2474 R & 2475 R. Dec. 1957.
4. Jacob, W.: Swed. Patent No. 164 938.

Manuscript received by the editors October 1960.